

IN THE UNITED STATES PATENT AND TRADEMARK OFFICE

In re Patent Application of

Date: May 15, 2008

Applicants: Bednorz et al.

Docket: YO987-074BZ

Serial No.: 08/479,810

Group Art Unit: 1751

Filed: June 7, 1995

Examiner: M. Kopec

For: NEW SUPERCONDUCTIVE COMPOUNDS HAVING HIGH TRANSITION
TEMPERATURE, METHODS FOR THEIR USE AND PREPARATION

Commissioner for Patents

United States Patent and Trademark Office

P.O. Box 1450

Alexandria, VA 22313-1450

**APPEAL BRIEF
PART IX**

CFR 37 § 41.37(c) (1) (ix)

SECTION 1

VOLUME 5

Part 3

BRIEF ATTACHMENTS AX TO BL

Respectfully submitted,

/Daniel P Morris/

Dr. Daniel P. Morris, Esq.

Reg. No. 32,053

(914) 945-3217

IBM CORPORATION

Intellectual Property Law Dept.

P.O. Box 218

Yorktown Heights, New York 10598

BRIEF ATTACHMENT AX

IN THE UNITED STATES PATENT AND TRADEMARK OFFICE

In re Patent Application of

Date: March 1, 2004

Applicants: Bednorz et al.

Docket: YO987-074BZ

Serial No.: 08/479,810

Group Art Unit: 1751

Filed: June 7, 1995

Examiner: M. Kopec

For: NEW SUPERCONDUCTIVE COMPOUNDS HAVING HIGH TRANSITION
TEMPERATURE, METHODS FOR THEIR USE AND PREPARATION

Commissioner for Patents
P.O. Box 1450
Alexandria, VA 22313-1450

FIFTH SUPPLEMENTAL AMENDMENT

Sir:

In response to the Office Action dated February 4, 2000:

ATTACHMENT 3

AX

Possible High T_c Superconductivity in the Ba-La-Cu-O System

J.G. Bednorz and K.A. Müller

IBM Zürich Research Laboratory, Rüschlikon, Switzerland

Received April 17, 1986

Metallic, oxygen-deficient compounds in the Ba-La-Cu-O system, with the composition $\text{Ba}_{1-x}\text{La}_x\text{Cu}_y\text{O}_{5(1-y)}$ have been prepared in polycrystalline form. Samples with $x=1$ and 0.75 , $y>0$, annealed below 900°C under reducing conditions, consist of three phases, one of them a perovskite-like mixed-valent copper compound. Upon cooling, the samples show a linear decrease in resistivity, then an approximately logarithmic increase, interpreted as a beginning of localization. Finally an abrupt decrease by up to three orders of magnitude occurs, reminiscent of the onset of percolative superconductivity. The highest onset temperature is observed in the 30 K range. It is markedly reduced by high current densities. Thus, it results partially from the percolative nature, but possibly also from $2D$ superconducting fluctuations of double perovskite layers of one of the phases present.

1. Introduction

"At the extreme forefront of research in superconductivity is the empirical search for new materials" [1]. Transition-metal alloy compounds of $A15$ (Nb_3Sn) and $B1$ (NbN) structure have so far shown the highest superconducting transition temperatures. Among many $A15$ compounds, careful optimization of Nb-Ge thin films near the stoichiometric composition of Nb_3Ge by Gavalev et al. and Testardi et al. a decade ago allowed them to reach the highest $T_c = 23.3\text{ K}$ reported until now [2, 3]. The heavy Fermion systems with low Fermi energy, newly discovered, are not expected to reach very high T_c 's [4].

Only a small number of oxides is known to exhibit superconductivity. High-temperature superconductivity in the Li-Ti-O system with onsets as high as 13.7 K was reported by Johnston et al. [5]. Their x-ray analysis revealed the presence of three different crystallographic phases, one of them, with a spinel structure, showing the high T_c [5]. Other oxides like perovskites exhibit superconductivity despite their small carrier concentrations, n . In Nb-doped SrTiO_3 , with $n = 2 \times 10^{19}\text{ cm}^{-3}$, the plasma edge is below the highest optical phonon, which is therefore unshielded

[6]. This large electron-phonon coupling allows a T_c of 0.7 K [7] with Cooper pairing. The occurrence of high electron-phonon coupling in another metallic oxide, also a perovskite, became evident with the discovery of superconductivity in the mixed-valent compound $\text{BaPb}_{1-x}\text{Bi}_x\text{O}_3$ by Sleight et al., also a decade ago [8]. The highest T_c in homogeneous oxygen-deficient mixed crystals is 13 K with a comparatively low concentration of carries $n = 2.4 \times 10^{21}\text{ cm}^{-3}$ [9]. Flat electronic bands and a strong breathing mode with a phonon feature near 100 cm^{-1} , whose intensity is proportional to T_c , exist [10]. This last example indicates that within the BCS mechanism, one may find still higher T_c 's in perovskite-type or related metallic oxides, if the electron-phonon interactions and the carrier densities at the Fermi level can be enhanced further.

Strong electron-phonon interactions in oxides can occur owing to polaron formation as well as in mixed-valent systems. A superconductivity (metallic) to bipolaronic (insulator) transition phase diagram was proposed theoretically by Chakraverty [11]. A mechanism for polaron formation is the Jahn-Teller effect, as studied by Höck et al. [12]. Isolated Fe^{4+} , Ni^{3+} and Cu^{2+} in octahedral oxygen environment

show strong Jahn-Teller (J.T.) effects [13]. While SrFe(IV)O_3 is distorted perovskite insulator, LaNi(III)O_3 is a J.T. undistorted metal in which the transfer energy b_u of the J.T. e_g electrons is sufficiently large [14] to quench the J.T. distortion. In analogy to Chakraverty's phase diagram, a J.T.-type polaron formation may therefore be expected at the borderline of the metal-insulator transition in mixed perovskites, a subject on which we have recently carried out a series of investigations [15]. Here, we report on the synthesis and electrical measurements of compounds within the Ba-La-Cu-O system. This system exhibits a number of oxygen-deficient phases with mixed-valent copper constituents [16], i.e., with itinerant electronic states between the non-J.T. Cu^{2+} and the J.T. Cu^{2+} ions, and thus was expected to have considerable electron-phonon coupling and metallic conductivity.

II. Experimental

1. Sample Preparation and Characterization

Samples were prepared by a coprecipitation method from aqueous solutions [17] of Ba-, La- and Cu-nitrate (SPECPURE JMC) in their appropriate ratios. When added to an aqueous solution of oxalic acid as the precipitant, an intimate mixture of the corresponding oxalates was formed. The decomposition of the precipitate and the solid-state reaction were performed by heating at 900 °C for 5 h. The product was pressed into pellets at 4 kbar, and reheated to 900 °C for sintering.

2. X-Ray Analysis

X-ray powder diffractograms (System D 500 SIEMENS) revealed three individual crystallographic phases. Within a range of 10° to 80° (2θ), 17 lines could be identified to correspond to a layer-type perovskite-like phase, related to the K_2NiF_4 structure ($a = 3.79$ Å and $c = 13.21$ Å) [16]. The second phase is most probably a cubic one, whose presence depends on the Ba concentration, as the line intensity decreases for smaller $x(\text{Ba})$. The amount of the third phase (volume fraction > 30% from the x-ray intensities) seems to be independent of the starting composition, and shows thermal stability up to 1,000 °C. For higher temperatures, this phase disappears progressively, giving rise to the formation of an oxygen-deficient perovskite ($\text{La}_x\text{Ba}_{3-x}\text{Cu}_3\text{O}_{7-x}$) as described by Michel and Raveau [16].

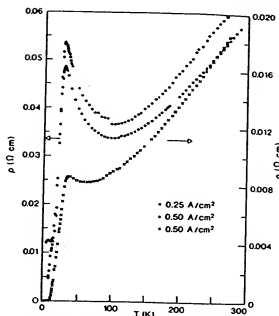


Fig. 1. Temperature dependence of resistivity in $\text{Ba}_x\text{La}_{3-x}\text{Cu}_3\text{O}_{7-x}$ for samples with $x(\text{Ba})=1$ (upper curves, left scale) and $x(\text{Ba})=0.75$ (lower curve, right scale). The first two cases also show the influence of current density

3. Conductivity Measurements

The dc conductivity was measured by the four-point method. Rectangular-shaped samples, cut from the sintered pellets, were provided with gold electrodes and contacted by In wires. Our measurements between 300 and 4.2 K were performed in a continuous-flow cryostat (Leybold-Heraeus) incorporated in a computer-controlled (IBM-PC) fully-automatic system for temperature variation, data acquisition and processing.

For samples with $x(\text{Ba}) \leq 1.0$, the conductivity measurements, involving typical current densities of 0.5 A/cm^2 , generally exhibit a high-temperature metallic behaviour with an increase in resistivity at low temperatures (Fig. 1). At still lower temperatures, a sharp drop in resistivity (> 90%) occurs, which for higher currents becomes partially suppressed (Fig. 1: upper curves, left scale). This characteristic drop has been studied as a function of annealing conditions, i.e., temperature and O_2 partial pressure (Fig. 2). For samples annealed in air, the transition from itinerant to localized behaviour, as indicated by the minimum in resistivity in the 80 K range, is not very pronounced. Annealing in a slightly reducing atmosphere, however, leads to an increase in resistivity and a more pronounced localization effect. At the same time, the onset of the resistivity drop is shifted

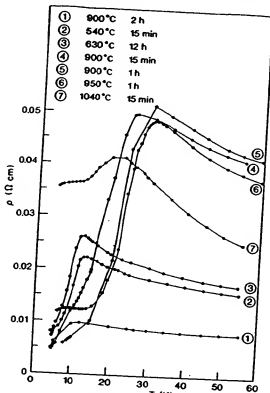


Fig. 2. Low-temperature resistivity of samples with $x(\text{Ba})=1.0$, annealed at O_2 partial pressure of 0.2 bar (curve ①) and 0.2×10^{-4} bar (curves ② to ⑦).

towards the 30 K region. Curves ④ and ⑤, recorded for samples treated at 900 °C, show the occurrence of a shoulder at still lower temperature, more pronounced in curve ⑤. At annealing temperatures of 1,040 °C, the highly conducting phase has almost vanished. As mentioned in the Introduction, the mixed-valent state of copper is of importance for electron-phonon coupling. Therefore, the concentration of electrons was varied by the Ba/La ratio. A typical curve for a sample with a lower Ba concentration of 0.75 is shown in Fig. 1 (right scale). Its resistivity decreases by at least three orders of magnitude, giving evidence for the bulk being superconducting below 13 K with an onset around 35 K, as shown in Fig. 3, on an expanded temperature scale. The latter figure also shows the influence of the current density, typical for granular compounds.

III. Discussion

The resistivity behaviour of our samples, Fig. 1, is qualitatively very similar to the one reported in the Li-Ti-O system, and in superconducting

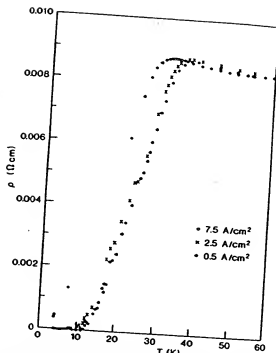


Fig. 3. Low-temperature resistivity of a sample with $x(\text{Ba})=0.75$, recorded for different current densities.

$\text{BaPb}_{1-x}\text{Bi}_x\text{O}_3$ polycrystalline thin films [5, 18]. Upon cooling from room temperature, the latter exhibit a nearly linear metallic decrease of $\rho(T)$, then a logarithmic type of increase, before undergoing the transition to superconductivity. One could, of course, speculate that in our samples a metal-to-metal structural phase transition occurs in one of the phases. The shift in the drop in $\rho(T)$ with increasing current density (Fig. 3), however, would be hard to explain with such an assumption, while it supports our interpretation that we observe the onset of superconductivity of percolative nature, as discussed below. In $\text{BaPb}_{1-x}\text{Bi}_x\text{O}_3$, the onset of superconductivity has been taken at the resistivity peak [18]. This assumption appears to be valid in percolative systems, i.e., in the thin films [18] consisting of polycrystals with grain boundaries, or when different crystalline phases with interpenetrating grains are present, as found in the Li-Ti-O [5] or in our Ba-La-Cu-O system. The onset can also be due to fluctuations in the superconducting wave functions. We assume one of the Ba-La-Cu-O phases exhibits this behaviour. Therefore, under the above premises, the peak in $\rho(T)$ at 35 K, observed for an $x(\text{Ba})=0.75$ (Fig. 1), has

to be identified as the start to superconductive cooperative phenomena in the isolated grains. It should be noted that in granular Al, Cooper pairs in coupled grains have been shown to exist already at a point where $\rho(T)$ upon cooling has decreased by only 20% of its highest value. This has been proven qualitatively [19] and more recently also quantitatively [20] by the negative frequency shift occurring in a microwave cavity. In 100 Å films, a shoulder in the frequency shift owing to 2D fluctuations was observed above the T_c of the grains. In our Ba-La-Cu-O system, a series of layer-like phases with considerable variety in compositions are known to exist [16, 21], and therefore 2D correlations can be present.

The granularity of our system can be justified from the structural information, and more quantitatively from the normal conductivity behaviour. From the former, we know that more than one phase is present and the question arises how large are the grains. This can be inferred from the logarithmic fingerprint in resistivity. Such logarithmic increases are usually associated with beginning of localization. A most recent example is the Anderson transition in granular Sn films [22]. Common for the granular Sn and our samples is also the resistivity at 300 K, lying in the range of 0.06 to 0.02 Ωcm , which is near the microscopic critical resistivity of $\rho_c = 10 L_0 \hbar / e^2$ for localization. From the latter formula, an interatomic distance L_0 in the range of 100 Å is computed, thus a size of superconducting grains of this order of magnitude must be present. Upon cooling below T_c , Josephson junctions between the grains phase-lock progressively [23] and the bulk resistivity gradually drops to zero by three orders of magnitude, for sample 2 (Fig. 1). At larger current densities, the weaker Josephson junctions switch to normal resistivity, resulting in a temperature shift of the drop, as shown in Fig. 3. The plateau in resistivity occurring below the 80% drop (Fig. 1) for the higher current density of 0.5 A/cm², and Fig. 2 curve (c) may be ascribed to switching of junctions to the normal state.

The way the samples have been prepared seems to be of crucial importance: Michel et al. [21] obtained a single-phase perovskite by mixing the oxides of La and Cu and BaCO₃ in an appropriate ratio and subsequent annealing at 1,000 °C in air. We also applied this annealing condition to one of our samples, obtained by the decomposition of the corresponding oxalates, and found no superconductivity. Thus, the preparation from the oxalates and annealing below 950 °C are necessary to obtain a non-perovskite-type phase with a limited temperature range of stability exhibiting this new behaviour. The formation of this phase at comparatively low temperatures is favoured by the intimate mixture of the compo-

nents and the high reactivity of the oxalates owing to the evolution of large amounts of H₂O and CO₂ during decomposition.

IV. Conclusion

In the concentration range investigated, compounds of the Ba-La-Cu-O system are metallic at high temperatures, and exhibit a tendency towards localization upon cooling. Samples annealed near 900 °C under reducing conditions show features associated with an onset of granular superconductivity near 30 K. The system consists of three phases, one of them having a metallic perovskite-type layer-like structure. The characterization of the new, apparently superconducting, phase is in progress. An identification of that phase may allow growing of single crystals for studying the Meissner effect, and collecting specific-heat data to prove the presence of high T_c bulk superconductivity.

The authors would like to thank H.E. Weibel for his help in getting familiar with the conductivity measurement system, E. Courtens and H. Thomas for discussions and a critical reading of the manuscript.

References

1. Tinkham, M., Beasley, M.R., Larbaestier, D.C., Clark, A.F., Finemore, D.K.: Workshop on Problems in Superconductivity, Copper Mountain, Colorado, August 1983, p. 12
2. Beasley, M.R., Geballe, T.H.: *Phys. Today* 36 (10), 60 (1984)
3. Müller, J.: *Rep. Prog. Phys.* 43, 663 (1980)
4. Ott, H.R.: *Unconventional Superconductivity*. Zürich Phys. Soc. Seminar, Zürich, February 13, 1986
5. Johnston, D.C., Prakash, H., Zachariasen, W.H., Viswanathan, R.: *Mater. Res. Bull.* 8, 777 (1973)
6. Baratoff, A., Binnig, G.: *Physica* 108 B, 1335 (1981)
7. Baratoff, A., Binnig, G., Bednorz, J.G., Gervais, F., Servoin, J.L.: In: *Superconductivity in d- and f-Band Metals*, Proceedings IV Conference in "Superconductivity in d- and f-Band Metals", Buckel, W. and Weber, W. (eds), p. 419, Kernforschungszentrum Karlsruhe 1982
8. Binnig, G., Baratoff, A., Hönig, H.E., Bednorz, J.G.: *Phys. Rev. Lett.* 45, 1352 (1980)
9. Batlogg, B.: *Physica* 126 B, 275 (1984)
10. Thanh, T.D., Koma, A., Tanaka, S.: *Appl. Phys.* 22, 205 (1980)
11. Mattheis, F., Hamann, D.R.: *Phys. Rev. B* 26, 2682 (1982); *Ibid.* 28, 4227 (1983)
12. Chakraverty, B.K.: *J. Phys. Lett.* 40, L99 (1979); *J. Phys.* 42, 1351 (1981)
13. Höck, K.-H., Nickisch, H., Thomas, H.: *Helv. Phys. Acta* 56, 237 (1983)
14. Englmann, R.: In: *The Jahn-Teller Effect in Molecules and Crystals*. London, New York: Wiley Interscience 1972
15. Goodenough, J.B., Longo, M.: Magnetic and other properties of oxide and related compounds. In: *Landolt-Börnstein New*

wing
CO₂unds
high
cool-
0 °C
ated
near
z of
like
ntly
ica-
rys-
ting
T_cting
tens
inu-F₀

iv.

)

ys.

in.

n.

d-

t-

t-

t.

t.

t.

t.

t.

t.

t.

t.

t.

t.

t.

t.

t.

t.

t.

t.

t.

t.

t.

t.

t.

t.

t.

t.

Series. Vol III/4a: Crystal and solid state physics. Hellwege, K.H., Hellwege, A.M. (eds.), p. 262, Fig. 73. Berlin, Heidelberg, New York: Springer-Verlag 1970

15. Bednorz, J.G., Müller, K.A.: (in preparation)
16. Michel, C., Raveau, B.: *Chim. Min.* 21, 407 (1984)
17. Bednorz, J.G., Müller, K.A., Arend, H., Gränicher, H.: *Mat. Res. Bull.* 18 (2), 181 (1983)
18. Suzuki, M., Murakami, T., Inamura, T.: *Shinku* 24, 67 (1981) (in Japanese)
- Enomoto, Y., Suzuki, M., Murakami, T., Inukai, T., Inamura, T.: *Jpn. J. Appl. Phys.* 20, L661 (1981)
19. Müller, K.A., Pomerantz, M., Knoedler, C.M., Abraham, D.: *Phys. Rev. Lett.* 45, 832 (1980)
20. Stocker, E., Buttat, J.: *Solid State Commun.* 53, 915 (1985)

21. Michel, C., Er-Rakho, L., Raveau, B.: *Mat. Res. Bull.* 20, 667 (1985)
22. Van Haeften, C., Bruynseraede, Y.: *Phys. Rev. B* 33, 1684 (1986)
23. Deutscher, G., Entin-Wohlman, O., Fishman, S., Shapira, Y.: *Phys. Rev. B* 21, 5041 (1980)

J.G. Bednorz
K.A. Müller
IBM Zürich Research Laboratory
Säumerstrasse 4
CH-8803 Rüschlikon
Switzerland

Note Added in Proof

Chemical analysis of the bulk composition of our samples revealed a deviation from the ideal La/Ba ratios of 4 and 5.66. The actual ratios are 16 and 18, respectively. This is in agreement with an identification of the third phase as CuO

BRIEF ATTACHMENT AY

INTRODUCTION

Exploring Superconductivity

Georg Bednorz

In 1987, Georg Bednorz shared the Nobel Prize in Physics with his partner and mentor, K. Alex Müller "For their important breakthrough in the discovery of superconductivity in ceramic materials." Their breakthrough, accomplished in an IBM research lab in Switzerland, centered around the fabrication of a new copper-oxide compound that was superconducting at temperatures high enough to dramatically extend the applications of superconductors. To comprehend the significance of Bednorz's work, one must first understand the history of research in superconductivity.


Early investigations of superconductors that operate at temperatures higher than 23.2° K focused on metallic compounds that are good conductors of current at room temperature. In 1957 John Bardeen, Leon N. Cooper, and J. Robert Schrieffer (Nobel Prize in Physics, 1972) of the University of Illinois presented a new theory of superconductivity that changed the focus of research. In ordinary conductors some energy is lost to resistance because the conducting electrons scatter off impurities and vibrating atoms, known as phonons. According to the BCS theory (named for the initials of its originators), superconducting current is carried by pairs of electrons. This pairing keeps individual electrons from scattering off impurities, thus preventing resistance and establishing the superconducting state. Furthermore, it is the interaction between the electrons and the atomic structure of the superconductor that is responsible for the electron pairing.

With this new theory, the search for high-temperature superconductors shifted from metals and metal alloys to materials that display a strong interaction between the electron pairs and the underlying atomic structure. Scientists turned to oxides, which are normally insulators.


The initial research led to modest advances. In 1973 David Johnston at the University of California at San Diego discovered superconductivity in lithium-titanium oxide at 13.7° K. In 1975 Arthur Sleight at Du Pont Research observed barium-lead-bismuth oxide superconducting at 13° K. X-ray analysis indicated the presence of significant interaction between electrons and the vibrations of the structural atoms (phonons). This fit the BCS theory and suggested that further research on metal oxides might prove rewarding.

In 1983 Alex Müller, who had been conducting research on insulators, proposed that Bednorz collaborate with him in a search for high-temperature superconductors in metal oxides. Bednorz agreed because he felt the combination of Müller's vision and his expertise in solid-state physics would lead to success.

They first experimented with nickel oxides, but had disappointing results. Progress was slow and the amount of time and energy they could devote to this work was limited because it was not a major focus at the IBM research facility. The two men persevered, however, because they knew that oxide materials satisfied the requirements of the current BCS theory and that under the proper conditions such a material should prove to be superconducting at high temperatures.


[Click here](#)  To hear Georg Bednorz describe their early work.

Then in the fall of 1985 Bednorz read a paper by Claude Michel, L. Er-Rakho, and Bernard Raveau (from the University of Caen) that described their work with copper-oxide compounds. Bednorz immediately realized that a mixture of copper and barium would have the properties he was seeking, and on that very day he fabricated the new compound, a ceramic insulator composed of lanthanum, barium, and copper oxide. Since he could not duplicate the exact conditions under which the French scientists prepared their compound, he used a different preparation scheme. As it turned out, that "chance" modification led to the Nobel Prize.

[Click here](#)  To hear Georg Bednorz describing the results of their modification.

In January 1986 the new material was tested and the resistance analysis indicated that it was superconducting. Bednorz recalls that "when it happened, I didn't trust my eyes." The fabrication scheme he used had a different amount of oxygen and a more moderate heating process than the original French one; this turned out to be a key to its superconducting character. Bednorz's compound--and all subsequent metal-oxide superconductors--contained very thin sheets of copper oxide separated by layers of other metal oxides. There appears to be a direct correlation between the number of copper-oxide layers in a superconductor and its critical temperature. In general, the greater the number of copper-oxide layers, the higher the critical temperature. By varying the barium content and heating conditions, Bednorz was able to produce a material that was superconducting at temperatures as high as 30° K, seven degrees higher than the existing record.

When Bednorz's laboratory detected the initial data supporting the high-temperature superconductivity of the copper-oxide ceramic material, Bednorz and Müller had to make a difficult decision. There had been many unsubstantiated and overrated claims of high-temperature superconductors, and they wondered if they should publish their results immediately in a prominent journal or wait until they substantiated their results with the more rigorous magnetic tests (to detect the Meissner effect). Delays at this stage would mean that others working on similar projects could publish their findings first and receive the credit. They decided to submit their results at once to a journal that would not have many specialists as readers. They also wanted a journal with a fair amount of time between submission and publication, which would allow them to complete the magnetic testing before the article appeared. Their initial results were submitted to the Swiss Journal Zeitschrift für Physik on April 17, 1986, and were published in the September issue. The paper received little attention, and by mid-October they had final confirmation of superconductivity.

[Click here](#)  To hear Georg Bednorz describing their thoughts on publishing their results.

Bednorz and Müller announced their discovery to the physics community, which was initially skeptical. Their colleagues questioned the validity of the data, and many laboratories throughout the world set out to verify their claims. After confirmation by the University of Tokyo, the University of Houston, and Bell Laboratories, the scientific community began to realize that their claim of high-temperature superconductivity was valid.

Attention in the scientific community then focused on raising the temperature, and by the end of 1986 Bednorz raised the critical temperature of the barium-lanthanum-copper oxide system to 40° K by replacing barium with strontium. Researchers from the University of Houston and the University of Alabama, led by Paul Chu, then found that they could raise the compound's critical temperature to 52° K by applying pressure to the present metal oxide superconductor. This connection between compression of a crystal and an elevated critical temperature led Paul Chu to replace lanthanum with a smaller atom, yttrium. On February 16, 1987, his research group established the critical temperature of yttrium-

barium-copper oxide at 92° K. This advance was particularly significant because this compound could be cooled with cheap and readily available liquid nitrogen. These new materials were dubbed high-temperature superconductors.

The newest members of the superconductor family contain bismuth or thallium. On January 22, 1988, Hiroshi Maeda of Tsukuba Laboratories of the National Research Institute of Metals discovered a critical temperature of 105° K for a bismuth-calcium-strontium-copper oxide compound. On January 26, 1988, Paul Chu reported a critical temperature of 120° K for the same system. On February 22, 1988, Zhengzhi Sheng and Allen Hermann of the University of Arkansas announced that a compound of thallium-calcium-barium-copper oxide exhibited an onset critical temperature of 120° K. Many research groups are now working diligently to find new materials that display even higher critical temperature.

It is worth noting that there is no accepted theory to explain the high-temperature behavior of this type of compound. The BCS theory, which has proven to be a useful tool in understanding lower-temperature materials, does not adequately explain how the Cooper pairs in the new compounds hold together at such high temperatures. When Bednorz was asked how high-temperature superconductivity works, he replied, "If I could tell you, many of the theorists working on the problem would be very surprised."

[Back to Interactive Learning Studio](#)

BRIEF ATTACHMENT AZ

April 2002

“A Snapshot View of High Temperature Superconductivity 2002”

Ivan K. Schuller¹, Arun Bansil², Dimitri N. Basov¹, Malcolm R. Beasley³, Juan C. Campuzano⁴, Jules P. Carbotte⁵, Robert J. Cava⁶, George Crabtree⁴, Robert C. Dynes¹, Douglas Finnemore⁷, Theodore H. Geballe³, Kenneth Gray⁴, Laura H. Greene⁸, Bruce N. Harmon⁷, David C. Larbalestier⁹, Donald Liebenberg¹⁰, M. Brian Maple¹, William T. Oosterhuis¹⁰, Douglas J. Scalapino¹¹, Sunil K. Sinha¹, Zhixun Shen³, James L. Smith¹², Jerry Smith¹⁰, John Tranquada¹³, Dale J. van Harlingen⁸, David Welch¹³

¹University of California, San Diego, ²Northeastern University, ³Stanford University, ⁴Argonne National Laboratory, ⁵McMaster University, ⁶Princeton University, ⁷Ames Laboratory, ⁸University of Illinois, ⁹University of Wisconsin, ¹⁰U.S. Department of Energy, ¹¹University of California, Santa Barbara, ¹²Los Alamos National Laboratory, ¹³Brookhaven National Laboratory

Table of Contents

- I. **Summary**
- II. **Structure, Bonding and New Systems**
 - 1. Synthesis and Fabrication
 - a) *Bulk*
 - b) *Thin films*
 - c) *Doping in the Cuprate Superconductors*
 - 2. Other Topics of Interest:
 - a) *Applied pressure*
 - b) *Spin, lattice, and charge correlations*
 - 3. Conclusion
- III. **Electronic structure and quasiparticle dynamics**
 - 1. Techniques
 - a) *Electron Tunneling*
 - b) *Angular Resolved Photoemission Spectroscopy (ARPES)*
 - c) *Infrared Spectroscopy*
 - 2. Magnetism, Competing Order, and Phonons
 - a) *Magnetism and Spin Fluctuations*
 - b) *Competing Orders*
 - c) *Phonons and Electron-Phonon Interactions*
- IV. **Vortices**
 - 1. Single Vortex Physics
 - a) *Confinement*
 - b) *Pseudovortices and Vortex Core States*
 - c) *Hybrid Materials*
 - 2. Multivortex Physics
 - a) *Disordered Glassy and Liquid States*
 - b) *Dynamic Phases*
 - c) *Josephson Vortices and Crossing Lattices*
 - 3. Instrumentation
- V. **Proximity and Interface Effects**
- VI. **Nonequilibrium Effects**
- VII. **Theory**
 - 1. Preamble
 - 2. Phenomenological Approach
 - a) *Status*
 - b) *Key issues and opportunities*
 - 3. Numerical Studies of Hubbard and t-J Models
 - a) *Status*
 - b) *Key issues and opportunities*
 - 4. Electronic Structure
 - a) *Status*
 - b) *Key issues and opportunities*
- VIII. **Defects and Microstructure with an Eye to Applications**

I. Summary

This report outlines the conclusions of a workshop on High Temperature Superconductivity held April 5-8, 2002 in San Diego. The purpose of this report is to outline and highlight some outstanding and interesting issues in the field of High Temperature Superconductivity. The range of activities and new ideas that arose within the context of High Temperature Superconductors is so vast and extensive that it is impossible to summarize it in a brief document. Thus this report does not pretend to be all-inclusive and cover all areas of activity. It is a restricted snapshot and it only presents a few viewpoints. The complexity and difficulties with high temperature superconductivity is well illustrated by the Buddhist parable of the blind men trying to describe "experimentally" an elephant. These very same facts clearly illustrate that this is an extremely active field, with many unanswered questions, and with a great future potential for discoveries and progress in many (sometimes unpredictable) directions.

It is very important to stress that independently of any current or future applications, this is a very important area of basic research.

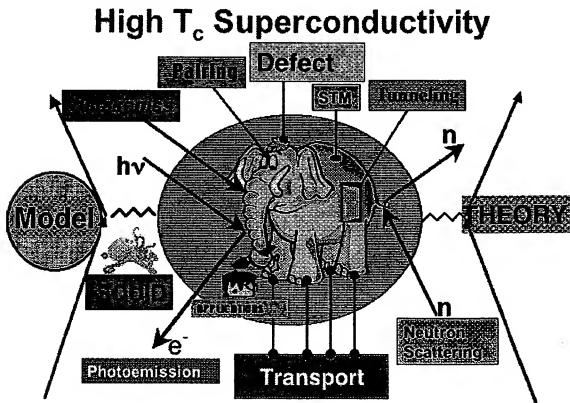


Fig. 1 Status of High Temperature Superconductivity.[1]

Basic research in high temperature superconductivity, because the complexity of the materials, brings together expertise from materials scientists, physicists and chemists, experimentalists and theorists. Much of the research in High T_c superconductivity has spilled over to other areas of research where complex materials play an important role such as magnetism in the manganites, complex oxides, two and one dimensional magnets, etc. Applications could greatly benefit from the discovery of new superconductors which are more robust and allow easier manufacturing. Perhaps this is not possible since a naive inspection of superconductors seems to indicate that the higher the T_c the more complex the material. An excellent review where many target needs for applications have been outlined is an NSF report of ~5 years ago. Many of the comments made there regarding applied needs, are still valid[2].

It is important to realize that this field is based on complex materials and because of this materials science issues are crucial. Microstructures, crystallinity, phase variations, nonequilibrium phases, and overall structural issues play a crucial role and can strongly affect the physical properties of the materials. Moreover, it seems that to date there are no clear-cut directions for searches for new superconducting phases, as shown by the serendipitous discovery of superconductivity in MgB_2 . Thus studies in which the nature of chemical bonding and how this arises in existing superconductors may prove to be fruitful. Of course, "enlightened" empirical searches either guided by chemical and materials intuition or systematic searches using well-defined strategies may prove to be fruitful. It is interesting to note that while empirical searches in the oxides, gave rise to many superconducting systems, similar (probable?) searches after the discovery of superconductivity in MgB_2 have not uncovered any new superconductors. Anyhow, this illustrates that superconductivity is pervasive in many systems and thus future work should not be restricted to a particular type of materials systems. See Chapter II.

Research in the electronic properties of High T_c superconductors has proven to be particularly fruitful. This has lead to improvements in electronic structure techniques which unquestionably have an effect on other fields. The improvement on real and reciprocal space resolution uncovered many interesting properties. However, it is not clear at the present time whether many of these properties are related in some essential way to superconductivity or they are just accidentally present. It seems that the presence of competing phenomena is present in most high temperature superconductors. Thus it is natural to investigate systems which are close to some form of instability such as the metal-insulator transition, magnetic phases, electronic instabilities such as stripe phases, etc. Comparisons of classical infrared spectroscopy, and photoemission measurements with tunneling may prove to be fruitful. In particular, mapping with high resolution (in real and reciprocal space) the electronic structure may prove to hold some of the keys to the mechanism of superconductivity. To make these useful, issues such as surface contamination, surface segregation, and in general heterogeneity of the materials close to surfaces or interfaces must be addressed, and are particularly important in these very short coherence length superconductors. This is particularly important for surface sensitive probes such as photoemission. Several techniques such as Raman scattering, NMR and muon spin depolarization are not addressed in this snapshot, although they give

valuable information and are heavily researched. Complementary measurements are particularly useful if a whole battery of tests, **in the same sample**, which are structurally characterized in detail, are performed. The "quality" of samples on the other hand, must be well established by structural criteria which are well defined "a-priori" and not based on circular or theoretical arguments. See Chapter III.

The properties of High Temperature Superconductors in a magnetic field have proven to be particularly interesting. A myriad of new phases have been uncovered in the vortex system and have lead to the establishment of a very complex phase diagram the details of which are still being established. The presence of many phases and the interaction/competition/closeness to magnetic phases allows for much new research using artificially structured pinning. New lithography and preparation techniques allow modifications and confinement of these materials in length scales approaching the superconducting coherence length and certainly the penetration depth. Moreover, novel imaging techniques are arising which can give detailed microscopic images of the vortex system. This of course can provide the microscopic picture of the magnetic state of high temperature superconductors and will probably also help improvements on their use. See Chapter IV.

Many basic research studies and a large number of applications require the High Temperature Superconductors to be in proximity with other materials. Thus issues of proximity effects, spatial variations close to an interface or surface, structural and materials variations are particularly important in thin film and/or nanoscopic structures. For this purpose it is important to investigate the mutual interaction between superconductors and other materials. This requires careful preparation and detailed characterization of inhomogeneous materials, together with superconducting measurements as a function of well-defined structural parameters. This may also allow addressing issues such as the importance of the proximity to other ordered phases such as magnetic and electronic inhomogeneities which are naturally existent or are artificially engineered. It is not even clear in the various models of high temperature superconductivity or even experimentally how the proximity effect occurs. What is the dependence of the order parameter in an ordinary or magnetic metal, or a low temperature superconductor when in proximity with a d-wave superconductor? See Chapter V.

Contrary to low temperature superconductors, high T_c ones have received very little attention under nonequilibrium (time dependent, strongly driven, exposed to varying radiations, etc.) conditions. This may prove to be a very interesting and novel direction for ceramic oxides. These types of studies may hold important clues to the mechanism of superconductivity, may unravel new physics and are important in many applications. For instance, simple issues such as the microscopic nature or even existence of critical slowing down close to the superconducting phase transition has not been firmly established. See Chapter VI.

The theory of high temperature superconductivity has proven to be elusive to date. This is probably as much caused by the fact that in these complex materials it is

very hard to establish uniquely even the experimental phenomenology, as well as by the evolution of many competing models, which seem to address only particular aspects of the problem. The Indian story[1] of the blind men trying to characterize the main properties of an elephant by touching various parts of its body seems to be particularly relevant. It is not even clear whether there is a single theory of superconductivity or whether various mechanisms are possible. Thus it is impossible to summarize, or even give a complete general overview of all theories of superconductivity and because of this, this report will be very limited in its theoretical scope. The general view point (determined by "majority vote") seems to be that low temperature superconductors are phonon mediated whereas high T_c ones are somehow "unconventional" and anisotropic, although the origin of the anisotropy remains controversial. Because of this, numerical studies in well-defined theoretical models may prove to be particularly illuminating and may help uncover the essence of superconductivity. Particularly, understanding and further developing the t-J model looks like a promising numerical direction. Electronic structure calculations combined with well developed methodologies seem to explain quantitatively many aspects of superconductors with moderate T_c s. How far can these type of approaches be pushed? Could they in fact explain ab-initio superconductivity in some of the cuprates? Moreover, first principle electronic calculations may be very useful in providing parameters for model hamiltonians. Another approach which at least allows parametrizing in some useful way the properties of superconductors has also been used. How far can these type of models go and how universally can they explain the (superconducting or normal) properties is not clear at this stage. There are several important issues which must be kept in mind. It may be that there is a theoretical model which has the essence of the problem in it and it either has not yet been developed or has not yet percolated to the conscience of the community. Moreover, it seems that to date no theory has been developed which has predictive power as far as materials system are concerned. Since purely theoretical approaches have difficulties so far in identifying a clear avenue for search, empirical studies in which materials parameters and properties are correlated with superconducting properties may prove useful[3]. This may serve at a later stage as a test ground for theories. Comparisons of theoretical ideas which rely only on the layered material of high T_c ceramics, with artificially engineered layered superlattices should not be neglected and may prove to be useful. See Chapter VII.

Finally, there seems to be still much work needed to understand in detail the connections, control and effect of defects on high temperature superconductivity. This of course is very important for applications, particularly those which require high critical currents such as power applications. Moreover, the intrinsic brittleness highlights that understanding and controlling the mechanical properties while not directly related to superconductivity, is a very important and promising new area of research, especially in connections with large scale applications. See Chapter VIII.

In the rest of this paper we will expand on these issues and attempt to outline some well defined promising directions of research. The focus is mostly on basic research challenges and opportunities, which hold back progress.

II. Structure, Bonding and New Systems

The discovery of new superconducting materials has played an important role in the advancement of the field of superconductivity research since its inception[4-7]. This was perhaps most dramatically displayed by the discovery of the high T_c cuprates in 1986. The influence of new superconducting systems continues to this day, for example through the discovery in 2001[8] of MgB_2 . Thus far, the existence of a totally new superconductor has proven impossible to predict from first principles. Therefore their discovery has been based largely 'on empirical approaches,' intuition, and even serendipity. This unpredictability is at the root of the excitement that the condensed matter community displays at the discovery of a new material that is superconducting at high temperature. New systems can be found by either bulk methods or thin film methods, each of which has its own advantages, disadvantages, challenges and opportunities. The search for new materials has always been[9], and remains an important area of research in the field of superconductivity.

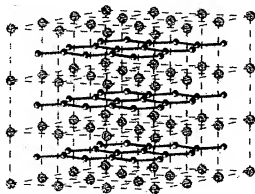


Fig. 2 The crystal structure of MgB_2 . The graphite-like array of boron (shown in black) is critical to the occurrence of high temperature superconductivity in this compound.

Also important for the development of potentially practical materials and the understanding of the complex physical phenomena which occur in superconducting materials has been the use of chemical doping or manipulation to influence the electronic and magnetic properties of the superconducting systems. An example of the former chemical doping is the introduction of small flux pinning chemical precipitates in conventional intermetallic superconductors and 123-type superconductors. Examples of the latter are found in the "lightly doped" cuprates and other perovskite structure transition metal oxides where the concepts of charge and orbital ordering have recently emerged as important considerations in attempts to understand magnetic and electronic properties. These cooperative states join other such states such as charge density waves and spin density waves as critically influential in determining the ultimate electronic

ground state of complex materials. Chemical doping has played an essential role in these areas. Importantly, it allows for the systematic variation of electronic properties as a function of variables such as lattice size, carrier concentration, and magnetic or non-magnetic disorder, providing a basis for the development of theoretical models. This area of research is highly active in the field of superconductivity, and will continue to be of great importance in the future.

1. Synthesis and Fabrication

a) Bulk

In the high density of states conventional intermetallic superconductors, the BCS coupling through the lattice may be viewed as a general lattice phenomenon. In more recently discovered superconductors, such as MgB_2 , it has been found that one particular phonon mode – an in-plane boron mode that modulates bond lengths and angles within the flat B honeycomb lattice in the case of MgB_2 – is responsible for coupling to the conduction electrons and is the driving force for superconductivity [10, 11]. Conclusions about the nature of the phonons and electrons that are responsible for the superconductivity in a particular material can be arrived at nowadays by sophisticated experimental study and theoretical analysis. In particular the band-structure experts can calculate the effect that a particular phonon has on the electrons at the Fermi energy in a particular superconductor by doing “frozen phonon calculations”. Such calculations are highly instructive for superconducting materials like MgB_2 .

This analysis is after the fact, unfortunately, for people whose interest is in finding the new superconductors in the first place. So given the fact that undirected combinatorial chemistry will never get through all the possible element/treatment combinations in a search for superconducting materials, one important issue to be resolved in future research is to translate the physics of superconductivity into a set of chemical hypotheses to guide the search for new ones. The era of finding new high temperature superconductors in intermetallic compounds like Nb_3Ge appears to be long gone. The new breed of high T_c superconductors is quite different – even beyond the cuprates, which are their own special case. The difference lies in the type of chemical bonding these superconductors display, even in what look like classic intermetallic compounds such as MgB_2 and $\text{LuNi}_2\text{B}_2\text{C}$ [12]. Thus one important issue for future research is to explore how the nature of the chemical bonding present influences the superconductivity in “conventional” intermetallic compounds.

Initially promising reports of electronic doping through charge injection into a variety of organic and inorganic compounds in FET device structures have recently been called into question [13]. Nonetheless, conceptually they point out that another area of future research in new superconducting systems should be that non-thermodynamic synthetic methods should be actively pursued. Modulation doping, the chemical analogue of charge injection, for transferring charge between layers in fine scaled multilayered films, has potential which is yet to be exploited. Other methods for non-thermodynamic synthesis with high potential for success include quenching from high pressure or from

the vapor, epitaxial thin film layer by layer or block-by-block growth, photodoping, electrochemical synthesis at low temperatures, ion exchange, framework stabilization of structures, and electrochemical intercalation.

b) *Thin Films.*

There are many examples of stabilization of non thermodynamic compounds in thin films in both the cuprate superconductors and in dielectric or ferroelectric materials by using epitaxy with substrate or buffer layers. In the most extreme examples of this type of metastable material it may be a single atomic layer or even an interface that has the desired properties. On such short length scales, chemical bonding is the predominant influencing factor. Different physical and chemical methods of growth influence the behavior of surfaces and very thin layers. Great progress has been made in characterization after growth – such as Transmission Electron Microscopy (TEM) and X-ray probes, but a great deal more may be gained in the future by incorporating techniques that can be used *in situ* to characterize surfaces during growth.

Of particular interest in the search for new materials is the “phase spread method” used with success by some materials physicists. In this method, thin films are made by intentionally introducing composition gradients, for example by having three atomic sources in a triangular geometry, such that their deposition areas only partially overlap. The film thus fabricated contains mixtures of the source atoms in systematically varying ratios depending on proximity of substrate to one or another of the source. Annealing of such composition spreads under different conditions can be employed to search significant areas of phase space.

Photoexcitation provides another non-thermodynamic method to perform doping studies on thin films in a reproducible way without changing material, thus avoiding the inherent difficulties with controlling stoichiometry, uniformity, and homogeneity of the samples[14, 15]. Persistent photoexcitation has been performed in many cuprate superconductors and on the magnetic manganites at low temperatures below 100K. Large changes in conductivity, Hall effect, mobility, and superconducting transition temperatures have been observed. In the best model for this process, light generates an electron hole pair and the electron is trapped in a defect thus changing the hole doping in the electronically active layer providing a potentially useful way to trim device properties and “write” artificial nanostructures without need for lithography.

c) *Doping in the Cuprate Superconductors.*

The properties of the cation-substituted and oxygen-doped high-temperature superconductors have been studied in detail since 1987. In general, the physical properties (temperature-dependent resistivity, superconducting transition temperature, Hall effect, etc.) and the structural properties of the HTS cuprates behave quite differently as a function of substitutions in comparison to conventional superconductors. Doping and ion-induced disorder have shown that a small change in physical structure can induce a dramatic change in the electronic structure in these materials. This was one

of the first indications that they were unconventional superconductors. The details of the effects of atomic substitutions or doping are not yet fully understood in the cuprate superconductors, and this represents an active area of current research. Concentrating on $\text{YBa}_2\text{Cu}_3\text{O}_{7-x}$ (YBCO) for example, some of these issues are:

i) *Doping on the Y-site.*

Doping with the heavy Rare Earth (RE) ions on the Y-site, even with Gd, does not affect T_c , except for substitutions of the Y with Pr. The effects of Pr-doping remain controversial.

ii) *Doping on the CuO chains.*

Substitutions of $3+$ ions (e.g., Al, Co, Fe) primarily replace Cu in the CuO chains. Extra oxygen is simultaneously incorporated into the chain layer, the c-axis lattice constant increases, and an orthorhombic to tetragonal transition occurs. Since the extra oxygen compensates for the valence of the substituted cation, it remains an open question as to whether the resulting doped materials are underdoped or overdoped. Also, it has long been known that not only is the T_c of YBCO dependent on the oxygen concentration, but also on how the oxygen is ordered. Open issues remain, such as why do the chain oxygens need to be ordered to maximize the T_c ?

iii) *Doping in the CuO_2 planes.*

Both Ni and Zn predominately replace copper in the CuO_2 planes without significant structural change. However, T_c falls faster in these cases than it does with increased $3+$ -cation doping on the chains or oxygen doping on the chains. That is an indication that the loss of structural continuity of the CuO_2 plane is more detrimental to the superconducting transition temperature than the lattice changes that occur due to doping on the CuO chains. There are interesting data comparing the Ni and Zn-doping: T_c falls faster with increasing the Zn doping than with increasing the Ni doping. Conversely, the room temperature resistivity increases faster and the Relative Resistance Ratio (RRR) [$R(300)/R(0)$ -extrapolated] reduces faster with increasing Ni doping than increasing Zn doping. Therefore, Zn destroys the superconducting phase faster and the Ni destroys the normal metal phase faster. Remaining issues are: Why do Ni and Zn substitution reduce T_c so dramatically? and Why does Zn suppress the superconducting state faster than Ni, while Ni suppresses the normal state faster than Zn?

iv) *The Role of the Charge Reservoir Layers.*

The cuprates containing Hg, Tl and Bi ions in their charge reservoir layers have unusually high T_c s. These ions are known to charge disproportionate, which makes them negative U-centers. Under some circumstances it is known that negative U-centers can be superconducting pairing centers. It is of great interest to determine whether superconducting pairing on the charge reservoir layers is responsible for the enhanced T_c s.

of the Hg, Bi and Tl cuprates, and if so whether the negative U approach can be turned into a general method for finding and enhancing superconductivity.

2. Other Topics of Interest

a) Applied Pressure.

The investigation of high temperature superconductors under high pressure has the advantage that the basic interactions responsible for superconductivity can be changed without introducing disorder into the system as encountered in alloying experiments. The drawback is that one has to deal with massive high pressure cells, small sample sizes, and technical difficulties that increase with the higher the pressure range of interest. Measurements of the pressure dependence of T_c are the most straightforward since this can be accomplished through measurements of the electrical resistivity and the ac magnetic susceptibility under pressure. The electrical resistivity in the normal state, which can be accessed even below T_c by suppressing superconductivity with a magnetic field, yields complimentary information about phonons and magnetic excitations that are responsible for the superconductivity. Other types of measurements such as NMR and specific heat have been made under pressure. It would be useful to develop techniques for making other types of measurements under pressure and extending the range of pressures currently accessible.

b) Spin, Lattice, and Charge Correlations.

"Doping" generally refers to the introduction of charge carriers into the conduction or valence bands of a material. However, because of the large coupling between charge, spin and lattice in the cuprate superconductors and other transition metal oxides, doping of these materials with charge carriers can also be accompanied by the formation of static and dynamic spin and/or charge ordered phases on a microscopic scale. These "stripe phases," have recently been observed in many perovskite based transition metal oxides, including several cuprates, and may be a general feature of transition metal oxides[16, 17]. The role these microscopic inhomogeneous spin or charge phases play in high temperature superconductivity, magnetism, and other effects that have been attributed to them, is, however, unclear at this time.

The comprehensive understanding of spin/charge self-organization in oxides is a challenging task. This is a new viewpoint in the survey of strongly correlated phenomena in solids – a field that until recently has been primarily focused on the properties of nominally homogeneous systems. Intrinsically inhomogeneous spin and charge systems in transition metal oxides call for both original theoretical approaches and for the development of novel experimental tools suitable to deliver important information. Existing experimental information on the electronic and lattice properties of stripes systems is incomplete and therefore many fundamental problems related to spin/charge ordered regime in solids remain unresolved.

3. Conclusion

We believe that the opportunities for new materials to greatly influence the future of superconductivity research remain large, both from the point of view of fundamental science and the development of practical superconducting materials. We believe that chemical doping, non-thermodynamic synthesis, the discovery of totally new materials, the investigation of strongly correlated charge and electronic systems, and the use of chemical principles to help answer questions about the nature of superconductivity are exciting areas for future research.

III. Electronic Structure and Quasiparticle Dynamics

High- T_c superconductivity is achieved when a moderate density of electrons or holes is introduced in antiferromagnetic (AF) Mott-Hubbard insulator hosts by chemical or field-effect doping. Gross features of the evolution of the electronic structure as doping progresses from Mott insulator to d-wave superconductor are known from the systematic transport, photoemission and optical studies[18-21]. The doping-driven phase diagram of high- T_c systems is exceptionally rich owing at least in part to the fact that at the verge of the metal-insulator transition boundary magnetic, electronic, lattice and orbital degrees of freedom are all characterized by similar energy scales. Optimally doped cuprates (having highest T_c for a given series) reveal a well-defined Fermi surface in close agreement with the results of the band structure calculations[22]. Nevertheless, the dynamics of charge carriers appears to be highly anomalous defying the grounding principles of the Fermi liquid theory. Numerous attempts to describe the electronic properties using strong coupling Eliashberg theory have been only partially successful[23-25]. Using this approach it became possible to find a consistent description of many of the features established through a combination of tunneling, photoemission, optical and neutron scattering measurements for YBCO and the Bi2212 families of materials. However, many other systems of cuprates fail to follow the same patterns[26, 27]. Moreover, because of the extremely strong inelastic scattering established for most high T_c superconductors the concept of strongly interacting quasiparticles underlying the Eliashberg formalism is in question.

Early on it became established that superconducting currents in cuprates are carried by *pairs* of holes or electrons similar to that of conventional BCS superconductors. However, a viable description of the pairing interaction is yet to be found. Numerous experimental results indicate that the process of the condensate formation in cuprates is much more complex than the BCS picture of a pairing instability of the Fermi gas. One example of a radical departure from the BCS scenario is that the opening of the superconducting gap in cuprates is preceded by the formation of a partial gap (pseudogap)[28]. There is still a debate as to whether this pseudogap is related to the superconductivity. The pseudogap appears to be strongly anisotropic around the Fermi surface mirroring the anisotropy of the superconducting gap. These observations prompted the "precursor to superconductivity" scenarios for the pseudogap. Within this

view, the formation of pairs precedes the development of global phase coherence between paired states[29]. Observations of vortex-like excitations[30] as well as of finite superfluid stiffness[31] at $T > T_c$ are in accord with the preformed pairs hypothesis. The process of the superconducting condensate formation in high- T_c cuprates also appears to be notably different from the BCS scenario. In particular, the energy scales involved in the formation of the superconducting condensate are anomalously broad and exceeds the magnitude of the superconducting energy gap by more than one order of magnitude[32, 33]. These latter results inferred from optical spectroscopy are consistent with the view that the kinetic energy is lowered in the superconducting state. Similar conclusions also emerged from the detailed analysis of the photoemission spectra[34]. The electronic properties of the high- T_c superconductors have been probed by several complementary techniques. These techniques have shown substantial technological improvements in part driven by the need for higher energy and k resolution. In addition there is a growing belief that these materials may have real space inhomogeneities and so that a high resolution real space probe is desirable. Among the techniques that have revealed substantial insight because of technical improvements, we discuss electron tunneling, angular resolved photoemission spectroscopy, and infrared spectroscopy.

1. Techniques

a) *Electron Tunneling.*

Electron tunneling (both quasiparticle and Josephson tunneling) has been a powerful technique to probe the excitation spectrum, the superfluid density and the pair wave function phase of conventional superconductors. With high T_c cuprates, the technique has been no less informative. Currently, much of our understanding of the order parameter symmetry has come from Josephson effect studies[35] and the non-BCS nature of the excitation spectrum that comes about from the symmetry has been clearly observed[36]. C-axis and a-b plane quasiparticle tunneling have illustrated the extreme anisotropy of these superconductors and shown that surfaces are very different with possible bound states due to the broken symmetry at the a-b interface[37]. Intrinsic c-axis tunneling[38] has attempted to address the relationship between the superconducting gap and the pseudo gap. The debate over whether the pseudogap and the gap are intrinsically coupled continues.

STM studies offer an important additional feature that has already yielded some surprises. STM quasiparticle tunneling has allowed both microscopy and spectroscopy with good energy resolution and the spatial resolution to study the gap parameter on a length scale smaller than the superconducting coherence length[39]. Some of the current thinking on the high T_c superconductors concludes that there are intrinsic inhomogeneities (especially in the underdoped limits) in the superconducting properties. Coupling the high energy resolution with the high spatial resolution, along with the recently developed superconducting STM[40] will allow direct spatial studies of the energy gap, bound states and the superfluid density. Recent investigations have illustrated the local effects of non-magnetic and magnetic impurities[41] in the high T_c materials and a background periodicity in the electronic density[42] (charge density wave

or spin density wave?) which requires further investigation. It is not clear whether this periodicity in the electronic density is associated with the superconductivity in these materials. Finally, the combination of high resolution quasiparticle spectroscopy and Josephson probe will allow quantitative investigation of spatial variations of the order parameter and superfluid density around impurities, at interfaces and proximity junctions. In conventional superconductors these two quantities are related but with spatial inhomogeneities, it is no longer required. For the high T_c materials, some theoretical models require inhomogeneities that would result in the superfluid density having different behavior than the energy gap. This will allow us to address both fundamental issues and applications. For example, current studies show that a magnetic impurity does not suppress the energy gap[31]. It has been concluded that superconductivity is not affected but the superfluid density has not yet been investigated. In addition, much is still to be learned about the proximity effect at the interface between the high T_c materials and other metals. Tunneling will allow us to probe this interface.

b) Angular Resolved Photoemission Spectroscopy (ARPES).

ARPES experiments have contributed to our understanding of the electronic structure and superconducting properties by revealing the Fermi surface information,[43] and a large superconducting gap anisotropy that is consistent with d-wave pairing state.[44]

Recent improved resolution, both in energy and in k have resulted in unprecedented data which allow us to map the electronic dispersion curves (E vs. k) for bands below the Fermi level E_F [45, 46]. Angle resolved photoemission studies are now mapping the dispersion curves for several cuprates (and other perovskite oxides). As a result of the enhanced energy and k resolution, it has been demonstrated that in addition to E and k , the linewidths ΔE (related to scattering rate $1/\tau$) and Δk (related to the inverse mean free path $1/\ell$) can also be determined. While mapping these quantities over an extensive phase space of E and k is still to be done, these measurements have revealed some very important insight already. Close to E_F an electron mass enhancement[47-49] (E vs. k measures the velocity and hence the effective mass m^*) is observed in the dispersion curves which is both energy and temperature dependent. These measurements can be thought of as directly probing the self-energy of the carriers with all their dressings as a result of the interactions the carriers experience. In conventional superconductors, these interactions and mass enhancements are a result of the electron-phonon interaction; the mechanism responsible for superconductivity in the simple materials. Indeed, for many in the field it was the measurement of the strength of the electron-phonon interaction (via tunneling for example) which confirmed the phonon mechanism of superconductivity. The measurements of ARPES are being carried out in several laboratories in the U.S. and elsewhere and the mass renormalization effects are observed at several facilities and in several materials.

There is still disagreement as to some of the details of these measurements and to their interpretation[48, 50, 51]. Electron-phonon interactions, electron-spin interactions and electron-electron interactions have all been suggested and all result in enhanced mass

due to the interactions. Temperature dependent studies also illustrate that these interactions are at low energy and result from strong interactions.

It is clear that mapping of these dispersion curves over a wider volume of the E-k phase space is important. It is especially critical with the high T_c cuprates because of the large electronic anisotropy of the materials. Furthermore, because of the symmetry of the order parameter, mapping of the self energy effects as a function of k around the Fermi surface is especially critical. If these observed renormalizations are the signature of the mechanism responsible for superconductivity in the high T_c materials, an extensive map of the electronic renormalized map will be valuable if the analogy with low T_c superconductors is relevant. In the case of low T_c materials the renormalized mass $m^* = m(1 + \lambda)$ where λ = electron-phonon interaction averaged over the Fermi surface.

Current ARPES measurements could be determining quantitatively the strength of the interaction and the mechanism of superconductivity. As a final caveat, it must be remembered that both APRES and tunneling are surface probes.

In this connection, inelastic X-ray scattering (IXS), which is not sensitive to surfaces or defects, is a valuable probe of bulk states. For high momentum and energy transfers IXS directly measures the ground state momentum density of electrons, while spin density is measured in magnetic IXS scattering. With improved resolution that has been achieved with synchrotron light sources, IXS has revealed surprising electron correlation effects with simple metals and has been extended to study the electronic excitations of the present compound of high T_c superconductors. Its application to ceramic superconductors would be most worthwhile.[52, 53]

c) *Infrared Spectroscopy.*

Infrared (IR) and optical spectroscopy is ideally suited for the studies of superconductivity because of the ability of these techniques to probe such fundamental parameters as the energy gap and the super fluid density[54]. Notably, IR spectroscopy allows one to investigate the *anisotropy* in these parameters through measurements performed with the polarized light[55]. Because IR/optical information is representative of the bulk and measurements can be performed on the micro-crystals, these studies allow one to examine common patterns of a large variety of materials which may not be suitable for examination with other techniques. Optical techniques offer means to probe strong coupling effects in the response of quasiparticles. In this context IR, tunneling and ARPES results are complementary to each other. It is therefore desirable to "map" renormalization effects using a combination of several spectroscopic methods. Charge- and spin-ordered states in solids can be conveniently examined through the analysis of the IR-active phonon modes. The latter circumstance is important for the investigation of self-organization effects which dominate the dynamics of charge carriers at least in under-doped cuprates.

IR measurements can be performed in high magnetic field. Present work in the use of IR in high field experiments is restricted to a few experiments but several groups

are actively involved into adapting IR instrumentation for these challenging measurements. These studies promise to yield detailed information on dynamics of both pancake and Josephson vortices. More importantly, DC fields currently available in optical cryostats (up to 33 T) are sufficient to destroy superconductivity thus giving spectroscopic access to the *normal* state properties at $T \ll T_c$. Transport measurements in strong magnetic field highlighted anomalies of the normal state in LaSrCuO (LSCO) series of cuprates[56]. Spectroscopic measurements will be instrumental in distinguishing between (conflicting) interpretations of these results and will also help to unravel generic trends of the normal state behavior at $T \ll T_c$ between several classes of superconductors.

2. Magnetism, Competing Order, and Phonons

a) Magnetism and Spin Fluctuations.

As discussed earlier, superconductivity in the cuprates is achieved by doping holes or electrons into an antiferromagnetic-insulator state. The magnetism is essentially an electronic effect, as it results from strong Coulomb repulsion between pairs of conduction electrons on the same Cu atom, together with the Pauli exclusion principle. Considerable knowledge of antiferromagnetism (AF) and spin fluctuations in the cuprates[57, 58], has been obtained experimentally using neutron scattering, nuclear magnetic resonance (NMR), and muon spin rotation (μ SR) spectroscopy. The general significance of antiferromagnetic correlations and spin fluctuations in theoretical mechanisms of high-temperature superconductivity is motivated by this experimental work.

In hole-doped cuprates, 2% holes doped into the CuO_2 planes are generally sufficient to destroy AF long-range order, but a minimum of 5-6% are necessary to induce superconductivity. Considerable attention has been devoted to characterizing the evolution of the AF spin fluctuations with doping. The bandwidth of the magnetic excitations, ~ 300 meV in the ordered AF, appears to change relatively little with doping. In LSCO, the low-energy spin fluctuations become incommensurate as doping increases, with a characteristic wave vector displaced from that of the AF by an amount δ . Similar incommensurability has been observed in YBCO, but additional features are the presence of a gap in the low-energy fluctuation spectrum followed by a commensurate "resonance" peak. The gap and peak energies both increase with hole concentration up to optimum doping, at which the resonance-peak energy is ~ 40 meV. Recent results on other families of superconducting cuprates indicate that the resonance peak is a common, although not universal, feature[59].

Electron doping has a weaker effect on the AF state, with a transition directly from AF order to superconductivity occurring at an electron concentration near 12%. Initial neutron measurements indicate that the AF spin fluctuations remain commensurate in the superconducting phase. Studies over a broad energy range are made challenging by the presence of crystal-field excitations from the rare-earth ions.

Progress in the characterization of spin fluctuations has been enabled by the development and improvement of techniques for growing large single crystals and by forming large-volume mosaics of small crystals. Neutron scattering studies of hole-doped cuprate systems other than LSCO and YBCO are in early stages, and considerable progress is likely in the next few years. Improvement in the homogeneity of large underdoped YBCO crystals would be helpful for some of the issues discussed below. The availability of sufficient access to appropriate neutron scattering facilities may also be a limiting factor.

b) Competing Orders.

A phenomenon known as "stripe" order has been observed by neutron and X-ray diffraction in several variants of the LSCO family[60, 61]. Spin-stripe order is indicated by the appearance of elastic magnetic superlattice peaks at the same incommensurate wave vectors at which the low-energy spin fluctuations occur. These are usually accompanied by the observation of another set of superlattice peaks split about fundamental Bragg points, indicative of charge-stripe order. The presence of stripe order is generally (although not always, as in the case of $\text{La}_2\text{CuO}_{4-x}$) associated with a reduction in the superconducting transition temperature. However, there is also a linear correlation between T_c and the incommensurability of the spin fluctuations in the absence of stripe order.

There is also some evidence of stripe correlations in $\text{YBa}_2\text{Cu}_3\text{O}_{6-x}$ O chains. The temperature dependence of the associated superlattice intensities suggests a coupling to electronic correlations, and possibly to charge stripes[62]. Certain spin fluctuations have been found to have an incommensurability similar to that found in LSCO; however, the cause of the incommensurability is controversial.

The recent scanning tunneling microscope (STM) observations of spatial modulations of the electronic density of states (DOS) in the CuO_2 planes of BSCCO has stimulated considerable speculation. The observed period of $4a$ (a, the in-plane lattice constant) suggests a connection with the charge and spin stripes found in LSCO. Clearly, a combination of tunneling and scattering studies is needed to clarify the nature of the modulations.

There are many unresolved issues associated with the problem of stripes. Is stripe order a type of electronic instability, like conventional charge-density-wave order, that only competes with and limits superconductivity? Is it possible for a stripe-liquid phase to exist? Are stripe correlations common to all superconducting cuprate families, or do they only occur in special cases? Are spin stripes always associated with charge stripes, or are these distinct types of order? Do stripes (or possibly another type of inhomogeneity) exist in electron-doped cuprates? Studies with a wide range of techniques will be needed to answer these questions. Stripes are but one kind of order that has been proposed to have a connection with the various "pseudogap" phenomena that are observed in underdoped cuprates[63]. A number of theories have put forward the hypothesis that a new order parameter appears in the pseudogap regime. Two particular

examples are quadrupolar orbital currents, and the staggered flux phase or d-density-wave (DDW) state. In both cases, orbital currents result in local magnetic moments that should be, in principle, detectable by neutron scattering. So far, neutron scattering experiments have been unable to find evidence for such phases, which predict no breaking of translational symmetry; however, the presence of quadrupolar currents provides a possible explanation for the recent observation of time-reversal-symmetry breaking by photoemission[64]. The possible existence of orbital moments remains an open issue.

c) *Phonons and Electron-Phonon Interactions.*

The role of electron-phonon interactions in the cuprates has been the subject of renewed interest, motivated in part by a recent interpretation of ARPES data[28]. An important technique for characterizing phonon dispersions and densities of states is inelastic neutron scattering. (Note that neutron measurements of the phonon DOS in MgB_2 provided an important validation of the theoretical evaluations of electron-phonon coupling in that system.) Dispersion anomalies in the Cu-O bond-stretching modes, clearly associated with some kind of electron-phonon coupling, have been the subject of controversy for several years. The experiments are constrained by weak scattering cross sections and limited crystal size. Further experimental studies, together with serious theoretical analysis, are necessary in order to make real progress in this area. Inelastic X-ray scattering has also been used recently to study optical phonons in a cuprate.

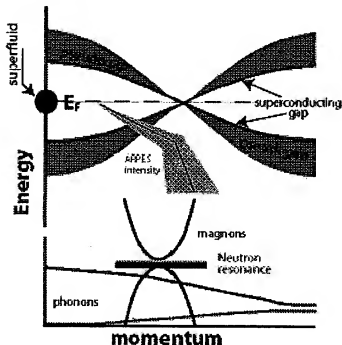


Figure 3. Schematic representation of excitations and collective modes in high- T_c superconductors. A remarkable variety of effects in these materials have typical energy scales of about 50-70 meV, including: phonons, magnetic resonance, superconducting gap and pseudogap as well as "kinks" in the ARPES spectra. Competition, interplay and interdependence between these effects are responsible for complexity of the strongly correlated state in these materials.

IV. Vortices

Most of the electromagnetic properties of Type II superconductors are determined by vortices in static and dynamic configurations. Rapid progress in manipulating and measuring vortices in recent years has greatly expanded the limits of known and imaginable vortex phenomena. This chapter outlines several research directions that are now within reach and that will develop new concepts and strategies for fundamental science and applications.

1. Single Vortex Physics.

a) Confinement.

Advances in micro- and nano-scale patterning and in high sensitivity measurements now enable studies of *single* vortices, allowing a wide range of new physics to be explored. Vortices enter mesoscopic samples[65-68] one-at-a-time at field intervals determined by flux quantization, $\Delta H \sim \Phi_0/L^2$ where Φ_0 is the flux quantum and L the sample dimension. The entry of each vortex produces a step change in the magnetization, corresponding to a *first order* phase transition. In circular disks, vortices are predicted to configure in shell patterns[69] reminiscent of electrons in atoms and leading to magic numbers of high stability. At certain fields a collection of discrete Abrikosov vortices transforms to a single *giant vortex* containing the same number of flux quanta and a circulating current at the outer edge of the sample. This phase transition is reminiscent of Wigner localization in electronic systems. In lower symmetry disks such as squares, vortices and antivortices coexist to simultaneously satisfy flux quantization and rotational symmetry[67].

Studies of confined vortices can be extended to layered superconductors such as NbSe₂ and the cuprates, where the superconducting coherence length ξ and the magnetic penetration depth λ are quite different, and to other experimental probes like STM that directly image the superconducting order parameter. Confinement need not be limited to a single disk. Arrays of disks, each containing confined vortices, can interact through a superconducting substrate. Confinement in a line geometry[65] allows *motion* of confined vortices to be studied[70]. Confined disks connected by lines offer many analogies to single electron behavior including the Coulomb blockade and single electron tunneling.

Individual vortices in an array can be manipulated by imposing an artificial mesoscopic template. One approach is to lithographically pattern a superconducting film with an array of holes, or antidots, each of which traps one or more vortices[71-74]. Trapping vortices one-by-one has practical implications: it can dramatically enhance the pinning effectiveness and critical current, and it can lead to extremely sharp switching effects at matching fields. These switching features offer the potential for three terminal devices, where the supercurrent across the antidot array is modulated by a control magnetic field operating near the matching field. Antidots are predicted to trap vortices

with multiple flux quanta if the hole size is large compared to the coherence length. The properties of these multi-quantum vortices are largely unexplored. Such antidots, for example, could enable the construction of information storage devices operating with integer rather than conventional binary bits.

Mesoscopic templating can be extended in several exciting directions. The technique can be applied to cuprate high temperature superconductors[75], where the nanoscale coherence length enables many tens of flux quanta to be trapped in a single mesoscopic hole. Unlike low T_c superconductors, the cuprates have clearly defined lattice, liquid, and glassy phases that will react quite differently to the imposed order of the templates. First order vortex lattice melting, for example, is expected to be fundamentally modified by commensurate or incommensurate templates. Aperiodic templates provide another new direction. The vortices trapped in the holes create aperiodic scattering centers for free interstitial vortices whose dynamics will be quite different from those in ordered or random pinning arrays. Templates created to date have been limited by lithography to lattice spacings slightly less than one micron, putting the first matching field at about 20 Gauss. Electron beam and self-assembly techniques, for example based on diblock copolymers[76] anodic aluminum oxide[77] or inverse micelles[78], can be used to make templates with nanometer lattice constants. This much smaller spacing puts the commensurate vortex lattice in the strong interaction limit where collective effects dramatically alter its behavior. The one study on dense templates reported so far[79] shows that strong pinning persists well below T_c . High density templates bring the first matching field up to the kG range, much more interesting for applications than the tens of Gauss range accessible to lithographic templates. High density templates offer an intriguing new strategy for pinning the vortex liquid, where eliminating shear motion requires one pin site per vortex. In BSCCO and YBCO this opens large areas of the H-T phase diagram to practical use.

b) Pseudovortices and Vortex Core States.

The observation of unusual thermomagnetic effects in the underdoped region of LSCO above the superconducting transition temperature and below the pseudogap temperature[80] suggests that vortex-like excitations may be associated with the pseudogap state. The properties of these pseudovortices are still under examination and may hold important insights into the underdoped state. Pseudovortices may be observable as fluctuations using experiments with short time scales and local resolution, such as magnetic resonance or muon spin rotation.

The suppression of the superconducting energy gap in the vortex core creates a natural potential well that captures observable bound states in cuprate superconductors[81, 82]. These bound states provide a window on the nature of pairing, because they are sensitive to the presence of nodes in the gap that distort the core potential. STM sees not only the bound state, but also the anisotropy of the energy gap around the core, providing direct information on the nodal structure. These experiments would be particularly valuable if performed systematically for under and over doped regimes, where the nature of the normal and superconducting states changes

continuously. In other organic and heavy fermion superconductors where the order parameter is a complex vector, the core states will display subtle details reflecting the exotic pairing. These core states are within reach experimentally but remain unexplored.

In the vortex core the superconducting order parameter is suppressed, providing a fascinating opportunity to search for competing types of order without physically altering the material. Indications of spin density waves[42] and pseudogaps[83] in the cores of BSCCO suggest a strong interplay of these types of order with superconductivity. The same approach could be employed to search for competition with antiferromagnetism[84] charge stripes, and other proposed ordered states.

The existence of two superconducting gaps[85] in MgB_2 raises fundamental questions about their effect on the core states. Strong variations in the core potential and the bound states are expected as the relative strength of the two gaps varies with temperature and field. This fascinating area is now within reach and is virtually unexplored.

c) *Hybrid Materials.*

We are now entering a new era of materials sophistication allowing studies of superconductors exposed to *internal* magnetic fields. Such internal fields arise in magnetic/superconducting hybrid structures[86], including naturally occurring $\text{RuSr}_2\text{GdCu}_4\text{O}_8$ [87] and the magnetic borocarbides[88, 89], and artificial hybrid structures containing patterned magnetic and superconducting layers[90]. There are fundamental questions regarding how superconductors respond to internal magnetic fields: the conventional mechanisms of Meissner shielding and vortex penetration for external fields are not necessarily adequate.

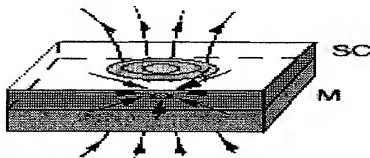


Fig 4. Superconductor/magnet bilayer. The vortex field polarizes the magnet locally, producing a radial magnetic texture.

In bilayer hybrids, the field of an individual vortex in the superconducting layer locally polarizes the adjacent magnetic layer creating a tiny *magnetic texture*. [91] Fig 4 shows a radial magnetic texture, where the vertical arrows represent the vortex magnetic

field and the horizontal arrows the induced polarization of the magnetic layer. The coupled vortex-magnetic texture pair is a new compound object whose static and dynamic properties are virtually unexplored. One important element is the interaction between pairs, which is mediated by dipole and exchange interactions in the magnetic layer, Lorentz forces in the superconducting layer, and magnetostatic interactions between the layers. The resultant interaction potential is distinctively more complex than the simple repulsive potential of bare vortices. Dynamics brings in yet another element, the de-polarization and re-polarization of the magnetic layer that is required if a vortex in the superconducting layer is to move. Beyond the new physics of vortex-texture pairs, there is an additional attractive feature. The properties of the hybrid can be tuned by selecting the materials (e.g., the easy direction and the anisotropy in the magnetic layer), the relative thickness of the two layers, and the magnetic field direction. In multilayer hybrids with parallel applied field, an array of π -Josephson vortices can be formed, while tipping the field away from the layers induces Abrikosov-texture pairs.

There are equally fascinating possibilities in hybrids composed of magnetic dots deposited on a superconducting layer. Here the magnetic dot is a pin site that is isolated from the superconductor, avoiding deleterious effects of the pinning defect on current flow. Recent work on superconducting/magnetic dot hybrids[92-94] has defined several important issues, such as (i) the spontaneous creation of vortices and antivortices in zero applied field, (ii) the annihilation of antivortices by external field-generated vortices, (iii) the nature of matching field effects, (iv) the effect of magnetic dot repolarization at high field, and (v) the dynamics of dot-generated vortices under a driving Lorentz force. These basic unexplored issues become even more fascinating when the scale of the magnetic dot array is reduced from present day lithographic dimensions to much smaller self-assembled dimensions. The interaction of flexible and compressible vortex lattices with rigid pinning geometries has many analogies in epitaxial growth, absorption of noble gases on surfaces and even plasma physics in confined geometries. Thus progress in this area has broad relevance well beyond the field of superconductivity.

2. Multivortex Physics

a) *Disordered Glassy and Liquid States.*

The *collective behavior* of vortices is much like that of atoms: their mutual interaction energy creates lattices, quenched disorder by random pinning produces glasses, and thermal disorder melts the lattice or glass to a novel liquid state. The liquid and glassy states of vortex matter offer major challenges for understanding the magnetic properties of superconductors. Two kinds of glassy state have been proposed, the vortex glass[95] for disorder by point defects, and the Bose glass[96] for disorder by line defects. While experiments confirm the second order Bose glass melting transition, the tilt modulus and the resistive behavior of these disordered systems are at odds with each other and with theory[97]. For point disorder, even the voltage-current scaling behavior expected at melting is not observed[98]. Experimentally, lattice and glassy melting coexist in the same phase diagram[99-101], sometimes accompanied by novel "inverse melting" regions. Quasi crystals are another disordered phase of vortex matter, triggered

by pentagonal or decagonal boundaries. The thermodynamics of melting in this phase intermediate between lattice and glass will be fascinating.

The vortex liquid shows equally fascinating behavior arising from *thermal* disorder rather than quenched disorder. Recent specific heat measurements[102] reveal two liquid phases separated by a second order phase transition. Understanding the nature of these two phases and the transition between them is a challenge not only for vortex matter but also other line liquids like polymers and liquid crystals. The vortex liquid offers another promising opportunity, to study the *interplay* of thermal and quenched disorder. The addition of quenched disorder to the liquid shifts the freezing transition up for columnar defects, down for point defects. The effect of the two kinds of quenched disorder on liquid state thermodynamics and on its driven dynamics is ripe for incisive experiments. Disordered vortices offer a rich complexity that is easily accessible experimentally yet so far defies theoretical description. Their behavior is fundamental to applications of superconductivity, and to the basic science of condensed matter systems generally.

b) Dynamic Phases.

The rich equilibrium phase diagram of vortices is matched by its driven dynamic behavior. The onset of motion at the critical current is a complex dynamic process governed by the distribution of pinning strengths, the vortex-vortex interactions, the temperature, and the driving Lorentz force. The plastic motion that normally accompanies depinning can now be directly observed through Lorentz microscopy[103] and magneto-optical imaging[104]. This emerging spatio-temporal resolution opens possibilities for systematic experimental studies to characterize the depinning process as a function of the basic variables. Such previously hidden onset phenomena as vortex channeling, vortex hopping from pin site to pin site, and the distinction between avalanche and continuous onset are becoming observable. This wealth of experimental information drives new theoretical descriptions of the depinning process. The plastic motion inherent in depinning makes its description in terms of partial differential equations of hydrodynamics challenging. However, statistical descriptions in terms of time dependent position and velocity correlation functions can be created that break new ground for describing the onset of plastic motion. Beyond depinning, there are a host of dynamic phenomena that are now amenable to observation, including vortex creep, thermally assisted flux flow, hysteresis in I-V curves, and memory effects. The concept of vortex *focusing* and *rectification* through the ratchet effect is especially interesting[105]. A fundamental microscopic understanding of these phenomena would lead to better engineered superconducting devices where stability and high depinning forces are crucial [106].

c) Josephson Vortices and Crossing Lattices.

Highly layered cuprates such as BSCCO support naturally occurring Josephson vortices, where the absence of a core and the large lateral penetration depth fundamentally alter the behavior typical of Abrikosov vortices. The two kinds of vortices co-exist and interact in the presence of a tilted applied field, where the perpendicular field

induces a pancake vortex lattice and the parallel field induces a Josephson vortex lattice. The two *crossing lattices* interact to produce a complex phase diagram[107], containing spontaneous vortex stripes and intricate melting behavior for fields very close to the ab plane[108]. Advances in scanning Hall probe technology[109] and magneto-optical imaging[110] now allow these crossing lattice states to be imaged, directly illuminating these phase transitions in real space. The dynamic properties of Josephson lattices are also fascinating. Because they have no core and no conventional pinning, Josephson vortices can be driven at very high speeds. They are predicted to undergo a dynamic phase transition, from a highly distorted hexagonal structure at low speed to a stacked configuration at high speed[111]. The most remarkable prediction is that the high speed Josephson lattice emits Terahertz radiation with a frequency inversely proportional to the transit time for one lattice constant[112]. This offers the appealing possibility to create a new class of Terahertz radiation sources from dc components, with an adjustable frequency determined by the driving current and applied magnetic field.

3. Instrumentation.

Advances in STM, scanning Hall probes, magneto-optical imaging, Lorentz microscopy, high sensitivity specific heat and magnetization have driven recent and rapid progress in vortex physics. Further advances in instrumentation are on the horizon. Lorentz microscopy of vortex systems has recently been achieved at 1 MeV, showing unexpected changes in vortex orientation in BSCCO films[113] and dynamic structure in apparently static crossing lattices[114]. Magneto-optical imaging can now see single vortices[104], opening a new window on real space dynamics. Higher resolution can be achieved with development of *near field* magneto-optical imaging, an advance that is within reach using available techniques. Specific heat experiments are ripe for much higher sensitivity using MEMS (micromachines) to eliminate addenda corrections and innovative temperature sensing. This new instrumentation will drive not only vortex physics but also will advance many other areas of condensed matter physics.

V. Proximity and Interface Effects

The superconducting proximity effect involves the mutual influence of neighboring superconducting and non-superconducting materials across an interface[115]. Such mutual influences can be profound. They can affect greatly the physical properties of both materials and are important in any application or scientific measurement that involves interfaces. Related effects occur at vacuum interfaces at the surface of a superconductor. The proximity effect is central to the physics of the coupling of superconductivity across non-superconducting barriers that make possible the Josephson junctions used in high- T_c superconducting electronics[116] and the grain boundary interfaces that are presently the primary factor limiting current flow in high-current superconducting tapes[117]. The proximity effect is also central to the broader application of the extremely powerful but surface sensitive techniques of photoemission spectroscopy and the growing arsenal of scanning local probes to these materials. The importance of grain boundaries as current limiting factors in HTS tapes is also discussed in

Chapter VII of this report. And the importance of surface effects in the application of ARPES and scanning probes is discussed in Chapter III.

To all of this must be added the possibility of surface doping through the use of charge transfer from deposited over-layers or the electrostatic field effect. The recent determination of scientific misconduct in some reported results using field-effect doping to induce high-temperatures superconductivity does not undermine the basic scientific rationale for such work. Indeed, field effect doping (both capacitive[118] and ferroelectric[119]) has a long history that continues up to today. The situation has been reviewed recently[120]. Clearly, charge transfer and field-effect doping remain potentially elegant approaches to creating new superconductors and developing model systems for studying two-dimensional superconductivity.

For all these reasons mastery of the proximity and interface effects in the high temperature superconductors is essential to progress in the field.

In conventional, low- T_c superconductors the understanding of the proximity effect is relatively well developed for interfaces with normal metals[121]. The reasons are the power of BCS theory along with the simplification provided by the generally long superconducting coherence lengths typical of low- T_c materials (and conventional normal metals). These long coherence lengths tend to average out and temper interface effects and thereby permit the use of simple, phenomenological boundary conditions for most purposes. The proximity effect with a ferromagnet is qualitatively different, however, and its understanding remains under developed. The new twist here is that the pair wave function has an oscillatory decay in the ferromagnetic (FM) material[122], in contrast to the simple exponential decay found in the normal-metal case.

High- T_c superconductors are very different. The very short coherence lengths characteristic of these materials make them much more susceptible to the influence of neighboring materials and internal defects virtually at the atomic level. Hence, the use of phenomenological boundary conditions is problematic, and microscopic theory will have to play a larger role. Of course, there is no well developed microscopic theory of the high- T_c superconductors. In addition, the strong doping dependence of the cuprate superconductors makes them sensitive to charge transfer at interfaces, where there is a tendency to form npn-like junctions[123], introducing further new complexity. The d-wave nature of the pairing also leads to new features in the proximity effect (and the related Andreev scattering process at interfaces) that have not been fully explored. One now well-accepted example is the reduction of the pair wave function to zero at surfaces whose normal points along the direction of the nodes in the energy gap[124].

There are also intriguing experimental results that suggest new physics is operating in the proximity effect with the high- T_c superconductors. The anomalous normal state properties of the cuprates, particularly in the pseudo-gap regime at low doping, seems incompatible with the use of the conventional theory (based on low- T_c

superconductors and normal metallic behavior) to describe the proximity effect with these phases. In addition, various systematic studies of the proximity Josephson coupling of the ab-planes of the cuprate superconductors across these normal phases imply characteristic lengths of the proximity coupling that are larger than can be readily explained with conventional ideas[125]. The alternative possibility that longer coherence lengths are possible in the normal planes and/or that the range of the proximity effect with conventional normal metals on the c-axis of BSCCO is shorter than can be readily explained with conventional ideas[126] is intriguing.

From the theoretical perspective, understanding of the proximity effect with a material near a quantum phase transition (such as the superconductor/insulator or metal/insulator transitions) with their associated quantum fluctuations is lacking even in the case of conventional superconductivity. It is presumably even more challenging in the case of the cuprates, which exhibit several such transitions as a function of doping, due to their highly correlated nature. In addition, there are speculations that negative U centers in the blocking layers are playing a role in the high- T_c of some cuprates in a kind of internal proximity effect[127].

Finally, the ability to exploit widely the powerful but inherently surface sensitive electronic probes of the high- T_c superconductors such as ARPES and the various emerging scanning probes will depend on dealing somehow with their complicated surface chemistry and altered doping of the CuO_2 planes near the surface due to the lack in general of a charge neutral cleavage plane in the unit cell of the cuprates, with the notable exception of $\text{Bi}_2\text{Sr}_2\text{CaCu}_2\text{O}_x$ (2212 BSCCO).

Key to understanding proximity and interface effects is the controlled preparation and characterization at the atomic level of the various interfaces of interest. Only by creating and understanding such model interfaces can the necessary phenomenology be developed that can guide applications (with their real, more complicated interfaces) and permit unambiguous scientific study of these materials with surface sensitive techniques.

Fortunately, recent advances in the controlled thin film deposition of highly refined interfaces of various kinds have been developed for the high- T_c superconductors and complex oxides more generally[128]. Atomic layer (or block by block) epitaxial growth has been achieved in some cases. Grading of individual layers as a film is built up may be necessary and likely is possible. The same techniques may also be useful in preparing the surfaces of bulk single crystals for study by ARPES and/or scanning probes.

The techniques capable of such refined interface preparation involve the combination of very well controlled deposition techniques with various *in-situ* means of monitoring the growth. These include Molecular Beam Epitaxy (MBE), Pulsed Laser Deposition (PLD) and sputtering. The need for an oxidizing atmosphere presents technical problems, but these are increasingly under control. *In-situ* Reflection High Energy Electron Diffraction (RHEED) is now commonly available for structural characterization and techniques to measure *in-situ* and in real time the temperature and

composition of a growing film are likely to become available. Such instrumentation will greatly facilitate progress. *Ex-situ*, post-deposition characterization is necessary, however, in order to confirm the structure away from the growth conditions.

At the same time, techniques for preparing well-defined grain boundaries of various types for physical study in both crystals and thin films have been developed. Advances in electron microscopy have also been developed that permit not only the structural characterization of the grain boundaries but also determination of the spatial dependence of the electric potential (and therefore the distribution of charge) across the boundary, at least on average. Such information will greatly facilitate progress in understanding the electrical properties of these grain boundaries. Still needing development are probes capable of characterizing the lateral dependence of the structure and properties of these interfaces (particularly electrical transport). Presumably local scanning probes can be brought to bear usefully on these questions. Similarly, techniques need to be developed that can reveal the point defects present near the boundaries that are not visible in TEM and may be playing a significant role in achieving charge neutrality near the boundary.

In concert with better sample preparation and more thorough physical study will need to be the systematic development of phenomenological theories that incorporate appropriately the known physics of the high- T_c superconductors and the realities of the materials themselves. First principle predictive value is probably not possible nor is it necessary from the point of view of furthering the science. Phenomenological models may provide useful models of interfaces for applications and guide the empirical process of materials optimization.

In summary, study of the proximity effect is a critical element in the evolving study of the high temperature superconductors. The key issues are: developing the model materials systems that will enable understanding at the required atomic level; developing tools to make and measure such interfaces, in particular scanning probes; surface doping and charge transfer studies, developing a unified theory of the proximity effect that deals with the material realities and the novel physics of the high- T_c superconductors; and applying all this knowledge in surface sensitive studies of these materials.

VI. Nonequilibrium Effects

A very general case of nonequilibrium dynamics in an electronic system starts by creating a high-energy electron (e.g., by optical absorption) followed by a cascade of excited states with smaller and smaller energies until the excess energy can escape the system, generally by phonons. In superconductors, nonequilibrium effects also occur with a transport current, for example, at interfaces exhibiting proximity effects, including grain boundaries (see Chapters V and VIII). The nonequilibrium effects of currents are especially important when magnetic vortices appear either from applied fields or the self-field of the current. The excitation energies are not too large ($< k_B T_c$) in these cases, which are discussed in the dynamic phases of vortices part of Chapter IV and under pinning in Chapter VIII.

Returning to the cascade processes mentioned at the start, these are indicated schematically in Fig. 5. They include electron-phonon and electron-electron scattering and are relatively fast, being $\sim 10^{-12}$ sec to achieve thermal energies[129]. The eventual loss of excess energy results from the escape of phonons from a finite sized sample and it is much slower, being generally $\sim 10^{-6}$ sec, due to the small velocity of sound and significant phonon-electron scattering. In the case of a superconductor, this strongly affects the final relaxation step, the recombination into Cooper pairs and escape of the excess energy by phonons. In superconductors, scattering between electron-like and hole-like branches (see Fig. 5) only occurs after 'thermalization' to energy scales of order of the energy gap. In high-temperature superconductors (HTS), the d-wave energy gap depends on the momentum direction, exhibiting nodes along the (π, π) wave vectors. Thus a new element of nonequilibrium processes in HTS is the relaxation of momentum around the Fermi surface.

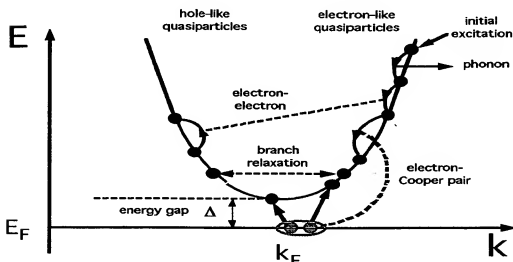


Fig. 5. Energy, E , versus momentum, k , for quasiparticle excitations in a superconductor with energy gap, Δ , showing electron-like ($k > k_F$) and hole-like ($k < k_F$) excitation branches. Also shown schematically are possible relaxation cascade processes for an initial electron-like excitation of energy, $E > \Delta$. Energy relaxation occurs by emission of a phonon, scattering off another quasiparticle or breaking a Cooper pair. Relaxation between the electron-like and hole-like branches occurs preferentially when $E \sim \Delta$. The final step (not shown) is the relaxation of the excess quasiparticle density back to Cooper pairs and the concomitant escape of a phonon with energy $\sim 2\Delta$.

Progress has been made to understand the fast scattering rates in HTS using thermal Hall conductivity[130], microwave absorption[131] and optical pump-probe experiments[132-136], but crucial pieces are missing. These include systematic studies

that cover a wide spectrum of pump and probe frequencies, other complementary experiments and connections to theoretical predictions. Less attention has been paid to the traditional nonequilibrium studies[137, 138] in LTS that have addressed a wide range of effects of excess quasiparticle densities and/or branch imbalances between electron-like and hole-like quasiparticles. The opportunities in the latter case are exotic, numerous and largely untapped.

It is quite interesting that the scattering times derived from thermal conductivity[130], microwave absorption[131] and optical pump-probe experiments[132] exhibit a very similar magnitude and temperature dependence. While the first two probe nodal quasiparticles at the (π, π) points of the k -dependent d -wave density of states at an energy scale of $\sim k_B T$, most pump-probe experiments excite the HTS with 1.5 eV photons whose energy is $\sim 200 k_B T_c$ and the cascade can include all k states. In addition, the probe response, which measures the reflectivity changes after optical pumping, varies dramatically with probe frequency (even changing sign) so the specific property of the nonequilibrium distribution being addressed is less clear. One expects that these probe-frequency dependencies will reflect features of the electronic system such as the plasma frequency as well as the changes due to these nonequilibrium states. For example, the temperature dependence of the amplitude of the 90 meV probe energy response to a 1.5 eV pump energy[133], shows a strong correlation with the amplitude of the neutron resonant spin excitation[139]. The resolutions of these fascinating mysteries promise a rich new field of research that can bring considerable insight into non-thermal processes in electronic oxides and possibly into the mechanism of HTS. For these experiments, it seems that much could be answered if another probe, like tunneling, could be done on such fast time scales (~ 10 psec) to complement the optical data.

The eventual recombination and energy transfer to phonons has been addressed in mm-wave absorption measurements that probe the reflectivity at a frequency of ~ 0.3 meV. The authors find relaxation times in the 10^{-6} sec range and intuit a more significant bottleneck than LTS due to the unique properties of the nodal quasiparticles. They also suggest an analogy to the T relaxation process[140] found for He. The long relaxation time means that the traditional nonequilibrium effects found in LTS, which have addressed the effects of excess quasiparticle densities and/or branch imbalances between electron-like and hole-like quasiparticles, should be observable in HTS. Such nonequilibrium effects in high-temperature superconductors (HTS) comprise a research area that is ready for exploitation.

Numerous effects of perturbations by tunnel-junction injection of quasiparticles (unpaired electrons), microwave or optical illumination, etc. are readily observed in low T_c superconductors (LTS) and these have been understood in terms of electron-phonon scattering[137, 138]. This is consistent with the electron-phonon coupling mechanism for these superconductors. Occasionally the effects of direct electron-electron (Coulomb) scattering must also be considered. In HTS the situation is potentially much more interesting for at least two reasons. The d -wave symmetry of the order parameter admits a momentum-dependence to the quasiparticle energy spectrum and there are additional spin and charge excitations that have been suggested as potential candidate bosons for the

attractive interaction. The latter excitations are seen by neutron scattering and would be expected to interact with quasiparticles. By studying the relaxation processes in nonequilibrium it may be possible to address the importance of these excitations if their effects on the relaxation of nonequilibrium quasiparticle distributions can be identified.

Nonequilibrium states are here classified as those states for which the quasiparticle (or, e.g., phonon) distribution exhibits an energy profile different from thermal equilibrium. No matter how high the energy of the fundamental excitation process, in a fairly short time the excess energy of the perturbation relaxes, predominantly, into a state for s-wave superconductors in which it resonates between phonons of energy 2Δ and quasiparticles of energy $\sim\Delta$. This is due to the high density of quasiparticle states near Δ in the BCS density of states and it results in a bottleneck for the escape of the 2Δ recombination phonons into the thermal bath since they are resonantly reabsorbed by the high density of Cooper pairs. This increases the effective recombination time above the bare value (typically by one to two orders-of-magnitude).

The observations of many diverse nonequilibrium effects observed in low T_c superconductors (LTS) benefit from the long time constants for the ultimate recombination into Cooper pairs. This is due to the 2Δ -phonon bottleneck and the small energy scale of Δ in LTS also contributes to a long bare recombination time due to the small phase space available in the decay channel via phonons (density of phonon states $\sim\omega^2$). Nonequilibrium studies in LTS have discovered new effects, like energy gap enhancement by microwave or tunnel-junction injection, branch or charge imbalance and new applications, like weak-link Josephson devices, superconducting three-terminal devices and particle detectors. See Ref. 9 for more complete reviews of these topics. The greater richness of the interactions in HTS, together with the nonconventional order parameter, large energy gap and the naturally layered structure can be anticipated to provide additional phenomena and applications. Examples include the coupling of ac Josephson oscillations to phonons or the possibility of terahertz oscillators enabled by the coupling of coherent Josephson vortex flow in BSCCO to Josephson plasmons to produce electromagnetic radiation. For instance, in the latter case, one can test predictions of the occurrence of dynamically stabilized vortex configurations and the interaction with Josephson vortices with Josephson plasmons. In addition, the large energy gap in HTS cuprates make them attractive candidates to extend the frequency range of tunnel-junction mixers beyond that of LTS junctions. Although energy gap enhancement, by microwave illumination[141, 142] or tunnel junction injection[143], is well established in LTS, the discovery of photoinduced superconductivity in underdoped cuprates is unique and unexpected—it produces substantial increases in T_c that are persistent[14].

The large Δ_0 in HTS, compared to LTS, may be expected to lead to shorter bare recombination times, but under many circumstances nonequilibrium effects can still occur. For example, the longer effective relaxation time due to resonant 2Δ -phonon adsorption mentioned above is largely a geometrical escape factor that may be quite similar[134] to that found in LTS. This resonant adsorption is usually referred to as phonon trapping since the nonequilibrium perturbation energy must be converted into,

and carried away by, phonons. Phonons can be expected to play that same role in HTS, since, e.g., spin and charge excitations cannot leave the electronic system. But also, an additional trapping mechanism may occur due to the nodes of the d-wave order parameter. This proposed effect is the momentum-space analogy of the real-space quasiparticle traps devised for LTS superconductive detectors[144]. In such detectors, Cooper pairs in a large volume of superconductor (with a relatively large gap, Δ_s) interact strongly with incident irradiation to produce excess quasiparticles. The detector is arranged so that the quasiparticles have a high probability of diffusing into an attached superconductor with a smaller gap, Δ_s , before the energy escapes the system via phonons. The smaller Δ_s results in a *longer bare recombination time* due to the smaller phase space of phonons of energy $\omega=2\Delta_s$. In addition, the excess energy of quasiparticles, $\sim\Delta_s$, converts into a greater number of quasiparticles with $E\sim\Delta_s$.

In a proposed relaxation mechanism, quasiparticles produced in the high- Δ regions away from the nodes at the (π, π) points would diffuse to traps in momentum space at the lower energy states near the nodes. Several mechanisms can be envisioned, e.g., direct scattering of quasiparticles by phonons or spin excitations and pair breaking into near-nodal quasiparticle states by nonequilibrium phonons or spin excitations. The interpretation of nonequilibrium data in these regimes could be connected to models for the mechanism of HTS (see Chapter VII). It will be interesting to explore the relation of the specific momenta of spin excitations with relaxation processes across the d-wave Fermi surface. The multiplying factor upon energy degradation implies that a single 1.5 eV photon could create up to 4000 quasiparticles trapped at the nodal points with an energy scale of ~ 4 K. As pointed out above, measurable recombination times in excess of 10^{-6} sec have been reported in HTS.

The ease of fabrication of thin-film superconductor-insulator-superconductor tunnel junctions was also a vital component of previous studies of LTS materials. Making junctions with two HTS electrodes has proved much more difficult and most tunneling studies have relied on point-contact or STM tunnel junctions. However significant progress has been made using MBE growth of multilayers of HTS with lattice-matched insulators as well as the internal junctions of BSCCO crystals offer another opportunity that is unique to the HTS cuprates. In the latter case, it seems necessary to intercalate molecules (e.g., iodine or mercury bromide) between the Bi-O bilayers to reduce the current for injection near the energy gap, 2Δ , and avoid a significant weakening of the superconducting state[145].

VII. Theory

1. Preamble

Since the discovery of high T_c superconducting materials, there have been many ideas put forth to explain their unusual and often perplexing physical properties. Here, rather than attempting to survey the field, we offer three individual perspectives.

2. Phenomenological Approach

a) Status.

The cuprates are highly correlated systems close to the Hubbard-Mott antiferromagnetic insulating state. In the underdoped regime, pseudogap signatures[28] go well beyond ordinary metallic behavior. Here we will limit the discussion to the optimally doped case where Hubbard-Mott modifications may not be so severe. In this case generalizations of techniques developed for ordinary superconductors may be applicable with appropriate modifications and give valuable insight. For conventional superconductors phonon structures in current-voltage characteristics of planar tunneling were exploited to derive a complete picture of the electron-phonon spectral density $\alpha^2F(\omega)$ [146]. This function defines the kernels that enter the Eliashberg equations. The theory accurately predicts (at the 10% level) the many deviations from universal BCS laws which have been seen in a broad range of experiments[146]. Similar equations suitably generalized to include d-wave symmetry[23, 147, 148] can lead to an equally good understanding of the observed superconducting properties of optimally doped YBCO. In this approach the general framework of a boson exchange mechanism is retained with a boson exchange spectral density (denoted by $I^2\chi(\omega)$), to be determined from experimental data. In the high temperature oxides, rather than tunneling, including STM, the technique of choice has so far been the infrared conductivity, from which one can construct a model of $I^2\chi(\omega)$. [23, 147, 148] When applied to the conventional s-wave case the method reproduces the tunneling derived model for $\alpha^2F(\omega)$ [149, 150]. In the oxides the optical scattering is dominated by a fluctuation spectrum which is largely featureless and which extends over a large energy scale of order several hundred meV (the order of J in the t-J model). Such a spectrum is expected in spin fluctuation theories such as the nearly antiferromagnetic Fermi liquid (NAFL)[151, 152] or in the marginal Fermi liquid (MFL)[153].

In the superconducting state a new phenomenon has been identified. One finds increased scattering at some definite finite value of ω associated with the growth of a new optical resonance in the charge carrier boson spectral density, the energy of which (ω_n) corresponds exactly to the energy of the spin resonance measured by inelastic neutron scattering (when available). This correspondence does not prove, but provides support for a spin fluctuation mechanism (rather than the MFL). Moreover the spectral density derived from the infrared data, (at T_c in optimally doped YBCO) shows a form characterized by a spin fluctuation energy ω_{sf} [152]. This form is progressively modified by the growth of the resonance at ω_n and attendant reduction of spectral weight at smaller energies as the temperature is lowered below T_c . The spectrum obtained depends on temperature (through feedback effects due to the onset of superconductivity)[154, 155], and leads to good agreement with observed properties of the superconducting state. While the generalized (for d-wave) Eliashberg equations are not as firmly grounded in

the basic microscopic theory as in the phonon case, they do offer a phenomenology within which superconducting properties can be understood. These include the condensation energy per copper atom, the fraction of total spectral weight which condenses into Cooper pairs at $T=0$, the temperature dependence of the superfluid density, the peak observed in microwave data as a function of temperature and its shift in position with microwave frequency, the similar peak in the thermal conductivity, and the frequency dependence of the infrared conductivity

b) Key Issues and Opportunities.

An important issue for the future is to extend the calculations to the underdoped regime. There is as yet no systematic quantification of pseudogap effects and contradictory views exist as to their origin. In the preformed pair model[29] the pseudogap and superconducting gap have a common origin with the superconducting transition related to the onset of phase coherence. In the d-density wave model[156] (DDW) a new order parameter competes with superconductivity. Another problem that needs resolution is understanding the new ARPES data which have been interpreted as giving strong signatures of phonon effects[157-159]. The dressed quasiparticle energies must also contain important renormalization due to the spin fluctuations. Certainly a pure phonon model is incompatible with the infrared optical data. However, it is well known that transport and quasiparticle scattering rates are different. In transport, backward collisions assume additional importance in the depletion of current, as compared with quasiparticle scattering. The quasiparticle electron-boson spectral density may have important contributions from both phonons and spin fluctuations, while the transport spectral density may be dominated by spin fluctuations. An important aim for the future should be to achieve a common understanding of ARPES, optical and tunneling data simultaneously.

3. Numerical Studies of Hubbard and t-J Models

a) Status.

Numerical studies of the high T_c cuprate problem have been used to determine what types of correlations are significant in specific models. They have shown that the 2D Hubbard and t-J models exhibit antiferromagnetic[160, 161], striped domain wall[162], and $d_{x^2-y^2}$ pairing correlations[162-165]. The similarity of this behavior to the phenomena observed in the cuprate materials support the notion that the Hubbard and t-J models contain much of the essential physics of the cuprate problem.

This is really quite remarkable when one considers that these are basically two parameter models involving U/t or J/t and the doping $x = 1-n$. Furthermore, boundary conditions or added next-nearest-neighbor hopping terms can shift the nature of the dominant correlations showing that the antiferromagnetic, stripe, and pairing correlations are delicately balanced in these models, reminding us of the behavior of the materials themselves.

b) Key Issues and Opportunities.

While we have seen that many of the basic cuprate phenomena appear as properties of these models, the interplay of the various correlations and the nature of the underlying pairing mechanism remain open. Thus a key issue is to determine whether the underlying physics is to be understood in terms of spin-charge separation[166, 167], SO(5) symmetry[130], stripes[168], spin-fluctuation exchange[169], or whether additional phonon mediated interactions may play a supporting role[46, 170]. With the understanding which has been gained and with further development of computational techniques, we have the opportunity of addressing these issues. Here it is important to realize that the search for the appropriate theoretical framework for understanding the cuprates also includes seeking to determine what type of models (and ultimately materials) are described by various scenarios. For example, we would like to understand what types of strongly correlated models exhibit spin-charge separation or more generally some type of fractionalization. Is there a sufficient temperature range for strongly correlated 2-leg ladders to renormalize so that an SO(5) description is appropriate? Do stripes suppress or enhance pairing? What role do phonons play and how is the electron-phonon interaction affected by strong Coulomb interactions? What is the structure of the phase diagram for these models? What new materials or material modifications will the answers to these questions suggest?

It should also be noted that theoretical progress in first-principles band theory simulations of ARPES intensities in the high- T_c 's has been made and the inclusion of the electron-phonon and strong correlation effects in these simulations can advance the interpretation of the data[171].

We are in a position to address these issues and we also have the opportunity to take advantage of more than a decade and a half of advances driven by the cuprate discovery. As part of this effort we need to continue the development of numerical techniques. We should also work to establish closer connections to the electronic structure and quantum chemistry communities for key information on the basic orbitals and effective parameters that enter model descriptions of real materials.

4. Electronic Structure

a) Status.

The discovery of superconductivity in MgB_2 and the subsequent response by the computational community demonstrated the remarkable progress that has been achieved in first principles calculations for the electronic properties of conventional (phonon mediated) superconductors. Indeed, $\alpha^2F(\omega)$ can now be calculated accurately for fairly complex materials using density functional methods. For example, first principles evaluation of the electron-phonon interaction was used to calculate the superconducting transition temperature of the simple hexagonal phase of Si under high pressure[172]. Not only can the electron-phonon coupling be obtained, but also complete phonon dispersion curves for the whole Brillouin Zone (BZ) are being calculated using perturbation theory

(harmonic approximation). If anharmonic terms are important, frozen phonon calculations yield total energies as a function of the relevant lattice distortions. Indeed, structural phase transitions involving soft phonon modes are frequently analyzed via such total energy calculations. While phonon frequencies and eigenvectors are needed to

evaluate $\alpha^2F(\omega)$, it is difficult to draw conclusions about superconductivity from phonon dispersion curves. It is interesting however, that first principles calculations of phonons in the cuprates have in general yielded good agreement with neutron scattering experiments (see for example [173] and references therein).

When Local Density Approximation (LDA) calculations were unable to produce the insulating antiferromagnetic state in the cuprate phase diagram [174], it became clear that new approaches for dealing with correlation and moving beyond standard band structure techniques were needed. The first of these new "band structure" approaches, the LDA+U method, introduces a Hubbard U term into the LDA equations, affecting the orbitals for which the correlations are strong [175]. The more recent LDA++, and Dynamical Mean Field Theory (DMFT) methods make a more direct attack at calculating the electron self-energy, $\Sigma(\mathbf{k}, \omega)$ [176-179]. The computational resources for evaluating the dynamics are demanding, and while good progress is being made, results have only been obtained for prototype systems. Although there is not yet a satisfactory band structure based technique for treating spin fluctuations when going from the Mott-Hubbard insulating state to optimally doped high T_c materials, straight forward band structure calculations of the doped cuprates yield Fermi surface geometries in remarkably good agreement with precise angle resolved photoemission experiments. Band structure calculations have also been valuable in identifying the relevant orbitals and in estimating values of the parameters that enter more phenomenological models.

b) Key Issues and Opportunities.

A key ingredient in solving the Eliashberg equation for phonon mediated superconductivity is the simplification made possible by Migdal's theorem. In exploring other boson mechanisms with higher frequency spectra the role of the retarded Coulomb interaction, μ^* , needs to be revisited [180]. It has been suggested that for vanadium the effective μ^* is larger than expected because of the pair-breaking influence of spin fluctuations [181]. In the one band Hubbard model it has also been argued that strong correlations suppress the electron phonon coupling in α^2F and transport quantities [182]. The recent angle resolved photoemission measurements which show mass renormalization for bands passing through the Fermi energy may provide a quantitative measure of the electron-phonon interaction for specific states [159]. A comparison with first principles calculated values would be most interesting.

There are many other questions, many identified in this document, which are now being approached with model Hamiltonians. While electronic structure practitioners are eager to participate in and learn from such studies, and to provide parameters and insights where possible, there is a strong desire to develop the apparatus required for a real first principles treatment of the phenomena. There are many insights and ideas that need to be

developed first. Perhaps the situation today is not so different than in the early 1960s when the Fermi surface was considered exotic. The dividends from the investment in physics of that period are the basis for what is now considered "routine" materials science, with applications ranging from Stockpile Stewardship to material processing to drug design. Solving the "high T_c problem" will likewise result in valuable tools and insights leading to future applications.

VIII. Defects and Microstructure with an Eye to Applications

Crystal lattice defects and their organization on the scale of nanometers to micrometers ("microstructure" for short) play a very significant role in the science and technology of superconducting materials: [183-188] For one thing, defects are unavoidable in the world of "real materials," and it is vital to characterize their nature and distribution so as to understand their effects on superconductivity. It is also vital to control the defect distribution in the polycrystalline, large-scale microstructure of conductors since appropriate nanoscale defects are responsible for developing high critical current densities, J_c , within grains. But planar defects, especially grain boundaries, block grain-to-grain transmission of the current, dictating the geometry of conductors because of the sensitivity of J_c to strain defects, etc. Defects can also provide insights into fundamental questions, e.g., the use of grain-boundary junctions in the investigation of order-parameter symmetry in cuprate superconductors. HTS conductors are available from several companies worldwide and have been used to demonstrate large components of the electric power grid such as power cables, motors, transformers and fault current limiters. Josephson-junction devices and other electronic devices based on HTS technology are in an advancing state of commercial development. However, we are still far from understanding or being able to optimize HTS material properties in the way that we have learned to do for the workhorse conductor of LTS (Nb-Ti). The main point is that our ability to adequately control defects and microstructures is still rudimentary. Some of the remaining key issues derive from the anisotropic nature of the cuprates and their low carrier density. These characteristics result in inadequate magnetic flux pinning, percolative current flow past many interfacial barriers, inability to control the phase state, and a general lack of materials control.

Extensive investigation of the cuprates has developed a firm understanding of some of their microstructure-sensitive properties. First of all, it is painfully clear that crystallographic texture and phase purity must be tightly controlled for high J_c in cuprates. It also seems unavoidable that magnetic flux pinning at temperatures, above about 30K, is inadequate in the present conductor material, Bi-2223. It is just too anisotropic for magnetic field applications, though adequate for self-field use in power cables at 77K. YBCO has much greater potential for applications in fields at 77K than Bi-2223, because its mass anisotropy is about 7, rather than the ~100 of Bi-2223, even though its T_c is 92 K rather than the 110 K of Bi-2223. By contrast it has been quickly established that MgB_2 has only a small anisotropy (values vary from about 2 to 7, though with a greater weight on lower numbers) and that grain boundaries are not serious obstacles to current flow. Flux pinning also appears to be strong, leading to high critical current densities in prototype wires. In many respects MgB_2 appears to be exactly what

its 39 K T_c suggests, intermediate in properties between LTS and HTS, benefiting in particular from lower anisotropy and relatively insensitive to planar defects.

It is not surprising at all that understanding of defects in cuprate superconductors is such a hard-won commodity, because these are very complex materials (the most practically important material, Bi-2223 ($\text{Bi,Pb})_2\text{Sr}_2\text{Ca}_2\text{Cu}_3\text{O}_{10-x}$) forms a 7-component system when embedded in Ag). The continued attention to grain boundaries and to the search to understand flux-pinning defects has enhanced and will continue to increase our knowledge of defects in complex oxides in a much wider context, e.g., the understanding of defects in manganites, ferroelectric perovskites, etc. Continued investment in the materials physics of defects in HTS materials is attractive, not just because of the implications for superconductivity technology

What, then, are some of the outstanding issues in this field and how can we solve them? We need a new phenomenology, which combines the new physics of HTS with a realistic description of defects and microstructure in these complex materials. At present, almost all of the phenomenological discussion of the effects of defects and microstructure on the superconducting properties of HTS materials is based on theoretical concepts appropriate to s wave LTS. How do defects in HTS materials really interact with correlated-electron phenomena, stripe-phases, and electronic phase separation? We will not understand the answers to such questions without a basic theory of defects in complex oxides that takes account of their complex electronic state and proximity to the metal insulator transition.

Knowledge of lattice defects and microstructure in HTS materials is mostly confined to YBCO (and other 123-structure cuprates) and to the 2212 and 2223 phases of BSCCO. Why stick to these "old favorites?" To a very large degree, this reflects a "tyranny of practicality and materials complexity," which inhibits the development of a wider knowledge needed to understand broader aspects of the materials physics of HTS materials. Many HTS materials are much more complex to make and appropriate recipes for "good sample" manufacture are lacking. It is believed that much might be learned from infinite layer materials. For example, their structures are not neatly divisible into charge reservoir and superconducting blocks. Since grain boundaries in HTS are believed to be disruptive to current precisely because charge transfer to the conducting cuprate planes is perturbed, their study in infinite layers might be particularly valuable.

Many issues involving magnetic flux pinning in HTS materials remain to be clarified. Although much is known about the thermodynamics and phase-diagrams of vortex matter in HTS materials, (see Chapter IV), much remains to be learned about the elementary interactions between vortices and defects, e.g., the physics of the elementary pinning forces, f_p , for various types of defects and their systematic variation among various cuprates. Furthermore, the knowledge of the behavior of defects, such as dislocations and plastic flow in vortex lattices themselves, is mostly extrapolated from the LTS case and almost certainly needs revision in such strongly anisotropic cases as Bi-2223, where line vortices in LTS materials break up into largely, but not completely disconnected pancake vortices. Experiments need to be designed specifically to

illuminate the fundamental nature of defect-vortex interactions in HTS materials. These would be particularly valuable when combined with parallel conductor development activities. The intermediate nature of MgB_2 makes the nature of elementary pinning forces, vortex-lattice elasticity and plasticity very interesting. Are these properties fundamentally different or similar to those of Nb_3Sn and other LTS intermetallic compounds? Does the complex electronic band structure and anisotropy of MgB_2 make it's flux-pinning fundamentally different from that in the A15 compounds?

What is learned about the interactions between defects and correlated-electron phenomena in HTS materials will pay dividends in a wider range of materials, e.g., manganites, and phenomena, e.g., magnetism and metal-insulator transitions. In fact, the interactions between defects and transport properties in the normal state of cuprates are very poorly understood, too. A better understanding here would greatly improve the ability to characterize the nature and concentration of defects in cuprates in a quantitative manner.

There are many needs and opportunities in the science of defects and microstructure of cuprates, in addition to the direct connection to superconductivity (e.g., flux-pinning and weak links). The latter provides the motivation for microstructural control, but understanding of the basic materials science of defects and microstructure is needed to exercise such control efficiently. Here, too, experiments and theory designed to gain basic understanding that can couple to the activity driven by practical considerations would be very valuable. For example, there is a considerable lack of serious theory and modeling, as well as of basic experimental studies, of the thermodynamics, kinetics, and mechanisms of nucleation and growth of epitaxial oxides of relevance to coated conductors (including buffer layers, etc.), despite there being a large amount of process development in this area. Understanding of the fundamentals of phase formation in cuprate systems is sparse. There is also a serious need for quantitative understanding of the elementary defects, such as point defects, dislocations, twin boundaries, stacking faults, etc., which are the "elementary particles" of microstructure in HTS phases. This, together with quantitative descriptions of microstructure and defect chemistry, is needed to develop an adequate phenomenology of current transport and flux pinning in HTS systems.

Another area of fundamental materials physics that is relatively unexplored for HTS materials is that of mechanical properties, especially elasticity, anelasticity, and fracture. There is a paucity of basic experimental data, and these complex materials require theoretical methods more advanced than those needed for simpler materials, including ferroelasticity, non-linear and microcontinuum elasticity, and models of non-linear lattice statics and dynamics. Furthermore, an understanding of the coupling of elastic strain fields to the superconductivity of HTS materials is needed to understand interactions between defects and superconductivity, as well as to predict the behavior of conductors in devices such as high field magnets where large stresses arise during device operation.

The quantitative description of HTS-based conductors also requires improved methods of modeling the physical properties of composites, including mechanical, thermal and electromagnetic properties. The latter is particularly challenging, involving current and magnetic induction distributions in polycrystalline, defect-containing, multiphase composites.

The discussion above indicates the great complexity of the defect physics and microstructural science of HTS superconductors, which are both of fundamental interest and of enormous relevance to practical applications. However, powerful instrumental tools are available to help meet this challenge, especially modern transmission electron microscopy and local scanning probe microscopies and spectroscopies. These tools now permit the characterization of atomic and electronic structure, as well as elastic strain fields, over length scales ranging from atomic resolution to micrometers. This affords an unprecedented ability to obtain images and spectroscopy of atomic, charge, and strain distributions, which will revolutionize our quantitative understanding of defects and microstructure. The use of such instrumental tools, together with microscale electromagnetic characterization, coupled with the development of HTS-appropriate theoretical phenomenology, has the potential to yield important new insights into this complex problem, with wider implications for many complex new materials of the future.

References

1. Buddhist Udana, Circa 100 B.C..
2. B.J. Battlogg. 1997, National Science Foundation.
3. J.E. Hirsch, Phys. Rev. B 55, 9007 (1997).
4. R. Flukiger, in *Concise Encyclopedia of Magnetic and Superconducting Material*, Jan Evetts, Editor. 1992, Pergamon Press, Inc. p. 1.
5. O. Fisher and M.B. Maple, in *Superconductivity in Ternary Compound*, I. O. Fischer and M.B. Maple, Editors. 1982, Springer-Verlag: Berlin. p. 1.
6. J. Etourneau, in *Solid State Chemistry: Compounds*, A.K. Cheetham and Peter Day, Editors. 1992, Clarendon Press: Oxford. p. 60.
7. S.V. Vonsovsky, Yu A. Izyunov, and E.Z. Kurmaev, in *Springer Series in Solid State Sciences*. 1982, Springer-Verlag: Berlin. p. 259.
8. J. Nagamatsu, N. Nakagawa, Y.Z. Murakana, and J. Akimitsu, Nature **410**, 63 (2001).
9. C.M. Varma, W. Buckel and W. Weber, Editors. 1982, Kernforschungszentrum Karlsruhe, GmbH: Karlsruhe. p. 603.

10. S. L. Bud'ko, G. Lapertot, C. Petrovic, C.E. Cunningham, N. Anderson, and P.C. Canfield, *Phys. Rev. Lett.* **86**, 1877 (2001).
11. T. Yildirim, O. Gulseren, J.W. Lynn, and C.M. Brown, *Phys. Rev. Lett.* **87**, 037001 (2001).
12. T. Siegrist, H. W. Zandbergen, R. J. Cava, J. J. Krajewski, and W.F. Peck, Jr., *Nature* **367**, 254 (1994).
13. http://www.lucnt.com/news_events/researchreview.html
14. A. Gilabert, A. Hoffmann, M.-G. Medici and I.K. Schuller, *J. Supercond.* **13**, 1 (2000).
15. R. Cauro, A. Gilabert, J. P. Contour, R. Lyonnet, M.-G. Medici, J. C. Grenet, C. Leighton, and I. K. Schuller, *Phys. Rev. B* **63**, 174423 (2001).
16. J.M. Tranquada, B.J. Sternlieb, J.D. Axe, Y. Nakamura, and S. Uchida, *Nature* **375**, 561 (1995).
17. M. Abu-Shiekh, O. Bakharev, H. B. Brom, and J. Zaanen, *Phys. Rev. Lett.* **87**, 237201 (2001).
18. J. Orenstein, G.A. Thomas, A.J. Millis, S.L. Cooper, D.H. Rapkine, T. Timusk, L.F. Schneemeyer, and J.V. Waszczak, *Phys. Rev. B* **42**, 6342 (1990).
19. S. Uchida, T. Ido, H. Takagi, T. Arima, Y. Tokura, and S. Tajima, *Phys. Rev. B* **43**, 7942 (1991).
20. M. Imada, A. Fujimori, and Y. Tokura, *Rev. Mod. Phys.* **70**, 1039 (1998).
21. A. Damascelli, Z.-X. Shen, and Z. Hussain, *Cond-Matt/0208504*, (2002).
22. W.E. Pickett, H. Krakauer, R.E. Cohen, and D.J. Singh, *Science* **225**, 46 (1992).
23. J.P. Carbotte, E. Schachinger, and D.N. Basov, *Nature* **401**, 354 (1999).
24. A. Abanov, A.V. Chubukov, and J. Schmalian, *J. Jour. El. Spect. Rel. Phen.* **117-118**, 129 (2001).
25. M.R. Norman and H. Ding, *Phys. Rev. B* **57**, 11088 (1998).
26. A. Lanzara, P.V. Bogdanov, X.J. Zhou, S.A. Kellar, D.L. Feng, E.D. Lu, Yoshida T, H. Elsaki, A. Fujimori, K. Kishio, J.-I. Shimoyama, T. Noda, S. Uchida, Z. Hussain, and Z.-X. Shen, *Nature* **412**, 510 (2001).

27. E.J. Singley, D.N. Basov, K. Kurahashi, T. Uefuji, and K. Yamada, *Phys. Rev. B* **64**, 224503 (2001).
28. T. Timusk and B. Statt, *Rep. Prog. Phys.* **62**, 61 (1999).
29. V. J. Emery and S. A. Kivelson, *Nature* **374**, 434 (1995).
30. Z.A. Xu, N.P. Ong, Y. Wang, T. Kakeshita, and S. Uchida, *Nature* **406**, 486 (2000).
31. J. Corson, R. Mallozzi, J. Orenstein, J.N. Eckstein, and I. Bozovic, *Nature* **398**, 221 (1999).
32. D.N. Basov, S.I. Woods, A.S. Katz, E.J. Singley, R.C. Dynes, M. Xu, D.C. Hinks, C.C. Homes, and M. Strongin, *Science* **283**, 49 (1999).
33. H.J.A. Molengraaf, C. Pressura, D. Van Der Marel, P.H. Kes, and M. Li, *Science* **295**, 2239 (2002).
34. M.R. Norman, M. Randeria, B. Janko, and J.C. Campuzano, *Phys. Rev. B* **61**, 14742 (2000).
35. D. van Harlingen, *DOE Workshop, High Temperature Superconductivity*. April 2002.
36. Ch. Renner, B. Revaz, J.-Y. Genoud, K. Kadowaki, and O. Fischer, *Phys. Rev. Lett.* **80**, 149 (1998).
37. M. Covington and L.H. Greene, *Phys. Rev. B* **62**, 12440 (2002).
38. V.M. Krasnov, *Arxiv: Condensed Matter/0201287*.
39. S.H. Pan, J.P. O'Neal, R.L. Badzey, C. Chamon, H. Ding, J.R. Engelbrecht, Z. Wang, H. Eisaki, S. Uchida, A.K. Gupta, K.-W. Ng, E.W. Hudson, K.M. Lang, and J.C. Davis, *Nature* **413**, 282 (2001).
40. O. Naaman, W. Teizer, and R.C. Dynes, *Phys. Rev. Lett.* **87**, 097004 (2001).
41. E.W. Hudson, K.M. Lang, V. Madhavan, S.H. Pan, H. Eisaki, S. Uchida, and J.C. Davis, *Nature* **411**, 920 (2001).
42. J. E. Hoffman, E. W. Hudson, K. M. Lang, V. Madhavan, H. Eisaki, S. Uchida, and J.C. Davis, *Science* **295**, 466 (2002).

43. C.G. Olson, R. Liu, A.B. Yang, D.W. Lunch, A.J. Arko, R.S. List, B.W. Veal, Y.C. Chang, P.Z. Jiang, and A.P. Paulikas, *Science* **245**, 731 (1989).
44. Z.X. Shen, D.S. Dessau, B.O. Wells, D.M. King, W.E. Spicer, A.J. Arko, D.S. Marshall, L.W. Lambardo, A. Kapitulnik, P. Dickinson, S. Doniach, and J. Dicarilo, *Phys. Rev. Lett.* **70**, 1553 (1993).
45. A. Kaminski, M. Randeria, J.C. Campuzano, M.R. Norman, H. Fretwell, J. Mesot, T. Sato, Takahashi, and K. Kadowaki, *Phys. Rev. Lett.* **86**, 1070 (2002).
46. P.V. Bogdanov, A. Lanzara, S.A. Kellar, Z.J. Zhou, E.D. Lu, W.J. Zheng, G. Gu, J.-I. Shinoyama, K. Kishio, H. Ikeda, R. Yoshizaki, Z. Hussain, and Z.X. Shen, *Phys. Rev. Lett.* **85**, 2581 (2000).
47. A. D. Gromko, A. V. Fedorov, Y. -D. Chuang, J. D. Koralek, Y. Aiura, Y. Yamaguchi, K. Oka, Yoichi Ando, and D. S. Dessau, *Arxiv.: Condensed Matter/0203239*.
48. Z.-X. Shen, A. Langara, S. Ishihara, and N. Nagaosa, *Phil Mag.* **B82**, 1349 (2002).
49. T. Valla, *Arxiv.: Condensed Matter/0204003*.
50. P.D. Johnson, T. Valla, A. V. Fedorov, Z. Yusof, B.O. Wells, Q. Li, A.R. Moodenbaugh, G.D. Gu, N. Koshizuka, C. Kendziora, C. Sha Jian, and D.G. Hinks, *Phys. Rev. Lett.* **87**, 177077 (2002).
51. M.R. Norman, M. Eschrig, A. Kaminski, and J.C. Campuzano, *Phys. Rev. B* **64**, 184508 (2001).
52. Y. Sakurai, Y. Tanaka, A. Bansil, S. Kaprzyk, A.T. Stewart, Y. Nagashima, T. Hyodo, S. Nanao, H. Kawata, and N. Shiotani, *Phys. Rev. Lett.* **74**, 2252 (1995).
53. J. Laukkanen, K. Hamalainen, S. Manninen, A. Shukla, T. Takahashi, K. Yamada, B. Barbiellini, S. Kaprzyk, and A. Bansil, *J. Phys. Chem. Sol.* **62**, 2249 (2001).
54. D.N. Basov and T. Timusk, in *Handbook on the Physics and Chemistry of Rare Earths*. 2001, Elsevier Science B.V. p. 437.
55. D.N. Basov, R. Liang, D.A. Bonn, W.N. Hardy, B. Dabrowski, M. Quijada, D.B. Tanner, J.P. Rice, D.M. Ginsberg, and T. Timusk, *Phys. Rev. Lett.* **74**, 598 (1995).

56. G.S. Boebinger, Y. Ando, A. Passner, T. Kimura, M. Okuya, J. Shimoyama, K. Kishio, K. Tamasaku, N. Ichikawa, and S. Uchida, *Phys. Rev. Lett.* **77**, 5417 (1996).
57. T. E. Mason, in *Handbook on the Physics and Chemistry of Rare Earths*, K. A. Gschneidner, Jr., L. Eyring, and M. B. Maple, Editors. 2001, Elsevier: Amsterdam.
58. M.A. Kastner, R.J. Birgeneau, G. Shirane, and Y. Endoh, *Rev. Mod. Phys.* **70**, 897 (1998).
59. H. He, P. Bourges, Y. Sidis, C. Ulrich, L.P. Regnault, S. Pailhes, N.S. Berzigiarova, N.N. Kolesnikov, and B. Keimer, *Science* **295**, 1045 (2002).
60. J. Orenstein and A. J. Millis, *Science* **288**, 468 (2000).
61. V.J. Emery, S.A. Kivelson, and J.M. Tranquada, *Proc. Natl. Acad. Sci.* **96**, 8814 (1999).
62. Z. Islam, Arxiv: Condensed Matter/0110390.
63. M. Buchanan, *Nature* **409**, 8 (2001).
64. A. Kaminski, S. Rosenkranz, H. M. Fretwell, J. C. Campuzano, Z. Li, H. Raffy, W. G. Cullen, H. You, C. G. Olson, C. M. Varma, and H. Höchst, *Nature* **416**, 610 (2002).
65. J. Guimpel, L. Civalé, F. de la Cruz, J.M. Murduck, and I.K. Schuller, *Phys. Rev. B* **38**, 2342 (1988).
66. A. K. Geim, S.V. Dubonos, J.J. Palacios, I.V. Grigorieva, M. Henini, and J.J. Schermer, *Phys. Rev. Lett.* **85**, 1528 (2000).
67. L. F. Chibotaru, A. Ceulemans, V. Bruyndoncx, and V.V. Moshchalkov, *Nature* **408**, 833 (2000).
68. B. J. Baelus and F. M. Peeters, *Phys. Rev. B* **65**, 104515 (2002).
69. Yu. E. Lozovik, E.A. Rakoch, and S. Yu. Volkov, *Phys. Solid State* **44**, 22 (2002).
70. R. Besseling, R. Niggebrugge, and P. H. Kes, *Phys. Rev. Lett.* **82**, 3144 (1999).
71. J. I. Martin, M. Velez, E.M. Gonzalez, A. Hoffmann, D. Jaque, M.I. Montero, E. Navarro, J.E. Villegas, I.K. Schuller, and J.L. Vicent, *Physica C* **369**, 135 (2002).

72. A. Grigorenko, G.D. Howells, S.J. Bending, J. Bekaert, M.J. Van Bacl, L. Van Look, V.V. Moshchalkov, Y. Bruynseraede, G. Borghs, I.I. Kaya, and R.A. Stradling, *Phys. Rev. B* **63**, 052504 (2001).
73. M. Baert, V.V. Metlushko, R. Jonckheere, V.V. Moshchalkov, and Y. Bruynseraede, *Phys. Rev. Lett.* **74**, 3269 (1995).
74. V. Metlushko, U. Welp, G.W. Crabtree, R. Osgood, S.D. Bader, L.E. DeLong, Zhao Zhang, S.R.J. Brueck, B. Illic, K. Chung, and P.J. Hesketh, *Phys. Rev. B* **60**, R12585 (1999).
75. A. Castellanos, R. Wordenweber, G. Ockenfuss, A. V.D. Hart, and K. Keck, *Appl. Phys. Lett.* **71**, 962 (1997).
76. M. Park, C. Harrison, P. Chaikin, R.A. Register, and D.H. Adamson, *Science* **276**, 1401 (1997).
77. H. Masuda and H. Fukuda, *Science* **268**, 1466 (1995).
78. B. Koslowski, S. Strobel, Th. Herzog, B. Heinz, H.G. Boyen, R. Notz, P. Ziemann, J.P. Spatz, and M. Moller, *J. Appl. Phys.* **87**, 7533 (2000).
79. U. Welp, Z. L. Xiao, J. S. Jiang, V. K. Vlasko-Vlasov, S. D. Bader, G. W. Crabtree, J. Liang, H. Chik, and J. M. Xu, *Arxiv Condensed Matter/0204535*.
80. Yayu Wang, Z.A. Xu, T. Kakeshita, S. Uchida, S. Ono, Y. Ando, and N.P. Ong, *Phys. Rev. B* **64**, 224519 (2001).
81. S.H. Pan, E.W. Hudson, A.K. Gupta, K.-W. Ng, H. Elsakki, S. Uchida, and J.C. Davis, *Phys. Rev. Lett.* **85**, 1536 (2000).
82. I. Maggio-Aprile, Ch. Renner, A. Erb, E. Walker, and O. Fischer, *Phys. Rev. Lett.* **75**, 2754 (1995).
83. B.W. Hoogenboom, K. Kadowaki, B. Revaz, M. Li, Ch. Renner, and O. Fischer, *Phys. Rev. Lett.* **87**, 267001 (2001).
84. S.-C. Zhang, *Science* **275**, 1089 (1997).
85. A.Y. Liu, I.I. Mazin, and J. Kortus, *Phys. Rev. Lett.* **87**, (2001).
86. C. Uher, R. Clarke, G.-G. Zheng, and I.K. Schuller, *Phys. Rev. B* **30**, 453 (1984).
87. J. Jorgensen, *Phys. Rev. B* **63**, 054440 (2001).
88. T.K. Ng and C.M. Varma, *Phys. Rev. Lett.* **78**, 330 (1997).

89. S.-M. Choi, J.W. Lynn, D. Lopez, P.L. Gammel, P.C. Canfield, and S.L. Bud'ko, *Phys. Rev. Lett.* **87**, 107001 (2001).
90. M.I. Montero, Kai Liu, O.M. Stoll, A. Hoffmann, Ivan K. Schuller, Johan J. Åkerman, J.I. Martin, J.L. Vicent, S.M. Baker, T.P. Russell, C. Leighton and J. Nogues, *J. Phys. D*, **35**, 2398 (2002).
91. S. Erdin, I.F. Lyuksyutov, V.L. Pokrovsky, and V.M. Vinokur, *Phys. Rev. Lett.* **88**, 017001 (2002).
92. O.M. Stoll, M.I. Montero, J. Guimpel, J.J. Åkerman, and I.K. Schuller, *Phys. Rev. B* **65**, 104518 (2002).
93. M. Velez, D. Jaque, J.I. Martin, M.I. Montero, I.K. Schuller, and J.L. Vicent, *Phys. Rev. B* **65**, 104511 (2002).
94. M.J. Van Bael, J. Bekaert, K. Temst, L. Van Look, V.V. Moschchalkov, Y. Bruynseraede, G.D. Howells, A.N. Grigorenko, S.J. Bending, and G. Borghs, *Phys. Rev. Lett.* **86**, 155 (2001).
95. D. S. Fisher, M.P. A. Fisher, and D. A. Huse, *Phys. Rev. B* **43**, 130 (1991).
96. David R. Nelson and V. M. Vinokur, *Phys. Rev. B* **48**, 13060 (1993).
97. A. W. Smith, H.M. Jaeger, T.F. Rosenbaum, W.K. Kwok, and G.W. Crabtree, *Phys. Rev. B* **63**, 064514 (2001).
98. A. M. Petrean, L.M. Paulius, W.-K. Kwok, J.A. Fendrich, and G.W. Crabtree, *Phys. Rev. Lett.* **84**, 5852 (2000).
99. Y. Paltiel, E. Zeldov, Y. Myasoedov, M.L. Rappaport, G. Jung, S. Bhattacharya, M.J. Higgins, Z.L. Xiao, E.Y. Andrei, P.L. Gammel, and D.J. Bishop, *Phys. Rev. Lett.* **85**, 3712 (2000).
100. W. K. Kwok, R.J. Olsson, G. Karapetrov, L.M. Paulius, W.G. Moulton, D.J. Hoffman, and G.W. Crabtree, *Phys. Rev. Lett.* **84**, 3706 (2000).
101. N. Avraham, B. Khaykevich, Y. Myasoedov, M. Rappaport, H. Shtrikman, D.E. Feldman, T. Tamegai, P.H. Kes, Ming Li, M. Konczykowski, K. Van der Beek, K. Yamada, and E. Zeldov, *Nature* **411**, 451 (2001).
102. F. Bouquet, C. Marcenat, E. Steep, R. Calemczuk, W.K. Kwok, U. Welp, G.W. Crabtree, R.A. Fisher, N.E. Phillips, and A. Schilling, *Nature* **411**, 448 (2001).

103. T. Matsuda, K. Harada, H. Kasai, O. Kamimura, and A. Tonomura, *Science* **271**, 1393 (1996).
104. P.E. Goa, H. Hauglin, M. Baziljevich, E. Il'yashenko, P.L. Gammel, and T.H. Johansen, *Supercond. Sci. Tech.* **14**, 729 (2001).
105. C.J. Olson, C. Reichhardt, B. Janko, and F. Nori, *Phys. Rev. Lett.* **87**, 177002 (2001).
106. M.N. Kunchur, B.I. Ivlev, and J.M. Knight, *Phys. Rev. Lett.* **87**, 177001 (2001).
107. A. E. Koshelev, *Phys. Rev. Lett.* **83**, 187 (1999).
108. J. Mirkovic, S.E. Savelev, E. Sugahara, and K. Kadowaki, *Phys. Rev. Lett.* **86**, 886 (2001).
109. A. Grigorenko, S. Bending, T. Tamegal, S. Ooi, and M. Henini, *Nature* **414**, 728 (2001).
110. V.K. Vlasko-Vlasov, *Arxiv Condensed Matter/0203145*.
111. A.E. Koshelev and I. Aranson, *Phys. Rev. B* **64**, 174508 (2001).
112. M. Machida, T. Koyama, and M. Tachiki, *Phys. Rev. Lett.* **83**, 4618 (1999).
113. A. Tonomura, H. Kasai, O. Kamimura, T. Matsuda, K. Harada, Y. Nakayama, J. Shimoyama, K. Kishio, T. Hanaguri, K. Kitazawa, M. Sasase, and S. Okayasu, *Nature* **412**, 620 (2001).
114. T. Matsuda, O. Kamimura, H. Kasai, K. Harada, T. Yoshida, T. Akashi, A. Tonomura, Y. Nakayama, J. Shimoyama, K. Kishio, T. Hanaguri, and K. Kitazawa, *Science* **294**, 2136 (2001).
115. For a good classic discussion of proximity effects, see the chapter by G. Deutscher and P.G. de Gennes, in *Superconductivity*, R. D. Parks, Editor. 1969, Marcel Dekker.
116. For a useful entrée into the literature, see: L. Antognazza, B.H. Moockly, T.H. Geballe and K. Char, *Phys. Rev. B* **52**, 4559 (1995).
117. For an authoritative review, see: H. Hilgenkamp and J. Mannhart, *Rev. Mod. Phys.* **74**, 485 (2002).
118. R.E. Glover and M.D. Sherill, *Phys. Rev. Lett.* **5**, 248 (1960).
119. H.L. Stradler, *Phys. Rev. Lett.* **14**, 979 (1965).

120. C.H. Ahn, J.-M. Triscone, and J. Mannhart, (To be published in Nature).
121. For a contemporary entrée into the literature, see: Y.V. Fominov, N.M. Chitchev, and A.A. Golubov, Arxiv-cond. matt. *Nonmonotonic critical temperature in superconductor/ferromagnet bilayers*.
122. See for example: A. Rusanov, R. Boogaard, M. Hesselberth, H. Sellier and J. Aarts, Arxiv.: Condensed Matter/0111178.
123. See section VII-D, Rev. Mod. Phys. **74**, 485 (2002).
124. Y. Tanaka, and S. Kashiwaya, Phys. Rev. Lett. **74**, 3451 (1995).
125. For one example and useful references, see Y. Suzuki, J.M. Triscone, E.B. Eom, M.R. Beasley, and T.H. Geballe, Phys. Rev. Lett. **73**, 328 (1994).
126. R.C. Dynes, this DOE Workshop.
127. T.H. Geballe and B.Y. Mozysh, Physica C **341**, 1821 (2000).
128. See, for instance, I. Bozovic IEEE Trans. Appl. Superconductivity **11**, 2686 (2001).
129. Philip B. Allen, Phys. Rev. Lett. **59**, 1460 (1987).
130. Y. Zhang, N. P. Ong, P. W. Anderson, D. A. Bonn, R. Liang, and W. N. Hardy, Phys. Rev. Lett. **86**, 890 (2001).
131. A. Hosseini, R. Harris, S. Kamal, P. Dosanjh, J. Preston, Ruixing Liang, W.N. Hardy, and D.A. Bonn, Phys. Rev. B **60**, 1349 (1999).
132. G.P. Segre, N. Gedik, J. Orenstein, D.A. Bonn, Ruixing Liang, and W.N. Hardy, Phys. Rev. Lett. **88**, 137001 (2002).
133. R.A. Kaindl, M. Woerner, T. Elsaesser, D.C. Smith, J.F. Ryan, G.A. Farnan, M.P. McCurry, and D.G. Walmsley, Science **287**, 470 (2000).
134. B.J. Feenstra, J. Schuttmann, D. van der Marel, R. Perez Pinaya, and M. Decroux, Phys. Rev. Lett. **79**, 4890 (1997).
135. R.D. Averitt, G. Rodriguez, A. I. Lobad, J. L. W. Siders, S. A. Trugman, and A. J. Taylor, Phys. Rev. B **63**, 140502 (2001).
136. J. Demsar, R. Hudej, J. Karpinski, V.V. Kabanov, and D. Mihailovic, Phys. Rev. B **63**, 054519 (2001).

137. *Nonequilibrium Superconductivity, Phonons, and Kapitza Boundaries*, ed. K.E. Gray. 1981, New York: Plenum Press.
138. D.N. Langenberg and A.I. Larkin. 1986, New York: North-Holland.
139. P. Dai, H.A. Mook, S.M. Hayden, G. Aeppli, T.G. Perring, R.D. Hunt, and F. Dogan, *Science* **284**, 1344 (1999).
140. D. Vollhardt and P. Wölfle. 1990, London: Taylor & Francis.
141. A.F.G. Wyatt, V. M. Dmitriev, W. S. Moore, and F. W. Sheard, *Phys. Rev. Lett.* **16**, 1166 (1966).
142. A.H. Dayem and J.J. Wiegand, *Phys. Rev.* **155**, 419 (1967).
143. K.E. Gray, *Solid State Commun.* **26**, 633 (1978).
144. N.E. Booth, *Appl. Phys. Lett.* **50**, 293 (1987).
145. A. Yurgens, D. Winkler, T. Claeson, Seong-Ju Hwang, and Jin-Ho Choy, *Int. J. Mod. Phys.* **13**, 3758 (1999).
146. J. P. Carbotte, *Rev. Mod. Phys.* **62**, 1027 (1990).
147. E. Schachinger, J.P. Carbotte, and D.N. Basov, *Europhys. Lett.* **54**, 380 (2001).
148. E. Schachinger and J. P. Carbotte, *Phys. Rev. B* **65**, 064514 (2002).
149. A. Puchkov, D.N. Basov, and T. Timusk, *J. Phys: Condens. Matter* **8**, 10049 (1996).
150. F. Marsiglio, T. Startseva, and J.P. Carbotte, *Phys. Lett. A* **245**, 172 (1998).
151. N. E. Bickers, D. J. Scalapino, and S. R. White, *Phys. Rev. Lett.* **62**, 96 (1989).
152. A. J. Millis, H. Monien, and D. Pines, *Phys. Rev. B* **42**, 167 (1990).
153. C.M. Varma, P.B. Littlewood, S. Schmitt-Rink, E. Abrahams, and A.E. Ruckenstein, *Phys. Rev. Lett.* **63**, 1996 (1989).
154. C.H. Pao and N.E. Bickers, *Phys. Rev. Lett.* **72**, 1870 (1994).
155. P. Monthoux and D.J. Scalapino, *Phys. Rev. Lett.* **72**, 1874 (1994).

156. S. Chakravarty, R.B. Laughlin, D.K. Morr, and C. Nayak, Phys. Rev. B **63**, 094503 (2001).
157. P.D. Johnson, T. Valla, A.V. Fedorov, Z. Yusof, B.O. Wells, Q. Q. Li, A.R. Moodenbaugh, G.D. Gu, N. Koshizuka, C. Kendziora, Sha Jian, and D.G. Hinks, Phys. Rev. Lett. **87**, 177007 (2001).
158. A. Lanza, Arxiv: Condensed Matter/10102227.
159. Z. X. Shen, Arxiv: Condensed Matter/10102244.
160. J. E. Hirsch, Phys. Rev. B **31**, 4403 (1985).
161. J. D. Reger and A. P. Young, Phys. Rev. B **37**, 5978 (1988).
162. D. J. Scalapino and S. R. White, Phys. Rev. **31**, 5978 (2001).
163. S. Sorella, G.B. Martins, F. Becca, C. Gazza, L. Capriotti, A. Parola, and E. Dagotto, Arxiv: Condensed Matter/0110460.
164. D. Poilblanc, J. Riera, and E. Dagotto, Phys. Rev. B **49**, 12318 (1994).
165. P. W. Leung, Arxiv: Condensed Matter/0201031.
166. G. Baskaran, Z. Zou, and P. W. Anderson, Sol. State. Comm. **63**, 973 (1987).
167. T. Senthil and M. P. A. Fisher, Arxiv: Condensed Matter/9910224.
168. V. J. Emery, S. A. Kivelson, and O. Zachar, Phys. Rev. **56**, 6120 (1997).
169. V. Chubukov, D. Pines, and J. Schmalian, Arxiv: Condensed Matter/9910224.
170. D.J. Scalapino, Phys. Reports **250**, 329 (1995).
171. A. Bansil and M. Lindroos, Phys. Rev. Lett. **83**, 5154 (1999).
172. K.J. Chang, M.M. Dacorogna, M.L. Cohen, J.M. Mignot, G. Chouteau, and G. Martinez, Phys. Rev. Lett. **54**, 2375 (1985).
173. Cheng-Zhang Wang, Rici Yu, and H. Krakauer, Phys. Rev. B **59**, 9278 (1999).
174. T. C. Leung, X. W. Wang, and B. N. Harmon, Phys. Rev. B **37**, 384 (1988).
175. V. I. Anisimov, F. Aryasetiawan, and A.I. Lichtenstein, J. Phys.: Condens. Matter **9**, 767 (1997).

176. M.I. Katsnelson and A.I. Lichtenstein, *J. Phys.: Condens. Mat.* **11**, 1037 (1999).
177. A. Georges, G. Kotliar, W. Krauth, and M.J. Rozenberg, *Rev. Mod. Phys.* **68**, 13 (1996).
178. For a recent cluster DMFT application to the Hubbard model and d-wave superconductivity, see A. I. Lichtenstein and M. I. Katsnelson, *Phys. Rev. B* **62**, R9283 (2000).
179. An application of DMFT to ARPES spectra see Th. A. Meier, Th. Pruschke, and M. Jarrell, *cond-mat/0201037*.
180. H. Rietschel and L. J. Sham, *Phys. Rev. B* **28**, 5100 (1983).
181. H. Rietschel, H. Winter, and W. Reichardt, *Phys. Rev. B* **22**, 4284 (1980).
182. Miodrag L. Kulić and Roland Zeyher, *Phys. Rev. B* **49**, 4395 (1994).
183. Z.-X. Cai and Yimei Zhu. 1998: World Scientific.
184. M.E. McHenry and R.A. Sutton, *Prog. Mater. Sci.* **38**, 159 (1994).
185. G. Blatter, M.V. Feigel'man, V.B. Geshkenbein, A.I. Larkin, and V.M. Vinokur, *Revs. Mod. Phys.* **66**, 1125 (1994).
186. *Superconductors Science and Technology*, July 1997. Special issue to mark 10 years of high-T_c superconductivity, .
187. C. Buzea and T. Yamashita, *Superconductor Science and Technology* **14**, R115 (2001).
188. D. Larbaestier, A. Gurevich, D.M. Feldman, and A. Polyanskii, *Nature* **414**, 368 (2001).

BRIEF ATTACHMENT BA

IN THE UNITED STATES PATENT AND TRADEMARK OFFICE

In re Patent Application of

Applicants: Bednorz et al.

Serial No.: 08/479,810

Filed: June 7, 1995

For: NEW SUPERCONDUCTIVE COMPOUNDS HAVING HIGH TRANSITION
TEMPERATURE, METHODS FOR THEIR USE AND PREPARATION

Date: March 1, 2004

Docket: YO987-074BZ

Group Art Unit: 1751

Examiner: M. Kopec

Commissioner for Patents
P.O. Box 1450
Alexandria, VA 22313-1450

FIFTH SUPPLEMENTAL AMENDMENT

Sir:

In response to the Office Action dated February 4, 2000:

ATTACHMENT 43



http://catnyp.nypl.org/search/q

**CATNYP: The Online Catalog of The New York Public Library
The Research Libraries**

ANOTHER SEARCH **START OVER** **EXPORT**

You searched **AUTHOR** **rao** in **Entire**

Limited to: Words in the TITLE "new directions in s"

Call # JSD 88-446
Author Rao, C. N. R. (Chintamani Nagesa Ramachandra), 1934-
Title New directions in solid state chemistry : structure, synthesis, properties, reacr
Rao, J. Gopalakrishnan.
Imprint Cambridge [Cambridgeshire] : New York : Cambridge University Press, 1986

LOCATION	CALL #
Science & Business Lib	JSD 88-446

Location Science & Business Lib
Descript x, 516 p. : ill. ; 23 cm.
Series Cambridge solid state science series
Note Includes index
 Bibliography: p. [475]-503.
Subject Solid state chemistry.
Add'l name Gopalakrishnan, J. (Jagannatha), 1939-

ANOTHER SEARCH **START OVER** **EXPORT**

CATNYP: The Online Catalog of The New York Public Library

Daniel P. Morris, Ph.D.
 Staff Counsel
 IBM Research
 IP Law Department Yorktown
 Tie line: 8-862-3217
 Phone: 914-945-3217
 Fax: 914-945-3281

RECEIPT

IN THE UNITED STATES PATENT AND TRADEMARK OFFICE

In re Patent Application of

Applicants: Bednorz et al.

Serial No.: 08/479,810

Filed: June 7, 1995

For: NEW SUPERCONDUCTIVE COMPOUNDS HAVING HIGH TRANSITION
TEMPERATURE, METHODS FOR THEIR USE AND PREPARATION



Date: March 1, 2004

Docket: YO987-074BZ

Group Art Unit: 1751

Examiner: M. Kopec

Commissioner for Patents
P.O. Box 1450
Alexandria, VA 22313-1450

FIFTH SUPPLEMENTAL AMENDMENT

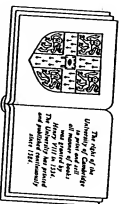
Sir:

In response to the Office Action dated February 4, 2000:

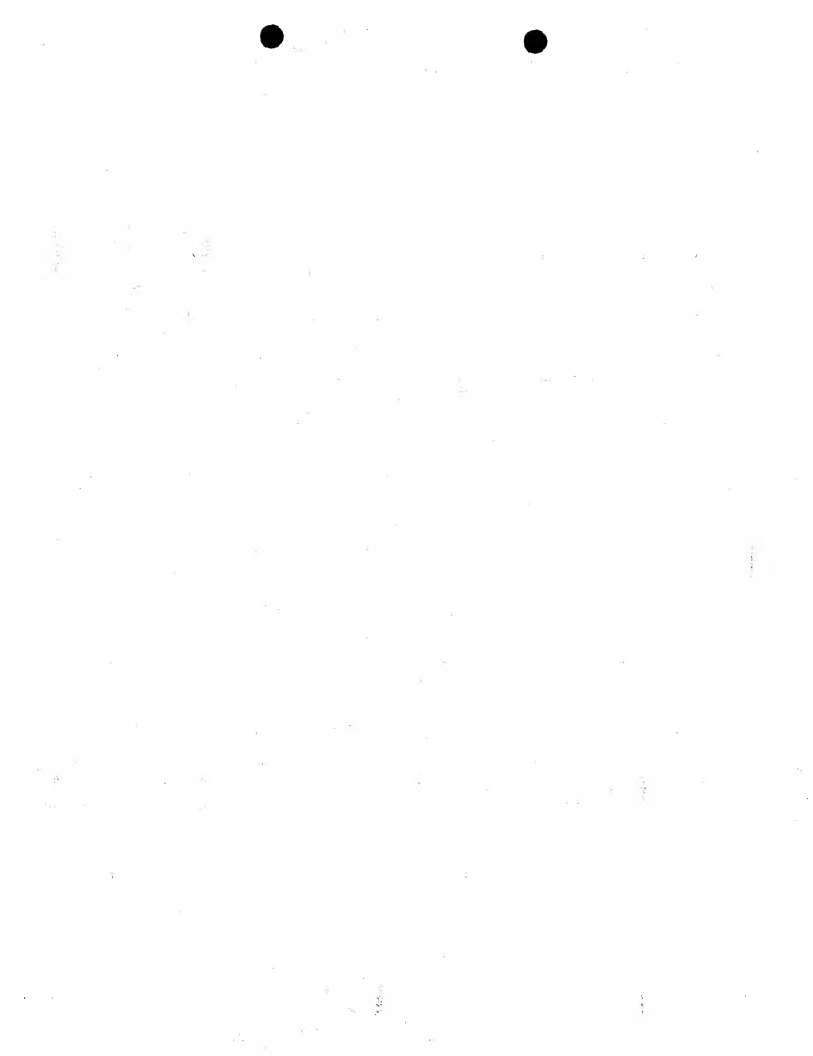
C. N. R. RAO, FRs
J. GOPALAKRISHNAN
*Solid State and Structural Chemistry Unit, Indian Institute of Science,
Bangalore, India*

New directions in solid state chemistry

Structure, synthesis, properties, reactivity
and materials design



CAMBRIDGE UNIVERSITY PRESS
Cambridge
London New York New Rochelle
Melbourne Sydney



bulk metals. Metal particulates (similar to those on the surfaces of supported metal catalysts (Chapter 8)) constitute a type of metal aggregate somewhere between high nuclearity metal clusters and bulk metals.

There are families of metal cluster compounds (Fig. 6.37) containing metal clusters surrounded by ligands (Lewis & Green, 1982). In small cluster compounds, the electrons are paired, but in large clusters there will be closely spaced electronic levels, as in metal particles. In such clusters, quantum size effects would be expected. Benfield *et al.* (1982) have found intrinsic paramagnetism in $H_2O_6(\text{CO})_{12}$ below 70 K as expected of an osmium particle of approximate diameter of 10 Å; the excess paramagnetism increases with cluster size in osmium compounds (Johnson *et al.*, 1985).

Metal cluster compounds simulate surface species produced by the interaction of molecules with metal surfaces (Materies *et al.*, 1979) and this is of value in understanding heterogeneous catalysis. The development of selective catalysts for the C_1 chemical industry employing CO (and possibly CO_2) as the raw material has resulted in major efforts in metal cluster research. Criteria have been developed to distinguish between cluster catalysts and mononuclear catalysis. Typical of the catalysts investigated hitherto are $[\text{Ir}_4(\text{CO})_{12-x}(\text{PPh}_3)_x]$ where $\text{Ph} = \text{phenyl}$ and $x = 1, 2$ or 3.

6.7 Mixed-valence compounds

Chemical compounds consisting of an element (usually a metal) in two different formal oxidation states are said to exhibit mixed valency. Mixed-valence chemistry is as old as chemistry itself, some of the well-known mixed-valence compounds being Prussian blue ($\text{Fe}_4[\text{Fe}(\text{CN})_6]_3 \cdot 14\text{H}_2\text{O}$), magnetite (Fe_3O_4), and heteropoly tungsten and molybdenum blues. Mixed-valence chemistry, however, encompasses a large variety of solids with fascinating properties (Table 6.6) formed by nearly a third of the elements in the periodic table, and there has been a recent upsurge of interest in the subject (Day, 1981). Since variable valency is a prerequisite for mixed valency, it is quite common among the compounds of transition metals, Cu, Eu and Ti, as well as some of the post-transition elements with stable ns^2 and nd^0 electronic configurations such as Ga, Sn, Sb, Ti, Pb and Bi. Most mixed-valency compounds contain electronegative counterpart anions such as halides, oxide, sulphide or molecular ligands containing electronegative atoms. In order for a solid to be called a mixed-valence compound, we should be able to assign definite oxidation states that differ by integral numbers (one or at the most two units) to the element showing mixed valency.

Fe_3O_4 , consisting of iron in the 2⁺ and 3⁺ oxidation states, is a mixed-valence compound, whereas the alloy Nb_3Ge , where we cannot specify the oxidation states of the constituents, is not. We should also make a distinction between the mixed-valence compounds of the Fe_3O_4 type and valence-fluctuating systems such as CeAnd SmS , where a fluctuation in the electron configuration between $4f^7$ and $4f^7 + 1d^1$ occurs (Fallon *et al.*, 1981). (see Section 2.2.7). Electronic properties associated with *heavy fermion behaviour* (e.g. CeCuSi_2 , UPt_3) wherein the carriers exhibit large effective masses (Stewart, 1984).

In certain mixed-valence compounds, the presence of more than one oxidation state can be recognized from the formula, as for example Pb_3O_4 and $\text{V}_6\text{O}_{13-11}$, while in some others the formula indicates an apparently integral oxidation state although the oxidation state is rather unusual for the element in question. Typical examples of the latter category are Sb_2O_3 , BaBiO_3 and $\text{Pb}(\text{NH}_3)_2\text{Cl}_2$; experimental evidence shows that we are not dealing with $\text{Sb}(\text{IV})$, $\text{Bi}(\text{IV})$ and $\text{Pb}(\text{IV})$ states in these compounds but with $\text{Sb}(\text{III})$, V , $\text{Bi}(\text{III})$ and $\text{Pb}(\text{III})$ and these solids should indeed be formulated as $\text{Sb}^{2+}\text{Sb}^{3+}\text{O}_3$, $\text{BaBi}_{0.5}\text{Bi}_{1.5}^{3+}\text{O}_3$ and $[\text{Pb}(\text{NH}_3)_2]^+[\text{PbCl}_3]^{2-}$. In all such systems, X-ray photoelectron

Table 6.6 Typical mixed-valence solids

Compound	Classification in the Robin-Day scheme	Importance
Pb_3O_4	Class I	Red lead
Sb_2O_3	Class I	Mineral cerussite
$\text{Fe}_4[\text{Fe}(\text{CN})_6]_3 \cdot 14\text{H}_2\text{O}$	Class II	Dye and pigment (Prussian blue)
$\text{V}_6\text{O}_{13-11}$	Class II	Semiconductor-metal transitions
$\text{LiNi}_{0.5}\text{Co}_{0.5}\text{O}_2$	Class II	Hopping semiconductor
$\text{La}_2\text{Sb}_2\text{MnO}_7$	Class II	Ferroparamagnetism
$\text{BaBi}_{1-x}\text{Pb}_x\text{O}_3$	Class III	Superconductivity
LiTi_2O_4	Class III	Superconductivity
$\text{K}_2\text{Pt}(\text{CN})_4\text{Br}_{0.38} \cdot 3\text{H}_2\text{O}$	Class III	Molecular metal; Peierls instability
Na_2WO_4	Class III	Bronze lustre and metallic at high x
$\text{M}_x\text{Mo}_6\text{S}_8$	Class III	Superconductivity
Fe_2S_3 , Ferrodioxins	Class III	Electron transfer (enzymes)

spectroscopy can readily identify the presence of mixed valency (Rao *et al.*, 1979).

Robin & Day (1967) have proposed a classification of mixed-valence compounds based on the valence delocalization coefficient, α , the magnitude of which depends on the energy difference between the two states $M^{2+}M^{0+}$ and $M^{1+}M^{1+}$, where A and B are two different sites. When ΔE is large as in Pb_2O_3 , α is small; such compounds belong to class I. If the two sites are similar but crystallographically distinguishable, the compounds are considered to belong to class II. In class III, α becomes large and the two sites occupied by the mixed-valent cations are identical. Properties associated with the mixed-valent classes would be different (Table 6.6). For example, in class I compounds, electron hopping between the sites is not favoured since ΔE is large. In class III compounds, on the other hand, the electrons would be delocalized. The ligands which bridge the cations play a role in determining the intervalence transfer; the greater the metal-ligand overlap, the higher the probability of electron transfer (Mayoh & Day, 1972). In order to describe the electron transfer in mixed-valence compounds properly, one would have to consider the coupling between the electronic and vibrational motions. Experimentally, the frequency of optical intervalence transition gives an estimate of the energy required for thermally activated electron transfer. The intensity of the optical intervalence transition gives information on α . One of the most characteristic features of mixed-valent class II compounds is the structureless broad intervalence absorption band in the visible and infrared. A vibrational coupling model has been developed to calculate the absorption profiles (Phepho *et al.*, 1978); a good example of analysis of such absorption profiles is the recent study of $(CH_3NH_3)_2Sb_2Sn_2Cl_6$ by Prasidas & Day (1984). When the electrons are not completely delocalized and they hop from site to site in marginal semiconductors, the strength of interaction between the electrons and the lattice (polarons) becomes an important factor.

Mixed valency occurs in minerals (e.g. Fe_3O_4), metal-chain compounds, dimers and oligomers and metal complexes, and even in organic and biological systems (Brown, 1980; Day, 1981). Among the dimeric and oligomeric metal complexes exhibiting mixed valency, the pyrazine-bridged Ru (II, III) ammine complex,



synthesized by Creutz & Taube (1973), has received much attention. The important question with regard to this family of complexes is whether they belong to class II or III. With identical ligands around each metal ion, the first impression is to consider the Creutz-Taube complex as belonging to class III. Optical absorption shows an intense band in the visible (550 nm), which is characteristic of Ru(II). It certainly supports the idea that a distinct Ru(II) can be identified on the time scale of optical transition (10^{-14} s). However, the intervalence band centred at ~ 1550 nm is insensitive to solvent effects and a bit too narrow to be called a class II behaviour. XPS shows doublets in the core-level Ru(2d) and (3p) spectra, indicating that the individual oxidation states can be distinguished on this time scale (10^{-15} s) as well. Hush (1975) has argued that the creation of core-hole by photoionization would relax the system into a localized state even if it were originally delocalized; core-shell photoelectron spectroscopy, therefore does not appear to provide the means to determine the extent of localization or delocalization in the valence shell. Infrared spectroscopy has shown that the NH_3 rocking mode (800 cm^{-1}), $Ru-NH_3$ stretching mode (449 cm^{-1}) and Ru -pyrazine stretching mode (316 cm^{-1}) of the Creutz-Taube complex all occur at values intermediate between those of the corresponding Ru(II) and Ru(III) complexes. This has been taken as evidence that the valence electron is delocalized in the time scale of infrared spectroscopy (10^{-12} – 10^{-13} s). Results of the various measurements on this complex are somewhat conflicting because of the different time scales; it appears that the electron-transfer rate is somewhere between 10^6 – 10^{12} s^{-1} . Mixed valency in compounds like $La_{1-x}Sr_xCoO_3$ (Rao *et al.*, 1975, 1977) is determined by rate of electron transfer and so by composition, that is in $MoFe_2O_4$ and other solids resulting from fast electron transfer is discussed (Randall *et al.*, 1985).

In the metal-chain compounds, we can distinguish two types of mixed valent systems, one where the chain is entirely composed of metal atoms (class III) and the other in which the metal and the bridging ligand alternate (class II). Wolfman's red salt, $[PtCl_2(H_2NH_2)_2] [PtCl_2(H_2NH_2)_2Cl_2] \cdot 4H_2O$ is an example of the former, consisting of Pt(II) and Pt(IV) ions bridged by chloride ions. In KCP type of mixed-valent compounds, mixed valency is achieved by partly oxidizing the Pt ions to an average oxidation state $(2+x)$ with $x \approx 0.3$. Partial oxidation is accomplished by removing some of the cations as in $K_{1-x}Pt(CN)_3 \cdot 1.5H_2O$ or by introducing extra anions in $K_2Pt(CN)_3 \cdot 0.3 \cdot 3H_2O$. Even the Hg chain compound $Hg_{1-x}AsF_6$ (see Section 4.9) is mixed-valent.

Fe_3O_4 has the inverse spinel structure, with all the Fe^{2+} ions and half of the Fe^{3+} ions located in octahedral sites (B sites) in the oxygen network and the remaining half of the Fe^{3+} ions located on tetrahedral sites (A sites). It undergoes a ferrimagnetic-paramagnetic transition around 830 K and another transition around $T_V = 123$ K (Verwey transition). The material is a semiconductor both above and below the Verwey transition. Some changes in properties have also been observed near 200 K and 12 K, but these are not very significant. The properties of Fe_3O_4 in the region of the Verwey transition and above have been a subject of great interest, and an entire issue of the *Philosophical Magazine* (B42, No. 10, 1980) was devoted to the transition.

Detailed structural investigations employing neutron diffraction and other techniques suggest that charge ordering of Fe^{2+} and Fe^{3+} ions (and therefore the long-range order) is established below T_V . Cation strings, *a* and *b*, run along the [110] and [110] directions respectively (on alternate (001) planes). While three Fe^{2+} ions in succession are followed by a Fe^{3+} ion along one *a* chain, on an adjacent *a* chain three Fe^{3+} ions are followed by one Fe^{2+} . In the *b* chain, cation ordering occurs with a pair of Fe^{2+} ions followed by a pair of Fe^{3+} ions in alternation. Successive *b*-*a*-*b*-*a* planes are stacked, perpendicular to the *c* axis, in such a way that proximate cations in three successive planes are in groups, forming hexagonal rings of alternate Fe^{2+} and Fe^{3+} ions. All the cations along *b* strings are members of rings and only a quarter of the *a*-string cations are involved in ring formation. The synchronous displacement of three electrons to their nearest-neighbour position inside any ring produces an interchange of Fe^{2+} with Fe^{3+} . A significant fraction of hexagonal rings always exists in the 'inverted' charge configuration, thereby randomizing charge along the *b* strings, but leaving three-quarters of the *a*-chain constituents in an ordered arrangement below T_V . This rationalizes earlier experimental findings that it is the *a*-plane cations which order at low temperatures.

The existence of superstructure lines just above T_V in critical neutron scattering show the detailed investigation of elastic and inelastic neutron scattering show the existence of a soft mode with wave vector $k = (00\frac{1}{2})$ that 'condenses' at $k = (00\frac{1}{2})$. Proceeding from one Fe^{2+} (or from one Fe^{3+}) ion in the *a* plane at $z = \frac{1}{2}$ to the corresponding position in the *a* plane at $z = \frac{3}{2}$, one arrives at the complementary charge (namely, Fe^{3+} or Fe^{2+}) respectively. One has to advance by twice the unit lattice distance along *c* to duplicate the same ionic configuration at $z = \frac{1}{2}$ that prevails at $z = \frac{3}{2}$. Formally, this corresponds to the existence of a charge-density wave (with wave length $\lambda = 2c$) which couples strongly to the corresponding phonon mode with the same wave vector. At the transition, the ordering of the charges (leading to the establishment of the CDW)

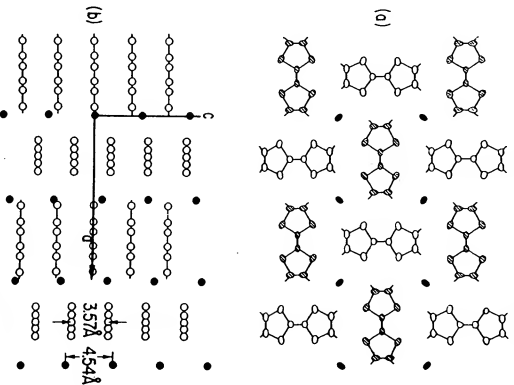
occurs simultaneously with a net atomic displacement that lowers the symmetry.

Although the structural characterization of Fe_3O_4 near the Verwey transition is fairly satisfactory, many finer details are not yet understood. (Honig, 1982, 1986), including the actual structure of the low-temperature phase (rhombohedral, orthorhombic, monoclinic or triclinic). Electrical properties around T_V are also not fully characterized. There is uncertainty regarding the nature of variation of conductivity with temperature. It is not clear whether the inherent character of charge carriers assumed by some workers is valid. Most of the data on transport properties seem to suggest a small polaron model. What is rather puzzling is that the resistivity decreases by two orders of magnitude at T_V , accompanied by the loss of long-range order. Recent studies have shown that the Verwey transition and the associated changes in conductivity and heat capacity are very sensitive to oxygen stoichiometry (Honig, 1986).

There are several interesting families of inorganic mixed-valence compounds that we have not discussed here (see Y'von, 1979; McCarty, 1982). For example, there are metal-cluster compounds such as the Chevrel phases, $\text{M}_6\text{Mo}_6\text{X}_8$ (*X* = S or Se) and condensed metal-cluster chain compounds such as TiMo_3Se_8 , Ti_2Fe_2 , NaMo_6O_6 and $\text{M}_6\text{P}_6\text{O}_6$. TTF halides and TTF-TCNQ complexes (Section 1.9) constitute molecular mixed-valent systems in which the mixed valency is associated with an entire molecule; the charge on TTF in such compounds is non-integral. The structure of TTF- BrO_3 and such solids consists of stacks of TTF molecules parallel to the *c*-axis. The Br^- ions are also arranged in columns parallel to the *c*-axis. However, the repeat distances of the cation (3.57 Å) and anion (4.54 Å) columns are different (Fig. 6.38). The structure is incommensurate along the *c*-axis because the lattice periodicities of the two subunits are not simple multiples (or fractions) of one another. It is important to note that the periodicity of the TTF subunit is independent of stoichiometry, whereas that of the bromide subunit is stoichiometry dependent. Hence the charge transfer in the salt can be expressed as $f = 3.57/(\text{DB})$. Nonstoichiometric compositions in the TTF-halide systems seem to be stabilized because of electrostatic (Madelung) factors. Calculations show that the Madelung energy is maximum around a halogen content of 0.7 to 0.8. Beyond this composition, repulsion between like charges along the stacking axis begins to dominate, decreasing the net binding energy. Optical absorption shows a new peak around 0.7 eV in TTF- BrO_3 . The peak, which is not present in the spectra of stoichiometric salts, has been assigned to a mixed-valence intrastack charge-transfer transition between a neutral TTF and adjacent TTF $^{+}$.

The structure of HMTTF-TCNQ, a typical TTF-TCNQ-type complex, is shown in Fig. 6.9. The segregated stacking in this structure is a characteristic feature of the highly conducting organic charge-transfer system of the TTF-TCNQ family. In HMTTF-TCNQ (HMTTF: hexamethylbenzothia[3,4]valene), the separation between donor molecules is 3.57 Å while that between TCNQ molecules is 3.23 Å along the stacks. To make the anion and cation sublattices com-

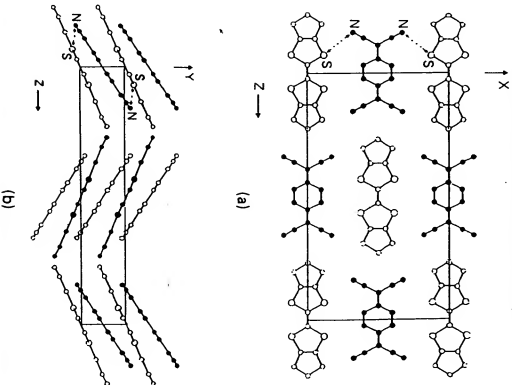
Figure 6.38. Crystal structure of TTF-Br_{0.19}. Projections (a) down the *a*-axis and (b) down the *b*-axis. (After Torrance & Silverman, 1977.)



ment with each other, the molecules are stacked in a staggered configuration such that the normals to the molecular planes are not parallel to the stacking axis but make an angle with it. The angles are different for the donor and acceptor stacks; in the HMTTF-TCNQ structure, the values are respectively 23.8° and 34.2°.

What makes the TTF-TCNQ family distinct from the other salts of TCNQ with cations, such as alkali metals and tetramethylammonium, is

Figure 6.39. Crystal structure of HMTTF-TCNQ. (a) Projection on the plane perpendicular to the stacking axis and (b) projection on a plane containing the stacking axis. (After Greene *et al.*, 1976.)



that the charge transfer, f , in the TTF-TCNQ family is incomplete ($f < 1$). TTF-TCNQ members are also different from the TTF-halides, in the TTF-halides, where the charge on each halide atom is unity, partial charge transfer (mixed valency) is realized by the formation of non-stoichiometric materials, while in the TTF-TCNQ family, the composition is stoichiometric (1:1), but mixed valence arises because of partial electron-transfer.

Evidence for incomplete electron transfer (mixed valency) has come from a number of physical studies. Optical absorption studies show a low energy peak at 0.3 eV, which is not present in insulating salts such as $K^+(TCNQ)^-$. Moreover, the absorption is polarized parallel to the stack axis. The absorption is therefore clearly due to mixed-valence intrastack electronic transition. TTF-TCNQ undergoes a transition from conducting to insulating state at 59 K. This transition is characterized by a subtle periodic modulation of the lattice due to a coupling of the conduction electrons with the lattice (CDW). This shows up in the form of satellite reflections surrounding the Bragg peaks in the diffraction experiment. Because the structure is sinusoidally modulated, the Bragg peaks caused by the average structure remain essentially unchanged. Since the satellite peaks are the result of interaction between conduction electrons and the lattice, their positions are determined by the extent of charge transfer, f ; a value of $f = 0.59$ has been obtained for TTF-TCNQ from the diffraction satellites. A comparison of charge transfer in a variety of TCNQ salts with the reduction potential of cations shows that only those cations with a reduction potential $E_r = 0.0$ to 0.5 V vs. SCE lead to mixed-valence or incomplete transfer (Torrance, 1979). When the potential is too high (perylene, pyrene, anthracene etc.), there is no charge transfer and when it is too low, the transfer is complete.

The effect of f on the conductivity of TCNQ salts can be visualized as follows: for electrical conduction to occur, electrons must move from one TCNQ to another. When the charge transfer is complete, the process can be represented as



which involves creation of a dianion. Understandably the energy involved would be prohibitive and hence TCNQ salts with $f = 1$ are insulators. In the mixed-valence salts, the electrons can move easily along the stack by the process, $TCNQ^- + TCNQ^0 \longrightarrow TCNQ^0 + TCNQ^0$, which does not require creation of dianions. This localized picture is, however, only qualitative. A more accurate description would involve the band model. The relation between mixed-valence and

electrical properties is seen in HMTF-TCNQ and HMTF-TCNQF₄. Both are isostructural but HMTF-TCNQ is metallic, while the tetrafluoro-substituted TCNQ salt is semiconducting; the conductivity of the latter is about seven orders of magnitude less than the former. This difference arises because TCNQF₄ is a much stronger acceptor than TCNQ and hence the charge transfer is complete in HMTF-TCNQF₄.

6.8 Low-dimensional solids

Chemists are by and large preoccupied with three-dimensional structures and most of solid state chemistry deals with three-dimensional solids. However, there has been increasing interest in lower-dimensional solids which show spectacular anisotropy in their properties. One is familiar with graphite that is metallic in two dimensions and a semiconductor in the third dimension; the striking directional differences in the properties of mica(sheet) and asbestos (fibres) are common experience. The platinum chain compound KCP referred to earlier reflects visible light and conducts electrically like a metal only in the chain direction. If one looks at a crystal of KCP with a polaroid oriented so that the electric vector of the light is parallel to the chain axis, it is highly reflecting and copper-coloured; if the polaroid is turned through a right angle, it is pale yellow and transparent like any other ionic crystal. The situation is similar with Wolfram's red salt. Most of the synthetic metals or molecular metals are low-dimensional solids; many of the exotic materials being tried for superconductivity are also low-dimensional (Keller 1975, 1977; Miller & Epstein, 1978; Hatfield, 1978; Alcaeer, 1980; Miller, 1987).

It is convenient to classify low-dimensional solids into two categories, chain (essentially one-dimensional) and layer (essentially two-dimensional). Examples of the chain compounds are KCP and other Pt-chain compounds, polymeric (SN)_x, polycyclopentadiene, Hg₂-AsF₆ with Hg chains, [C(CH₃)₂NMnCl], KCuF₃ and RbFeCl₃. Examples of layer compounds are graphite-related systems, Ti and Nb chalcogenides, K₂NiF₆, (RNH₃)₂MoCl₄ and CoCl₂ ($R = CH_3$, etc., $M = Cr, Mn$ etc.). We shall briefly examine the magnetic, electrical and optical properties as well as phase transitions of typical members of this extraordinary class of materials (Day, 1983; Subramanyam & Nalini, 1985; also see Phil. Trans. Roy. Soc. London 1985, A314).

In understanding the magnetic behaviour of solids it is necessary to take into account not only the dimensionality of the lattice (1 to 3), but also the dimensionality of the spin or of the order parameter (1 to 3), which give rise to nine possible types of magnetic systems. In addition,

BRIEF ATTACHMENT BB

IN THE UNITED STATES PATENT AND TRADEMARK OFFICE

In re Patent Application of

Applicants: Bednorz et al.

Serial No.: 08/479,810

Filed: June 7, 1995

For: NEW SUPERCONDUCTIVE COMPOUNDS HAVING HIGH TRANSITION
TEMPERATURE, METHODS FOR THEIR USE AND PREPARATION

Date: March 1, 2004

Docket: YO987-074BZ

Group Art Unit: 1751

Examiner: M. Kopec

Commissioner for Patents
P.O. Box 1450
Alexandria, VA 22313-1450

FIFTH SUPPLEMENTAL AMENDMENT

Sir:

In response to the Office Action dated February 4, 2000:

ATTACHMENT 49

The following tables give properties of a number of high temperature superconductors. Table 1 lists the crystal structure (space group and lattice constants) and the critical transition temperature T_c for the more important high temperature superconductors so far studied. Table 2 gives energy gap, critical current density, and penetration depth in the superconducting state. Table 3 gives electrical and thermal properties of some of these materials in the normal state. The tables were prepared in November 1992 and updated in November 1994.

REFERENCES

- Ginsburg, D.M., Ed., *Physical Properties of High-Temperature Superconductors*, Vols. I—III, World Scientific, Singapore, 1989—1992.
- Rao, C.N.R., Ed., *Chemistry of High-Temperature Superconductors*, World Scientific, Singapore, 1991.
- Shackelford, J.F., *The CRC Materials Science and Engineering Handbook*, CRC Press, Boca Raton, 1992, 98—99 and 122—123.
- Kaldos, E., Ed., *Materials and Crystallographic Aspects of HT_c Superconductivity*, Kluwer Academic Publ., Dordrecht, The Netherlands, 1992.
- Malik, S.K. and Shah, S.S., Ed., *Physical and Material Properties of High Temperature Superconductors*, Nova Science Publ., Commack, N.Y., 1994.
- Chmaissem, O. et al., *Physica*, C230, 231—238, 1994.
- Antipov, E.V. et al., *Physica*, C215, 1—10, 1993.

Table 1
Structural Parameters and Approximate T_c Values of High-Temperature Superconductors

Material	Structure	T_c/K (maximum value)
1 $\text{La}_2\text{CuO}_{4.8}$	Bmab; $a = 5.355$, $b = 5.401$, $c = 13.15 \text{ \AA}$	39
2 $\text{La}_{2-x}\text{Sr}_x\text{CuO}_4$	14/mmm; $a = 3.779$, $c = 13.23 \text{ \AA}$	35
3 $\text{La}_{2-x}\text{Ce}_x\text{Sr}_y\text{Cu}_2\text{O}_6$	14/mmm; $a = 3.825$, $c = 19.42 \text{ \AA}$	60
4 $\text{YBa}_2\text{Cu}_3\text{O}_7$	Pmmn; $a = 3.821$, $b = 3.885$, $c = 11.676 \text{ \AA}$	93
5 $\text{YBa}_2\text{Cu}_3\text{O}_8$	Amnm; $a = 3.84$, $b = 3.87$, $c = 27.24 \text{ \AA}$	80
6 $\text{Y}_2\text{BaCu}_3\text{O}_{15}$	Amnm; $a = 3.851$, $b = 3.869$, $c = 50.29 \text{ \AA}$	93
7 $\text{Bi}_2\text{Sr}_2\text{CuO}_6$	Amma; $a = 5.362$, $b = 5.374$, $c = 24.622 \text{ \AA}$	10
8 $\text{Bi}_2\text{CaSr}_2\text{Cu}_2\text{O}_8$	A_{2ga} ; $a = 5.409$, $b = 5.420$, $c = 30.93 \text{ \AA}$	92
9 $\text{Bi}_2\text{CaSr}_2\text{Cu}_2\text{O}_{10}$	A_{2ga} ; $a = 5.39$, $b = 5.40$, $c = 37 \text{ \AA}$	110
10 $\text{Bi}_2\text{Sr}_2(\text{La}_{1-x}\text{Ce}_x)_2\text{Cu}_2\text{O}_{10}$	P4/mmm; $a = 3.888$, $c = 17.28 \text{ \AA}$	25
11 $\text{Ti}_2\text{Ba}_2\text{CuO}_6$	A_{2ga} ; $a = 5.468$, $b = 5.472$, $c = 23.238 \text{ \AA}$; 14/mmm; $a = 3.866$, $c = 23.239 \text{ \AA}$	92
12 $\text{Ti}_2\text{CaBa}_2\text{Cu}_2\text{O}_8$	14/mmm; $a = 3.855$, $c = 29.318 \text{ \AA}$	119
13 $\text{Ti}_2\text{Ca}_2\text{Ba}_2\text{Cu}_2\text{O}_{10}$	14/mmm; $a = 3.85$, $c = 35.9 \text{ \AA}$	128
14 $\text{Ti}(\text{BaLa})\text{CuO}_5$	P4/mmm; $a = 3.83$, $c = 9.55 \text{ \AA}$	40
15 $\text{Ti}(\text{SrLa})\text{CuO}_5$	P4/mmm; $a = 3.7$, $c = 9 \text{ \AA}$	40
16 $(\text{Ti}_2\text{PbO}_3)\text{Sr}_2\text{Cu}_2\text{O}_5$	P4/mmm; $a = 3.738$, $c = 9.01 \text{ \AA}$	40
17 $\text{TiCaBa}_2\text{Cu}_2\text{O}_7$	P4/mmm; $a = 3.856$, $c = 12.754 \text{ \AA}$	103
18 $(\text{Ti}_2\text{PbO}_3)\text{CaSr}_2\text{Cu}_2\text{O}_7$	P4/mmm; $a = 3.80$, $c = 12.05 \text{ \AA}$	90
19 $\text{TiSr}_2\text{Y}_2\text{Cu}_2\text{O}_7$	P4/mmm; $a = 3.80$, $c = 12.10 \text{ \AA}$	90
20 $\text{TiCa}_2\text{Ba}_2\text{Cu}_2\text{O}_8$	P4/mmm; $a = 3.853$, $c = 15.913 \text{ \AA}$	110
21 $(\text{Ti}_2\text{PbO}_3)\text{Sr}_2\text{Cu}_2\text{O}_9$	P4/mmm; $a = 3.81$, $c = 15.23 \text{ \AA}$	120
22 $\text{TiBa}_2(\text{La}_{1-x}\text{Ce}_x)_2\text{Cu}_2\text{O}_9$	14/mmm; $a = 3.8$, $c = 29.5 \text{ \AA}$	40
23 $\text{Pb}_2\text{Sr}_2\text{La}_2\text{Cu}_2\text{O}_9$	Cmmm; $a = 5.435$, $b = 5.463$, $c = 15.817 \text{ \AA}$	70
24 $\text{Pb}_2(\text{SrLa})_2\text{Cu}_2\text{O}_6$	P22 ₁ 2; $a = 5.333$, $b = 5.421$, $c = 12.609 \text{ \AA}$	32
25 $(\text{PbCu})\text{Sr}_2(\text{LaCa})\text{Cu}_2\text{O}_7$	P4/mmm; $a = 3.820$, $c = 11.826 \text{ \AA}$	50
26 $(\text{PbCu})(\text{SrEu})(\text{EuCe})\text{Cu}_2\text{O}_7$	14/mmm; $a = 3.837$, $c = 29.01 \text{ \AA}$	25
27 $\text{Nd}_2\text{CeCu}_2\text{O}_7$	14/mmm; $a = 3.95$, $c = 12.07 \text{ \AA}$	30
28 $\text{Ca}_2\text{SrCu}_2\text{O}_7$	P4/mmm; $a = 3.902$, $c = 3.35 \text{ \AA}$	110
29 $\text{Sr}_2\text{NdCu}_2\text{O}_7$	P4/mmm; $a = 3.942$, $c = 3.393 \text{ \AA}$	40
30 $\text{Ba}_2\text{K}_2\text{BiO}_3$	Pmm3m; $a = 4.287 \text{ \AA}$	31
31 $\text{Rb}_2\text{Cu}_2\text{O}_7$	$a = 14.493 \text{ \AA}$	31
32 $\text{NdBa}_2\text{Cu}_2\text{O}_7$	Pmmn; $a = 3.878$, $b = 3.913$, $c = 11.753$	58

HIGH TEMPERATURE SUPERCONDUCTORS (continued)

Table 1
Structural Parameters and Approximate T_c Values of High-Temperature Superconductors
(continued)

Material	Structure	T_c /K (maximum value)
33 SmBaSrCu ₃ O ₇	14/mmm; $a = 3.854$, $c = 11.62$	84
34 EuBaSrCu ₃ O ₇	14/mmm; $a = 3.845$, $c = 11.59$	88
35 GdBaSrCu ₃ O ₇	14/mmm; $a = 3.849$, $c = 11.53$	86
36 DyBaSrCu ₃ O ₇	Pmmn; $a = 3.802$, $b = 3.850$, $c = 11.56$	90
37 HoBaSrCu ₃ O ₇	Pmmn; $a = 3.794$, $b = 3.849$, $c = 11.55$	87
38 ErBaSrCu ₃ O ₇ (multiphase)	Pmmn; $a = 3.787$, $b = 3.846$, $c = 11.54$	82
39 TmBaSrCu ₃ O ₇ (multiphase)	Pmmn; $a = 3.784$, $b = 3.849$, $c = 11.55$	88
40 YBaSrCu ₃ O ₇	Pmmn; $a = 3.803$, $b = 3.842$, $c = 11.54$	84
41 HgBa ₂ Cu ₃ O ₄	14/mmm; $a = 3.878$, $c = 9.507$	94
42 HgBa ₂ CaCu ₃ O ₈ (annealed in O ₂)	14/mmm; $a = 3.862$, $c = 12.705$	127
43 HgBa ₂ Ca ₂ Cu ₃ O ₈	Pmmn; $a = 3.85$, $c = 15.85$	133
44 HgBa ₂ Ca ₃ Cu ₄ O ₁₀	Pmmn; $a = 3.854$, $c = 19.008$	126

Table 2
Superconducting Properties

$J_c(0)$: Critical current density extrapolated to 0 K

λ_{ab} : Penetration depth in a - b plane

k_B : Boltzmann constant

Material	Form	Energy gap (Δ)		$10^{-4} \times J_c$ (0)/A cm ⁻²	λ_{ab}/λ
		$2\Delta_{90}/k_B T_c^*$	$2\Delta_{10}/k_B T_c^*$		
YBa ₂ Cu ₃ O ₇	Single Crystal	5-6	4-5	30 (film)	1400
Bi ₂ Sr ₂ CaCu ₂ O ₈	Single Crystal	8-9	5.5-6.5	2	2700
Tl ₂ Ba ₂ CaCu ₂ O ₈	Ceramic	6-7	4-6	10 (film, 80 K)	2000
La _{2-x} Sr _x CuO ₄ , $x = 0.15$	Ceramic	7-9	4-6		
Nd _{2-x} Ce _x CuO ₄	Ceramic	8	4-5	0.2 (film)	

* Obtained from peak to peak value.

† Obtained from fit to BCS-type relation.

BRIEF ATTACHMENT BC

IN THE UNITED STATES PATENT AND TRADEMARK OFFICE

In re Patent Application of

Applicants: Bednorz et al.

Serial No.: 08/479,810

Filed: June 7, 1995

For: NEW SUPERCONDUCTIVE COMPOUNDS HAVING HIGH TRANSITION
TEMPERATURE, METHODS FOR THEIR USE AND PREPARATION

Date: March 1, 2004

Docket: YO987-074BZ

Group Art Unit: 1751

Examiner: M. Kopec

Commissioner for Patents
P.O. Box 1450
Alexandria, VA 22313-1450

FIFTH SUPPLEMENTAL AMENDMENT

Sir:

In response to the Office Action dated February 4, 2000:

ATTACHMENT 50

ERCONDUCTIVITY

Temperature

Temperature

Temperature

Superconductivity

Physics

conductors

Superconductivity

(ma)

Workshop on Towards the
conductors

ity

Topics — 1st Asia-Pacific

1 Superconductivity

Temperature

Superconductivity

PHYSICAL PROPERTIES OF HIGH TEMPERATURE SUPERCONDUCTORS I

Editor

Donald M. Ginsberg

Professor of Physics

University of Illinois at Urbana-Champaign



World Scientific

Singapore • New Jersey • London • Hong Kong

Published by

World Scientific Publishing Co. Pte. Ltd.
P O Box 128, Farrer Road, Singapore 9128

USA office: World Scientific Publishing Co., Inc.
687 Hartwell Street, Teaneck, NJ 07666, USA

UK office: World Scientific Publishing Co. Pte. Ltd.
73 Lynton Mead, Totteridge, London N20 8DH, England

PHYSICAL PROPERTIES OF HIGH TEMPERATURE SUPERCONDUCTORS I

Copyright © 1989 by World Scientific Publishing Co. Pte. Ltd.

All rights reserved. This book, or parts thereof, may not be reproduced in any form or by any means, electronic or mechanical, including photocopying, recording or any information storage and retrieval system now known or to be invented, without written permission from the Publisher.

ISBN 9971-50-683-1
9971-50-894-X (pbk)

Printed in Singapore by Utopia Press.

537.623

Physic

1989

*This book is de
rised to the big*

537.623

CONTENTS

Preface	vii
Chapter 1: Introduction, History, and Overview of High Temperature Superconductivity <i>D.M. Ginsberg</i>	1
Chapter 2: Thermodynamic Properties, Fluctuations, and Anisotropy of High Temperature Superconductors <i>M.B. Salamon</i>	39
Chapter 3: Macroscopic Magnetic Properties of High Temperature Superconductors <i>A.P. Malozemoff</i>	71
Chapter 4: Neutron Scattering Studies of Structural and Magnetic Excitations in Lamellar Copper Oxides — A Review <i>R.J. Birgeneau and G. Shirane</i>	151
Chapter 5: Normal State Transport and Elastic Properties of High T_c Materials and Related Compounds <i>P.B. Allen, Z. Fisk, and A. Migliori</i>	213
Chapter 6: Rare Earth and Other Substitutions in High Temperature Oxide Superconductors <i>J.T. Markert, Y. Dalichaouch, and M.B. Maple</i>	265
Chapter 7: Infrared Properties of High T_c Superconductors <i>T. Timusk and D.B. Tanner</i>	339
Chapter 8: Raman Scattering in High- T_c Superconductors <i>O. Thomsen and M. Cardona</i>	409
Subject Index	509

PHYSICAL PROPERTIES OF HIGH TEMPERATURE SUPERCONDUCTORS II

Editor

Donald M. Ginsberg

Department of Physics

University of Illinois at Urbana — Champaign



World Scientific

Singapore • New Jersey • London • Hong Kong

Published by

World Scientific Publishing Co. Pte. Ltd.

P O Box 128, Farrer Road, Singapore 9128

USA office: 687 Hartwell Street, Teaneck, NJ 07666

UK office: 73 Lynton Mead, Totteridge, London N20 8DH

*Thi
John*

**PHYSICAL PROPERTIES OF HIGH TEMPERATURE
SUPERCONDUCTORS II**

Copyright © 1990 by World Scientific Publishing Co. Pte. Ltd.

All rights reserved. This book, or parts thereof, may not be reproduced in any form or by any means, electronic or mechanical, including photocopying, recording or any information storage and retrieval system now known or to be invented, without written permission from the Publisher.

ISBN 981-02-0124-9
981-02-0190-7 (pbk)

Printed in Singapore by JBW Printers & Binders Pte. Ltd.

CONTENTS

Preface	vii
Chapter 1. Introduction: A Description of Some New Materials and An Overview of This Book <i>D.M. Ginsberg</i>	1
Chapter 2. Specific Heat of High Temperature Superconductors: A Review <i>A. Junod</i>	13
Chapter 3. Crystal Structures of High-Temperature Superconductors <i>R.M. Hazen</i>	121
Chapter 4. The Microstructure of High-Temperature Oxide Superconductors <i>C.H. Chen</i>	199
Chapter 5. Nuclear Resonance Studies of $\text{YBa}_2\text{Cu}_3\text{O}_{7-\delta}$ <i>C.H. Pennington and C.P. Slichter</i>	269
Chapter 6. Electronic Structure, Surface Properties, and Interface Chemistry of High Temperature Superconductors <i>H.M. Meyer III and J. H. Weaver</i>	369
Chapter 7. The Hall Effect and its Relation to other Transport Phenomena in the Normal State of the High-Temperature Superconductors <i>N.P. Ong</i>	459
Chapter 8. Oxygen Stoichiometric Effects and Related Atomic Substitutions in the High- T_c Cuprates <i>L.H. Greene and B.G. Bagley</i>	509
Chapter 9. The Pairing State of $\text{YBa}_2\text{Cu}_3\text{O}_{7-\delta}$ <i>J.F. Annett, N. Goldenfeld and S.R. Renn</i>	571
Subject Index	687
Appendix A	697
Appendix B	699

BRIEF ATTACHMENT BD

IN THE UNITED STATES PATENT AND TRADEMARK OFFICE

In re Patent Application of

Applicants: Bednorz et al.

Serial No.: 08/479,810

Filed: June 7, 1995

For: NEW SUPERCONDUCTIVE COMPOUNDS HAVING HIGH TRANSITION
TEMPERATURE, METHODS FOR THEIR USE AND PREPARATION

Date: March 1, 2004

Docket: YO987-074BZ

Group Art Unit: 1751

Examiner: M. Kopec

Commissioner for Patents
P.O. Box 1450
Alexandria, VA 22313-1450

FIFTH SUPPLEMENTAL AMENDMENT

Sir:

In response to the Office Action dated February 4, 2000:

ATTACHMENT 51

CHEMISTRY OF HIGH TEMPERATURE SUPERCONDUCTORS

Edited by

C. N. R. RAO, F. R. S.

*CSIR Centre of Excellence in Chemistry and
Solid State and Structural Chemistry Unit
Indian Institute of Science, Bangalore, India*



World Scientific

Singapore • New Jersey • London • Hong Kong

UK office: 73 Lynton Mead, Totteridge, London N20 8DH

All rights reserved. This book, or parts thereof, may not be reproduced in any form by any means, electronic or mechanical, including photocopying, recording or by any information storage and retrieval system now known or to be invented, without written permission from the Publisher.

Printed in Singapore by Utopia Press.

Library

University of Miami

C.N.R.
Ban
Juli

CONTENTS

Preface	v
Crystal Chemistry and Superconductivity in the Copper Oxides <i>J. B. Goodenough and A. Manthiram</i>	1
Defects and Microstructures in Layered Copper Oxides <i>M. Hervieu, B. Domengès, C. Michel, and B. Raveau</i>	57
Important Common Features of the Cuprate Superconductors: Relation Between the Electronic Structure and Superconductivity <i>C. N. R. Rao</i>	87
Design of New Cuprate Superconductors and Prediction of Their Structures <i>Takahisa Arima and Yoshinori Tokura</i>	104
Structure and Superconductivity in Y-123 and Related Compounds <i>G. V. Subba Rao and U. V. Varadaraju</i>	126
Chemistry of Superconducting Bismuth, Thallium and Lead Cuprates <i>J. Gopalakrishnan</i>	156
The Modulation in Bismuth Cuprates and Related Materials <i>J. W. Tarascon, W. R. McKinnon, and Y. LePage</i>	186
Electron-Doped High T_c Cuprate Superconductors <i>Carmen C. Almasan and M. Brian Maple</i>	205
Application of High-Pressure and High Oxygen Pressure to Cu-Oxides <i>M. Takano, Z. Hiroi, M. Azuma, and Y. Takeda</i>	243
Copper-Less Oxide Superconductors <i>A. M. Umarji</i>	267
Synthesis, Structure and Properties of $\text{La}_2\text{NiO}_{4+\delta}$ <i>Douglas J. Buttrey and Jurgen M. Honig</i>	283

Thermodynamics of Y-Ba-Cu-O System and Related Aspects	306
<i>S. F. Pashin and Yu. D. Tretyakov</i>	
Investigation of the Electronic Structure of the Cuprate Superconductors Using High-Energy Spectroscopies	348
<i>D. D. Sarma</i>	
Field Modulated Microwave Absorption in High-Temperature Superconducting Oxides	379
<i>Micky Puri and Larry Kevan</i>	
Grain Alignment and its Effect on Critical Current Properties of $\text{Bi}_2\text{Sr}_2\text{Ca}_1\text{Cu}_2\text{O}_x/\text{Ag}$ Superconducting Tape	399
<i>K. Togano, H. Kumakura, H. Maeda, and J. Kase</i>	
High T_c Superconducting Thin Films - Processing Methods and Properties	411
<i>S. Mohan</i>	
High Temperature Superconductor Thin Films by Pulsed Laser Ablation	454
<i>S. B. Ogale</i>	
Magnetic Properties and Field Modulated Microwave Absorption of $\text{YBa}_2\text{Cu}_3\text{O}_7$ Thin Films	484
<i>C. Schlenker, J. Dumas, C. L. Liu, and S. Revenaz</i>	

Published by

World Scientific Publishing Co. Pte. Ltd.

P O Box 128, Farrer Road, Singapore 9128

USA office: Suite 1B, 1060 Main Street, River Edge, NJ 07661

UK office: 73 Lynton Mead, Totteridge, London N20 8DH

Library of Congress Cataloging-in-Publication Data

Chemistry of high-temperature: superconductors/edited by C.N.R. Rao.

p. cm.

Includes bibliographical references.

ISBN 98 10208057

1. High temperature superconductors. 2. Superconductivity-
Chemistry. 3. Solid state chemistry. I. Rao, C.N.R.
(Chintamani Nagasa Ramachandra), 1934-

QC611.98.H54C47 1991

527.623--dc20

91-32649

CIP

Copyright © 1991 by World Scientific Publishing Co. Pte. Ltd.

All rights reserved. This book, or parts thereof, may not be reproduced in any form or by any means, electronic or mechanical, including photocopying, recording or any information storage and retrieval system now known or to be invented, without written permission from the Publisher.

Printed in Singapore by Utopia Press.

Library

University of Miami

BRIEF ATTACHMENT BE

IN THE UNITED STATES PATENT AND TRADEMARK OFFICE

In re Patent Application of

Applicants: Bednorz et al.

Serial No.: 08/479,810

Filed: June 7, 1995

For: NEW SUPERCONDUCTIVE COMPOUNDS HAVING HIGH TRANSITION
TEMPERATURE, METHODS FOR THEIR USE AND PREPARATION

Date: March 1, 2004

Docket: YO987-074BZ

Group Art Unit: 1751

Examiner: M. Kopec

Commissioner for Patents
P.O. Box 1450
Alexandria, VA 22313-1450

FIFTH SUPPLEMENTAL AMENDMENT

Sir:

In response to the Office Action dated February 4, 2000:

ATTACHMENT 52

BE

The CRC Materials Science and Engineering Handbook

Editor

James F. Shackelford

Professor of Materials Science and Engineering

Division of Materials Science and Engineering

and

Associate Dean of the College of Engineering

University of California, Davis

Associate Editor

William Alexander

Research Engineer

Division of Materials Science and Engineering

University of California, Davis



CRC Press

Boca Raton Ann Arbor London

Library of Congress Cataloging-in-Publication Data

Catalog record is available from the Library of Congress

ISBN 0-8493-4276-7

This book represents information obtained from authentic and highly regarded sources. Reprinted material is quoted with permission, and sources are indicated. A wide variety of references are listed. Every reasonable effort has been made to give reliable data and information, but the author and the publisher cannot assume responsibility for the validity of all materials or for the consequences of their use.

All rights reserved. This book, or any parts thereof, may not be reproduced in any form without written consent from the publisher.

Direct all inquiries to CRC Press, Inc., 2000 Corporate Blvd., N. W., Boca Raton, Florida, 33431.

© 1992 by CRC Press, Inc.

International Standard Book Number 0-8493-4276-7

Printed in the United States 0 1 2 3 4 5 6 7 8 9

TABLE OF CONTENTS

The Elements	1
Elements for Engineering Materials	2
Elements in the Earth's Crust	4
The Periodic Table of The Elements	6
The Metallic Elements	7
The Elements in Ceramic Materials	8
The Elements in Polymeric Materials	9
The Elements in Semiconducting Materials	10
Available Stable Isotopes of the Elements	12
Properties of Selected Elements	20
Melting Points of Selected Elements	26
Densities of Selected Elements	28
Crystal Structure of the Elements	30
Atomic and Ionic Radii of the Elements	34
Atomic Radii of the Elements	39
Ionic Radii of the Elements	41
Selected Properties of Superconductive Elements	43
T_c for Thin Films of Superconductive Elements	44
Engineering Compounds	47
Engineering Ceramics	48
Refractories, Ceramics, and Salts	53
Type II Superconducting Compounds:	
Critical Temperature and Crystal Structure Data	65
High Temperature Superconducting Compounds:	
Critical Temperature and Crystal Structure Data	98
Crystal Structure Types	101
Critical Temperature Data for	
Type II Superconducting Compounds	104
Selected Superconductive Compounds And Alloys:	
Critical Field Data	121
T_c Data for High Temperature Superconducting Compounds	122
Bonding, Thermodynamic, and Kinetic Data	125
Bond Strengths in Diatomic Molecules	
(Listed by Molecule)	126
(Listed by Bond Strength)	135
Bond Strengths of Polyatomic Molecules	
(Listed by Molecule)	144
(Listed by Bond Strength)	147

terial is quoted
has been made
e validity of all

n consent from

Table of Contents (Continued)

Carbon Bond Lengths (Periodic Table Presentation)	150
Carbon Bond Lengths	151
Bond Length Values Between Elements	
(Listed by Bond)	154
(Listed by Bond Length)	156
Bond Angle Values Between Elements	
(Listed by Bond)	158
(Listed by Bond Angle)	159
Heat of Formation of Selected Inorganic Oxides	160
Heats of Sublimation (at 25°C) of Selected Metals	
and their Oxides	173
Melting Points of Selected Elements and Inorganic Compounds	
(Listed by Element or Compound)	174
(Listed by Melting Point)	186
Melting Points of Ceramics	
(Listed by Compound)	198
(Listed by Melting Point)	202
Heat of Fusion For Selected Elements and	
Inorganic Compounds	206
Surface Tension of Liquid Elements	218
Vapor Pressure of the Elements	
(Very Low Pressures)	235
(Moderate Pressures)	237
(High Pressures)	240
Specific Heat of Selected Elements at 25 °C	
(Listed by Element)	243
(Listed by Specific Heat)	248
Heat Capacity of Selected Ceramics	253
Specific Heat of Selected Polymers	255
Phase Change Thermodynamic Properties	
for Selected Elements	260
for Selected Oxides	269
Thermodynamic Coefficients	
Description	281
for Selected Elements	283
for Selected Oxides	292
Thermal Conductivity of Metals	
at Cryogenic Temperatures	305
at 100 to 3000 K	321

Table of Contents (Continued)

Thermal Conductivity of Selected Ceramics	334
Thermal Conductivity of Special Concretes	345
Thermal Conductivity of Cryogenic Insulation and Supports	346
Thermal Conductivity of Selected Polymers	348
Thermal Expansion of Selected Tool Steels	355
Thermal Expansion and Thermal Conductivity of Selected Alloy Cast Irons	356
Thermal Expansion of Selected Ceramics	357
Thermal Expansion Coefficients for Materials used in Integrated Circuits	374
Thermal Expansion of Selected Polymers	376
Values of The Error Function	384
Diffusion in Selected Metallic Systems	385
Diffusivity Values of Metals into Metals	406
Diffusion in some Non-Metallic Systems	416
Diffusion in Semiconductors	417
Temper Designation System for Aluminum Alloys	424
Structure, Compositions, and Phase Diagram Sources	425
The Seven Crystal Systems	426
The Fourteen Bravais Lattices	427
Structure of Selected Ceramics	428
Density of Selected Tool Steels	434
Density of Selected Alloy Cast Irons	435
Density of Selected Ceramics	436
Specific Gravity of Selected Polymers	439
Composition Limits of Selected Tool Steels	450
Composition Limits of Selected Gray Cast Irons	459
Composition Limits of Selected Ductile Irons	464
Composition Ranges for Selected Malleable Irons	468
Composition Ranges for Selected Carbon Steels	470
Composition Ranges for Selected Resulfurized Carbon Steels	475
Composition Ranges for Selected Alloy Steels	478
Composition Ranges for Selected Cast Aluminum Alloys	498
Composition Ranges for Selected Wrought Aluminum Alloys	502
Typical Composition of Selected Glass-Ceramics	506
Phase Diagram Sources	510

Table of Contents (Continued)

Mechanical Properties	511
Mechanical Properties of Selected Tool Steels	512
Tool Steel Softening After 100 Hours for Various Temperatures	518
Mechanical Properties of Selected Gray Cast Irons	519
Mechanical Properties of Selected Ductile Irons	521
Average Mechanical Properties of Treated Ductile Irons	523
Mechanical Properties of Selected Malleable Iron Castings	525
Young's Modulus of Selected Ceramics	528
Modulus of Elasticity in Tension for Selected Polymers	534
Poisson's Ratio for Selected Ceramics	538
Yield Strength of Selected Cast Aluminum Alloys (Listed by Alloy)	541
(Listed by Yield Strength)	544
Yield Strength of Selected Wrought Aluminum Alloys (Listed by Alloy)	547
(Listed by Yield Strength)	555
Yield Strength of Selected Polymers	563
Tensile Strength of Selected Aluminum Casting Alloys (Listed by Alloy)	567
(Listed by Tensile Strength)	570
Tensile Strength of Selected Wrought Aluminum Alloys (Listed by Alloy)	573
(Listed by Tensile Strength)	581
Tensile Strength of Selected Ceramics	589
Tensile Strength of Selected Polymers	593
Total Elongation of Selected Cast Aluminum Alloys (Listed by Alloy)	601
(Listed by Total Elongation)	604
Total Elongation of Selected Polymers	607
Elongation at Yield of Selected Polymers	615
Shear Strength of Selected Wrought Aluminum Alloys (Listed by Alloy)	617
(Listed by Shear Strength)	624
Hardness of Selected Wrought Aluminum Alloys (Listed by Alloy)	631
(Listed by Hardness)	636
Hardness of Selected Ceramics	641
Hardness of Selected Polymers	647

EI

CI

Table of Contents (Continued)

Impact Strength of Selected Polymers	657
Compressive Yield Strength of Selected Polymers	666
Compressive Strength of Selected Polymers	669
Modulus of Elasticity in Flexure of Selected Polymers	674
Flexural Strength of Selected Polymers	683
Fatigue Strength of Selected Wrought Aluminum Alloys (Listed by Alloy)	691
(Listed by Fatigue Strength)	695
Coefficient of Static Friction for Selected Polymers	699
Abrasion Resistance of Selected Polymers	701
Electrical, Magnetic, and Optical Properties	705
Electrical Resistivity of Selected Alloy Cast Irons	706
Resistivity of Selected Ceramics	707
Volume Resistivity of Selected Polymers	713
Dielectric Strength of Selected Polymers	722
Dielectric Constant of Selected Polymers	731
Dissipation Factor for Selected Polymers	740
Arc Resistance of Selected Polymers	751
Dispersion of Optical Materials at 298 K	757
Transmission Range of Glass Ceramics	766
Transparency of Selected Polymers	770
Refractive Index of Selected Polymers	776
Chemical Properties	781
Composition of Sea Water	782
Anions in Sea Water	783
Water Absorption of Selected Polymers	784
Flammability of Selected Polymers	793

BRIEF ATTACHMENT BF

IN THE UNITED STATES PATENT AND TRADEMARK OFFICE

In re Patent Application of

Applicants: Bednorz et al.

Serial No.: 08/479,810

Filed: June 7, 1995

Date: March 1, 2004

Docket: YO987-074BZ

Group Art Unit: 1751

Examiner: M. Kopec

For: NEW SUPERCONDUCTIVE COMPOUNDS HAVING HIGH TRANSITION
TEMPERATURE, METHODS FOR THEIR USE AND PREPARATION

Commissioner for Patents
P.O. Box 1450
Alexandria, VA 22313-1450

FIFTH SUPPLEMENTAL AMENDMENT

Sir:

In response to the Office Action dated February 4, 2000:

ATTACHMENT 53

BF

Materials and Crystallographic Aspects of HT_C-Superconductivity

edited by

E. Kaldis

Laboratorium für Festkörperphysik,
Eidgenössische Technische Hochschule Hönggerberg,
Zürich, Switzerland



Kluwer Academic Publishers

Dordrecht / Boston / London

Published in cooperation with NATO Scientific Affairs Division

Proceedings of the NATO Advanced Study Institute on
Materials and Crystallographic Aspects of HT_C-Superconductivity
Erice, Sicily, Italy
May 17-30, 1993

A C.I.P. Catalogue record for this book is available from the Library of Congress.

ISBN 0-7923-2773-X

Published by Kluwer Academic Publishers,
P.O. Box 17, 3300 AA Dordrecht, The Netherlands.

Kluwer Academic Publishers incorporates the publishing programmes of
D. Reidel, Martinus Nijhoff, Dr W. Junk and MTP Press.

Sold and distributed in the U.S.A. and Canada
by Kluwer Academic Publishers,
101 Philip Drive, Norwell, MA 02061, U.S.A.

In all other countries, sold and distributed
by Kluwer Academic Publishers Group,
P.O. Box 322, 3300 AH Dordrecht, The Netherlands.

Printed on acid-free paper

All Rights Reserved

© 1994 Kluwer Academic Publishers and copyright holders as specified on appropriate pages within

No part of the material protected by this copyright notice may be reproduced or utilized in any form or by any means, electronic or mechanical, including photocopying, recording or by any information storage and retrieval system, without written permission from the copyright owner.

Printed in the Netherlands

TABLE OF

Preface

Part I: Stru

M. Marezio

A classification
between the

A.W. Hewat
Neutron pow
superconduct

T. Egami
Local structu
temperature s

D. Hohlwein
Superstructun

V.I. Simonov
Accurate X-ra
materials

C. Chaillout
Structural and

John B. Good
Electron energ

John B. Good
The system La

John B. Good
The n-type co

TABLE OF CONTENTS

Preface

ix

Part I: Structure and Structure-Properties Relationship

M. Marezio and C. Chaillout

A classification of the copper oxide superconductors and the relationship between the Cu valence and the superconducting properties

3

A.W. Hewat

Neutron powder diffraction on the ILL high flux reactor and high T_c superconductors

17

T. Egami

Local structural distortion: implication to the mechanism of high temperature superconductivity

45

D. Hohlwein

Superstructures in 123 compounds X-ray and neutron diffraction

65

V.I. Simonov

Accurate X-ray structural investigations of single crystals of high- T_c materials

83

C. Chaillout and M. Marezio

Structural and physical properties of superconducting $\text{La}_2\text{CuO}_{4+x}$

129

John B. Goodenough

Electron energies in oxides

145

John B. Goodenough

The system $\text{La}_{2-x}\text{Sr}_x\text{CuO}_4$

161

John B. Goodenough

The n-type copper oxide superconductors

175

<i>Shin-ichi Uchida</i> Charge dynamics in high T_c copper oxides	187	<i>J. Mannhart, J.</i> High- T_c thin film
<i>Y. Maeno</i> Lattice instabilities and superconductivity in La-214 compounds	203	<i>J. Alarco, Yu. E.</i> <i>Z. Ivanov, V.K.</i> <i>J. Ramos, E. St.</i> Engineered grain applications
Part II: Physics of HTSC		
<i>D. Brinkmann</i> Probing crystallographic and materials properties of Y-Ba-Cu-O superconductors by NMR and NQR	225	Part IV: Organ
<i>Z. Schlesinger, R.T. Collins, L.D. Rotter, F. Holtzberg, C. Feild, U. Welp, G.W. Crabtree, J.Z. Liu and Y. Fang</i> Infrared properties of selected high T_c superconductors	249	<i>J. Fink, P. Adeln</i> <i>M. Knupfer, M. A</i> <i>and E. Sohmen</i> High-energy spec superconductors
<i>H. Keller</i> Probing high-temperature superconductivity with positive muons	265	<i>G. van Tendeloo</i> Electron microscop materials and full
<i>T. Schneider</i> Extreme type II superconductors: Universal properties and trends	289	<i>Jack M. Williams,</i> <i>Urs Geiser, John</i> <i>Eugene L. Venturi</i> Structure-property and anion-based (use in the design o
<i>G. Ruani</i> IR-excited Raman spectroscopy on HT $_c$ superconductors	311	Part V: Phase Dis
<i>I. Morgenstern, J.M. Singer, Th. Hußlein and H.-G. Matuttis</i> Numerical simulation of high temperature superconductors	331	<i>J. Karpinski, K. Co</i> <i>and E. Kaldis</i> Phase diagram, syn oxygen pressure P_c
<i>J. Röhler</i> Evidence from EXAFS for an axial oxygen centered lattice instability in $YBa_2Cu_3O_{7.8}$?	353	<i>G.F. Voronin</i> Thermodynamic st
<i>A.M. Hermann, M. Paranthaman and H.M. Duan</i> Single crystal growth and characterization of thallium cuprate superconductors - A review	373	
Part III: Flux Pinning, Pinning Centers, Applications		
<i>P.H. Kes</i> Flux pinning in high-temperature superconductors	401	
<i>M. Murakami</i> Flux pinning of high temperature superconductors and their applications	433	

187	<i>J. Mannhart, J.G. Bednorz, A. Catana, Ch. Gerber and D.G. Schlom</i> High-T _c thin films. Growth modes - structure - applications	453
203	<i>J. Alarco, Yu. Boikov, G. Brorsson, T. Claeson, G. Daalmans, J. Edstam, Z. Ivanov, V.K. Kaplunenko, P.-Å. Nilsson, E. Olsson, H.K. Olsson, J. Ramos, E. Stepanov, A. Tzalenchuk, D. Winkler and Y.-M. Zhang</i> Engineered grain boundary junctions - characteristics, structure, applications	471
225	Part IV: Organic Superconductors	
249	<i>J. Fink, P. Adelman, M. Alexander, K.-P. Bohnen, M.S. Golden, M. Knupfer, M. Merkel, N. Nücker, E. Pellegrin, H. Romberg, M. Roth and E. Soimen</i> High-energy spectroscopic studies of fullerene and cuprate superconductors	493
265	<i>G. van Tendeloo and S. Amelinckx</i> Electron microscopy and the structural studies of superconducting materials and fullerenes	521
289	<i>Jack M. Williams, K. Douglas Carlson, Aravinda M. Kini, H. Hau Wang, Urs Geiser, John A. Schluter, Arthur J. Schultz, James E. Schirber, Eugene L. Venturini, Donald L. Overmyer and Myung-Hwan Whangbo</i> Structure-property relationships in radical-cation (electron-donor molecule) and anion-based (including fullerides) organic superconductors and their use in the design of new materials	539
311	Part V: Phase Diagrams of HTSC	
331	<i>J. Karpinski, K. Conder, Ch. Krüger, H. Schwer I. Mangelschots, E. Jilek and E. Kaldis</i> Phase diagram, synthesis and crystal growth of YBaCuO phases at high oxygen pressure $P_{O_2} < 3000$ bar.	555
353	<i>G.F. Voronin</i> Thermodynamic stability of superconductors in the Y-Ba-Cu-O system	585



BRIEF ATTACHMENT BG

IN THE UNITED STATES PATENT AND TRADEMARK OFFICE

In re Patent Application of

Applicants: Bednorz et al.

Serial No.: 08/479,810

Filed: June 7, 1995

Date: March 1, 2004

Docket: YO987-074BZ

Group Art Unit: 1751

Examiner: M. Kopec

For: NEW SUPERCONDUCTIVE COMPOUNDS HAVING HIGH TRANSITION
TEMPERATURE, METHODS FOR THEIR USE AND PREPARATION

Commissioner for Patents
P.O. Box 1450
Alexandria, VA 22313-1450

FIFTH SUPPLEMENTAL AMENDMENT

Sir:

In response to the Office Action dated February 4, 2000:

ATTACHMENT 54

**PHYSICAL AND MATERIAL
PROPERTIES OF
HIGH TEMPERATURE
SUPERCONDUCTORS**

**Edited by
S.K. Malik and S.S. Shah**

NOVA SCIENCE PUBLISHERS, INC.

Vol. 301

QC
611
.98
H54 P43
1993

Art Director: Christopher Concannon
Graphics: Elenor Kallberg and Maria Ester Hawrys
Book Production: Michael Lyons, Roseann Pena,
Casey Pfalzer, June Martino,
Tammy Sauter, and Michelle Lalo
Circulation: Irene Kwartiroff, Annette Hellingner,
and Benjamin Fung

Library of Congress Cataloging-in-Publication Data

Physical and material properties of high temperature
superconductors / edited by S.K. Malik and S.S. Shah.
p. cm.

Includes bibliographical references and index.
ISBN 1-56072-114-6 : \$145.00

1. High temperature superconductors. 2. High
temperature superconductivity. I. Malik, S.K. II. Shah, S.S.
QC611.98.H54P48 1993 93-8788
537.623-dc20 CIP

© 1994 Nova Science Publishers, Inc.
6080 Jericho Turnpike, Suite 207
Commack, New York 11725
Tele. 516-499-3103 Fax 516-499-3146
E Mail Novasci1@aol.com

All rights reserved. No part of this book may be reproduced,
stored in a retrieval system or transmitted in any form or by any
means: electronic, electrostatic, magnetic, tape, mechanical,
photocopying, recording or otherwise without permission from
the publishers.

Printed in the United States of America

LIBRARY
University Of Miami

Contents

Preface	xi
Chemistry and Superconductivity of $(\text{Ti}, \text{La})(\text{Ba}, \text{Sr}, \text{Ln})_2(\text{Cu}, \text{MO})_{5 \pm \delta}$ 1201 Thallium Cuprates <i>M. Greenblatt and M.-H. Pan</i>	1
Phase Formation and Superconducting Properties of $\text{LnBaSrCu}_3\text{O}_7$ Compounds <i>V. Badri, U.V. Varadaraju, and G.V. Subba Rao</i>	35
Structure and Properties of Electron Superconductors <i>G. Balakrishnan</i>	49
The Influence of Pr and Cm on the Superconducting Properties of High- T_c Oxides <i>L. Soderholm and C.W. Williams</i>	59
Synthesis, Crystal Structure and Physical Properties of the $\text{Pb}_2\text{Sr}_2\text{RCu}_3\text{O}_{8+\delta}$ System <i>J.S. Xue, M. Reedyk and J.E. Greedan</i>	77
Current Directions in the Architecture of High- T_c Superconducting Oxides — A Review <i>Y.V. Yakhtsi and R.M. Iyer</i>	121
Characterization of Superconducting Fullerenes <i>J.D. Thompson, G. Sparr, K. Holczer, O. Klein, G. Gruner, R.B. Kaner, F. Diederich, and R.L. Whetten</i>	139
Transport Properties in Y-Doped Bi- and Tl-Based Superconductors <i>B. Ghosh, A. Poddar, P. Mandal, A.N. Das, and P. Choudhury</i>	149
On the Magnitude of Resistivity in High-Temperature Cuprate Superconductors <i>P. Ganguly</i>	163
Chemical Doping and Charge Balance in High Temperature Superconductors <i>E.E. Alp and S.M. Mini</i>	181

Hidden Aspects of the Valence and Superconductivity
X.Oudet

Valence Fluctuation in Metallic and Superconducting Oxides
M.S. Hegde

Magnetic Ordering in Oxide Superconductors
J.W. Lynn

Rare Earth Magnetism and Superconductivity in $\text{Pr}_{2-x}\text{Ce}_x\text{CuO}_4$ and $\text{Y}_{1-x}\text{Pr}_x\text{Ba}_2\text{Cu}_3\text{O}_{7-\delta}$: A Neutron Scattering Study
C.-K. Loong and L. Soderholm

Magnetism, Superconductivity and Upper Critical Fields in $\text{R}_{1-x}\text{Pr}_x\text{Ba}_2\text{Cu}_3\text{O}_{7-\delta}$ (R = Rare Earth) Compounds
S.K. Malik and C.V. Tommy

Low Temperature Specific Heat and AC-Susceptibility of $\text{REBa}_2\text{Cu}_3\text{O}_{7-\delta}$ (RE = Y, Nd, Eu, Gd, Dy, Ho, Er, Tm and Yb)
H. Kierspel, F. Oster, H. Drössler, U. Callies, H. General, H. Geus, G. Jackel, H.D. Jostardt, J. Langen, A. Waldorf, R. Müller, W. Schlätz, and D. Wohlleben

Fluctuation Diamagnetic Susceptibility in High Temperature Superconductors
R. Srinivasan

Flux-Lattice Melting in High-Temperature Superconductors
K.N. Shrivastava

Reversible Magnetization of Copper Oxide Superconductors in the Mixed State
U. Welp, S. Fleshler, W.K. Kwok, R.A. Klemm, V.M. Vinokur, J. Downey, and G.W. Crabtree

Vibrating Reed Studies of Flux Line Dynamics in Superconductors
Lance E. De Long, Zhigang Xu, Ji-Chang Hou and Joseph Brill

Diffraction from the Flux-Line Lattice in High Temperature Superconductors
D. McKenzie Paul and T. Forgan

	Measurements on Inhomogeneous Magnetic States and Irreversibility Line in Type-I and Type-II Superconductors R. Kumar, S. Ramakrishnan, and A.K. Grover	421
ides	Quantized Lorentz Force, Microwave Absorption and Magnetic Resonance in High Temperature Superconductors K.N. Shrivastava	445
	Crystal Growth and Characterization of Oxide Superconductors S.C. Gadkari, M.K. Gupta, and S.C. Sabharwal	477
xCuO ₄ and	Magnetic Properties in Bi ₂ Sr ₂ CaCu ₂ O _x Single Crystals Ming Xu	497
in	Recent Theories of High T _c Superconductivity K.P. Sinha	529
nd Yb)	Critical Current in High Temperature Superconductors P. Bhattacharyya	541
eral, orf,	Critical State Model for Samples with Non-Zero Demagnetization Factor P. Chaddah and K.V. Bhagwat	557
	High-T _c Josephson Junctions—A Review A.K. Gupta	571
s	Structural, Morphological and Superconducting Properties of the Thin Films of High-T _c Oxide Superconductors Deposited by Pulsed Laser Ablation S.B. Ogale, S.M. Kanetkar, R.D. Vispute, R. Viswanathan, and S.T. Bendre	591
s in the Vinokur,	In-Situ Growth of Superconducting YBa ₂ Cu ₃ O _{7-δ} Thin Films R. Pinto	629
uctors ' Brill	Preparation and Characterization of YBa ₂ Cu ₃ O _{7-δ} Thick Films D.K. Aswal, M.K. Gupta, A.K. Debnath, S.K. Gupta, and S.C. Sabharwal	649

Containerless Melt Processing of $\text{REBa}_2\text{Cu}_3\text{O}_{7-x}$ (RE = Y, Gd, Nd)
High Temperature Superconductors
R.W. McCallum, M.J. Kramer, T.J. Folkerts, S.R. Arrasmith,
B.D. Merkle, S.I. Yoo, Youwen Xu and K.W. Dennis

Fabrication of High T_c Oxide Superconductors
R. Prasad, N.C. Soni, K. Adhikary, and S.K. Malik

Influence of Zn, Ni and Co Substitution on Flux-Pinning and Critical
Current in $\text{YBa}_2\text{Cu}_3\text{O}_{7-5}$
R.G. Kulkarni

Magnetic Resonance Imaging (MRI)—A Programme in Superconductivity
R.S. Chaugule

Subject Index

The idea of a
Temperature Superconductivity
during February
ment of Physics,
by the Department
Institute of Fund
Aurangabad, and Ind

It was decided
in the form of a
Workshop many to
was, therefore, felt
should invite articles
are very happy to

We are indebted
and made it self-sufficient
Science and Technology
Research, Marathwada
Colleges and Industries

S.K. Malik
Data Institute of Physics
Bombay 400 005, 1

S.S. Shah
Marathwada University
Aurangabad 431 001

BRIEF ATTACHMENT BH

IN THE UNITED STATES PATENT AND TRADEMARK OFFICE

In re Patent Application of

Applicants: Bednorz et al.

Serial No.: 08/479,810

Filed: June 7, 1995

For: NEW SUPERCONDUCTIVE COMPOUNDS HAVING HIGH TRANSITION
TEMPERATURE, METHODS FOR THEIR USE AND PREPARATION

Date: March 1, 2004

Docket: YO987-074BZ

Group Art Unit: 1751

Examiner: M. Kopec

Commissioner for Patents
P.O. Box 1450
Alexandria, VA 22313-1450

FIFTH SUPPLEMENTAL AMENDMENT

Sir:

In response to the Office Action dated February 4, 2000:

ATTACHMENT 55

Synthesis and characterization of $\text{HgBa}_2\text{Ca}_{n-1}\text{Cu}_n\text{O}_{2n+2+\delta}$ ($n=1, 2, \text{ and } 3$)

O. Chmaissem, L. Wessels, Z.Z. Sheng *

Department of Physics, and High Density Electronics Center, University of Arkansas, Fayetteville, AR 72701, USA

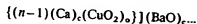
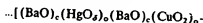
Received 17 May 1994; revised manuscript received 20 June 1994

Abstract

We have successfully prepared the first three members of the mercury-based superconducting compounds $\text{HgBa}_2\text{Ca}_{n-1}\text{Cu}_n\text{O}_{2n+2+\delta}$, namely Hg-1201, Hg-1212 and Hg-1223 with high purity and very good quality. The influence of the synthesis parameters is studied in detail. Using the sealed quartz tube method, very simple procedures are found to ensure a 100% reproducibility of nearly 100% pure Hg-1201 and 85-90% Hg-1212 and Hg-1223. Oxygen annealing of the sample Hg-1201 at 300°C for 18 h results in an enhancement of its critical temperature up to 97 K. The symmetry of the first and second members is tetragonal with lattice parameters $a=3.8831(1)$ Å, $c=9.5357(2)$ Å, and $a=3.8624(1)$ Å, $c=12.7045(2)$ Å, respectively. X-ray diffraction lines of Hg-1223 can be indexed in a tetragonal cell with $a=3.8564(1)$ Å and $c=15.8564(9)$ Å as well as in an orthorhombic cell with lattice parameters $a=5.4537(1)$ Å, $b=5.4247(1)$ Å, and $c=15.8505(7)$ Å.

1. Introduction

Following the discovery of superconductivity with $T_c=94$ K in the one-layer $\text{HgBa}_2\text{CuO}_{4+\delta}$ compound [1], a variety of new mercury cuprates have been synthesized [2-10]. $\text{HgBa}_2\text{CuO}_{4+\delta}$ (Hg-1201) is the first member of the homologous series $\text{HgBa}_2\text{Ca}_{n-1}\text{Cu}_n\text{O}_{2n+2+\delta}$. The $T_{\text{c onset}}$ of the first, second and third members are 94 K, 127 K and 134 K, respectively. $\text{HgBa}_2\text{Ca}_{n-1}\text{Cu}_n\text{O}_{2n+2+\delta}$ are isostructural to the Tl based superconductors $\text{TlBa}_2\text{Ca}_{n-1}\text{Cu}_n\text{O}_{2n+3}$ [11,12] but unlike the thallium compounds the mercury layers are heavily oxygen deficient. The structure of the Hg based superconductors $\text{HgBa}_2\text{Ca}_{n-1}\text{Cu}_n\text{O}_{2n+2+\delta}$ can be described as a sequence of layers:



in which blocks $(\text{BaO})_c(\text{HgO})_o(\text{BaO})_c$ having the rock-salt structure and a thickness of about 5.5 Å alternate with blocks $(\text{CuO}_2)_o\{[(n-1)(\text{Ca})_c(\text{CuO}_2)_o]\}$ having a perovskite-like structure and an approximate thickness $[4.00 + (n-1) \times 3.16]$ Å. The subscripts o and c indicate if the cation is at the origin or at the center of the mesh in each layer. All Hg-1201 [13,14], Hg-1212 [3] and Hg-1223 [15] are found to crystallize with symmetry of space group P4/mmm. An orthorhombic symmetry was also proposed by Meng et al. [16] for Hg-1223.

The research conducted on the thallium-based compounds showed that these materials offer a wide variety of possible substitutions on the different sites of their structures. Many compounds were prepared having their T_c above 100 K. As we mentioned above many new mercury-related compounds were already successfully synthesized with T_c around 100 K. Fur-

* Corresponding author.

thermore, Chu et al. [17] found that under very high pressures of about 150 kbar, the third member Hg-1223 becomes superconducting at 153 K. This result was confirmed by Nunez Regueiro et al. [18] who showed that their Hg-1223 samples if pressed to 235 kbar have a T_c as high as 157 K. As these results have no practical value because of the enormous pressure required, one may speculate that substituting some elements by smaller ions could imitate the effect of the high pressures and increase T_c to much higher values. The search for such new elements of substitution requires a well-controlled synthesis technique.

The synthesis of the Hg-Ba-Ca-Cu-O superconducting compounds of high purity remained a serious challenge until this date. One of the reasons for the fact that the preparation of these materials is so delicate is the decomposition of the mercury oxide HgO at low temperature (between 500 and 600°C), and by consequence, the formation of the superconducting phases is due to the reaction between vapor and solid. Two major methods were used:

- (1) the high-pressure methods in which the decomposition of HgO is slow, and
- (2) the sealed quartz tube methods.

Several groups reported their success in preparing samples of good quality using the sealed quartz tube method. Using this method, many classical synthesis routes were employed. Meng et al. [16] reported the synthesis of the mercury compounds ($n=2$ and 3) using an original method in which the Hg vapor is controlled by the insertion of precursor pellets in the sealed quartz tube together with pellets of nominal composition $\text{HgBa}_x\text{Ca}_{1-x}\text{Cu}_n\text{O}_y$. However, the synthesis of the mercury compounds has proved to be very delicate and requires good control of all the different preparation procedures such as starting materials, heating temperature, heating time, etc. The aim of our work was to study the influence of all these parameters and to find a more convenient method which guarantees to us the high reproducibility of the desired superconducting phases with high purity. We report herein the optimization of the synthesis of samples of good quality and 100% reproducibility using the sealed quartz tube method.

2. Experimental

Several methods were tried before we finally succeeded in synthesizing samples of high purity at 100% reproducibility. Attempts were first made to prepare superconducting samples using the single-step method (mixing the high-purity oxides all together and heating between 750°C and 850°C. The other preparations were all based on the two-step method in which we first prepared precursors of $\text{Ba}_2\text{Ca}_{n-1}\text{Cu}_n\text{O}_x$. The best precursors were those obtained by mixing $\text{Ba}(\text{NO}_3)_2$, CaO and CuO in appropriate amounts corresponding to the stoichiometric formula [19]. The mixture is placed in an alumina crucible and introduced into a preheated furnace at 650°C for 1-2 h, the temperature is then increased to 750°C and maintained for 1-2 h before the temperature is increased to 800-930°C. The sample is heated at this temperature for 16-18 h before being cooled down to room temperature by turning the furnace off. All of the heating cycle is done under a flowing gas of oxygen. The resulting materials are immediately transferred to a dry box. Some of the precursors are pelletized and the remaining powder is mixed with HgO in a molar ratio of 1:1 and then pelletized. Pellets of $\text{Ba}_2\text{Ca}_{n-1}\text{Cu}_n\text{O}_x$ (P) and of $\text{HgBa}_2\text{Ca}_{n-1}\text{Cu}_n\text{O}_{x+2+2s}$ (non-reacted HBCCO) (total weight about 1.8 g) were sealed together in a vacuum quartz tube (0.6 cm inner diameter, 1.0 cm outer diameter, and 8-9 cm long) which was in turn placed in a steel container as a safety precaution against possible explosion and then slowly heated (1-3.5°C/min) to 800-950°C. The temperature was maintained for 3 to 10 h before cooling slowly (1-3.5°C/min.) to 20-600°C. The furnace was then turned off.

The as-prepared samples were subjected to a heating treatment in a flowing gas of oxygen: the samples were introduced into a preheated furnace at 300°C and heated for a period of 18 h. The samples were then pulled out and quenched to room temperature in a dry box.

The samples were characterized using the X-ray diffraction technique, the AC magnetic susceptibility and the resistivity measurements. X-ray experiments were performed on a "Philips 1830" diffractometer with Cu K α radiation and showed that the superconducting phases were the majority phases in all the

samples prepared under the conditions described above together with some impurity phases which may be estimated to be in the order of 5–20%. These impurity phases are mainly CaHgO_2 and CaO . The AC magnetic susceptibility measurements showed that the samples prepared at temperatures above 900°C and the samples heated for more than 10 h were not superconducting. These experiments also showed sharp transitions from the normal state to the superconducting state with ΔT_c in the order of 5 K.

3. Results

3.1. Hg-1201

As the first member of the homologous series $\text{HgBa}_2\text{Ca}_{n-1}(\text{Cu}_2\text{O}_{2n+2+4})$, Hg-1201 does not contain calcium; its synthesis can be done very easily using our procedures with very good quality and a sharp superconducting transition. The precursor was first heated at 750°C (1–2 h) and after the total decomposition of the barium nitrate the temperature was raised to 900°C for 20 h before being pulled out and quenched to room temperature in the dry box. Slow cooling in the furnace gave the same good quality of precursors. The resulting precursor was partially melted and very well crystallized. An appropriate amount of HgO was added to the precursor and pelletized. Pellets of both precursor (P) and non-reacted mixture of HgO +precursor (HBCCO) were sealed together at a weight ratio (P/HBCCO) of 0.48 and slowly heated ($3^\circ\text{C}/\text{min}$) to 810°C maintained for 6 h, and then slowly cooled ($3.5^\circ\text{C}/\text{min}$) to 575°C . The power was then shut off and the furnace was naturally cooled to room temperature.

X-ray diffraction pattern of a Hg-1201 sample prepared under these conditions is presented in Fig. 1 and shows that Hg-1201 is the majority phase (>95%) and that the compound is nearly single phased. The structure is tetragonal with the space group $P4/\text{mmm}$, and there is no evidence of any kind of special extinction. The refined cell parameters of the as-synthesized sample are: $a=3.8831(1) \text{ \AA}$ and $c=9.5357(2) \text{ \AA}$.

AC magnetic susceptibility and resistivity measurements (Fig. 2) performed on Hg-1201 samples show a sharp superconducting transition and a zero

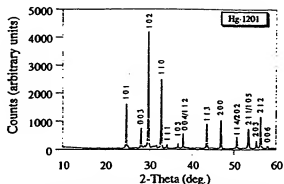


Fig. 1. X-ray diffraction pattern of an as-prepared Hg-1201 sample. The lines are indexed in a tetragonal cell with lattice constants $a=3.8831(1) \text{ \AA}$ and $c=9.5357(2) \text{ \AA}$.

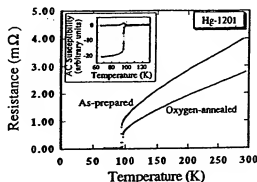


Fig. 2. Resistivity measurements carried out on a Hg-1201 sample. A sharp drop of the resistivity is observed at 94 K in the as-synthesized sample, it increases up to 97 K in the oxygen-annealed sample (300°C , 18 h). AC magnetic measurements (real and imaginary parts) are shown in the inset.

resistance at 94 K. Annealing the sample in O_2 at 300°C for 18 h results in an increase of its critical temperature up to 97 K. The curves presented in Fig. 2 show the resistivity measurements of the as-prepared and the oxygen-annealed sample. The oxygen-annealed samples were checked by X-ray diffraction and found to be remaining intact with no sign of any apparent change in the structure.

3.2. Hg-1212

With the introduction of the calcium into the structure, the synthesis procedures become more del-

icate and special care should be taken in the different stages of the preparation.

Some groups have reported the successful synthesis of Hg-1212 and Hg-1223 using the single-step method [20-24]. However, their procedures included the preparation of fresh oxides of BaO and CaO and the isolation of the sample from the quartz walls by wrapping the materials with a gold or silver foil [21-23] or even by using alumina tubes to be inserted in the quartz tubes [24]. Our experiments using this method were not successful probably because the samples were introduced in the quartz tubes without wrapping. Unlike the preparations based on the two-step method, the samples are rudely reacted with the quartz even at temperature as low as 750°C and the resulting materials were multi-colored powders with no sign of any homogeneity and particularly no superconductivity.

Our Hg-1212 samples were prepared by repeating the same procedures employed for the synthesis of Hg-1201. The purity of the samples was estimated by both the X-ray diffraction patterns and the AC magnetic-susceptibility measurements. We found that samples prepared at temperatures between 825°C and 860°C contain not more than 65% of the superconducting phase Hg-1212. Table 1 shows the dependence of the Hg-1212 volume percentage on the preparation conditions. The best samples were obtained by heating at relatively low temperature 790°C for 10 h. X-ray diffraction pattern and the superconducting properties are shown in Figs. 3 and 4, respectively. Hg-1212 is also tetragonal with lattice param-

eters $a=3.8624(1)$ Å and $c=12.7045(2)$ Å. The T_{onset} of the as-prepared samples is between 110 K and 120 K. Samples annealed in O₂ at 300°C for 18 h have their $T_{\text{c zero R}}$ increased up to 127 K.

3.3. Hg-1223

Ba₂Ca₂Cu₃O₇ precursors were prepared by heating the starting materials at 935°C for 7 h. Details are in the experimental section. The first preparations based on these precursors were partially successful as we were able to obtain a superconducting volume in the order of 60%. However, the superconducting phase was Hg-1212 rather than Hg-1223 (according to the X-ray diffraction patterns). Table 2 shows two sets of experiments with detailed synthesis conditions of Hg-1212 from nominal 1223 composition. The upper part of the table concerns the preparations in which the weight ratio P/HBCCO=0. The introduced pellets were only those with the nominal composition Hg_{0.8}Ba₂Ca₂Cu₃O₇, assuming that the prepared precursors had their initial composition. The mercury oxide was added in excess to the stoichiometric formula in order to compensate the loss resulting from its reaction with the quartz tube. In the lower part of the table are presented the experiments of the Hg controlled vapor by using the method described in the experimental section with the weight ratio P/HBCCO>0. In these preparations the estimated superconducting volume (Hg-1212) is ranging between 0 and 60%. These estimations are based on the X-ray diffraction patterns which also showed

Table 1

Selected experiments carried out for the preparation of Hg-1212. The nominal composition of the precursors used in these experiments is Ba₂CaCu₂O₇. Column 2 gives the weight ratio Precursor/HgBa₂CaCu₂O₇.

Name	Weight ratio	Heating rate (°C/min)	Cooling rate (°C/min)	Temp. (°C)	Time (h)	Hg-1212 vol. (%)
ch26	0.386	3	2→565°C	825	6	65
ch27	0.412	3	2→565°C	845	8	65
ch28	0.388	2.5	1→515°C	860	5	25
ch30	0.257	3	2→515°C	835	6	65
ch31	0.184	3	2→515°C	835	6	65
ch32	0.314	3	2→515°C	835	6	65
ch33	0.398	2	1→565°C	835	6	55
ch34	0.325	2	1→565°C	835	6	50
ch35	0.410	3	2→565°C	790	10	85
ch36	0.210	3	2→565°C	790	10	25

2) Å. The
vein 110 K
0°C for 18

l by heating
etails are in
rtions based
ssful as we
lume in the
cting phase
rding to the
ws two sets
nditions of
on. The up-
parations in
The intro-
minal com-
at the pre-
ssion. The
he stoichio-
the loss re-
tute. In the
experiments
method de-
the weight
ons the esti-
12) is rang-
ns are based
also showed

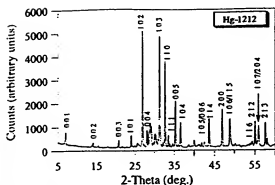


Fig. 3. X-ray diffraction pattern of an as-prepared Hg-1212 sample. The diffraction lines are indexed in a tetragonal cell with the lattice parameters $a = 3.8624(1)$ Å and $c = 12.7045(2)$ Å.

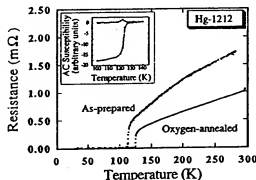


Fig. 4. Resistivity measurements of a sample Hg-1212. The figure shows clearly the increase of the T_{onset} from 117 K (as-synthesized sample) to 127 K (oxygen-annealed sample). The inset shows the AC magnetic measurements (real and imaginary parts) performed on an oxygen-annealed sample.

that the impurity phases are CaHgO_2 and CaO , with traces of a weak unknown phase. It is clear from the table that the formation of the superconducting phase is favored by the presence of the precursor pellets. The highest superconducting volume is obtained when heating to temperatures close to 850°C . At 870°C the sample (ch11) is still superconducting but with a decreased volume down to 40% and the sample is partially melted, indicating that preparations above this temperature could not be carried out successfully.

This work was carried out simultaneously with attempts to synthesize the fourth member of the mercury-based series, namely Hg-1234. The first results showed that the superconducting phase obtained with precursors assumed to be $\text{Ba}_2\text{Ca}_3\text{Cu}_4\text{O}_9$ (234) was

Hg-1223. By consequence, we started a new series of experiments based on the 234 precursors for the synthesis of Hg-1223.

Nominal $\text{Hg}_x\text{Ba}_y\text{Ca}_z\text{Cu}_w\text{O}_9$ pellets and $\text{Ba}_2\text{Ca}_3\text{Cu}_4\text{O}_9$ pellets were sealed together and treated as described in Table 3. Very good Hg-1223 samples with a volume $\approx 90\%$ were obtained with temperatures between 870°C and 885°C . The samples prepared at 900°C were partially melted and presented only 30 to 40% superconducting volume (samples ch2 and ch5), a longer reaction time at this temperature results in the destruction of the superconducting phase (sample ch19). The reproducibility of the Hg-1223 phase using these procedures is 100%. Using precursors obtained from different batches and following the same conditions given in Table 3 gave 90% Hg-1223 at each time. Together with the superconducting pellets were found drops of mercury inside the closed quartz tube.

X-ray diffraction pattern is given in Fig. 5 which shows the good quality of our Hg-1223 sample. Based on the tetragonal symmetry [4,15] of space group $P4/mmm$, the refined lattice parameters were found to be $a = 3.8564(1)$ Å and $c = 15.8564(9)$ Å. During indexing the diffraction pattern we found that many peaks were doubled and cannot all be indexed in the tetragonal symmetry, indicating that the symmetry might be orthorhombic. Refinements in an orthorhombic cell were equally successful and the doubled strong lines were all indexed in a unit cell of lattice parameters $a = 5.4537(1)$ Å, $b = 5.4247(1)$ Å and $c = 15.8505(7)$ Å.

The AC magnetic susceptibility and the resistivity measurements for a Hg-1223 phasic sample are given in Fig. 6. The T_{onset} is around 105 K for the as-prepared samples. A T_{onset} of 135 K can be easily obtained by following the same annealing treatment performed on Hg-1201 and Hg-1212 (O_2 , 300°C , 18 h). The resistivity measurement shows a sharp transition at 135 K and a zero resistance is achieved around 134 K.

4. Discussion

As we stated above, the preparation of Hg-1201, Hg-1212, and Hg-1223 was carried out using the sealed quartz tube method. The insertion of

se experiments

1212
(%)

Table 2

Selected preparation conditions of samples in the phase-formation experiments. The resultant superconducting phase is Hg-1212, and the nominal composition of the precursors is $\text{Ba}_2\text{Ca}_x\text{Cu}_2\text{O}_y$. Column 2 gives the weight ratio Precursor/ $\text{Hg}_8\text{Ba}_2\text{Ca}_x\text{Cu}_2\text{O}_y$, where $x=1$ for the preparation marked with an asterisk and $x=1.5$ for all the other preparations

Name	Weight ratio	Heating rate ($^{\circ}\text{C}/\text{min}$)	Cooling rate ($^{\circ}\text{C}/\text{min}$)	Temp. ($^{\circ}\text{C}$)	Time (h)	Hg-1212 vol. (%)
Hg1*	0	4	1.5 \rightarrow room temp.	800	8	0
Hg2	0	30	power shut off	850	7	7
Hg3	0	preheated furnace	power shut off	750	7	2
hg12	0	1.5	power shut off	860	8	6
hg16	0	3.5	power shut off	850	5	10
hg11	0.33	4.5	power shut off	850	5	55
hg13	0.35	4.5	power shut off	850	5	55
hg14	0.50	3.5	power shut off	830	5	50
hg15	0.40	2.5	power shut off	850	5	55
hg17	0.26	2.5	power shut off	850	8	65
ch11	0.40	3.5	power shut off	870	5	40

Table 3

Selected experiments carried out for the preparation of Hg-1223. The nominal composition of the precursors used in these experiments is $\text{Ba}_2\text{Ca}_x\text{Cu}_2\text{O}_y$. Column 2 gives the weight ratio Precursor/ $\text{Hg}_8\text{Ba}_2\text{Ca}_x\text{Cu}_2\text{O}_y$, where $x=1.5$ for the preparations marked with an asterisk and $x=1.0$ for all the other preparations

Name	Weight ratio	Heating rate ($^{\circ}\text{C}/\text{min}$)	Cooling rate ($^{\circ}\text{C}/\text{min}$)	Temp. ($^{\circ}\text{C}$)	Time (h)	Hg-1223 vol. (%)
ch14	0	1.5	1.0 \rightarrow room temp.	870	5	50
ch10	0.40	3.5	2.5 \rightarrow 600 $^{\circ}\text{C}$	870	5	90
ch15	0.40	3.5	2.5 \rightarrow 600 $^{\circ}\text{C}$	870	5	90
ch16	0.40	3.5	2.5 \rightarrow 600 $^{\circ}\text{C}$	870	5	90
ch13	0.40	3.5	1.5 \rightarrow 550 $^{\circ}\text{C}$	870	5	90
ch17	0.40	3.5	2.5 \rightarrow 600 $^{\circ}\text{C}$	880	8	90
ch18	0.38	3.5	2.5 \rightarrow room temp.	885	5	90
ch19	0.49	1.0	1.0 \rightarrow room temp.	900	10	0
ch4*	0.41	2.5	power shut off	880	10	0
hg1*	0.39	2.5	power shut off	870	8	65
hg3*	0.35	2.5	power shut off	900	5	40
ch2*	0.40	2.5	2.5 \rightarrow 140 $^{\circ}\text{C}$	900	10	40
ch3*	0.42	2.5	power shut off	950	3	0
ch5*	0.40	1.0	power shut off	900	3	30

$\text{Ba}_2\text{Ca}_{n-1}\text{Cu}_n\text{O}_y$ pellets (P) together with $\text{Hg-Ba}_2\text{Ca}_{n-1}\text{Cu}_n\text{O}_y$ pellets (HBCCO) in the sealed quartz tubes suggests that the total amount of the material inside the tube is mercury deficient. Surprisingly, drops of mercury were observed in almost all the experiments. The formation of Hg-1212 instead of Hg-1223 from nominal 1223 composition and the formation of Hg-1223 instead of Hg-1234 from nominal 1234 composition mean that there are some calcium and copper left. CaHgO_2 was observed as the major impurity phase and there are negligible traces

of CuO and its related compounds. One may speculate that the copper and the mercury cations are mixed. The substitution of Cu for 8% Hg was observed by Wagner et al. [13] in their Hg-1201 sample. As a consequence, they found additional extra oxygen atoms on the edges of the mercury layer ($\frac{1}{2}, 0, z$) together with the already existing extra oxygen atoms at ($\frac{1}{2}, \frac{1}{2}, 0$). In the first, second, third and fifth member of the mercury-based series the mercury atoms are found to have an unusually high temperature factor [14,15,25-27]. This can be reduced to a more

base is Hg-1212, and
 Cu_2O_x where $x=1$ for
 n.

Hg-1212 vol. (%)	
0	
7	
2	
6	
10	
55	
55	
50	
55	
65	
40	

in these experiments
 uted with an asterisk

Hg-1223 vol. (%)	
50	
90	
90	
90	
90	
90	
0	
0	
65	
40	
40	
0	
30	

One may specu-
 cations are
 8% Hg was ob-
 air Hg-1201 sam-
 additional extra
 mercury layer ($\frac{1}{2}$
 ing extra oxygen
 d, third and fifth
 s the mercury at-
 high temperature
 educed to a more

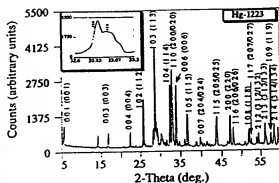


Fig. 5. X-ray diffraction pattern of an as-prepared Hg-1223 sample. The diffraction lines are indexed in both tetragonal cell with lattice constants $a=3.8564(1)$ Å and $c=15.8565(9)$ Å and orthorhombic cell (in parentheses) with lattice constants $a=5.4537(1)$ Å, $b=5.4247(1)$ Å and $c=15.8505(7)$ Å. The inset shows the splitting of the line (110) (tetragonal symmetry) into two lines, 200 and 020 (orthorhombic symmetry).

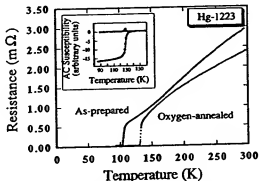


Fig. 6. Resistivity measurements carried out on both as-synthesized and oxygen-annealed Hg-1223 samples. The $T_{c, \text{onset}}$ (originally 105 K) is increased up to 135 K. The curve shows a sharp transition around 135 K with a zero resistance at about 134 K. The real and imaginary parts of the AC magnetic-susceptibility measurements carried out on an oxygen-annealed sample are shown in the inset.

reasonable value by mixing the mercury cations with atoms like copper for example. This possibility was investigated but not proved. The successful preparation of nearly "100%" pure Hg-1201 samples using our method where the mercury cations enclosed in the quartz tube present only 0.57 mole to 1 mole of the precursor $\text{Ba}_2\text{CuO}_{3+x}$ confirms that the mixing of Cu and Hg is very possible. The increase of $T_{c, \text{onset}}$ (97 K) might be due to this mixing. However, this conclusion must be interpreted with some caution. A

molar ratio Hg/Cu of 0.57 seems to be rather small compared to 0.85 found by Wagner et al. Even though our sample looks pure using the X-ray diffraction technique, it might not really be the case. An undetectable (by X-rays) amorphous Ba-Cu-O substance could exist in the powder as well. Such observation was reported by Dolhert et al. [28] who studied the low detectability of excess yttrium and barium in $\text{YBa}_2\text{Cu}_3\text{O}_x$ by X-ray diffraction. Thus the X-ray "pure" sample may not be actually very pure. However, the formation of $(\text{Hg}, \text{Cu})\text{Ba}_2\text{Ca}_{n-1}\text{Cu}_n\text{O}_{2n+2+x}$ is possible and seems to be dependent on the preparation conditions. More details need to be studied. As the X-rays are not too sensitive to the oxygen anions, neutron experiments are needed to determine the value of the extra oxygen atoms and their location and to confirm the occupancy of the mercury sites and also to investigate the possibility of any change in the structure.

Our Hg-1223 phase is very likely to be orthorhombic. The orthorhombicity of our samples is observed by the splitting of some of the X-ray diffraction lines. The possibility of the coexistence of two phases with very high rate of overlapped lines would suggest that these two phases are both members of the mercury-based series and by consequence we must be able to observe at least two well-defined superconducting transitions in our measurements. As this was not the case and as the lines (001) are singles and not split we may conclude that our Hg-1223 phase is orthorhombic. The refined cell parameters are in good agreement with those reported by Meng et al. [16] and Huang et al. [29] for their orthorhombic samples.

Acknowledgements

We thank John Shultz for his assistance in powder X-ray diffraction. This work was supported by the Advanced Research Projects Agency and the Arkansas Energy Office, USA.

References

- [1] S.N. Putilin, E.V. Antipov, O. Chmaissem and M. Marzorio, *Nature* (London) 362 (1993) 226.

- [2] A. Shilling, M. Cantoni, J.D. Guo and M.R. Ott, *Nature* (London) 363 (1993) 56.
- [3] S.N. Putlin, E.V. Antipov and M. Marezio, *Physica C* 212 (1993) 266.
- [4] E.V. Antipov, S.M. Loureiro, C. Chaillout, J.J. Capponi, P. Bordet, J.L. Tholence, S.N. Putlin and M. Marezio, *Physica C* 215 (1993) 1.
- [5] C. Martin, M. Huve, G. Van Tendeloo, A. Maignan, C. Michel, M. Hervieu and B. Raveau, *Physica C* 212 (1993) 274.
- [6] A. Maignan, C. Michel, G. Van Tendeloo, M. Hervieu and B. Raveau, *Physica C* 216 (1993) 1.
- [7] R.S. Liu, D.S. Shy, S.F. Hu and D.A. Jefferson, *Physica C* 216 (1993) 237.
- [8] F. Goutenoire, P. Daniel, M. Hervieu, G. Van Tendeloo, C. Michel, A. Maignan and B. Raveau, *Physica C* 216 (1993) 243.
- [9] D. Pelloquin, M. Hervieu, C. Michel, G. Van Tendeloo, A. Maignan and B. Raveau, *Physica C* 216 (1993) 257.
- [10] M. Hervieu, G. Van Tendeloo, A. Maignan, C. Michel, F. Goutenoire and B. Raveau, *Physica C* 216 (1993) 264.
- [11] Z.Z. Sheng and A.M. Hermann, *Nature* (London) 332 (1988) 55.
- [12] Z.Z. Sheng and A.M. Hermann, *Nature* (London) 332 (1988) 138.
- [13] J.L. Wagner, P.G. Radaelli, D.G. Hinks, J.D. Jorgensen, J.F. Mitchell, B. Dabrowski, G.S. Knapp and M.A. Beno, *Physica C* 210 (1993) 447.
- [14] O. Chmaissem, Q. Huang, S.N. Putlin, M. Marezio and A. Santoro, *Physica C* 212 (1993) 259.
- [15] O. Chmaissem, Q. Huang, E.V. Antipov, S.N. Putlin, M. Marezio, S.M. Loureiro, J.J. Capponi, J.L. Tholence and A. Santoro, *Physica C* 217 (1993) 265.
- [16] R.L. Meng, L. Beauvais, X.N. Zhang, Z.J. Huang, Y.Y. Sun, Y.Y. Xue and C.W. Chu, *Physica C* 216 (1993) 21.
- [17] C.W. Chu, L. Gao, F. Chen, Z.J. Huang, R.L. Meng and Y.Y. Xue, *Nature* (London) 365 (1993) 323.
- [18] M. Nunez-Regueiro, J.L. Tholence, E.V. Antipov, J.J. Capponi and M. Marezio, *Science* 262 (1993) 97.
- [19] Z.Z. Sheng, Y.F. Li and K.C. Goretta, *Mod. Phys. Lett. B*, to be published.
- [20] P.G. Radaelli, J.L. Wagner, B.A. Hunter, B.A. Beno, G.S. Knapp, J.D. Jorgensen and D.G. Hinks, *Physica C* 216 (1993) 29.
- [21] M. Itoh, A. Tokiwa-Yamamoto, S. Adachi and H. Yamauchi, *Physica C* 212 (1993) 271.
- [22] A. Tokiwa-Yamamoto, K. Isawa, M. Itoh, S. Adachi and H. Yamauchi, *Physica C* 216 (1993) 250.
- [23] W.J. Zhu, Y.Z. Huang, L.Q. Chen, C. Doag, B. Yin and Z.X. Zhao, *Physica C* 218 (1993) 5.
- [24] M. Paranthaman, *Physica C* 222 (1994) 7.
- [25] S.M. Loureiro, E.V. Antipov, J.L. Tholence, J.J. Capponi, O. Chmaissem, Q. Huang and M. Marezio, *Physica C* 17 (1993) 253.
- [26] E.V. Antipov, J.J. Capponi, C. Chaillout, O. Chmaissem, S.M. Loureiro, M. Marezio, S.N. Putlin, A. Santoro and J.L. Tholence, *Physica C* 218 (1993) 348.
- [27] Q. Huang, O. Chmaissem, J.J. Capponi, C. Chaillout, M. Marezio, J.L. Tholence and A. Santoro, *Physica C* 227 (1994) 1.
- [28] L.E. Dolther and N.D. Spencer, *Mater. Lett.* 9 (1990) 537.
- [29] Z.J. Huang, R.L. Meng, X.D. Qiu, Y.Y. Sun, J. Kulik, Y.Y. Xue and C.W. Chu, *Physica C* 217 (1993) 1.

The synthesis and characterization of the $\text{HgBa}_2\text{Ca}_2\text{Cu}_3\text{O}_{8+\delta}$ and $\text{HgBa}_2\text{Ca}_3\text{Cu}_4\text{O}_{10+\delta}$ phases

E.V. Antipov ^{a,b}, S.M. Loureiro ^b, C. Chaillout ^b, J.J. Capponi ^b, P. Bordet ^b, J.L. Tholence ^c, S.N. Putilin ^a and M. Marezio ^{b,d}

^a Department of Chemistry, Moscow State University, 119899 Moscow, Russian Federation

^b Laboratoire de Cristallographie CNRS-UJF, BP 166, 38042 Grenoble Cedex 09, France

^c CRTBT, CNRS-UJF, BP 166, 38042 Grenoble Cedex 09, France

^d AT&T Bell Laboratories, Murray Hill, NJ 07974, USA

Received 28 June 1993

Revised manuscript received 9 July 1993

The third (Hg-1223) and the fourth (Hg-1234) members of the recently-discovered homologous series $\text{Hg-Ba}_2\text{Ca}_{n-1}\text{Cu}_n\text{O}_{2n+2+\delta}$ have been synthesized by solid state reaction, carried out at 950°C under 50 kbar at different annealing times. These phases have a tetragonal cell with lattice parameters: $a=3.8532(6)$ Å, $c=15.818(2)$ Å and $a=3.8540(3)$ Å, $c=19.006(3)$ Å, respectively. The c parameters are in agreement with the formula $c \approx 9.5 + 3.2(n-1)$. Electron microscopy study showed similar lattice parameters as well as the occurrence of different intergrowths and stacking faults. A periodicity of 22 Å has also been detected, which may be attributed to the existence of the Hg-1245 phase. EDS analysis data of several grains of Hg-1223 and Hg-1234 are in agreement with the proposed chemical formulae. AC susceptibility measurements show that an increase of the superconducting transition temperature with n in the $\text{Hg-Ba}_2\text{Ca}_{n-1}\text{Cu}_n\text{O}_{2n+2+\delta}$ series occurs till the third member, after which a saturation seems to be achieved.

1. Introduction

Superconductivity at about 94 K and well above 120 K has been recently reported for $\text{HgBa}_2\text{CuO}_{4+\delta}$ (Hg-1201) [1] and $\text{HgBa}_2\text{CaCu}_2\text{O}_{6+\delta}$ (Hg-1212) [2], respectively. These phases are the first and the second members of the Hg-based homologous series of layered Cu mixed oxides. Their structures contain rock-salt-like slabs, such as $(\text{BaO})(\text{HgO}_2)(\text{BaO})$ alternating with either one (CuO_2) layer in the former or an anion-deficient perovskite-like slab, such as $(\text{CuO}_2)(\text{CaE})(\text{CuO}_2)$, in the latter. A superconducting transition temperature as high as 133 K has been reported for a multiphase sample in the Hg-Ba-Ca-Cu-O system by Schilling et al. [4]. These authors could not identify by X-ray diffraction the phases responsible for the superconductivity at this temperature, but proved by high resolution electron microscopy that the sample contained the Hg-1212 and Hg-1223 phases as well as different intergrowths. Putilin et al. [2] showed that in the sample

containing Hg-1212 as the majority phase, a small drop on the AC susceptibility curve versus T occurred at about 132 K which could be attributed to the third member of the Hg-bearing series.

Putilin et al. also showed [2] that it was possible to synthesize the Hg-1212 phase, practically in pure form, under high pressure (40–60 kbar) and at 800°C for about 1 h. The high pressure synthesis allows one to lower the mercury oxide decomposition. This decomposition occurs at ambient pressure at a temperature at which the reactivity of the other components is very low. It was suggested that the same technique could be used for obtaining the higher members of the series. We found that the reactions have to be carried out at higher temperatures (950°C) and for longer annealing times. The same occurs for the higher members of the Bi- or Tl-based Cu oxide series, which are formed by the formation, at the initial stages of the reaction, of the lower members of the corresponding families. We report herein the synthesis and characterization of the Hg-

$\text{Ba}_2\text{Ca}_2\text{Cu}_3\text{O}_{8+x}$ (Hg-1223) and $\text{HgBa}_2\text{Ca}_2\text{Cu}_4\text{O}_{10+x}$ (Hg-1234) phases. The reactions were carried out in a belt-type apparatus under high pressure (50 kbar) at 950°C for 3 and 3.5 h, respectively.

2. Synthesis and characterization by X-ray and EDS analysis

Powder samples containing the $\text{HgBa}_2\text{Ca}_2\text{Cu}_3\text{O}_{8+x}$ and $\text{HgBa}_2\text{Ca}_2\text{Cu}_4\text{O}_{10+x}$ phases were obtained by high-pressure and high-temperature reactions using the belt-type apparatus of the Laboratoire de Cristallographie. A precursor with the nominal composition $\text{Ba}_2\text{Ca}_2\text{Cu}_3\text{O}_x$ was prepared by mixing high-purity nitrates: $\text{Ba}(\text{NO}_3)_2$ (Aldrich, >99%), $\text{Ca}(\text{NO}_3)_2 \cdot 4\text{H}_2\text{O}$ (Normapur Prolabo, analytical reagent) and $\text{Cu}(\text{NO}_3)_2 \cdot 3\text{H}_2\text{O}$ (Strem Chemical Inc., 99.5%). The mixture thus obtained was initially heated at 600°C in air for 12 h, then regrinded and annealed at 925°C for 72 h in an oxygen flow with three intermediate regrindings. Then, the stoichiometric amount of yellow HgO (Aldrich, >99%) was added and the mixture was thoroughly grounded in an agate mortar and sealed in a Pt capsule specific for high pressure synthesis. Various temperatures and annealing times at a pressure of 50 kbar were tried in order to obtain the Hg-1223 and Hg-1234 phases. In these experiments the pressure was first increased to 50 kbar, subsequently the temperature was raised to the desired value during 1 h, then the temperature and the pressure were kept constant for 1–4 h. After this, the furnace power was shut off and the pressure decreased to normal conditions in 30 min.

The samples were studied by X-ray powder diffraction, performed with a Guinier focusing camera and $\text{Fe K}\alpha$ radiation (1.93730 Å). Finely powdered silicon ($a = 5.43088$ Å at 25°C) was used as an internal standard. The intensities of the reflections were evaluated by an automatic film scanner. The SCAN3 and SCANPI programs were used for processing the data [5].

The phase $\text{HgBa}_2\text{Ca}_2\text{Cu}_3\text{O}_{8+x}$ was present in the sample synthesized at 950°C for 3 h (sample 1) together with a smaller amount of Hg-1212, CaO and CuO , and traces of CaHgO_2 [6] and of an unknown phase whose intensities were less than 4%. The X-ray

diffraction pattern of sample 1 after background subtraction is shown in fig. 1. The 20 reflections corresponding to Hg-1223 were indexed on a tetragonal cell with lattice parameters $a = 3.8532(6)$ Å, $c = 15.818(2)$ Å. The characteristic 001 reflection is shown in the insert. No systematic absences were observed, leading to space group $\text{P4}/\text{mmm}$ and one formula per unit cell. The measured value of the c parameter of Hg-1223 corresponded to the expected value calculated by the formula $c \approx 9.5 + 3.2(n-1)$ with $n=3$ [1].

A scanning electron microscope JEOL 840A equipped with an energy-dispersive spectroscopy (EDS) attachment was used for the analysis of the cation composition of the two prepared samples. K α lines were used for the analysis of the Ca and Cu cations, and La α lines for the Ba and Hg ones. EDS analysis of several well crystallized and flat grains showed that besides Hg, Ba, Ca, Cu and O no other element was present in the samples. The average metal ratio found for four grains was $\text{Hg}:\text{Ba}:\text{Ca}:\text{Cu} = 13(2):24(1):26(1):38(1)$, with standard deviations between parentheses. The cation stoichiometry is in good agreement with the expected formula of the Hg-1223 phase.

The lattice parameters of Hg-1212 refined from ten reflections ($a = 3.859(4)$ Å, $c = 12.68(2)$ Å) are in agreement with the data of Putilin et al. [2]. It should be noted that there is severe overlapping between the $hk0$ reflections of the Hg-1212 and those of the Hg-1223 phases. Moreover, the $hk4$ reflections of Hg-1212 overlap with the $hk5$ reflections of Hg-1223. These overlappings did not allow us to determine all the intensities of the two phases. However, the ratio of the intensities of the strongest lines for Hg-1212 (102 and 103) and Hg-1223 (103 and 104) shows clearly that the Hg-1223 is the predominant phase in sample 1 (fig. 1).

The presence in sample 1 of the lower member together with the initial oxides, CuO and CaO , obviously indicates that the formation of Hg-1223 was not complete after a 3 h annealing period. The synthesis carried out at 900°C for 2 h led to the formation of Hg-1212 which was found to be the main phase in the sample together with the starting compounds. These data show that the formation of Hg-1223 occurs through the synthesis of the lower members of the series. The increase of the annealing

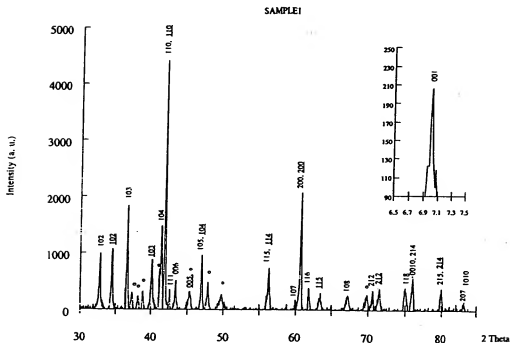


Fig. 1. X-ray powder pattern for sample I. Indexed XRD intensities correspond to Hg-1223 and Hg-1212 (underline). Impurities of CaO , CuO , CaHgO_2 and an unknown phase are marked by (*). The inset displays the characteristic intensity of 001 for Hg-1223.

time up to 3.5 and 4 h at 950°C and the same pressure led to the expected disappearance of Hg-1212 as well as of CaO . In these samples the formation of a new phase was detected. Its amount was relatively high (more than 50%) in samples annealed for 3.5 h (sample II). A total of 17 reflections of this phase were indexed on a tetragonal cell with lattice parameters $a = 3.8540(3)$ Å, $c = 19.006(3)$ Å. As for Hg-1223 no systematic absences were observed, leading to space group $P4/mmm$. Similar parameters were found by electron diffraction (see below). The c parameters of this phase corresponded to the value calculated from the formula $c \approx 9.5 + 3.2(n-1)$ for $n=4$. This strongly suggested that the new phase was the fourth member of the Hg-based series: $\text{Hg-Ba}_2\text{Ca}_3\text{Cu}_4\text{O}_{10+x}$. The approximate cations ratio determined by EDS analysis of five well-crystallized and flat grains was $\text{Hg:Ba:Ca:Cu} = 9(1):18(1):29(2):44(2)$. These data are in good agreement with the proposed formula for the new compound.

Besides Hg-1234 as the main phase, a smaller amount of Hg-1223 was present in sample II together with small amounts of CuO and of an unknown phase. This unknown phase was predominant in a sample treated for 5 h in the same conditions which did not contain any member of the Hg-based series and did not exhibit any superconductivity. The presence of the latter oxides can be explained as a result of the decomposition of Hg-1223 and the formation of Hg-1234. Hg-1212 was absent in this sample as well as in that annealed for 4 h. The X-ray diffraction pattern of sample Ii after background subtraction is shown in fig. 2. The ratio of the main intensities for both Hg-based layered cuprates, 104 for Hg-1223 and 105 for Hg-1234, shows that the latter was the main phase in this sample. As for sample I the overlapping of $hk0$ reflections for both phases occurs because of the similarity of the two a parameters. Moreover, the $hk6$ reflections of Hg-1234 are overlapped with the $hk5$ ones of Hg-1223.

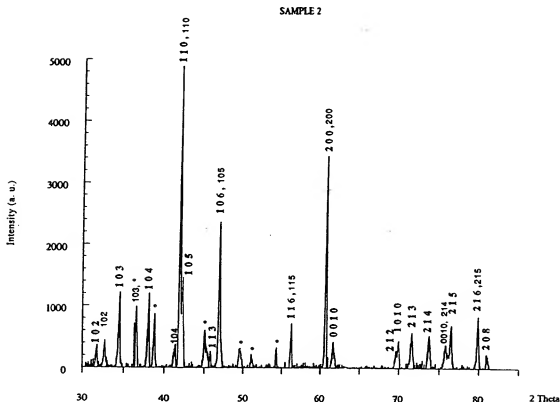


Fig. 2. X-ray powder pattern for sample 11. Indexed XRD intensities correspond to Hg-1234 (bold) and Hg-1223. Impurities of CuO and an unknown phase are marked by (*).

3. Electron microscopy

The I and II samples were studied by electron microscopy. A suspension of crystals in acetone was grounded in an agate mortar. The crystallites were recovered from the suspension on a porous carbon film. A Philips EM 400T operating at 120 kV was used.

Figure 3 (a) and (b) shows two diffraction patterns obtained for sample 1 corresponding to the $[001]$ and the $\langle 110 \rangle$ zone axes of the $\text{HgBa}_2\text{Ca}_3\text{Cu}_4\text{O}_{10.8}$ (Hg-1223) phase, respectively. In both cases, the diffraction spots are sharp, which indicates that the crystal is well ordered. In fig. 3(b), one can notice a modulation of the intensity of the diffraction spots along the c^* -axis, with maxima for hkl reflections with $l = 5n$ ($n=0, 1, 2, \dots$). On the micrograph (fig. 3(c)) corresponding to the diffraction pattern shown in fig. 3(b), one can see the very

regular periodicity of the fringes separated by 15.8 Å. During the observation under the electron beam, dark spots appeared near the edge of the crystal, probably due to the decomposition of the crystal.

Some diffraction patterns obtained for other crystals present diffuse lines parallel to the c^* -axis and passing through the Bragg spots (fig. 4 (a)). They are due to the presence of intergrowths as given evidence for by fig. 4(b). On this micrograph, two different spacings of 15.8 Å and 12.7 Å can be measured, attributed to Hg-1223 and Hg-1212, respectively.

In the case of sample 11, almost all the observed crystallites have diffraction patterns corresponding to the Hg-1234 phase ($\text{HgBa}_2\text{Ca}_3\text{Cu}_4\text{O}_{10.4}$) with cell parameters $a=b=3.85$ Å and $c=19$ Å. Figure 5(a) and (b) give examples of the $[001]$ and $\langle 100 \rangle$ zone axes, respectively. As for Hg-1223, also for Hg-1234 the intensity of the Bragg spots varies according to

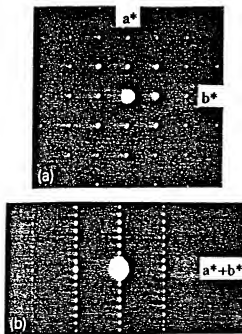


Fig. 3. Electron diffraction patterns of Hg-1223 taken along [001] (a) and $\langle 110 \rangle$ (b) zone axes. (c) Micrograph corresponding to the diffraction pattern (b). The interfringe spacing is 15.8 Å.

the value of the l index, the maxima of intensity being obtained for $l = 6n$ ($n = 0, 1, 2, \dots$). This intensity pattern might be explained by the fact that $c/6$ is equal to 3.17 Å, which corresponds to the distance between two neighboring (CuO_2) layers. The increase of the layer number n in the structure leads to the increase of the intensity of the hkl reflections with

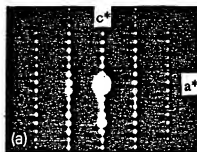


Fig. 4. Electron diffraction pattern of sample 1 along $\langle 100 \rangle$ and corresponding micrograph showing the intergrowths of Hg-1223 and Hg-1234.

$l = n + 2$. These periodicities of the (CuO_2) layers explain the overlapping of such reflections on the X-ray powder pattern (see above). Most of the images taken along the $\langle 100 \rangle$ zone axis show very regular fringes separated by 19 Å (fig. 5(c)). However, some crystals present intergrowths between the Hg-1223 and Hg-1234, as revealed in fig. 6. In this case, the following sequence is observed over about 500 Å: $-19 \text{ Å} - 19 \text{ Å} - 19 \text{ Å} - 19 \text{ Å} - 22 \text{ Å} -$. On the corresponding diffraction pattern, besides the diffraction spots of the Hg-1234 phase, additional spots related to the 22 Å periodicity are present. Such a periodicity may be attributed to a 1245 phase ($\text{HgBa}_2\text{Ca}_2\text{Cu}_3\text{O}_{12+x}$). The fact that the extra diffraction spots are sharp indicates that this phase is well ordered at least over a certain number of cells in these crystals.

4. AC susceptibility measurements

The critical temperature T_c , and the apparent su-

Theta

es of CuO

by 15.8
on beam,
crystal,
her crys-
axis and
)). They
even evi-
two dif-
mea-
Hg-1212.

observed
spending
with cell
ure 5(a)
00) zone
Hg-1234
ording to

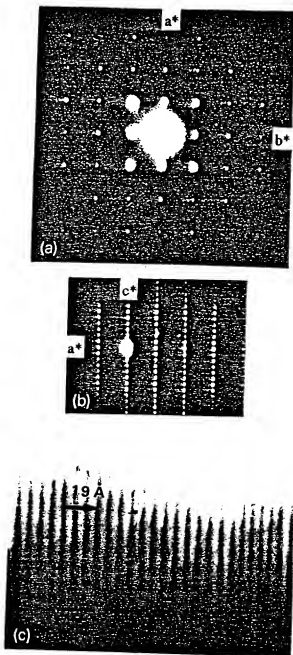


Fig. 5. Electron diffraction patterns of Hg-1234 taken along [001] (a) and $\langle 100 \rangle$ (b) zone axes. (c) Micrograph corresponding to the diffraction pattern of (b). The interfringe spacing is 19 Å.

perconducting volume of samples I and II have been determined from AC susceptibility measurements on fine powder samples. This avoids overestimates of the superconducting volume due to the larger screenings in sintered samples. The AC susceptibility was measured with an alternating maximum field of 0.01 Oe and a frequency of 119 Hz. The temperature was measured by a calibrated 100 Ω platinum thermometer.

The as-synthesized sample I undergoes a transition from the paramagnetic to the diamagnetic state with an onset above 133 K (fig. 7). Several measurements were made with the same sample and the reproducibility of T_c is ± 1 K (mainly due to the thermal contact between the sample and the thermometer). The estimated magnetic susceptibility at 4 K corresponds to a large volume of ideal diamagnetism indicating the bulk nature of superconductivity. We can suggest that the sharp and large drop on the AC susceptibility curve above 133 K should correspond to the Hg-1223 phase because Hg-1212, which is present in this sample as the minority phase, has a T_c not higher than 126 K [3].

The as-synthesized sample II undergoes a transition from the paramagnetic to the diamagnetic state with an onset as high as 132 K. Actually, two onsets at two different temperatures are visible, the smaller one at 132 K and the larger one at about 126 K. There are two Hg-based layered cuprates in this sample: Hg-1234 as the main phase and Hg-1223 as the minority one. Taking into consideration the results of sample I, we might suggest that the first onset (132 K) corresponds to Hg-1223 and the larger one at the lower temperature (126 K) to Hg-1234. In any case, it is obvious that T_c for Hg-1234 is not higher than that for Hg-1223.

5. Discussion

The synthesized $\text{HgBa}_2\text{Ca}_2\text{Cu}_3\text{O}_{8+\delta}$ (Hg-1223) and $\text{HgBa}_2\text{Ca}_2\text{Cu}_4\text{O}_{10+\delta}$ (Hg-1234) phases are the third and the fourth members of the $\text{HgBa}_2\text{Ca}_{n-1}\text{Cu}_n\text{O}_{2n+2+\delta}$ series, in analogy with those of Hg-1201 [1,7,8] and Hg-1212 [2] their structures can be schematized as containing rock-salt-like slabs, $(\text{BaO})(\text{HgO}_2)(\text{BaO})$, alternating with perovskite-like slabs, consisting in three (Hg-1223) or

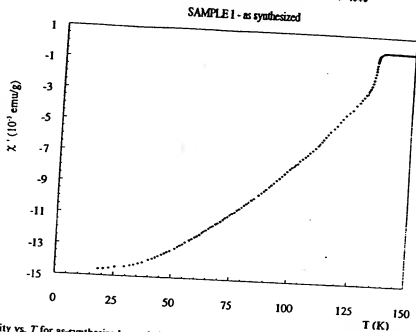


Fig. 7. AC susceptibility vs. T for as-synthesized sample I, where Hg-1223 is present as the main phase and Hg-1212 as the minority phase.

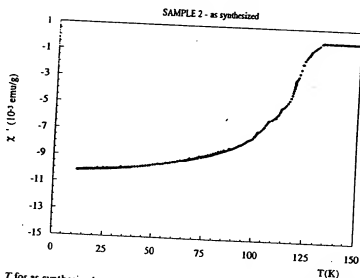


Fig. 8. AC susceptibility vs. T for as-synthesized sample II showing the presence of Hg-1234 as the main phase and of Hg-1223 as the minority phase.

1212. The appropriate treatment for Hg-1234 can possibly change T_c for this phase. Therefore, we can only conclude that for the as-prepared samples a saturation of T_c seems to occur in the Hg-Ba-Ca-Cu-O system at the third member. A similar behavior

occurs for the $\text{TlBa}_2\text{Ca}_{n-1}\text{Cu}_n\text{O}_{2n+3+x}$ homologous series, for which T_c increases up to the third member (120 K) also [9].

One can see in table 1 that for the Hg series, the increase of T_c is accompanied by a decrease of the a

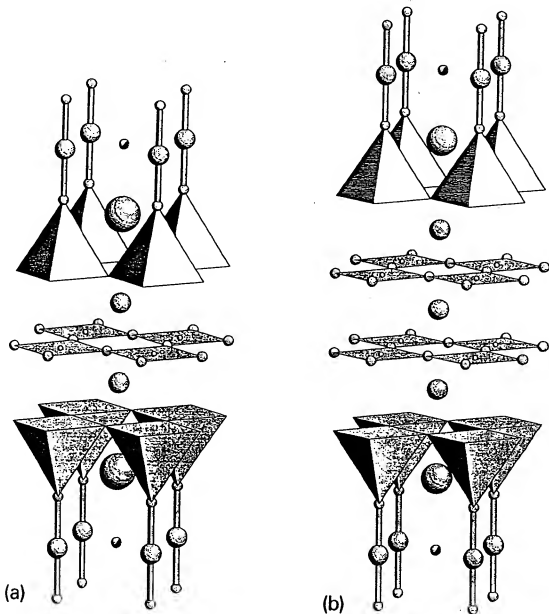


Fig. 9. The crystal structures of Hg-1223 (a) and Hg-1234 (b). The largest and medium large circles refer to Ba and Ca atoms, respectively. The Cu atoms are the smallest circles. Those at the base of the shaded pyramids are not shown. The circles forming the squares around the Cu are oxygen atoms. The dumbbells around the Hg atoms are formed by apical oxygen atoms. Partially filled circles refer to the partially occupied oxygen sites on the Hg layer.

parameter and just at T_c it remains practically constant between Hg-1223 and Hg-1234.

The electron microscopy study of Hg-1201 [10]

revealed the absence of intergrowths and this was attributed to the absence of the Ca^{2+} cations in the system. On the contrary, the addition of Ca layers in

Table I
Lattice parameters and transition temperatures for Hg-based Cu oxides

Formula	Short form	<i>a</i> (Å)	<i>c</i> (Å)	<i>T_c</i> (K)	Ref.
$\text{HgBa}_2\text{CuO}_{4+x}$	Hg-1201	3.8797(5)	9.509(2)	94	[1]
$\text{HgBa}_2\text{CaCu}_2\text{O}_{4+x}$	Hg-1212	3.8556(8)	12.652(4)	121	[2]
$\text{HgBa}_2\text{Ca}_2\text{Cu}_2\text{O}_{8+x}$	Hg-1223	3.8532(6)	15.818(2)	126	[3]
$\text{HgBa}_2\text{Ca}_2\text{Cu}_2\text{O}_{10+x}$	Hg-1234	3.8540(3)	19.006(3)	133	[4], this work
				< 132	this work

the system leads to intergrowths due to different numbers of (CuO_2) and Ca layers in the perovskite-like slabs. Such intergrowths were already reported in ref. [4]. Possibly, the occurrence of different intergrowths may explain why the variation versus temperature of the AC susceptibility does not present distinct and abrupt transitions which could be attributed to pure Hg-1212, 1223 and 1234 phases.

The synthesis of the higher members of the Hg-based homologous series as bulk samples has been performed at higher temperatures than that used for Hg-1212 and with longer treatment times. We suggest that the synthesis of such phases occurs through the formation at an initial state and subsequent decomposition of the lower members of the series. This feature is similar to that existing for the $\text{Ti-Ba}_2\text{Ca}_{n-1}\text{Cu}_n\text{O}_{2n+3-4}$ homologous series [9]. The use of high pressure, possibly, lowers the mercury oxide decomposition. It also leads to a decrease of stability of CaHgO_2 , whose synthesis at the first stage of the reaction inhibits the formation of Hg-based compounds.

Acknowledgements

The authors would like to thank M.F. Gorius, M.

Perroux and R. Argoud for their technical assistance. The visit of EVA has been supported by the fund from the French Ministry of Foreign Affairs. EVA and SNP would like to thank the support of the Russian Scientific Council on Superconductivity (Project "Poisk"). SML was supported by the Erasmus Students Exchange Program.

References

- [1] S.N. Putilin, E.V. Antipov, O. Chmaissem and M. Marezio, *Nature* (London) 362 (1993) 226.
- [2] S.N. Putilin, E.V. Antipov and M. Marezio, *Physica C* 212 (1993) 266.
- [3] S.M. Loureiro and J.J. Capponi, private communication.
- [4] A. Schilling, M. Cantoni, J.D. Guo and H.R. Ott, *Nature* (London) 363 (1993) 56.
- [5] K.E. Johansson, T. Palm and P.-E. Werner, *J. Phys. E: Sci. Instrum.* 13 (1980) 1289.
- [6] S.N. Putilin, M.G. Rozova, D. Kashporov, E.V. Antipov and L.M. Kovba, *Zh. Neorganicheskoi Khimii* 36 (1991) 1645 (in Russian).
- [7] O. Chmaissem, Q. Huang, S.N. Putilin, M. Marezio and A. Santoro, *Physica C* 212 (1993) 259.
- [8] J.L. Wagner, P.G. Radaelli, D.G. Hinks, J.D. Jorgensen, J.F. Mitchell, B. Dabrowski, G.S. Knapp and M.A. Beno, *Physica C* 210 (1993) 447.
- [9] S. Nakajima, M. Kikuchi, Y. Syono, T. Oku, D. Shindo, K. Hiraga, N. Kobayashi, H. Iwasaki and Y. Muto, *Physica C* 158 (1989) 471.
- [10] J. Bryntse and S.N. Putilin, *Physica C* 212 (1993) 223.

BRIEF ATTACHMENT BI

IN THE UNITED STATES PATENT AND TRADEMARK OFFICE

In re Patent Application of

Applicants: Bednorz et al.

Serial No.: 08/479,810

Filed: June 7, 1995

For: NEW SUPERCONDUCTIVE COMPOUNDS HAVING HIGH TRANSITION
TEMPERATURE, METHODS FOR THEIR USE AND PREPARATION

Date: March 1, 2004

Docket: YO987-074BZ

Group Art Unit: 1751

Examiner: M. Kopec

Commissioner for Patents
P.O. Box 1450
Alexandria, VA 22313-1450

FIFTH SUPPLEMENTAL AMENDMENT

Sir:

In response to the Office Action dated February 4, 2000:

ATTACHMENT 56

BI

The synthesis and characterization of the $\text{HgBa}_2\text{Ca}_2\text{Cu}_3\text{O}_{8+\delta}$ and $\text{HgBa}_2\text{Ca}_3\text{Cu}_4\text{O}_{10+\delta}$ phases

E.V. Antipov^{a,b}, S.M. Loureiro^b, C. Chaillout^b, J.J. Capponi^b, P. Bordet^b, J.L. Tholence^c,
S.N. Putilin^a and M. Marezio^{b,d}

^a Department of Chemistry, Moscow State University, 119899 Moscow, Russian Federation

^b Laboratoire de Cristallographie CNRS-UJF, BP 166, 38042 Grenoble Cedex 09, France

^c CRTBT, CNRS-UJF, BP 166, 38042 Grenoble Cedex 09, France

^d AT&T Bell Laboratories, Murray Hill, NJ 07974, USA

Received 28 June 1993

Revised manuscript received 9 July 1993

The third (Hg-1223) and the fourth (Hg-1234) members of the recently-discovered homologous series $\text{HgBa}_2\text{Ca}_{n-1}\text{Cu}_n\text{O}_{2n+2+\delta}$ have been synthesized by solid state reaction, carried out at 950°C under 50 kbar at different annealing times. These phases have a tetragonal cell with lattice parameters: $a = 3.8532(6)$ Å, $c = 15.818(2)$ Å and $a = 3.8540(3)$ Å, $c = 19.006(3)$ Å, respectively. The c parameters are in agreement with the formula $c \approx 9.5 + 3.2(n-1)$. Electron microscopy study showed similar lattice parameters as well as the occurrence of different intergrowths and stacking faults. A periodicity of 22 Å has also been detected, which may be attributed to the existence of the Hg-1245 phase. EDS analysis data of several grains of Hg-1223 and Hg-1234 are in agreement with the proposed chemical formulae. AC susceptibility measurements show that an increase of the superconducting transition temperature with n in the $\text{HgBa}_2\text{Ca}_{n-1}\text{Cu}_n\text{O}_{2n+2+\delta}$ series occurs till the third member, after which a saturation seems to be achieved.

1. Introduction

Superconductivity at about 94 K and well above 120 K has been recently reported for $\text{HgBa}_2\text{CuO}_{4+\delta}$ (Hg-1201) [1] and $\text{HgBa}_2\text{CaCu}_2\text{O}_{6+\delta}$ (Hg-1212) [2], respectively. These phases are the first and the second members of the Hg-based homologous series of layered Cu mixed oxides. Their structures contain rock-salt-like slabs, such as $(\text{BaO})(\text{HgO}_x)$ (BaO) alternating with either one (CuO_2) layer in the former or an anion-deficient perovskite-like slab, such as $(\text{CuO}_2)_2(\text{CaO})$ (CuO_2) , in the latter. A superconducting transition temperature as high as 133 K has been reported for a multiphase sample in the Hg-Ba-Ca-Cu-O system by Schilling et al. [4]. These authors could not identify by X-ray diffraction the phases responsible for the superconductivity at this temperature, but proved by high resolution electron microscopy that the sample contained the Hg-1212 and Hg-1223 phases as well as different intergrowths. Putilin et al. [2] showed that in the sample

containing Hg-1212 as the majority phase, a small drop on the AC susceptibility curve versus T occurred at about 132 K which could be attributed to the third member of the Hg-bearing series.

Putilin et al. also showed [2] that it was possible to synthesize the Hg-1212 phase, practically in pure form, under high pressure (40–60 kbar) and at 800°C for about 1 h. The high pressure synthesis allows one to lower the mercury oxide decomposition. This decomposition occurs at ambient pressure at a temperature at which the reactivity of the other components is very low. It was suggested that the same technique could be used for obtaining the higher members of the series. We found that the reactions have to be carried out at higher temperatures (950°C) and for longer annealing times. The same occurs for the higher members of the Bi- or Tl-based Cu oxide series, which are formed by the formation, at the initial stages of the reaction, of the lower members of the corresponding families. We report herein the synthesis and characterization of the Hg-

$\text{Ba}_2\text{Ca}_2\text{Cu}_3\text{O}_{11.4}$ (Hg-1223) and $\text{HgBa}_2\text{Ca}_3\text{Cu}_4\text{O}_{10.4}$ (Hg-1234) phases. The reactions were carried out in a belt-type apparatus under high pressure (50 kbar) at 950°C for 3 and 3.5 h, respectively.

2. Synthesis and characterization by X-ray and EDS analysis

Powder samples containing the $\text{HgBa}_2\text{Ca}_x\text{Cu}_y\text{O}_{10+x}$ and $\text{HgBa}_2\text{Ca}_3\text{Cu}_4\text{O}_{10.4}$ phases were obtained by high-pressure and high-temperature reactions using the belt-type apparatus of the Laboratoire de Cristallographie. A precursor with the nominal composition $\text{Ba}_2\text{Ca}_2\text{Cu}_3\text{O}_x$ was prepared by mixing high-purity nitrates: $\text{Ba}(\text{NO}_3)_2$ (Aldrich, > 99%), $\text{Ca}(\text{NO}_3)_2 \cdot 4\text{H}_2\text{O}$ (Normapur Prolabo, analytical reagent) and $\text{Cu}(\text{NO}_3)_2 \cdot 3\text{H}_2\text{O}$ (Strem Chemical Inc., 99.5%). The mixture thus obtained was initially heated at 600°C in air for 12 h, then reground and annealed at 925°C for 72 h in an oxygen flow with three intermediate regrindings. Then, the stoichiometric amount of yellow HgO (Aldrich, > 99%) was added and the mixture was thoroughly grounded in an agate mortar and sealed in a Pt capsule specific for high pressure synthesis. Various temperatures and annealing times at a pressure of 50 kbar were tried in order to obtain the Hg-1223 and Hg-1234 phases. In these experiments the pressure was first increased to 50 kbar, subsequently the temperature was raised to the desired value during 1 h, then the temperature and the pressure were kept constant for 1–4 h. After this, the furnace power was shut off and the pressure decreased to normal conditions in 30 min.

The samples were studied by X-ray powder diffraction, performed with a Guinier focusing camera and $\text{Fe K}\alpha$ radiation (1.93730 Å). Finely powdered silicon ($a = 5.43088$ Å at 25°C) was used as an internal standard. The intensities of the reflections were evaluated by an automatic film scanner. The SCAN3 and SCANPI programs were used for processing the data [5].

The phase $\text{HgBa}_2\text{Ca}_2\text{Cu}_3\text{O}_{10.4}$ was present in the sample synthesized at 950°C for 3 h (sample 1) together with a smaller amount of Hg-1212, CaO and CuO , and traces of CaHgO_3 [6] and of an unknown phase whose intensities were less than 4%. The X-ray

diffraction pattern of sample 1 after background subtraction is shown in fig. 1. The 20 reflections corresponding to Hg-1223 were indexed on a tetragonal cell with lattice parameters $a = 3.8532(6)$ Å, $c = 15.818(2)$ Å. The characteristic 001 reflection is shown in the insert. No systematic absences were observed, leading to space group $P4/mmm$ and one formula per unit cell. The measured value of the c parameter of Hg-1223 corresponded to the expected value calculated by the formula $c \approx 9.5 + 3.2(n-1)$ with $n=3$ [1].

A scanning electron microscope JEOL 840A equipped with an energy-dispersive spectroscopy (EDS) attachment was used for the analysis of the cation composition of the two prepared samples. K α lines were used for the analysis of the Ca and Cu cations, and L α lines for the Ba and Hg ones. EDS analysis of several well crystallized flat grains showed that besides Hg, Ba, Ca, Cu and O no other element was present in the samples. The average metal ratio found for four grains was $\text{Hg}:\text{Ba}:\text{Ca}:\text{Cu} = 13(2):24(1):26(1):38(1)$, with standard deviations between parentheses. The cation stoichiometry is in good agreement with the expected formula of the Hg-1223 phase.

The lattice parameters of Hg-1212 refined from ten reflections ($a = 3.859(4)$ Å, $c = 16.68(2)$ Å) are in agreement with the data of Putilin et al. [2]. It should be noted that there is severe overlapping between the $hk0$ reflections of the Hg-1212 and those of the Hg-1223 phases. Moreover, the $hk4$ reflections of Hg-1212 overlap with the $hk5$ reflections of Hg-1223. These overlappings did not allow us to determine all the intensities of the two phases. However, the ratio of the intensities of the strongest lines for Hg-1212 (102 and 103) and Hg-1223 (103 and 104) shows clearly that the Hg-1223 is the predominant phase in sample 1 (fig. 1).

The presence in sample 1 of the lower member together with the initial oxides, CuO and CaO , obviously indicates that the formation of Hg-1223 was not complete after a 3 h annealing period. The synthesis carried out at 900°C for 2 h led to the formation of Hg-1212 which was found to be the main phase in the sample together with the starting compounds. These data show that the formation of Hg-1223 occurs through the synthesis of the lower members of the series. The increase of the annealing

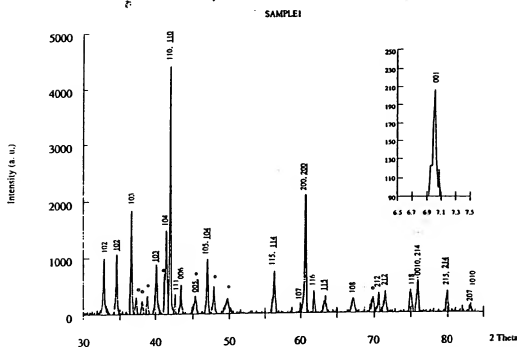


Fig. 1. X-ray powder pattern for sample I. Indexed XRD intensities correspond to Hg-1223 and Hg-1212 (underline). Impurities of CaO , CuO , CaHgO_3 and an unknown phase are marked by (*). The inset displays the characteristic intensity of 001 for Hg-1223.

time up to 3.5 and 4 h at 950°C and the same pressure led to the expected disappearance of Hg-1212 as well as of CaO . In these samples the formation of a new phase was detected. Its amount was relatively high (more than 50%) in samples annealed for 3.5 h (sample II). A total of 17 reflections of this phase were indexed on a tetragonal cell with lattice parameters $a = 3.8540(3) \text{ \AA}$, $c = 19.006(3) \text{ \AA}$. As for Hg-1223 no systematic absences were observed, leading to space group $P4/mmm$. Similar parameters were found by electron diffraction (see below). The c parameters of this phase corresponded to the value calculated from the formula $c \approx 9.5 + 3.2(n-1)$ for $n=4$. This strongly suggested that the new phase was the fourth member of the Hg-based series: $\text{Hg-Ba}_2\text{Ca}_2\text{Cu}_2\text{O}_{10+x}$. The approximate cations ratio determined by EDS analysis of five well-crystallized and flat grains was $\text{Hg:Ba:Ca:Cu} = 9(1):18(1):29(2):44(2)$. These data are in good agreement with the proposed formula for the new compound.

Besides Hg-1234 as the main phase, a smaller amount of Hg-1223 was present in sample II together with small amounts of CuO and of an unknown phase. This unknown phase was predominant in a sample treated for 5 h in the same conditions which did not contain any member of the Hg-based series and did not exhibit any superconductivity. The presence of the latter oxides can be explained as a result of the decomposition of Hg-1223 and the formation of Hg-1234. Hg-1212 was absent in this sample as well as in that annealed for 4 h. The X-ray diffraction pattern of sample II after background subtraction is shown in fig. 2. The ratio of the main intensities for both Hg-based layered cuprates, 104 for Hg-1223 and 105 for Hg-1234, shows that the latter was the main phase in this sample. As for sample I the overlapping of $hk0$ reflections for both phases occurs because of the similarity of the two a parameters. Moreover, the $hk6$ reflections of Hg-1234 are overlapped with the $hk5$ ones of Hg-1223.

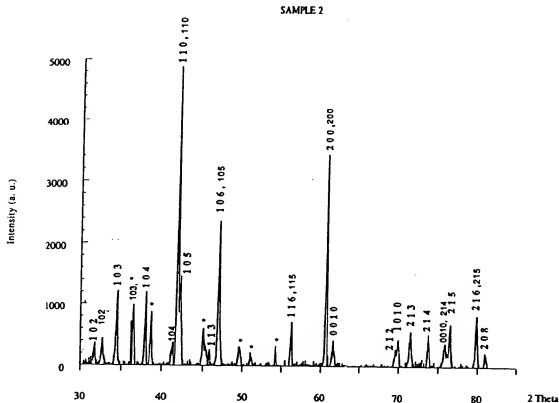


Fig. 2. X-ray powder pattern for sample II. Indexed XRD intensities correspond to Hg-1234 (bold) and Hg-1223. Impurities of CuO and an unknown phase are marked by (*).

3. Electron microscopy

The I and II samples were studied by electron microscopy. A suspension of crystals in acetone was grounded in an agate mortar. The crystallites were recovered from the suspension on a porous carbon film. A Philips EM 400T operating at 120 kV was used.

Figure 3 (a) and (b) shows two diffraction patterns obtained for sample I corresponding to the $[001]$ and the $\langle 110 \rangle$ zone axes of the $\text{Hg-Ba}_2\text{Ca}_2\text{Cu}_3\text{O}_{8+x}$ (Hg-1223) phase, respectively. In both cases, the diffraction spots are sharp, which indicates that the crystal is well ordered. In fig. 3(b), one can notice a modulation of the intensity of the diffraction spots along the c^* -axis, with maxima for hkl reflections with $l=5n$ ($n=0, 1, 2, \dots$). On the micrograph (fig. 3(c)) corresponding to the diffraction pattern shown in fig. 3(b), one can see the very

regular periodicity of the fringes separated by 15.8 Å. During the observation under the electron beam, dark spots appeared near the edge of the crystal, probably due to the decomposition of the crystal.

Some diffraction patterns obtained for other crystals present diffuse lines parallel to the c^* -axis and passing through the Bragg spots (fig. 4 (a)). They are due to the presence of intergrowths as given evidence for by fig. 4(b). On this micrograph, two different spacings of 15.8 Å and 12.7 Å can be measured, attributed to Hg-1223 and Hg-1212, respectively.

In the case of sample II, almost all the observed crystallites have diffraction patterns corresponding to the Hg-1234 phase ($\text{HgBa}_2\text{Ca}_3\text{Cu}_4\text{O}_{10+x}$) with cell parameters $a=b=3.85$ Å and $c=19$ Å. Figure 5(a) and (b) give examples of the $[001]$ and $\langle 100 \rangle$ zone axes, respectively. As for Hg-1223, also for Hg-1234 the intensity of the Bragg spots varies according to

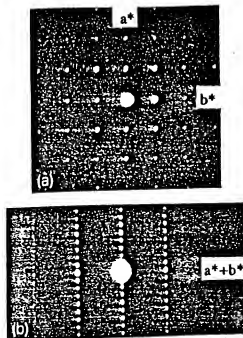


Fig. 3. Electron diffraction patterns of Hg-1223 taken along $[100]$ (a) and $[110]$ (b) zone axes. (c) Micrograph corresponding to the diffraction pattern (b). The interfringe spacing is 15.8 \AA .

the value of the l index, the maxima of intensity being obtained for $l=6n$ ($n=0, 1, 2, \dots$). This intensity pattern might be explained by the fact that $c/6$ is equal to 3.17 \AA , which corresponds to the distance between two neighboring (CuO_2) layers. The increase of the layer number n in the structure leads to the increase of the intensity of the hkl reflections with

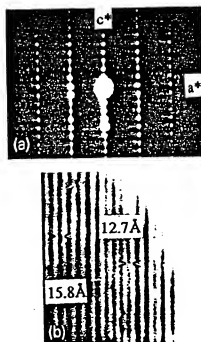


Fig. 4. Electron diffraction pattern of sample I along $\langle 100 \rangle$ and corresponding micrograph showing the intergrowths of Hg-1223 and Hg-1212.

$l=n+2$. These periodicities of the (CuO_2) layers explain the overlapping of such reflections on the X-ray powder pattern (see above). Most of the images taken along the $\langle 100 \rangle$ zone axis show very regular fringes separated by 19 \AA (fig. 5(c)). However, some crystals present intergrowths between the Hg-1223 and Hg-1234, as revealed in fig. 6. In this case, the following sequence is observed over about 500 \AA : $-19 \text{ \AA}-19 \text{ \AA}-19 \text{ \AA}-19 \text{ \AA}-19 \text{ \AA}-22 \text{ \AA}-$. On the corresponding diffraction pattern, besides the diffraction spots of the Hg-1234 phase, additional spots related to the 22 \AA periodicity are present. Such a periodicity may be attributed to a 1245 phase ($\text{HgBa}_2\text{Ca}_4\text{Cu}_5\text{O}_{12+x}$). The fact that the extra diffraction spots are sharp indicates that this phase is well ordered at least over a certain number of cells in these crystals.

4. AC susceptibility measurements

The critical temperature T_c , and the apparent su-

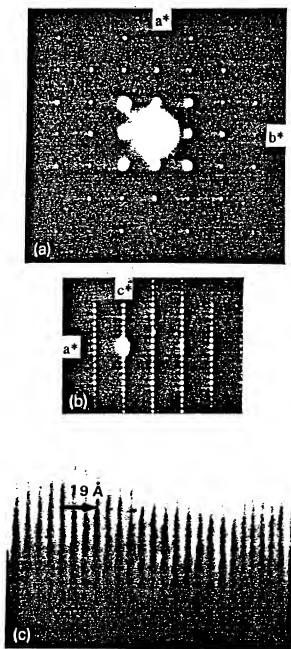


Fig. 5. Electron diffraction patterns of Hg-1234 taken along [001] (a) and [100] (b) zone axes. (c) Micrograph corresponding to the diffraction pattern of (b). The interfringe spacing is 19 Å.

perconducting volume of samples I and II have been determined from AC susceptibility measurements on fine powder samples. This avoids overestimates of the superconducting volume due to the larger screenings in sintered samples. The AC susceptibility was measured with an alternating maximum field of 0.01 Oe and a frequency of 119 Hz. The temperature was measured by a calibrated 100 Ω platinum thermometer.

The as-synthesized sample I undergoes a transition from the paramagnetic to the diamagnetic state with an onset above 133 K (fig. 7). Several measurements were made with the same sample and the reproducibility of T_c is ± 1 K (mainly due to the thermal contact between the sample and the thermometer). The estimated magnetic susceptibility at 4 K corresponds to a large volume of ideal diamagnetism indicating the bulk nature of superconductivity. We can suggest that the sharp and large drop on the AC susceptibility curve above 133 K should correspond to the Hg-1223 phase because Hg-1212, which is present in this sample as the minority phase, has a T_c not higher than 126 K [3].

The as-synthesized sample II undergoes a transition from the paramagnetic to the diamagnetic state with an onset as high as 132 K. Actually, two onsets at two different temperatures are visible, the smaller one at 132 K and the larger one at about 126 K. There are two Hg-based layered cuprates in this sample: Hg-1234 as the main phase and Hg-1223 as the minority one. Taking into consideration the results of sample I, we might suggest that the first onset (132 K) corresponds to Hg-1223 and the larger one at the lower temperature (126 K) to Hg-1234. In any case, it is obvious that T_c for Hg-1234 is not higher than that for Hg-1223.

5. Discussion

The synthesized $\text{HgBa}_2\text{Ca}_2\text{Cu}_4\text{O}_{8+x}$ (Hg-1223) and $\text{HgBa}_2\text{Ca}_2\text{Cu}_4\text{O}_{10+x}$ (Hg-1234) phases are the third and the fourth members of the $\text{Hg-Ba}_2\text{Ca}_{n-1}\text{Cu}_4\text{O}_{2n+2+x}$ series, in analogy with those of Hg-1201 [1,7,8] and Hg-1212 [2] their structures can be schematized as containing rock-salt-like slabs, $(\text{BaO})(\text{HgO}_4)(\text{BaO})$, alternating with perovskite-like slabs, consisting in three (Hg-1223) or

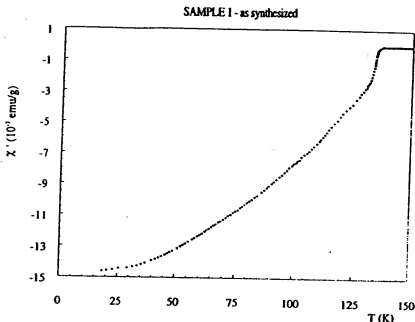


Fig. 7. AC susceptibility vs. T for as-synthesized sample I, where Hg-1223 is present as the main phase and Hg-1212 as the minority phase.

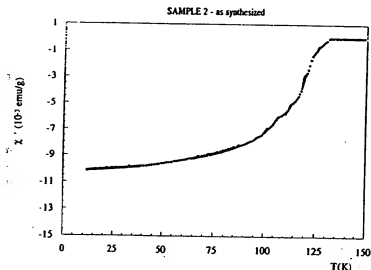


Fig. 8. AC susceptibility vs. T for as-synthesized sample II showing the presence of Hg-1234 as the main phase and of Hg-1223 as the minority phase.

1212. The appropriate treatment for Hg-1234 can possibly change T_c for this phase. Therefore, we can only conclude that for the as-prepared samples a saturation of T_c seems to occur in the Hg-Ba-Ca-Cu-O system at the third member. A similar behavior

occurs for the $\text{TlBa}_2\text{Ca}_{n-1}\text{Cu}_n\text{O}_{2n+3+x}$ homologous series, for which T_c increases up to the third member (120 K) also [9].

One can see in table I that for the Hg series, the increase of T_c is accompanied by a decrease of the a

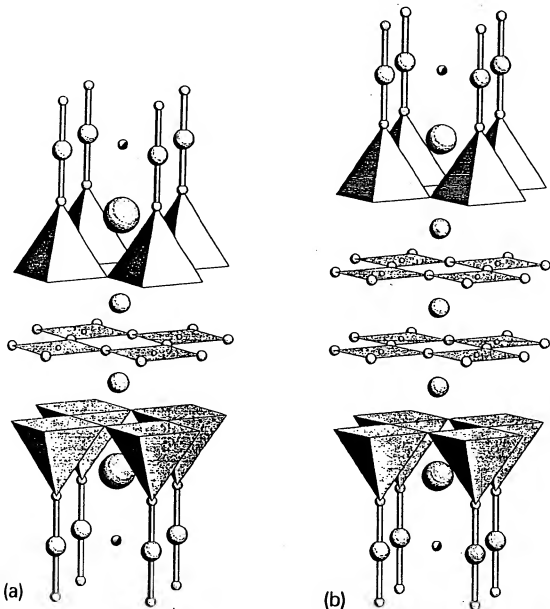


Fig. 9. The crystal structures of Hg-1223 (a) and Hg-1234 (b). The largest and medium large circles refer to Ba and Ca atoms, respectively. The Cu atoms are the smallest circles. Those at the base of the shaded pyramids are not shown. The circles forming the squares around the Cu are oxygen atoms. The dumbbells around the Hg atoms are formed by apical oxygen atoms. Partially filled circles refer to the partially occupied oxygen sites on the Hg layer.

parameter and just at T_c it remains practically constant between Hg-1223 and Hg-1234.

The electron microscopy study of Hg-1201 [10]

revealed the absence of intergrowths and this was attributed to the absence of the Ca^{2+} cations in the system. On the contrary, the addition of Ca layers in

Table 1
Lattice parameters and transition temperatures for Hg-based Cu oxides

Formula	Short form	a (Å)	c (Å)	T_{∞} (K)	Ref.
$\text{HgBa}_2\text{CuO}_{8+x}$	Hg-1201	3.8797(5)	9.509(2)	94	[1]
$\text{HgBa}_2\text{CaCu}_2\text{O}_{8+x}$	Hg-1212	3.8556(8)	12.652(4)	121	[2]
				126	[3]
$\text{HgBa}_2\text{Ca}_2\text{Cu}_3\text{O}_{8+x}$	Hg-1223	3.8532(6)	15.818(2)	133	[4], this work
$\text{HgBa}_2\text{Ca}_3\text{Cu}_4\text{O}_{10+x}$	Hg-1234	3.8540(3)	19.006(3)	<132	this work

the system leads to intergrowths due to different numbers of (CuO_2) and Ca layers in the perovskite-like slabs. Such intergrowths were already reported in ref. [4]. Possibly, the occurrence of different intergrowths may explain why the variation versus temperature of the AC susceptibility does not present distinct and abrupt transitions which could be attributed to pure Hg-1212, 1223 and 1234 phases.

The synthesis of the higher members of the Hg-based homologous series as bulk samples has been performed at higher temperatures than that used for Hg-1212 and with longer treatment times. We suggest that the synthesis of such phases occurs through the formation at an initial state and subsequent decomposition of the lower members of the series. This feature is similar to that existing for the $\text{Tl-Ba}_2\text{Ca}_{n-1}\text{Cu}_n\text{O}_{2n+3-x}$ homologous series [9]. The use of high pressure, possibly, lowers the mercury oxide decomposition. It also leads to a decrease of stability of CaHgO_2 , whose synthesis at the first stage of the reaction inhibits the formation of Hg-based compounds.

Acknowledgements

The authors would like to thank M.F. Gorius, M.

Perroux and R. Argoud for their technical assistance. The visit of EVA has been supported by the fund from the French Ministry of Foreign Affairs. EVA and SNP would like to thank the support of the Russian Scientific Council on Superconductivity (Project "Poisk"). SML was supported by the Erasmus Students Exchange Program.

References

- [1] S.N. Putilin, E.V. Antipov, O. Chmaissem and M. Marezio, *Nature* (London) 362 (1993) 226.
- [2] S.N. Putilin, E.V. Antipov and M. Marezio, *Physica C* 212 (1993) 266.
- [3] S.M. Loureiro and J.J. Capponi, private communication.
- [4] A. Schilling, M. Cantoni, J.D. Guo and H.R. Ott, *Nature* (London) 363 (1993) 56.
- [5] K.E. Johansson, T. Palm and P.-E. Werner, *J. Phys. E: Sci. Instrum.* 13 (1980) 1289.
- [6] S.N. Putilin, M.G. Rozova, D. Kashporov, E.V. Antipov and L.M. Kovba, *Zh. Neorganicheskoi Khimii* 36 (1991) 1645 (in Russian).
- [7] O. Chmaissem, Q. Huang, S.N. Putilin, M. Marezio and A. Santoro, *Physica C* 212 (1993) 259.
- [8] J.L. Wagner, P.G. Radaelli, D.G. Hinks, J.D. Jorgensen, J.F. Mitchell, B. Dabrowski, G.S. Knap and M.A. Beno, *Physica C* 210 (1993) 447.
- [9] S. Nakajima, M. Kikuchi, Y. Syono, T. Oku, D. Shindo, K. Hiraga, N. Kobayashi, H. Iwasaki and Y. Muto, *Physica C* 158 (1989) 471.
- [10] I. Brynse and S.N. Putilin, *Physica C* 212 (1993) 223.

BRIEF ATTACHMENT BJ

IN THE UNITED STATES PATENT AND TRADEMARK OFFICE

In re application of:

Date: November 6, 2006

Applicants: Bednorz, et al.

Docket: YO987-074BZ

Serial No.: 08/479,810

Group Art Unit: 1751

Filed: June 7, 1995

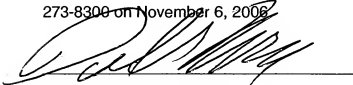
Examiner: M. Kopec

For: NEW SUPERCONDUCTIVE COMPOUNDS HAVING HIGH TRANSITION
TEMPERATURE, METHODS FOR THEIR USE AND PREPARATION

Commissioner for Patents
P.O. Box 1450
Alexandria, VA 22313-1450
(571) 273-8300

CERTIFICATE OF FACSIMILE TRANSMISSION

I hereby certify that this Ninth Response After Final Rejection (4 pages)
is being facsimile transmitted to the U.S. Patent and Trademark Office to (571)
273-8300 on November 6, 2006.



Dr. Daniel P. Morris, Esq.
Reg. No. 32,053

NINTH SUPPLEMENTAL RESPONSE

Sir:

In response to Office Action dated October 20, 2005, please consider the
following:

IN THE UNITED STATES PATENT AND TRADEMARK OFFICE

In re Patent Application of

Date: January 30, 2008

Applicants: Bednorz et al.

Docket: YO987-074BZ

Serial No.: 08/479,810

Group Art Unit: 1751

Filed: June 7, 1995

Examiner: M. Kopec

For: NEW SUPERCONDUCTIVE COMPOUNDS HAVING HIGH TRANSITION
TEMPERATURE, METHODS FOR THEIR USE AND PREPARATION

Commissioner for Patents
Box AF
P.O. Box 1450
Alexandria, VA 22313-1450

SIXTEENTH SUPPLEMENTARY RESPONSE

Submitted at the Suggestion of the Examiner in response to the
Advisory Action dated November 15, 2007

In response to the Advisory Action dated November 15, 2007 please consider the following:

Bismuth strontium calcium copper oxide

From Wikipedia, the free encyclopedia

Bismuth strontium calcium copper oxide, or **BSCCO** (pronounced "bisko"), is a family of high-temperature superconductors having the generalized chemical formula $\text{Bi}_2\text{Sr}_2\text{Ca}_n\text{Cu}_{n+1}\text{O}_{2n+6}$.

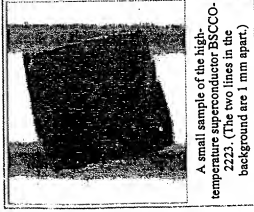
Specific types of BSCCO are usually referred to using the sequence of the numbers of the metallic ions. Thus **BSCCO-2212** ($\text{Bi}_2\text{Sr}_2\text{Ca}_1\text{Cu}_2\text{O}_8$) has a critical temperature of 95 K and **BSCCO-2223** ($\text{Bi}_2\text{Sr}_2\text{Ca}_2\text{Cu}_3\text{O}_9$) has $T_c = 107$ K. Both these critical temperatures are above the temperature of liquid nitrogen. BSCCO was also the first high-temperature superconductor to be discovered which did not contain a rare earth element.

BSCCO-2212 is the first high-temperature superconductor to be used for making conducting wires. Although it has the same problems with weak links at crystal grain boundaries as YBCO, for BSCCO this can be overcome by a texture evolution during the rolling process due to Van-der-Waals coupled BiO layers, which are not present in YBCO. However, its critical current density in magnetic fields at elevated temperatures is about a factor 10 less than that of YBCO.

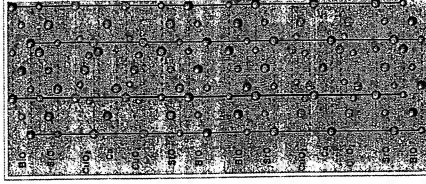
Retrieved from

"http://en.wikipedia.org/wiki/Bismuth_strontium_n_copper_oxide"

Categories: Bismuth compounds | Strontium compounds | Calcium compounds | High-temperature superconductors



A small sample of the high-temperature superconductor BSCCO-2223. (The two lines in the background are 1 mm apart.)



The unit cell of BSCCO-2212. The other BSCCO family members have very similar structures: 2201 has one less CuO_2 in its top and bottom half and no Ca layer, while 2223 has an extra CuO_2 and Ca layer in each half.

- This page was last modified 14:15, 14 July 2006.
 - All text is available under the terms of the GNU Free Documentation License. (See Copyrights for details.)
- Wikipedia® is a registered trademark of the Wikimedia Foundation, Inc.

ATTACHMENT BK

IN THE UNITED STATES PATENT AND TRADEMARK OFFICE

In re Patent Application of

Applicants: Bednorz et al.

Serial No.: 08/479,810

Filed: June 7, 1995

For: NEW SUPERCONDUCTIVE COMPOUNDS HAVING HIGH TRANSITION
TEMPERATURE, METHODS FOR THEIR USE AND PREPARATION

Date: November 25, 2006

Docket: YO987-074BZ

Group Art Unit: 1751

Examiner: M. Kopeck

Commissioner for Patents

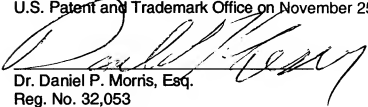
Box AF

P.O. Box 1450

Alexandria, VA 22313-1450

CERTIFICATE OF FIRST CLASS TRANSMISSION

I hereby certify that this Supplementary Response, (3 Pages Plus
Attachment A and Attachment B) is being transmitted by first class mail to the
U.S. Patent and Trademark Office on November 25, 2006.



Dr. Daniel P. Morris, Esq.
Reg. No. 32,053

FOURTEENTH SUPPLEMENTARY RESPONSE

In response to the Office Action dated October 20, 2005 please consider the
following:

IN THE UNITED STATES PATENT AND TRADEMARK OFFICE

In re Patent Application of

Applicants: Bednorz et al.

Serial No.: 08/479,810

Filed: June 7, 1995

Date: March 20, 2008

Docket: YO987-074BZ

Group Art Unit: 1751

Examiner: M. Kopec

For: NEW SUPERCONDUCTIVE COMPOUNDS HAVING HIGH TRANSITION
TEMPERATURE, METHODS FOR THEIR USE AND PREPARATION

Commissioner for Patents

Box AF

P.O. Box 1450

Alexandria, VA 22313-1450

ATTACHMENT FOR SEVENTEENTH SUPPLEMENTARY RESPONSE

Submitted at the Suggestion of the Examiner in response to the

Advisory Action dated November 15, 2007

In response to the Advisory Action dated November 15, 2007 please consider the following:

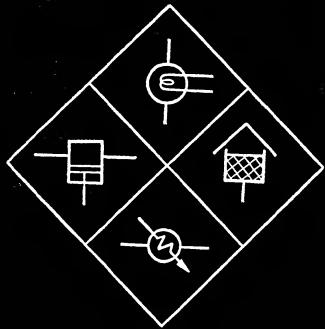
Respectfully submitted,

IBM CORPORATION
Intellectual Property Law Dept.
P.O. Box 218
Yorktown Heights, New York 10598

/Daniel P. Morris/
Dr. Daniel P. Morris, Esq.
Reg. No. 32,053
(914) 945-3217

ATTACHMENT A

Cryogenic Engineering



Edited by
B.A.HANDS

ORE

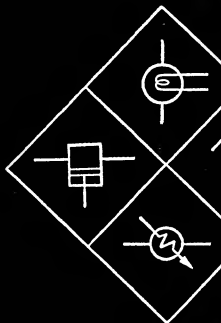
438929

TP 482.C74
1986
COPY 1

HANDS

Cryogenic Engineering

Cryogenic Engineering



Edited by
B.A.HAN

TP
482-
C74
1986

0.12.322990.1

YORE 1

Cryogenic Engineering

Edited by

B. A. Hands

*Department of Engineering Science, University of Oxford,
and St. Hilda's College, Oxford, England*

1986



Academic Press

Harcourt Brace Jovanovich, Publishers

London Orlando New York San Diego Austin
Boston Tokyo Sydney Toronto

ACADEMIC PRESS INC. (LONDON) LTD.
24/28 Oval Road, London NW1 7DX

United States Edition published by
ACADEMIC PRESS, INC.
Orlando, Florida 32887

Copyright © 1986 by
Academic Press Inc. (London) Ltd.

All rights reserved. No part of this book may be reproduced
or transmitted in any form or by any means, electronic or
mechanical, including photocopy, recording, or any
information storage and retrieval system without permission
in writing from the publishers

British Library Cataloguing in Publication Data

Cryogenic engineering.
I. Low temperature engineering
I. Hands, B.A.
621.5'9 TP482

ISBN 0-12-322990-1
ISBN 0-12-322991-X (Pbk)

Computer typeset and printed by
Page Bros (Norwich) Ltd

C. A. Bail
eering S
and Fell
R. A. Byrn
Formerly
Californ
D. Dew-H
versity o
versity C
D. Evans
0QX, Er
E. J. Grego
Fordhou
B. A. Hand
eering S
and G.E
G. Kraft
Karlsruh
J. T. Morg
OX11 0C
N. Nambud
Bombay
Engineer
B. W. Rich
inghamsh
J. M. Robe
Establish
H. Sixsmid
Hampshi
W. L. Swi
Hampshi
W. J. Tallis
Science, I
R. M. Tho
Chemical
T. J. Webst
England.

Contributors

- C. A. Bailey** University Lecturer, Cryogenics Laboratory, Department of Engineering Science, University of Oxford, Parks Road, Oxford OX1 3PJ, England and Fellow of Keble College, Oxford
- R. A. Byrns** Consultant, 2457 Marin Avenue, Berkeley, California 94708, U.S.A. *Formerly* Staff Senior Scientist, Lawrence Berkeley Laboratory, University of California, Berkeley, California 94720, U.S.A.
- D. Dew-Hughes** University Lecturer, Department of Engineering Science, University of Oxford, Parks Road, Oxford OX1 3PJ, England and Fellow of University College, Oxford
- D. Evans** Rutherford Appleton Laboratory, Chilton, Didcot, Oxfordshire OX11 0QX, England
- E. J. Gregory** Chief Process Engineer, Marston-Palmer Limited, Wobaston Road, Fordhouses, Wolverhampton WV10 6QJ, England
- B. A. Hands** Research Associate, Cryogenics Laboratory, Department of Engineering Science, University of Oxford, Parks Road, Oxford OX1 3PJ, England and G.E.C. Lecturer in Engineering, St. Hilda's College, Oxford
- G. Krafft** Koordinationstelle Technologietransfer, Kernforschungszentrum Karlsruhe GmbH, Postfach 3640, D-7500 Karlsruhe 1, West Germany
- J. T. Morgan** Rutherford Appleton Laboratory, Chilton, Didcot, Oxfordshire OX11 0QX, England
- N. Nambudripad** Tata Institute of Fundamental Research, Homi Bhabha Road, Bombay 400 005, India. *Formerly* of the Cryogenics Laboratory, Department of Engineering Science, University of Oxford
- B. W. Ricketson** Cryogenic Calibrations Limited, Pitchcott, Aylesbury, Buckinghamshire HP22 4HT, England
- J. M. Robertson** Heat Transfer and Fluid Flow Service, Atomic Energy Research Establishment, Harwell, Oxfordshire OX11 0RA, England
- H. Sixsmith** Creare Inc., PO Box 71, Great Hollow Road, Hanover, New Hampshire 03755, U.S.A.
- W. L. Swift** Creare Inc., PO Box 71, Great Hollow Road, Hanover, New Hampshire 03755, U.S.A.
- W. J. Tallis** Design Engineer, Cryogenics Laboratory, Department of Engineering Science, University of Oxford, Parks Road, Oxford OX1 3PJ, England
- R. M. Thorogood** Director, Cryogenic Research Programs, Air Products and Chemicals Inc., PO Box 538, Allentown, Pennsylvania 18105, U.S.A.
- T. J. Webster** Consultant, 38 Parkland Grove, Ashford, Middlesex TW15 2JR, England. *Formerly* Safety Manager, British Oxygen Company Ltd., England

Preface

The 1960s saw great activity in the field of cryogenic engineering, stimulated particularly by the American space effort and by developments in superconductivity. As a result, a number of books on cryogenic engineering in general were published. Since then, most volumes have concentrated on a particular aspect of the subject, rather than attempting a comprehensive review. In view of the steady, if unspectacular, advances made since that time, it seems opportune to attempt a new account of the basic science and of the engineering methods employed.

Cryogenic engineering covers a wide spectrum of disciplines, in traditional terms embracing much of electrical, mechanical and chemical engineering, its distinguishing feature being the use of temperatures well below ambient. In order to produce a volume of reasonable length, it was decided to assume that the reader should have knowledge appropriate to that of a final-year or graduate engineer or physicist. Further, since much of the body of knowledge of engineering at room-temperature can be applied directly to cryogenic problems, reference in such cases is made to standard textbooks, although since this book is biased towards engineering, the physicist may need to consult rather more of them than the engineer.

It was also decided, again on the grounds of overall length, to restrict the account of superconductivity. The design of superconducting magnets is very largely an electrical engineering problem, the cryogenic design, apart from training problems and stabilisation, being relatively straightforward. Further, the monograph "Superconducting Magnets" by M. N. Wilson (Oxford University Press, 1985) treats the subject comprehensively, and is required reading for anyone with other than a superficial interest in magnet design. Thus, the coverage of this topic is deliberately brief.

There are some other deliberate omissions, also. In particular, an account of refrigeration using hydrogen and neon is omitted, on the grounds that the techniques involved are broadly the same as those used for helium. Similarly, the particular problems involved with cryogenics in space are given only passing mention, since most of the design principles involved are also applicable to earth-based equipment. There is no attempt to provide complete property data; general trends are indicated, and, it is hoped, enough references for the reader to locate detailed data as necessary. However, since the book is intended for potential (and practising) cryogenic engineers, details of practical methods and current practices have been included.

The production of this book has been a co-operative effort, and I thank the authors for their tolerance of the editor's quirks. I should like to acknowledge those who have read parts of my own contributions and assisted with the provision of information, photographs and diagrams, particularly Dr A. Acton, Dr V. D. Arp, Mr R. J. Allam, Dr C. A. Bailey, Dr M. L. Christie, Dr. G. Davey, Prof G. B. Donaldson, Mr R. Harper, Dr D. B. R. Kenning, Dr R. D. McCarty, Dr W. Obert, Dr. C. Ruiz, Dr L. Solymar and Dr. R. M. Thorogood. Acknowledgements and sources for diagrams and photographs are given as appropriate in the text; I am most grateful to the organisations which supplied these and gave permission for their use. I am indebted to Johanne Beaulieu for preparing much of the text, to Mrs Judith Takacs for drawing the diagrams with her usual patience and skill, and to Mrs Stella Seddon for preparing the index. Finally, gratitude is due to my family for their tolerance, and for foregoing the use of the dining table for many months.

Oxford, 1985

B. A. Hands

Contributo
Preface

In the tables of data, a dash indicates that information was not available.

1.1 Introd
1.2 The C
1.3 Featu
1.4 Liquef
1.5 Air Se
1.6 Liquic
1.7 Liquic
1.8 Supen
1.9 Cryog
1.10 Cryog
1.11 Medic
1.12 Cryop
1.13 Instru
Refert
Journs
Gener
Bibliog
Non-sq

2.1 Introdu
2.2 Propert
2.3 Hydrog
2.4 Helium
2.5 Equatic

PREFACE

and I thank the
knowledge those
the provision of
Dr V. D. Arp,
by, Prof G. B.
Carty, Dr W.
acknowledgements
in the text; I
permission for
of the text, to
and skill, and
e to my family
many months.

A. Hands

ible.

Contents

Contributors
Preface

v
vii

1. A Survey of Cryogenic Engineering

B. A. Hands

1.1 Introduction	1
1.2 The Cryogenic Temperature Range	2
1.3 Features of Cryogenic Engineering	3
1.4 Liquefied Natural Gas (LNG)	6
1.5 Air Separation	10
1.6 Liquid Hydrogen	15
1.7 Liquid Helium	18
1.8 Superconducting Magnets and Machinery	19
1.9 Cryogenic Electronics	26
1.10 Cryogenics in Space	29
1.11 Medical and Biological Applications	29
1.12 Cryopumping	30
1.13 Instrumentation	33
References	34
Journals	36
General Bibliography	36
Bibliography of Specific Topics	36
Non-specialist Reading	37

2. Properties of the Cryogenic Fluids

B. A. Hands

2.1 Introduction	39
2.2 Property Data	40
2.3 Hydrogen	43
2.4 Helium	46
2.5 Equations of State	50

2.6 The Two-phase Region	54	5.9
2.7 Computer Packages	56	5.10
2.8 Approximate Equations	58	5.11
2.9 Properties of Mixtures	59	5.12
References	63	5.13
Sources of Data	63	5.14

3. Cryogenic Safety

T. J. Webster

3.1 Introduction	67	
3.2 Organisation for Safety	68	6.1 I
3.3 Relationship between Fluid Properties and Safety	68	6.2 I
3.4 First Aid	76	6.3 I
3.5 Combustion	77	6.4 I
3.6 Oxygen Hazards	79	6.5 I
3.7 Unexpected Hazards	83	6.6 I
3.8 Fluorine Safety	87	I
Bibliography	87	

4. Thermal Design

C. A. Bailey and B. A. Hands

4.1 Conservation of Energy Considerations	89	7.1 I
4.2 General Energy Requirements	90	7.2 F
4.3 Specific Heat	93	7.3 F
4.4 Thermal Contraction	97	7.4 F
4.5 Thermal Conductivity of Solids	100	F
4.6 Conduction through Gases	106	
4.7 Radiative Heat Transfer	107	
4.8 Thermal Insulations	112	
4.9 Applications to Design	116	
References	121	
Bibliography	121	

5. Fluid Dynamics

B. A. Hands

5.1 Introduction	123	8.1 I
5.2 Pressure Drop Calculations	124	8.2 R
5.3 Single-phase Pressure Drop	125	8.3 C
5.4 Characteristics of Two-phase Flow	128	8.4 P
5.5 Two-phase Pressure Drop	130	R
5.6 Critical (Choked) Flow	131	9.1 I
5.7 Cooldown Behaviour	131	9.2 S
5.8 Introduction to Instabilities	132	9.3 F

CONTENTS

CONTENTS

xi

54	5.9 Density Wave Oscillations	134
56	5.10 The Ledinegg Instability and Pressure-drop Oscillations	136
58	5.11 Geysering	138
59	5.12 Thermoacoustic Oscillations	141
63	5.13 Stratification, Thermal Overfill and Rollover	143
63	5.14 Sloshing	146
	References	148

6. Heat Transfer to Fluids

J. M. Robertson

67	6.1 Introduction	151
68	6.2 Heat Transfer to Single-phase Fluids	153
68	6.3 Heat Transfer Rates	156
76	6.4 Pool Boiling	157
77	6.5 Boiling in Channels	160
79	6.6 In-tube Condensing	166
83	References	168
87		

7. Heat Transfer Below 10 K

G. Kraft

89	7.1 Introduction	171
90	7.2 Basic Considerations	172
93	7.3 Heat Transfer to Supercritical Helium	174
97	7.4 Heat Transfer to Two-phase Helium	181
100	References	191

8. Heat Exchangers

E. J. Gregory

106	8.1 Introduction	193
107	8.2 Regenerators	195
112	8.3 Coiled Tube Heat Exchangers	197
116	8.4 Plate and Fin Heat Exchangers	199
121	References	216

9. Electrical Conductors at Low Temperatures

D. Dew-Hughes

123	9.1 Introduction	217
124	9.2 Simple Theory of Electrical Resistivity	219
125	9.3 Real Conductors at Low Temperatures	221
128		
130		
131		
131		
132		

9.4 Magnetoresistance	223
9.5 Superconductivity	225
9.6 Theories of Superconductivity	229
9.7 Flux-pinning and Critical Current Density	232
9.8 Conductor Stability	235
9.9 Stress Effects	236
9.10 Commercial Superconductors	238
Bibliography	240

10. Mechanical Design with Metals

B. A. Hands

10.1 Introduction	241
10.2 Elastic Moduli	242
10.3 Plastic Behaviour	243
10.4 Fracture Behaviour	246
10.5 Fatigue Behaviour	252
10.6 Aluminium Alloys	254
10.7 Stainless Steels	257
10.8 Nickel-Iron Alloys	262
10.9 Titanium Alloys	265
10.10 Copper Alloys	266
10.11 General Discussion	267
References	269
Bibliography	270

11. Design with Non-metallic Materials

D. Evans and J. T. Morgan

11.1 Introduction	271
11.2 Mechanical Properties of Polymers and their Relation to Structure	276
11.3 Thermal Contraction	285
11.4 Thermal Conductivity	289
Bibliography	292

12. Construction and Assembly Methods

W. J. Tallis

12.1 General Design Considerations	293
12.2 Permanent Joints	295
12.3 Demountable Joints	302
12.4 General Comments	309

CONTENTS

223
225
229
232
235
236
238
240

241
242
243
246
252
254
257
262
265
266
267
269
270

271
276
285
289
292

293
295
302
309

CONTENTS

xiii

13. Principles of Refrigeration, Liquefaction and Gas Separation

C. A. Bailey and B. A. Hands

13.1 Refrigeration	313
13.2 Liquefaction	314
13.3 Cooling Methods	316
13.4 Simple Cycles	320
13.5 Irreversibility	324
13.6 Second Law Violations	324
13.7 Compound Cycles	325
13.8 The Separation of Gases	328
13.9 Principles of Distillation	329
13.10 The Single Column Linde System	336
13.11 The Double Column	339
References	340

14. Cryogenic Turbines and Pumps

H. Sixsmith and W. L. Swift

14.1 Introduction	341
14.2 Turboexpander Design	342
14.3 Gas Bearings	344
14.4 Protective Devices	348
14.5 Turbine Performance	349
14.6 Pumps	352
14.7 Conclusions	355
References	355

15. Large Helium Refrigeration and Liquefaction Systems

R. A. Byrns

15.1 Specification of Heat Load and Capacity	357
15.2 Design of J-T Stage	360
15.3 The Claude Cycle	362
15.4 Design and Optimisation	364
15.5 Compressors	366
15.6 Heat Exchangers	368
15.7 Expanders	369
15.8 Control, Instrumentation, Purity and Gas Management	371
15.9 Distribution and Cooling Methods	372
15.10 Large Helium Plants	375
15.11 Large Purification Liquefiers	375
15.12 The 1500 W Refrigerator	376
15.13 Lawrence Livermore National Laboratory (3000 W) System	379
15.14 Fermi National Accelerator Laboratory (23 kW) System	381

15.15 Brookhaven 24.8 kW Refrigerator	388
15.16 Refrigeration Equipment Cost	389
References	389

16. Large Gas Separation and Liquefaction Plants

R. M. Thorogood

16.1 Introduction	391
16.2 Cryogenic Air Separation Processes	392
16.3 Natural Gas Processes	409
16.4 Natural Gas Liquefaction Processes	411
16.5 Equipment for Large Air Separation Plants	418
16.6 Equipment for Natural Gas Plants	424
16.7 Operation and Safety	427
Acknowledgements	428
References	428

17. Small Refrigerators

N. Nambudripad

17.1 Introduction	431
17.2 The Stirling Refrigerator	433
17.3 The Gifford-McMahon Refrigerator	438
17.4 The Pulse-tube Refrigerator	441
17.5 The Vuilleumier Refrigerator	443
17.6 Losses in Regenerative Mechanical Coolers	445
17.7 Regenerators	447
17.8 Magnetic Refrigeration	452
References	453

18. Thermometry

B. W. Ricketson

18.1 Introduction	457
18.2 Temperature and Accuracy	458
18.3 Criteria for Choosing a Sensor	459
18.4 Sensors	460
18.5 Thermal Anchorage for Electrical Leads	467
18.6 Measurement	468
18.7 Temperature from the Measurement	473
18.8 Conclusion	476
References	476

Appendix	477
Index	485

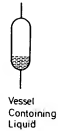
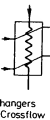
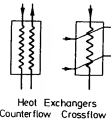
388
389
389

Symbols Used

391
392
409
411
418
424
427
428
428



431
433
438
441
443
445
447
452
453



457
458
459
460
467
468
473
476
476

477
485

A Survey of Cryogenic Engineering

B. A. HANDS

1.1 Introduction	1
1.2 The Cryogenic Temperature Range	2
1.3 Features of Cryogenic Engineering	3
1.4 Liquefied Natural Gas (LNG)	6
1.5 Air Separation	10
1.6 Liquid Hydrogen	15
1.7 Liquid Helium	18
1.8 Superconducting Magnets and Machinery	19
1.9 Cryogenic Electronics	26
1.10 Cryogenics in Space	29
1.11 Medical and Biological Applications	29
1.12 Cryopumping	30
1.13 Instrumentation	33
References	34
Journals	36
General Bibliography	36
Bibliography of Specific Topics	36
Non-specialist Reading	37

1.1 Introduction

Most of this book is concerned with an outline of the theory and practice of cryogenic engineering. It has not been possible within a volume of reasonable size to explore every aspect in detail, nor has it been possible to give a detailed account of all the applications of cryogenics. This chapter is intended to give an impression of the wide range of cryogenic engineering. After a discussion of the meaning of cryogenics, the chapter covers the uses of the commoner cryogenic liquids (natural gas, oxygen, nitrogen, hydrogen and helium), and then deals with superconductivity and cryo-

pumping. The chapter concludes with a brief outline of cryogenic instrumentation.

1.2 The Cryogenic Temperature Range

The 1960s were a decade which saw a rapid expansion both in low-temperature physics and in the commercial exploitation of low-temperature techniques. Towards the end of this period, a need was felt for the standardisation of low-temperature terminology, and, on the initiative of Professor Nicholas Kurti, the Comité d'étude des termes techniques français organised a meeting in 1969, at which was formed a small international committee to consider the terminology of low temperatures, remembering the necessity of unambiguous translation between English and French, and paying due regard to current practice in the United States. As an example of the confusion which then existed, temperature levels in Britain were, by some people, referred to as 'low' (below 0°C), 'very low' (around 100 K), 'deep low' (around 4 K) and 'ultra low' (less than 0.3 K), although the French had only two terms 'basse' and 'très basse'. It was never clear how the British users of this terminology would refer to temperatures in the microkelvin region!

The working group, with members from six countries, made its recommendations in 1971 [1.1], and these have largely been accepted by the scientific community. 'Cryogenics' and the corresponding prefix 'cryo' were to refer to 'all phenomena, processes, techniques or apparatus occurring or used at temperatures below 120 K' approximately, that is, around or below the normal boiling point of liquefied natural gas. It was recognised, however, that some inconsistencies were unavoidable, in particular the use, on historical grounds, of the terms cryohydrate, cryoscopy, cryochemistry and the French cryodessiccation, all of which refer to temperatures well above 120 K; and, because they use cryogenic fluids and techniques, cryosurgery, cryomedicine and cryobiology. Otherwise, the temperature range between 120 K and 0°C is covered by 'refrigeration' technology.

The scientific community has, on the whole, adhered to these proposals, but they have not been rigidly adopted by industry, where the technology of handling liquid ethylene (at around 150 K) is, with some justification on the grounds of the equipment used, included in the cryogenic domain, and 'cryogenic' is also used, with less justification, to describe equipment designed for use at still higher temperatures. However, since all fluids and materials used in cryogenics must at some time be brought to room temperature, properties and processes in the temperature range up to room temperature cannot be ignored.

1. A SURVEY OF CRYOGENICS

In this book, we are using the word 'engineering' to refer to the most widely used liquid liquefied natural gas (LNG) liquid hydrogen (LH2) importance of hydro range, the product is regarded as 'physics' at present to experience demagnetisation and be covered in this way.

1.3 Features of Cryogenics

It is worth considering 'ordinary' (or room temperature) that the properties of a particular material accepted that, in fact, they behave similarly to cryogenics. The ability to recognise and the use of low temperature different from that of cryogenics. The design criteria with identification of methods to achieve should, therefore, be in its own right.

There are, however, engineering temperature ranges—fluidity—the ability of the superfluid state. Theoretical physicists for many years has been achieved. It is because of the very high

The other phenomena of electrical resistance different for each material.

* According to [1.1], the wide acceptance.

cryogenic

In this book, we follow the 1971 recommendation and take 'cryogenic engineering' to refer to the temperature range below about 120 K. The most widely used liquids, in order of descending normal boiling point, are liquefied natural gas (LNG), liquid oxygen (LOX), liquid nitrogen (LIN), liquid hydrogen (LH₂) and liquid helium (LHe), although at present the importance of hydrogen has declined. At the lower end of the temperature range, the production of temperatures less than about 1.5 K may be regarded as 'physics' rather than 'engineering', since their use is restricted at present to experimental work. Therefore, techniques such as adiabatic demagnetisation and the use of the light isotope of helium (He³) will not be covered in this volume.

1.3 Features of Cryogenic Engineering

It is worth considering at this stage the differences between cryogenic and 'ordinary' (or room temperature) engineering. For a long time, it was felt that the properties of cryogenic fluids were in some way peculiar, so that a particular mystique arose around this area of engineering. It is now accepted that, in fact, cryogens (with the exception of superfluid helium) behave similarly to other fluids, and that the art of cryogenics lies in the ability to recognise and cater for the particular problems which arise through the use of low temperatures *per se*. This requirement is, of course, no different from that required in any other branch of engineering: an assessment of design criteria and possible causes of equipment failure, together with identification of the best techniques, materials and construction methods to achieve safe, efficient and reliable operation. Cryogenics should, therefore, be regarded more as a special art rather than as a subject in its own right.

There are, however, two phenomena peculiar to the cryogenic engineering temperature range which merit special consideration. One is superfluidity—the ability of liquid helium to behave as if it has zero viscosity. The superfluid state has been investigated by both experimental and theoretical physicists for many years, and a deep understanding of its behaviour has been achieved. From the engineer's point of view, it is of interest because of the very high rates of heat transfer which can be attained.

The other phenomenon is that of superconductivity,* the complete loss of electrical resistance below some well-defined temperature which is different for each metal. Superconductivity is of increasing technical import-

* According to [1.1], the proper term is superconduction, but this word has never achieved wide acceptance.

ance in the provision of high and very stable magnetic fields, and its application to heavy electrical engineering is being extensively studied. In 1962, the discovery of the Josephson effect opened the door to a new range of superconducting electronic devices.

The penalty of operating in the cryogenic temperature range is that work must be done to reach and maintain the low temperature required; from the second law of thermodynamics, it is clear that the work will increase roughly in inverse proportion to the magnitude of the absolute temperature. For instance, to extract 1 J of heat reversibly at 77 K requires about 3.7 J of work, while to extract 1 J at 4.2 K requires about 68 J of work. In practice, of course, reversibility cannot be achieved, and the work actually required is somewhat larger, by a few tens of percent at the higher cryogenic temperatures, to a factor of ten in the liquid helium range. Thus, on economic grounds there is every incentive to avoid the use of cryogenics wherever possible.

Cryogenics can be considered to have been born towards the end of 1877, when the first liquefaction of oxygen was achieved, by Raoul Pictet in Geneva, Switzerland, and by Louis Cailletet in Chatillon-sur-Seine in France.* Each used a different technique. Pictet's was to cool oxygen at 470 bars to about 140 K using successively liquid sulphur dioxide and solid carbon dioxide, at which temperature he allowed the oxygen to escape through a valve, and saw a mixture of liquid and vapour in the resulting jet. Cailletet, on the other hand, cooled his oxygen to only -29°C using liquid sulphur dioxide, and then performed an adiabatic expansion to form a mist of droplets in his glass vessel. It is perhaps of interest to observe that Pictet's method of 'cascade' cooling followed by Joule-Thomson expansion is still used in many designs of refrigerator and liquefier, although usually in association with external-work machines.

The next significant step was the invention of the vacuum flask by James Dewar, which enabled liquefied gases to be stored for long periods and paved the way for the liquefaction of hydrogen and helium. Until Dewar's invention, the liquids were stored in the innermost of a number of concentric vessels, each containing in turn a boiling liquid of higher temperature. The vacuum insulated, glass flask is now well known to the general public as a 'Thermos'; in the scientific community the name 'dewar' is preferred and is also used for small storage vessels of metallic or polymeric construction.

Developments during the next two decades proceeded apace, with Claude in France and Linde in Germany developing techniques for the liquefaction and fractional distillation of air to produce oxygen and nitrogen, and

* Which scientist was first is of no concern to us here, nor is the ensuing controversy, which has been discussed recently by Kurti [1.2].

1. A SURVE

forming cor
today to m
the 'perma
afterwards
above the li
plentiful su
Leiden fro
especially fo

Between t
production
process of a
100 m³ (100 t
was still a co
duction being
basis, and the
the world.

Immediate
Massachusset
liquefier usin
making liquid
the same tim
during the 19
comparatively

As a result,
produced in q
conducting me
was readily ava
those research
since the savir
water-cooled s
As confidence
constructed, so
tens of supercx
refrigerators in
engines were d
several kilowatt

As to the futu
argon by the frac
process for man
present forms a v
in importance as
are developed. f

elds, and its
y studied. In
a new range

is that work
quired; from
will increase
emperature.
; about 3.7 J
of work. In
ork actually
er cryogenic
e. Thus, on
f cryogenics

the end of
Raoul Pictet
sur-Seine in
d oxygen at
de and solid
n to escape
he resulting
-29°C using
sion to form
observe that
n expansion
ugh usually

sk by James
periods and
ntil Dewar's
f concentric
ature. The
l public as a
ferred and
nstruction.
with Claude
liquefaction
rogen, and

roversy, which

forming companies which are still in the forefront of cryogenic engineering today to market their inventions. Finally, in 1908, helium, the last of the 'permanent' gases, was liquefied by Kamerlingh Onnes, who shortly afterwards produced superfluid helium by reducing the vapour pressure above the liquid using a vacuum pump. It is worth noting, in these days of plentiful supplies, that Onnes's helium was painstakingly extracted at Leiden from large quantities of monazite sand imported from India especially for the purpose.

Between the two World Wars, there was a steady development in the production of oxygen and nitrogen by the distillation of liquid air (the process of 'air separation'), and during the 1930s plants producing around 100 m³ (100 t) of liquid oxygen per day were in operation. Liquid helium was still a comparatively rare and expensive commodity, the rate of production being limited to a litre or two per hour, often only on an intermittent basis, and the liquid being available in only very few laboratories throughout the world.

Immediately after the Second World War, Professor Sam Collins, at the Massachusetts Institute of Technology, developed a new design of helium liquefier using reciprocating expansion engines, which was capable of making liquid on a continuous basis at a rate of several litres per hour. At the same time, the extraction of helium from natural gas wells, begun during the 1920s, had greatly increased, so that helium gas, although still comparatively expensive, was no longer a rare commodity.

As a result, when, during the 1960s, Type II superconducting wire was produced in quantity on a commercial basis, enabling high-field superconducting magnets to be constructed for the first time, liquid helium was readily available for cooling. This development was quickly exploited by those research establishments concerned with high-energy nuclear physics, since the saving in energy costs compared with those of an equivalent water-cooled system quickly outweighed the much higher capital cost. As confidence was gained, magnets of increasingly complex design were constructed, so that each of the major laboratories now contain several tens of superconducting magnets. In parallel with these developments, refrigerators incorporating expansion turbines rather than reciprocating engines were developed; a number of refrigerators capable of extracting several kilowatts at 4 K have now been built.

As to the future, it is clear that the production of oxygen, nitrogen and argon by the fractional distillation of liquid air will remain a major industrial process for many years. The transport of liquefied natural gas by sea at present forms a vital link in the world's fuel supply system, but will decrease in importance as supplies of natural gas diminish and other energy sources are developed. Hydrogen may well be one of these fuels, but at present in

energy terms it is expensive to produce, requiring large amounts of primary energy, and the liquefaction process also consumes much energy. Liquid hydrogen, therefore, may never be economically viable as a fuel other than for a few specialised applications.

Superconducting magnet technology has assumed great importance, and since it is economically attractive compared with the use of conventional magnets and can also produce more uniform and time-invariant fields, applications are expanding. For a number of years, superconducting magnets have been routinely manufactured for experimental work in physics and chemistry, notably for nuclear magnetic resonance (NMR) and electron spin resonance (ESR). These methods have recently been extended to biological applications and now to medical diagnosis. This latter provides the first truly large-scale, commercial application of superconductivity.

Although superconducting motors, generators, transmission lines, and so on have been under active development in a number of countries, the scenario so far has been that each advance in superconducting electrical engineering has been matched by an advance in the corresponding room-temperature technology. Since the latter is usually less complex, it has been more attractive on the grounds of both cost and reliability.

In electronic engineering, the Josephson effect opened new prospects in the precise determination of voltage, in the measurement of very small magnetic fields and in rf applications. Devices based on the Josephson effect are now used on a routine basis.

Thus, although cryogenics is a field of relative antiquity, there has been an unusually long time between the discovery of some phenomena and their commercial exploitation. This was particularly so in the case of superconductivity, which was discovered in 1911 but only ceased to be a laboratory curiosity some 50 years later. On the other hand, devices using the Josephson effect were marketed within a few years of its prediction and discovery.

1.4 Liquefied Natural Gas (LNG)

Natural gas is typically composed of 85–95% methane, the remainder being mainly nitrogen, ethane, propane and butane, although quantities of heavier hydrocarbons, carbon dioxide, water, sulphur compounds and, occasionally, mercury, may also be present, the precise composition depending upon the reservoir from which it is extracted. Certain sources, notably in Kansas, are comparatively rich (about 0.4%) in helium and are the major sources of this element. Natural gas is extracted by drilling in a way similar to that used for oil production and is somewhat refined before

1. A SUR

use: the
or as liq
reduced.

Natur
century i
pipeline
of Amer
relied en
of Japan
Europe :

—

Y

15

15

15

15

—

1980

1990

° F

Sources
with the r
of large de
southward
is liquefie
decrease i
pressurisa

The firs
from Lake
and as a re
to Canvey
Twenty ye
Europe, fi

amounts of primary
uch energy. Liquid
as a fuel other than

at importance, and
use of conventional
ne-invariant fields;
erconducting mag-
tal work in physics
NMR) and electron
been extended to
This latter provides
perconductivity.
mission lines, and
er of countries, the
nducting electrical
rresponding room-
omplex, it has been
ility.
ed new prospects in
ment of very small
on the Josephson

uity, there has been
ne phenomena and
so in the case of
only ceased to be a
hand, devices using
of its prediction and

ine, the remainder
rough quantities of
ir compounds and,
recise composition
ed. Certain sources,
i) in helium and are
cted by drilling in a
what refined before

use: the heavier hydrocarbons are separated as natural gas liquid (NGL) or as liquefied petroleum gas (LPG), and the nitrogen content may be reduced.

Natural gas was used on a local basis in the United States during the 19th century for both fuel and heating; by the 1940s it was being distributed by pipeline throughout much of the country and now provides about a quarter of America's energy requirements. Since about 1975, Great Britain has relied entirely on natural gas for its gas supplies; it forms a significant part of Japan's energy consumption; and its use is widespread throughout Europe and the USSR (Table 1.1).

Table 1.1
Past and Projected Consumption of LNG (10^6 t/year)*

Year	Japan	United States	Western Europe	Total
1975	5.0	0.25	8	13.3
1980	19	11	11	41
1985	44	39	22-36	105-119
1990	47-55	50-105	33-39	130-199

Sources of natural gas (10^6 t/year)*

	Americas	USSR	Middle East	Far East	Africa	Total
1980	1	—	3	15	22	41
1990	6-30	9-35	13-17	35-39	67-78	130-199

* From Thorogood [1.3].

Sources of natural gas are scattered relatively evenly around the globe, with the result that a trade has developed in transferring the gas to areas of large demand. Thus there are, for instance, major pipelines from Alaska southwards, and from the USSR to Western Europe. However, much gas is liquefied for both transport and storage to take advantage of the large decrease in specific volume which is achieved without the necessity for pressurisation.

The first shipments of LNG by sea were made on an experimental basis from Lake Charles, United States, to Canvey Island, England, during 1959, and as a result of the success of these voyages a regular service from Algeria to Canvey Island was instituted in 1961, carrying about 700,000 t/year. Twenty years later, routes had been established from Algeria and Libya to Europe, from Algeria to the United States, and from Alaska, Abu Dhabi,

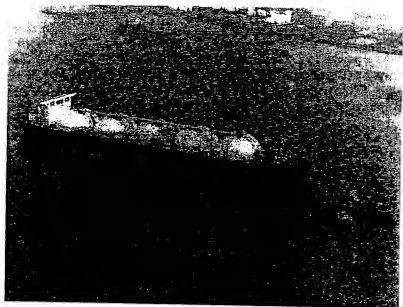
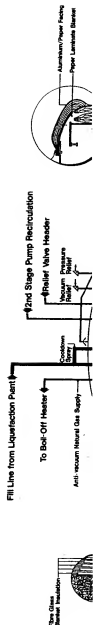


Fig. 1.1 The LNG tanker 'LNG Aquarius', launched in 1977, L.O.A. 285 m. The LNG is carried in 5 spherical aluminium tanks, each of 25,260 m³ capacity. (Courtesy of British Gas Corporation.)

Indonesia and Brunei to Japan, and another ten or so routes were under active development [1.4]. The shipping terminals are supplied by large liquefiers with up to 5000 t/day capacity in a single train (Fig. 16.22).

Apart from storage at liquefaction plants and trading terminals, natural gas is stored as liquid for 'peak shaving' operations, that is, to provide an additional source of gas during periods of peak demand when the normal supply system is inadequate (usually in winter). Liquefaction, using small (200 t/day) plants takes place during periods of low demand in the summer. Storage tanks may be as big as 100 m in diameter and 30 m in height, containing tens of thousands of tonnes of liquid (Fig. 1.2). In the past, they were usually constructed of either aluminium or 9% nickel steel; now, prestressed concrete (with a suitable thin metal liner to eliminate porosity problems) is being increasingly used. During the 1960s, a number of tanks were formed by excavating a hole in the ground and installing a thin steel liner, but this design has proved to be unsatisfactory due to large evaporation rates and to an ever-increasing area of frozen ground around the tank, although new designs are now being developed in Japan.



are under
by large
(.22).
s, natural
provide an
e normal
ing small
summer.
a height,
ast, they
el; now,
porosity
of tanks
g a thin
to large
d around
n.

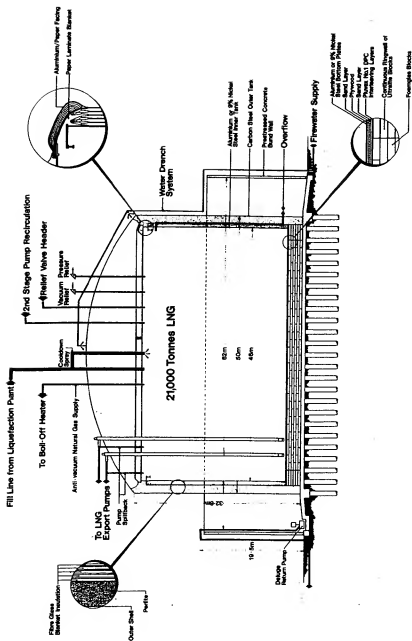


Fig. 1.2 A 50,000 m³ tank for the storage of liquefied natural gas for peak shaving. A bund is provided to retain the liquid in case of leakage. The insulated interspace, which contains natural gas vapour, is open to the vapour above the liquid, so that there will be no pressure differential. The horizontal ceiling above the liquid is insulated with glass fibre. The outer tank is designed as a pressure vessel, and in some designs might be reinforced concrete rather than carbon steel. (Courtesy of British Gas Corporation.)

Besides these large-scale facilities, in some areas it has proved economic to distribute LNG by truck and to keep it in small storage vessels close to the point of use. The technology adopted is similar to the well-established methods used for oxygen and nitrogen.

Purification ('upgrading') of natural gas is achieved by cryogenic methods. Many natural gas sources contain significant quantities of nitrogen and carbon dioxide, which reduce the calorific value and render the gas incompatible with other supplies to the pipeline distribution network. Upgrading plants are based on successive liquefaction and separation of the various components of natural gas and are frequently installed at the well-head. In these plants, solid impurities (sand, etc.) are filtered, and then water, sulphur compounds and carbon dioxide are removed using either molecular sieves or chemical absorption, for example, using glycol to absorb water or monoethanol amine to absorb carbon dioxide. Liquefaction can then take place without blocking the low-temperature heat exchangers with frozen components of the gas. Currently, natural gas companies are projecting a significant increase in the number and size of such plants. This increase is associated with the use of nitrogen injection into the gas wells to enhance gas recovery, thus creating a double use of cryogenics for both injection and rejection, since the nitrogen will be produced on-site by the fractional distillation of liquid air.

1.5 Air Separation

The production of oxygen, nitrogen and argon by the fractional distillation of air, or 'air separation' as it is known, forms a vital part of the infrastructure of the industrialised world. The major developments have occurred since the Second World War: in 1948, a system to produce 140 t/day of liquid oxygen was built in the United States; in the 1970s, plants with ten times that capacity were under construction in various parts of the world. The daily world production of oxygen is now about 5×10^5 t (Fig. 1.3), a purity of around 99.5% being easily achievable even on this scale.

By far the greatest amount of oxygen is consumed by the chemical and steel industries (Table 1.2). Since the daily consumption of a chemical or steel works may amount to several hundred tonnes per day, it has become common practice to build an air separation plant on an adjacent site and deliver the oxygen by pipeline. Because a continuous supply is essential, stringent conditions may be imposed by the user, and emergency electrical generators and back-up storage vessels may have to be provided to guarantee a supply until faults can be rectified or oxygen brought in by road.

A consic
compress
hospitals. C
oxidation o
methanol p
and in the t

Li

St

Nc
Fa
Ch

I

/

J

F

V

C

Pol.
Mis

a.

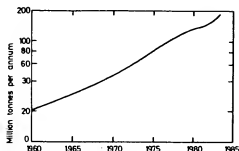


Fig. 1.3 Worldwide annual production rate of oxygen. (Courtesy of R. M. Thorogood.)

A considerable quantity of oxygen is produced in gaseous form and compressed into cylinders to be used, for instance, for welding, in diving and hospitals. Other important and growing uses for oxygen are in the partial oxidation of coal and heavy hydrocarbons to synthesise gas mixtures for methanol production and to produce hydrogen for ammonia production, and in the treatment of waste water by activated sludge processes. The use

Table 1.2
Industrial Consumption of Oxygen in the United States in 1979*

Percent of total consumption		
Steel making		
Basic oxygen process	39.6	
Open hearth process	9.3	
Electric furnace	1.7	
Cutting, welding, blast furnace air enrichment	14.8	
Total		65.4
Non-ferrous metals		3.0
Fabricated metal products		7.0
Chemicals		
Ethylene oxide	8.2	
Acetylene	3.8	
Titanium dioxide	2.8	
Propylene oxide	2.3	
Vinyl acetate	2.3	
Other	0.6	
Total		20.0
Pollution control		3.0
Miscellaneous		1.6

* From Thorogood [1.3].

of oxygen in the production of fuels from coal is expected to increase as oil reserves diminish, an important aspect of this being the very large consumption which will be required at an individual site, perhaps 20,000–30,000 t/day: the SASOL II complex which is operational in South Africa uses 15,000 t of oxygen per day.

Liquid oxygen is also produced in quantity for use in aerospace activities, both as a fuel oxidiser and for life support systems. The amounts required can be large: for instance, each Apollo flight to the moon consumed about 2000 t (Fig. 1.4), and the annual consumption of the American space programme at its peak was about 400,000 t [1.5].

At the same time as oxygen is separated from air, nitrogen is also, of

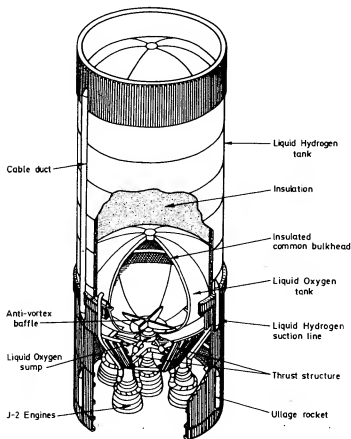


Fig. 1.4 Second stage of the Saturn V rocket launcher used for the Apollo flights to the moon. This stage was about 25 m high and 10 m diameter.

1. A SURVEY C

course, produ
oxygen. In th
by-product an
developed and
production.

Liquid nitro
cations, such as

(1) for coc
tamination mu

(2) for free
uses up to 700

(3) in the i
either side of t
whole system;

(4) in recla
of many metal
cold motor ve

constituents se
can be shattere

which does no
treated. In Bel;

being fragment
consumption o

from the non-f

(5) in defla:
deflashing can

each item indiv

(6) in the b
resistance of ce

(7) for the
the cattle indus

(8) in astro

(9) in grou
to be performe

(10) in bor
porarily harmle

However, th
for various che

dependent upor
for such applic

and chemical t

course, produced, the current world-wide consumption being about that of oxygen. In the early years of the industry, nitrogen was considered a by-product and sold relatively cheaply. However, new uses have been developed and some plants are now biased more towards nitrogen production.

Liquid nitrogen is a useful source of cold and finds a diversity of applications, such as:

- (1) for cooling cold traps in vacuum systems, especially where contamination must be avoided, as in semi-conductor device manufacture;
- (2) for freezing food: one major fast-food franchise in the United States uses up to 700 t/day for freezing hamburgers;
- (3) in the repair of pipelines: by freezing the liquid in the pipeline on either side of the fracture, a repair can be effected without emptying the whole system;
- (4) in reclamation processes, where use is made of the embrittlement of many metals and polymers at low temperatures, when, for instance, cold motor vehicle tyres can be pulverised, and the steel and polymer constituents separated and re-used; the polymer coating of electric cables can be shattered into small pieces while the copper or aluminium conductor, which does not become brittle, remains intact. Large items can also be treated. In Belgium, for example, complete automobiles are cooled before being fragmented; it is claimed that the process reduces the overall energy consumption of the process and makes it easier to separate the ferrous from the non-ferrous (non-embrittled) scrap;
- (5) in deflashing of moulded polymer products: in the embrittled state, deflashing can be achieved by a tumbling process rather than by treating each item individually;
- (6) in the heat treatment of metals: for instance, to improve the wear resistance of certain tool steels;
- (7) for the storage of biological specimens, especially bull semen for the cattle industry;
- (8) in astronautics, for pre-cooling fuel tanks prior to filling with oxygen;
- (9) in ground freezing, to enable tunnelling and excavation operations to be performed in wet and unstable soils;
- (10) in bomb disposal, for freezing explosives to render them temporarily harmless.

However, the widest use for nitrogen is as an inert blanketing gas for various chemical and metallurgical processes. The purity required is dependent upon use, with medium purities (1-3% oxygen) being acceptable for such applications as blast furnace feed systems, coal handling systems and chemical tank purging. High purity (less than 10 ppm oxygen) is

essential for many purposes, of which steel annealing, float glass manufacture and fabrication of semi-conducting devices are important examples. Gaseous nitrogen is also used as a feedstock for the production of some chemicals, particularly ammonia. For large-scale uses, the nitrogen is supplied by an on-site plant or by pipeline. In other cases, it is often convenient to store the nitrogen as liquid rather than as gas in cylinders and vaporise it as required.

As already mentioned, a relatively recent and growing use of nitrogen is as a displacing medium in the recovery of oil and gas. By forcing oil or natural gas out of the well under pressure, a significant increase in the percentage extracted can be achieved. Such applications are of large volume and require delivery pressures between 130 and 700 bars.

The other major constituent of air is argon, which is in great demand for inert blanketing when nitrogen is too reactive, and for inert gas-shielded welding (TIG, MIG, etc.), although helium tends to be preferred in the United States. Because a very high purity (>99.9%) is required for most purposes, the impure product from several air-separation plants may be sent to a central point for purification. The air-separation industry is, in fact, so competitive that the recovery of argon may be necessary to prevent a plant running at a loss. The demand for argon is increasing rapidly, and it is possible that in the future some air-separation plants will be operated for the production of argon only, the nitrogen and oxygen being discarded. Although much argon is supplied as compressed gas, it is more economical for even moderate users to receive and store argon as liquid.

Of the minor constituents of air (Table 1.3), neon, krypton and xenon are extracted mainly for use in the lamp industry and laboratory instruments. It is not at present economic to recover helium due to its availability from LNG wells.

Table 1.3
Potential Yield of Atmospheric Rare Gases from a 1000 t/day Oxygen Plant*

	Total in air passing through plant (m ³ /hr at NTP)	Typical yield (%)	Cylinders per day
Argon	1395	55	2800
Neon	2.7	60	6
Helium	0.75	60	2
Krypton	0.17	30	0.2
Xenon	0.014	30	0.015

* From Thorogood [1.3].

1.6 Liquid

Hydrogen explosive (0.02 mJ at no unusua 1970s, whe Its importe for exampl

Hydroge hydrocarb gas or fuel scale, elect due mainly hydrocarb burning hy Electrolytic hydrogen. since it clea the resultin tigation of thermoche

Hydroge (Chapters 1 higher. A co and para (C conversion being usual Care must a oxygen whic believed, ca perature pa

Liquid hy nuclear phys a target for from the enq to measure interactions: volume of lic of a charged a piston in on

1.6 Liquid Hydrogen

Hydrogen gas is a somewhat hazardous substance to handle due to its wide explosive concentration range with air (4–72%) and its low ignition energy (0.02 mJ at 30% concentration), although the liquid itself appears to present no unusual problems and was in wide use for cooling purposes until the 1970s, when liquid helium became more easily available in large quantities. Its importance as a cryogen has declined considerably since then, so that, for example, in Great Britain it is no longer commercially available.

Hydrogen gas is produced on a large scale by the reaction of steam with hydrocarbons, particularly natural gas, or by the partial oxidation of natural gas or fuel oil. The gasification of coal may also be used. On a smaller scale, electrolysis of water is used, in spite of its higher cost, which is due mainly to the higher binding energy of hydrogen in water than in hydrocarbons, to the high cost of electricity (itself often produced by burning hydrocarbons), and to the low efficiency of electrolytic cells. Electrolytic hydrogen may cost twice as much as the cheapest 'chemical' hydrogen. There is currently interest in developing hydrogen as a fuel, but since it clearly does not make sense to produce it from other fuels (with the resulting overall loss in available energy), there is widespread investigation of methods for producing hydrogen from water using various thermochemical methods.

Hydrogen may be liquefied using cycles similar to those in use for helium (Chapters 13 and 15), except that the cycle pressures are about five times higher. A complication is that, because hydrogen exists in two forms, ortho and para (Chapter 2), the inclusion of catalysts to promote ortho-to-para conversion must be considered. Great care must be taken with safety, it being usual to provide a blast wall between the liquefier and its operators. Care must also be taken to free the hydrogen from impurities, especially oxygen which can promote unwanted ortho-para conversion, and, it is believed, cause an explosion if accumulated as solid in the lower temperature parts of the plant.

Liquid hydrogen still finds two particular applications. In high-energy nuclear physics experiments, liquid hydrogen or deuterium may be used as a target for the particles produced from the accelerator. More interesting from the engineering point of view is the bubble chamber, which is used to measure the properties of charged particles and to elucidate their interactions and decays. A bubble chamber consists essentially of a closed volume of liquid held at a pressure well above saturation. On the passage of a charged particle, the pressure is rapidly reduced, usually by means of a piston in one wall of the chamber, so that the liquid is in the superheated

at glass manu-
rstant examples.
uction of some
nitrogen is sup-
then convenient
and vaporise

of nitrogen is
' forcing oil or
ncrease in the
of large volume

at demand for
rt gas-shielded
ferred in the
uired for most
plants may be
industry is, in
ary to prevent
g rapidly, and
ll be operated
ing discarded.
re economical
d.

and xenon are
nstruments. It
ilability from

n Plant"

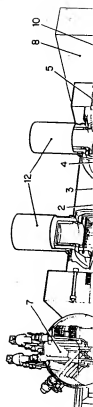
er day

5

state, and bubbles form along the track of the particle. A stereo photograph is taken, and the liquid is recompressed before bulk boiling occurs, the whole cycle taking a few tens of milliseconds. A large magnet surrounds the chamber so that the momentum of the particle can be deduced from the curvature of the track. Bubble chambers containing hydrocarbons and helium have been built, but hydrogen and deuterium are particularly favoured because their simpler nuclear structure allows a more straightforward interpretation of any interactions which occur. Hydrogen bubble chambers have been built as large as 3 m in length and containing several cubic metres of liquid, but they have now been superseded by other methods of detection, and the present tendency is to use smaller chambers surrounded by electronic detectors (Fig. 1.5).

The other application for which liquid hydrogen is still produced in quantity is as a fuel for space vehicles. When used with oxygen, it has a high propulsive energy per unit mass, and on this basis was, for instance, chosen for the fuel of the second and third stages of the rocket for the Apollo manned space flights to the moon, each of which consumed about 90 tonnes (1300 m^3) of liquid hydrogen (Fig. 1.4): in the late 1960s, the American space programme was using about 40,000 t/year [1.5]. In the 1980s, each launch of the space shuttle consumes about 120 tonnes (1700 m^3). Although on a mass basis hydrogen has a calorific value about three times higher than kerosene (which was used for the first stage of Apollo), its calorific value per unit volume is about three times lower. Thus rockets fuelled with hydrogen have to be much larger than those fuelled with kerosene, and this can entail problems of structural stability, particularly bending oscillations during flight.

There has been widespread discussion of the possibility of using hydrogen as a fuel for aircraft and automobiles as oil supplies diminish, although as already mentioned, a novel and energy-efficient means of producing hydrogen must be developed before this becomes a reality. On the question of safety, it can be argued that although hydrogen is more easily ignited than hydrocarbon fuels, its flame radiates little heat. Also, since hydrogen is lighter than air, it spreads upwards rather than outwards, so that overall there is probably little to choose between the two fuels. The storage of hydrogen is, however, a major problem. Storage as metal hydrides imposes a large weight and cost penalty because of the metals used and their low absorption capacity. Storage as liquid is clearly convenient, but requires large fuel tanks as mentioned earlier, although some saving in volume (about 15%) can be made by using a mixture of solid and liquid—'slush hydrogen'. Considerable care would have to be taken in the disposal of boil-off in a safe way. Perhaps a more serious drawback is the energy required for liquefaction, which may amount to as much as a third of the



B. A. HANDS

o photograph
g occurs, the
et surrounds
duced from
ocarbons and
: particularly
ore straight-
rogen bubble
ining several
led by other
ler chambers

produced in
gen, it has a
for instance,
cket for the
umed about
e 1960s, the
[1.5]. In the
120 tonnes
value about
irst stage of
lower. Thus
fuelled with
particularly

ugh hydrogen
h, although
f producing
he question
asily ignited
e hydrogen
that overall
: storage of
des imposes
d their low
ut requires
in volume
uid—slush
disposal of
the energy
hird of the

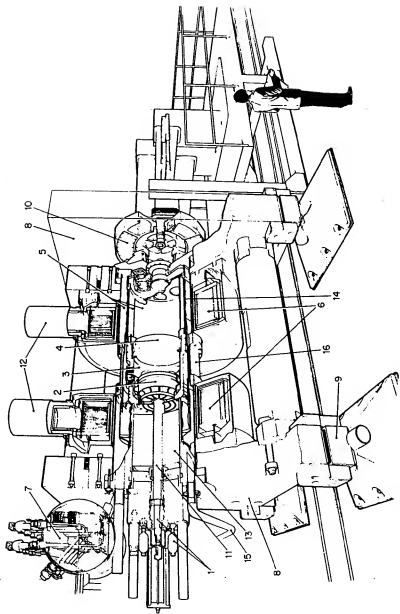


Fig. 1.5 Rapid-cycling hydrogen bubble chamber built for high-energy nuclear physics experiments. (1) Hydraulic actuator, (2) glass-reinforced plastic piston and bellows, (3) active volume (250 l), (4) main optical window, (5) vacuum enclosures, (6) vacuum enclosures, (7) chamber refrigeration control vessel, (8) iron support structure, (9) damped mountings, (10) cameras and light-source assembly, (11) piston shaft, (12) magnet lead and transfer line enclosures, (13) thermal insulation, (14) radiation shield cooled by helium gas at 20 K, (15) safety vent and (16) outer vacuum vessel. (Courtesy of the SERC, Rutherford Appleton Laboratory.)

calorific value of the fuel liquefied. This, together with the present high cost of production from non-hydrocarbon sources, makes hydrogen economically unattractive, although several experimental automobiles have been successfully run with liquid hydrogen as fuel for a number of years.

1.7 Liquid Helium

The importance of helium to the physicist and cryogenic engineer is that it is the only route to temperatures below about 10 K, apart from magnetic cooling methods which are unlikely to become practical on anything but a very small scale. The provision of helium refrigeration is, therefore, a necessary adjunct to the use of superconducting magnets.

The largest sources of helium in the western world are currently the natural gas wells of the states of Texas and Kansas in the United States. Wells in Poland, Northern Germany and the USSR (at Orenburg) also produce large quantities. Helium is present in these wells at a concentration of about 0.2–0.7% and is extracted by liquefying the other constituents. Although at present there is plenty of helium available, there are worries that if the growth in both size and number of superconducting magnets continues at the present pace, there could be a severe shortage in a few decades as natural gas wells become exhausted, even though the United States has considerable quantities of helium stored in underground porous rock—a result of the so-called 'conservation' programme which has now been discontinued [1.6]. Outside America, 'conservation' has a rather different connotation—that of recycling the gas after use, rather than exhausting it to the atmosphere. Such recovery is usually justifiable on economic grounds alone, since gaseous helium is not cheap, but it is worth noting that large quantities are used in welding and in oxygen–helium atmospheres for diving, from which helium recovery is not feasible.

A major landmark in the development of helium technology came in 1946 with the design by Professor Sam Collins of a liquefier which did not require the feed helium to be pre-cooled and which could be operated continuously for long periods. Previous to this, small-scale experiments were done by liquefying helium *in situ*, for example, by precooling with liquid hydrogen (sometimes itself produced *in situ*) and then adiabatically expanding. Continuous liquefaction was achieved using cascade cooling with liquid air (or nitrogen) and hydrogen followed by Joule–Thomson expansion. The latter method could produce a few litres of helium per hour, but required the simultaneous operation of both a hydrogen and a helium liquefier, the liquid air or nitrogen usually being available from a commercial source.

1. A SURVEY OF

The Collins proved to be a meant that fair still marketed to bearings were d liquefiers, and s refrigerators. TI engine, have no high efficiency. liquefiers.

Another prob to compress the since all will free is especially imp to be run conti contaminations I believed that w blockages in one received general based, piston rin compressors, bei reciprocating cor require a sophisti for a malfunction refrigerator itself more frequent m for more massiv tamination is sim

1.8 Superconduct

Perhaps the one has been the ex conductivity or tl phenomenon was major part in elec was destroyed by presence of a mag remained unfulfil 'high-field' supero remain supercond

present high
hydrogen econ-
omies have
been of years.

is that it
on magnetic
ity but a
therefore, a

currently the
United States.
enberg) also
concentration
constituents.
are worries
ing magnets
age in a few
the United
ound porous
ich has now
as a rather
rather than
ustainable on
it is worth
gen-helium
asible.

ogy came in
which did not
be operated
experiments
cooling with
adiabatically
ade cooling
le-Thomson
helium per
hydrogen and a
table from a

The Collins liquefier, which used a reciprocating expansion engine, proved to be a reliable machine, although the presence of rubbing seals meant that fairly frequent maintenance was required; its derivatives are still marketed today. During the 1950s, high-speed turbines running on gas bearings were developed as the external work components for hydrogen liquefiers, and soon afterwards this technique was incorporated in helium refrigerators. These turbines, although less robust than a reciprocating engine, have no rubbing surfaces and can achieve a large throughput at high efficiency. They are now usually specified for large refrigerators and liquefiers.

Another problem in the design of refrigerators arises from the necessity to compress the gas. The helium feed must be free of oil, water and air, since all will freeze at some point in the system and cause blockages: this is especially important today, when superconducting systems may have to be run continuously for many months. To achieve such service, oil contaminations less than 1 part in 10^7 may have to be specified, and it is believed that water contamination of about 3 parts in 10^8 has caused blockages in one system [1.7]. Two types of compressor appear to have received general acceptance, reciprocating compressors with dry, polymer-based, piston rings, and oil-flooded screw compressors. Oil-flooded screw compressors, being rotating machines, suffer from fewer problems than reciprocating compressors and are more compact and vibration-free, but require a sophisticated oil-removal system. Furthermore, it is not unknown for a malfunction to occur such that much of the oil is delivered into the refrigerator itself. Reciprocating compressors have the disadvantage of more frequent maintenance intervals, more vibration and a requirement for more massive foundations, but the equipment for removal of contamination is simpler.

1.8 Superconducting Magnets and Machinery

Perhaps the one major disappointment in the development of cryogenics has been the exploitation of the "electrical engineers' dream"—superconductivity or the complete absence of electrical resistivity. After this phenomenon was discovered in 1911, hopes persisted that it would play a major part in electrical engineering, even though the superconducting state was destroyed by the passage of a current of only a few amperes or the presence of a magnetic field of only a few tenths of a tesla, but the dream remained unfulfilled for some 50 years. In the late 1950s, a range of 'high-field' superconductors were discovered, so called because they would remain superconducting in fields of tens of tesla. Also, their critical tem-

peratures, instead of being at the most 9.25 K (niobium) were 5–10 K higher. It was discovered, however, that the construction of a superconducting magnet involved more than just winding the wire into a coil, and that copper had to be incorporated to 'stabilise' the magnet and allow it to operate at the fields which a short sample of the wire could sustain. In order to optimise the performance, many subtle techniques had to be learnt, and even today new designs are not always completely successful. Nevertheless, magnets are now made commercially on a production-line basis, and, for large magnets at least, at a cost less than their water-cooled copper equivalents, to which they are superior on running costs and in stability of field.

Superconducting magnets have found widespread applications in research

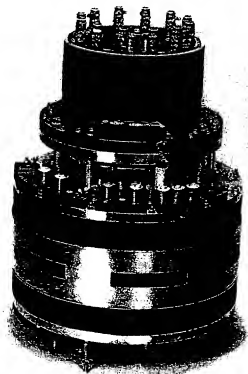


Fig. 1.6 Small superconducting magnet for research use. This is a split-pair magnet, wound partly from niobium-tin wire and partly from niobium-titanium, producing 10 T in a 70 mm bore. The maximum diameter is about 25 cm. The 12 resistors on top of the assembly are used to absorb energy should the magnet unexpectedly change from the superconducting to the normal state ('quench'). (Courtesy of Oxford Instruments Ltd.)

1. A SURVEY

laboratory cubic cent of NMR a use into ch which the coming into nucleus (p radiation, t magnetic fi between 0.: the x, y a correlating t mation may intensity of Since the w body, a 3-di abnormalitie lattice and s acquired. Th (Fig. 1.7), w and a stabilit

Still at a Spectroscopy nuclei due to resonant freq *vivo*. Process tissue during t ²³Na nucleus. Because the m of protons, m

No adverse MRI or MRS. field, which ca necessary), an ferrous objects

For MRS an used, the latter cryogenics for environments. conductivity, t per year world Large magne

(niobium) were 5–10 K construction of a superconducting wire into a coil, 'ise' the magnet and allow the wire could sustain. The techniques had to be used completely successful. Only on a production-line basis than their water-cooled on running costs and in

d applications in research


laboratories. Small magnets, providing a uniform field over a few tens of cubic centimetres, are mainly used by physicists (Fig. 1.6); the development of NMR and ESR techniques for analytical purposes has extended their use into chemistry and biology [1.8], and more recently, into medicine, in which the technique known as MRI (Magnetic Resonance Imaging) is coming into routine clinical use. In MRI, the resonance of the hydrogen nucleus (proton) is stimulated by applying radiofrequency electromagnetic radiation, the resonant frequency being directly proportional to the applied magnetic field. The patient is subjected to a uniform magnetic field of between 0.5 and 1.5 T, upon which are superimposed small gradients in the x , y and z directions. By changing the applied rf frequency and correlating the resonant frequency with the local field, 3-dimensional information may be obtained. The primary information is obtained from the intensity of the resonance, which depends upon the local proton density. Since the water and lipid content is different in the various tissues of the body, a 3-dimensional image of the body structure may be produced and abnormalities such as tumours may be located. Measurement of the spin-lattice and spin-spin relaxation times enable further information to be acquired. The magnets for whole-body MRI require a bore of about 1.0 m (Fig. 1.7), with a field homogeneity as good as 0.1 ppm of the main field and a stability of 0.1 ppm per hour [1.8].

Still at a more experimental stage is MRS (Magnetic Resonance Spectroscopy). Slight variations in the local magnetic environment of the nuclei due to different chemical surroundings produce small shifts in the resonant frequency, and this enables chemical reactions to be followed *in vivo*. Processes which have been investigated include changes in muscle tissue during exercise using the ^{31}P nucleus, cellular biochemistry using the ^{23}Na nucleus, and the kinetics of enzyme reactions using the ^{13}C nucleus. Because the magnetic moments of these nuclei are much weaker than those of protons, magnetic fields of about 6 T are generally required.

No adverse physiological effects are believed to occur with the use of MRI or MRS. The main safety problems are control of the stray magnetic field, which can be limited by the use of iron shielding (some 20 t may be necessary), and the prevention of personnel from inadvertently carrying ferrous objects into the region of the stray field.

For MRS and MRI, both conventional and superconducting magnets are used, the latter giving superior resolution but requiring some expertise in cryogenics for its operation which may not be available in some hospital environments. This is the first large-scale, non-research use of superconductivity, the current production rate being several hundred magnets per year worldwide.

Large magnets have been used since the mid-1960s by high-energy



is a split-pair magnet, wound producing 10 T in a 70 mm on top of the assembly are from the superconducting to Ltd.)

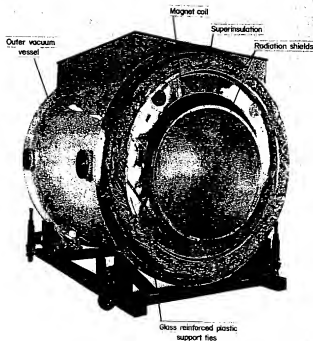


Fig. 1.7 A superconducting magnet, designed for whole-body scanning, during assembly. A field in the range 0.5–1.5 T is produced in a bore of 1 m. (Courtesy of Oxford Magnet Technology Ltd.)

nuclear physics establishments, at first for the focusing of ionised particle beams between the accelerator and the experiment, and lately in the accelerator itself. Such magnets are often one or two metres long with a bore of around 10 cm; besides simple solenoids, quadrupole and other configurations have been constructed. A great variety of superconducting magnets for other uses has now been made, for example, simple solenoids of several metres bore for use with bubble chambers; toroidal magnets for plasma physics experiments; and a 'yin-yang' configuration, weighing 341 t, for a nuclear fusion experiment (Fig. 1.8). Fields in the region of 10 T are commonplace, and some magnets are pulsed on a routine basis. High-energy nuclear physics and nuclear fusion have both given great stimulus to the development of magnet technology.

Applications in the generation and transmission of electric power have not been as successful, the enthusiasm of the manufacturers being counter-

1. A SURVEY

balanced by the story has ahead of the mission line system would [1.10]. Ten temperature studies had transmitter continuously overload.

Similarly, construction power generated 1000–3000 M over conversion smaller by a at the most, reliable than therefore, part the western programmes reported in 1 switched into construction

At present an electricity magnet capacity substation of Energy is transferred controlled with supply [1.13] time of 10 m shaving' energy way as pump

There has most promising given power, generator is generally of rapid speed thus removing

balanced by the caution (realism?) of the utility companies [1.9]. In general, the story has been that advances in 'conventional' technology have remained ahead of the possibilities of using superconductors. Superconducting transmission lines are a good example. In 1973, it seemed that a superconducting system would be economically viable for powers greater than about 1 GVA [1.10]. Ten years later, due to advances in insulation technology of room temperature systems, the figure had risen to 5 or 10 GVA, and experimental studies had been largely abandoned, even though in 1984 the prototype ac transmission line at the Brookhaven National Laboratory [1.11] was run continuously for 4 weeks at 1 GW, and its stability demonstrated at 100% overload.

Similarly, in the 1970s there was considerable activity in the design and construction of models and prototypes of superconducting alternators for power generation aimed at eventual machines in the capacity range of 1000-3000 MW. Superconducting alternators have two major advantages over conventional designs: a greater efficiency, and a size and weight smaller by a factor of about two. However, the increase in efficiency is 1% at the most, and this is easily negated if the alternators prove to be less reliable than the machines currently in use. The generating authorities are, therefore, proceeding with extreme caution, and again by 1985, activity in the western world in this field had considerably diminished, with only small programmes remaining in the USA, Japan and Germany. However, it was reported in 1985 [1.12] that in the USSR, an experimental alternator was switched into the Leningrad supply in the summer of 1984, and that construction of 300 MVA alternators is proceeding.

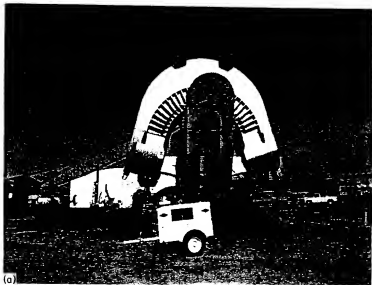
At present, only one superconducting device is believed to be in use by an electricity supply authority in the western world. A superconducting magnet capable of storing 38 MJ of energy has been installed at the Tacoma substation of the Bonneville Power Administration in the United States. Energy is transferred between the magnet and the transmission line in a controlled way to damp out subsynchronous oscillations in the ac electricity supply [1.13]. An advantage of the system is the relatively fast response time of 10 ms. Much larger magnets have also been proposed as 'peak shaving' energy storage devices, which would be used in much the same way as pumped water storage is now.

There has been considerable interest in superconducting motors. The most promising application appears to be for ship propulsion, where, for a given power, a superconducting motor combined with a superconducting generator is much smaller than a conventional system. The motors are generally of the dc homopolar type. The small rotating mass facilitates rapid speed changes, and the motor will operate efficiently at low speed, thus removing the need for a gear box. However, on economic grounds a

conventional system is still superior, and the main use for a superconducting unit may be in naval vessels, for which flexibility and small size are important advantages, and in icebreakers, because of the frequent reversals of direction at low speed.

A different form of power unit is the linear motor, which, when combined with magnetic levitation, forms a suitable system for driving high-speed trains. Japanese National Railways has pursued such a development [1.14], intended for the commuter line between Kobe and Tokyo, which was predicted to reach full capacity soon after 1980. Work started in the 1960s, and the first prototype was successfully tested in 1975. Since then, the design has been considerably refined, and in 1979 the version known as ML-500 ran at 517 km/hr, a world record. Propulsion is by linear synchronous motor, the high-frequency ac power being provided by coils mounted on the track. Guidance and support are both achieved using a repulsive electromagnetic inductive method, which requires the train itself to be equipped with powerful magnets. In the Japanese system, each vehicle (28.8 m long and weighing about 10 t) is provided with eight superconducting magnets of 700 kA-turns each and on-board refrigeration (Fig. 1.9). Although the project is well advanced, there are no plans yet to introduce the train into commercial service, since passenger density on the line has increased slower than originally predicted.

Finally, one other use of superconducting magnets is showing commercial promise. In the 1960s, it was established that kaolin, which is used in paper-



(b)

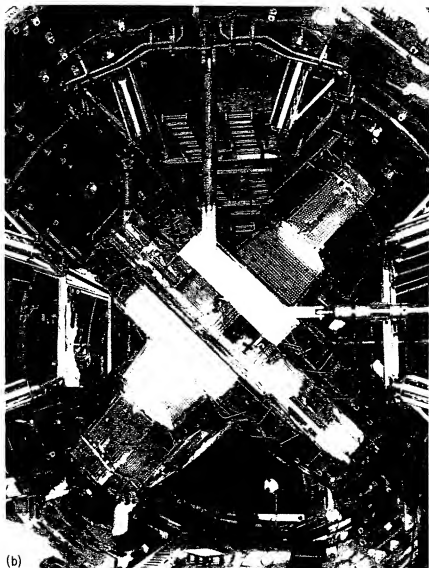
Fig. 1.8 'Yin
(a) Opposite: C
Laboratory). (b)
diameter. The (r
can also be seen
photograph indic
University of Cal
Energy.)

HANDS

ducting
portant
if direc-

mbined
h-speed
t [1.14],
ich was
s 1960s,
en, the
own as
chron-
ounted
pulsive
f to be
vehicle
super-
n (Fig.
yet to
on the

mercial
paper-



(b)

Fig. 1.8 'Yin-yang' magnet for the Mirror Fusion Test Facility in Berkeley, California. (a) *Opposite*: Coil-box assembly (courtesy of University of California Lawrence Berkeley Laboratory). (b) Magnet during installation in the vacuum vessel, which is about 20 m in diameter. The (rectangular) end views of six cryopump modules for maintaining a high vacuum can also be seen, arranged radially around the top two-thirds of the vacuum vessel. This photograph indicates the complexity of a modern large cryogenic installation. (Courtesy of University of California Lawrence Livermore National Laboratory and U.S. Department of Energy.)

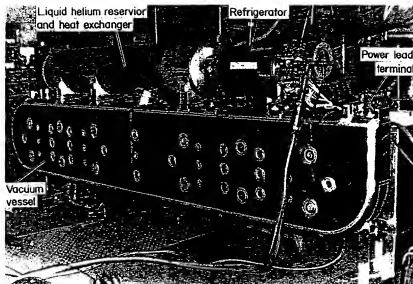


Fig. 1.9 A magnet-refrigerator assembly for the Japanese magnetically levitated train. The magnet coil is within the vacuum vessel. (Courtesy of Japanese National Railways.)

making, could be whitened by removing the discolourants, which are principally due to traces of iron, by passing the clay through a magnetic field gradient. Since then, applications have been found in the separation of ores, in the purification of chemicals, in the desulphurisation of coal and in the cleaning of flue gases and liquid effluents. The separation of red blood cells from plasma is also possible. Although many of these processes require only comparatively low magnetic fields, the use of superconducting magnets may be advantageous for certain applications [1.15].

1.9 Cryogenic Electronics

Many active electronic devices can be operated in a cryogenic environment [1.16]. They are generally of the field-effect transistor (FET) type and are based on silicon or gallium arsenide. For instrumentation purposes, there are clear advantages in placing at least some of the electronic circuitry close to the sensing head. However, there may also be inherent advantages in operating transistors at low temperatures, such as increased switching speed or lower noise. A serious problem is the effect on device reliability of the stresses induced by thermal cycling.

1. A SURVEY

Superconductivity is a phenomenon where the electrical resistance of a material drops to zero. This is due to the formation of Cooper pairs of electrons, which move through the material without scattering. Superconductors are used in a variety of applications, including magnetic levitation, power transmission, and medical imaging. The critical temperature of a superconductor is the temperature below which it becomes superconducting. The critical current is the maximum current that a superconductor can carry without losing its superconducting properties. The critical magnetic field is the maximum magnetic field that a superconductor can withstand without losing its superconducting properties.

The superconducting magnet is a key component of many applications. It is used to create strong magnetic fields for research and industrial purposes. The superconducting magnet is made of a superconducting material, which is cooled to its critical temperature. The current is then passed through the magnet, creating a strong magnetic field. The superconducting magnet is used in a variety of applications, including magnetic levitation, power transmission, and medical imaging.

The rf SQUID is a type of superconducting quantum interference device (SQUID). It is used to measure very small magnetic fields. The rf SQUID is made of a superconducting loop, which is coupled to a radio frequency (rf) circuit. The current in the loop is measured by the rf circuit. The rf SQUID is used in a variety of applications, including magnetic levitation, power transmission, and medical imaging.

Among the various applications of superconductivity, the most prominent are in the field of magnetic levitation, power transmission, and medical imaging. Superconducting magnets are used in magnetic levitation trains, which can travel at high speeds without the need for tracks. Superconducting magnets are also used in power transmission, where they can carry large currents without losing energy. Superconducting magnets are used in medical imaging, where they can create strong magnetic fields for imaging the body.



sted train.
lways.)

uch are
agnetic
variation
oal and
of red
ocesses
ducting

nment
nd are
there
close
ges in
speed
of the

Superconducting electronic devices are in a different class. They rely on two phenomena—the Josephson effect and the quantisation of magnetic flux, which are described in a simple way in [1.17], for example, while a more complete account is given in [1.18]. The quantum of magnetic flux is extremely small: 2.07×10^{-15} Wb, which is approximately equal to the amount of the earth's field enclosed by a ring $10 \mu\text{m}$ in diameter. The Josephson effect is observed when two pieces of superconductor (commonly lead or niobium) are separated by a very thin insulating layer, perhaps an oxide film about 20 nm thick. Not only can single electrons tunnel through such a layer, but so can the pairs of electrons (Cooper pairs) to which superconductivity is attributed, so that the insulating layer behaves as a superconductor, although there is a discontinuity in the phase of the wave function of the Cooper pairs across the junction. The characteristics of the Josephson junction are now used to define the volt, and have enabled the uncertainty in the maintained standard to be reduced to about $0.1 \mu\text{V}$.

The superconducting quantum interference device (SQUID) is formed from a superconducting loop containing at least one Josephson junction. If the loop encloses some magnetic flux, there must be a circulating current because it is superconducting. This current consists of Cooper pairs whose wave functions form standing waves round the ring. Across the junction, there is a phase discontinuity which is a function of the current flowing and hence of the magnetic flux.

The rf SQUID is formed from a single junction in a superconducting loop, which is inductively coupled to a resonant circuit. This is arranged to drive a current round the loop, so that the voltage across the circuit is a measure of the magnetic flux being measured. In the dc SQUID, two Josephson junctions are made in the loop, and a dc current is passed through the parallel circuit so formed. The voltage required to produce the current is then a function of the magnetic field trapped inside the loop. Superconducting quantum interference devices may be fabricated by technologies similar to those used for integrated circuits, although other methods may also be used. The rf device is the easier to make and use; the dc SQUID is the more sensitive, and the quantum limit of sensitivity can be approached. By forming the superconducting loop from two rings with a known distance between their planes, small magnetic field gradients may be measured in the presence of a large uniform field.

Among a variety of applications, SQUIDs have been used to map local anomalies in the earth's magnetic field (of interest to geologists and archaeologists, for example) and for navigational purposes. They are routinely used as mixers and amplifiers for receiving weak signals from satellite transmissions, and are also used in infra-red detectors. In medical investigations, SQUIDs are used to record the varying magnetic fields

associated with bodily activity, the fluctuations ranging from 10^{-11} T (from the heart) down to 10^{-15} T (from the brain) [1.19]. Gradiometer arrangements are often used in an attempt to reduce to an acceptably low level the effects of local field fluctuations due to electrical equipment and ionospheric phenomena. Advantages over the use of ECG and EEG are that electrodes do not have to be attached to the patient, and that the measurements are localised rather than averaged over some distance. By spatial scanning, a 3-dimensional image of, for example, brain activity can be constructed and the position of a malfunction pin-pointed. With a single detector, such an image may take several days to produce, but attempts are being made to develop multiple arrays using several tens of SQUIDS to reduce the scanning time. It may be observed that whereas MRI (Section 1.8) gives information about the structure of tissue, these magnetic field measurements give information about the functional behaviour of the tissue. SQUIDS have also been used to detect accumulations of ferromagnetic material in various parts of the body.

Josephson junctions may be arranged in a variety of ways for other purposes. For instance, a sampling oscilloscope has been made with a time resolution of 2 psec. But perhaps the best-known application is to computers. Combinations of Josephson junctions can be designed to act as a very fast switch with low power dissipation or as a memory element. The theoretical switching time is about 10 psec and the power dissipation about $1 \mu\text{W}$, giving a product of switching time and power consumption—the figure of merit used for switching devices—several orders of magnitude better than that of transistors. The fabrication of logic elements using such devices allows in principle the construction of a large capacity, compact, high-speed computer [1.20]. Much development work was carried out on this concept during the 1970s, especially by IBM. However, after '15 years and an estimated 100 million dollars' [1.21], IBM announced in 1983 that the project was abandoned, although development work in fact continues at a lower level. During that time, complete logic boards had been developed and tested. Major problems with the technology are that large fan-out ratios are difficult to achieve and that superconducting circuits have a very low inherent impedance and so are difficult to couple with conventional elements at room temperature. There were also manufacturing problems, since the boards could only be tested when in the superconducting state at a low temperature, and some logic gates were always destroyed due to thermal cycling. Another factor was that, as in other branches of superconductivity, room-temperature devices were being developed which approached the advantages offered by the superconducting system; for instance, at the end of 1985, it was reported that miniature ceramic circuit boards and hot electron devices were being developed by Fujitsu of Japan for use in an ambient-temperature computer which would be very much

1. A SUR

faster th
construct
there hav
architect

1.10 Cry

The large
eering ha
and hydr
precool
tanks. Th
is at a pr
insulation
problems
currents
these pro
small acc
fuel tank

The sn
urements
wavelength
of the ei
supercon
17) is al
utterly re
alternativ
then has

1.11 Met

Cryogen
fields. Th
been dis
more di
particula
difficult,
processe
by the th
chemical

ations ranging from 10^{-11} T (e brain) [1.19]. Gradiometer o reduce to an acceptably low ie to electrical equipment and he use of ECG and EEG are to the patient, and that the raged over some distance. By or example, brain activity can ion pin-pointed. With a single lays to produce, but attempts using several tens of SQUIDS ed that whereas MRI (Section of tissue, these magnetic field functional behaviour of the ectect accumulations of ferro-dy.

a variety of ways for other pe has been made with a time own application is to comput-in be designed to act as a very as a memory element. The id the power dissipation about and power consumption—the -several orders of magnitude n of logic elements using such of a large capacity, compact, nent work was carried out on BM. However, after '15 years , IBM announced in 1983 that pment work in fact continues : logic boards had been devel- technology are that large fan- perconducting circuits have a ult to couple with conventional also manufacturing problems, n the superconducting state at vere always destroyed due to is in other branches of super- vere being developed which : superconducting system; for that miniature ceramic circuit developed by Fujitsu of Japan er which would be very much

faster than a Josephson machine. However, work continues towards the construction of a complete superconducting computer in Japan, where there have recently been striking advances in fabrication technology and architecture.

1.10 Cryogenics in Space

The large-scale applications of cryogenic technology to aerospace engineering have already been mentioned, in particular the use of liquid oxygen and hydrogen to power launch vehicles, and the use of liquid nitrogen for precooling purposes. In addition, liquid or cold supercritical oxygen is carried for life support, and helium may be carried for pressurising fuel tanks. The technology is similar to that used on earth, except that weight is at a premium, and, once in the space environment, only minimal thermal insulation may be needed. However, the absence of gravity poses serious problems, since liquid no longer separates from vapour and convection currents are non-existent. Special devices have to be used to overcome these problems. In the case of rocket motors, the vehicle may be given a small acceleration by an auxiliary rocket to drive the liquid towards the fuel tank outlet so that the engines may be started reliably.

The small-scale applications are mainly concerned with scientific measurements, including astronomy covering the whole range of electromagnetic wavelengths, recording of magnetic fields and observations of the surface of the earth. The instruments used often include a cooled detector or a superconducting device. The provision of a small refrigerator (see Chapter 17) is attractive, but the device must be of long life (several years), utterly reliable and low in power consumption, weight and vibration. The alternative is to provide a store of cryogenic liquid, but the experiment then has a comparatively short lifetime. Both methods are, in fact, used.

1.11 Medical and Biological Applications

Cryogenics has found a number of applications in the medical and biological fields. The use of superconducting magnets in MRS and MRI has already been discussed, as has the use of SQUIDS. Low temperatures are used more directly to enable biological materials to be frozen and stored, particularly thin tissues and blood. The preservation of large items is more difficult, since the cells suffer damage during the cooling and warming processes, the rapidity of which is inevitably controlled to a great extent by the thermal conductivity of the material, although the injection of certain chemicals can minimise the damage in some cases. On the other hand, this

damage is put to good use in the elimination of tumours by freezing. A major difficulty here lies in the monitoring and control of the frozen region. There is also insufficient understanding of the mechanisms by which cells are killed. Nevertheless, successful results have been obtained in the treatment of some conditions, and it is probable that cryosurgery will be more widely used in the future [1.22].

In agriculture, for many years cattle semen has been routinely preserved in liquid nitrogen for subsequent artificial insemination, and this has made a major contribution to the development of the industry, especially in the underdeveloped countries.

1.12 Cryopumping

Cryopumping—the removal of gas from a system by solidification onto a cold surface—has a number of advantages over other methods of producing vacua. A cryopump consists essentially of a metal plate cooled to a low temperature, and, therefore, can be made easily and economically in a large size, with considerable freedom in design configuration [1.23]. It is a 'clean' pump, since the only working substance is the refrigerant used for cooling, which does not come into contact with the vacuum space. Lastly, all gases except helium can be pumped to extremely low partial pressures (Fig. 1.10).

Although the concept of the cryopump is straightforward, the construction requires some sophisticated design, since the low-temperature parts must be carefully shielded from room-temperature radiation while

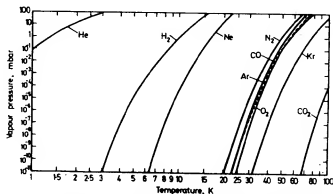


Fig. 1.10 Vapour pressure-temperature curves for atmospheric gases.

Down Lines for
Thermocouples

LN₂ Cooling

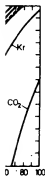
Top Menifold
and Radiation
Shield
Module
Manifolds

by freezing. A
e frozen region.
s by which cells
obtained in the
surgery will be

tinely preserved
d this has made
specially in the

ification onto a
ds of producing
ooled to a low
onomically in a
on [1.23]. It is a
gerant used for
n space. Lastly,
artial pressures

ward, the con-
w-temperature
radiation while



ic gases.

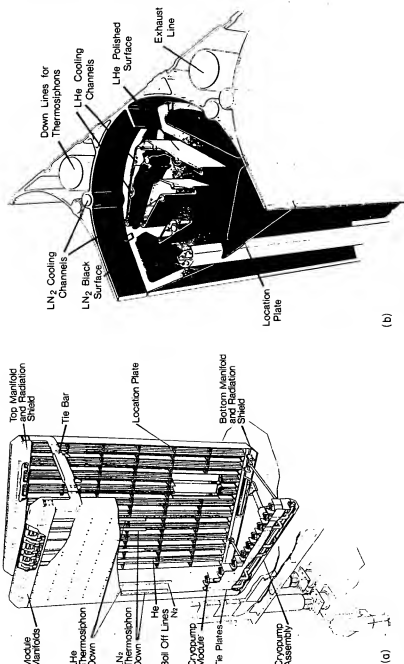


Fig. 1.11 Cryopump designed for the neutral injector assembly of the JET nuclear fusion experiment at Culham, England. The complete assembly is shown in (a). Each module (b) is 0.30×0.35 m in section and 6 m in height. (Courtesy of JET Joint Undertaking.)

allowing free access to gas molecules. This is especially so for cryopumps with stages at 20 K or 4 K, which must be shielded with panels at around 80 K. Since some molecules are scattered away from the cryopumping surface itself by the shields, the overall capture coefficient (which is usually between 0.35 and 0.5 depending on the design) is much less than that of the bare panel and, in fact, is not much different from that of a large diffusion pump.

Very large cryopumps were developed during the 1950s for use in space simulation chambers. Frequently, these used panels cooled to 20 K using a refrigerator with helium gas as the working fluid, and radiation shields cooled either with liquid nitrogen or with helium gas at around 100 K. The residual hydrogen and helium was extracted using conventional high-vacuum pumps. The cryopumps usually covered almost the whole of the interior surface of the vacuum vessel, which typically might be several hundred square metres in area.

Recently, attention has turned to the provision of cryopumps for nuclear fusion experiments. These are required to pump hydrogen at speeds of 10^6 – 10^7 l/sec and to pressures of the order of 10^{-5} mbar or better, so that the coolant must be liquid helium at around 3.5 K. A number of large pumps of this type have now been constructed; advantage has been taken of the geometrical freedom mentioned earlier to produce some interesting configurations [1.24] such as that shown in Fig. 1.11.

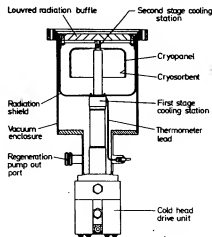


Fig. 1.12 Typical design of a small cryopump attached to a displacer refrigerator and intended to replace a diffusion pump.

At the other cryopumps for be scrupulously apertures of a direct replacement contained refrigerant provides refrigeration of course, pump temperature of residual hydrogen and zeolites has low pressures and restricted by a

1.13 Instrumentation

The instrument, probe, and probe. The latter if accurate and procedures, as examined in C

The measurement of liquids, float gauges allow the gas temperature of resistors or diodes measuring current in the liquid, a change in heat transfer is unreliable because heat transfer is a static liquid of the liquid alone.

In the author's hydrostatic heat to room temperature or rising up the n that the liquid

ryopumps
s at around
ryopumping
ch is usually
than that of
it of a large

use in space
20 K using
ation shields
und 100 K.
tional high-
whole of the
t be several

for nuclear
it speeds of
tter, so that
er of large
been taken
interesting

rigerator and

At the other end of the size scale, there is an increasing interest in small cryopumps for industrial purposes, especially where oil contamination must be scrupulously avoided as in the semi-conductor industry. These have apertures of a few tens of centimetres and are frequently designed to be a direct replacement for a diffusion pump. They are cooled with a small self-contained refrigerator based on a displacer cycle (see Chapter 17) which provides refrigeration at around 100 K for the radiation shield (which also, of course, pumps water vapour), and cooling at around 20 K for the lower temperature panel, which is equipped with a sorbent material to pump residual hydrogen (Fig. 1.12). Sorbent materials such as activated charcoal and zeolites have attracted attention on account of their ability to achieve low pressures at comparatively high temperatures. However, their use is restricted by a low pumping speed and a limited absorption capacity.

1.13 Instrumentation

The instrument most commonly used in cryogenic engineering is the thermometer, probably on account of its cheapness and simplicity of installation. The latter is deceptive, however, and great care must be taken if accurate and reliable measurements are to be obtained. Installation procedures, as well as the many different types of sensor available, are examined in Chapter 18.

The measurement of liquid level can present problems. For the denser liquids, float gauges can be used, provided that the float is designed to allow the gas inside to contract or even condense, depending on the temperature of the liquid. A popular electronic device is a chain of carbon resistors or diodes which essentially act as resistance thermometers. The measuring current is adjusted so that when the sensor ceases to be immersed in the liquid, a large temperature change of the sensor occurs due to the change in heat transfer coefficient. However, the method tends to be unreliable because the current must be carefully adjusted and because the heat transfer coefficient can be similar in a fast-flowing stream of vapour and a static liquid. Difficulties can also arise if the saturation temperature of the liquid alters due to a change in pressure.

In the author's view, the most reliable method is simply to measure the hydrostatic head of liquid, using pressure tappings which are brought up to room temperature to a suitable differential pressure gauge. At the low-temperature end, to eliminate hydrostatic head errors due to the liquid rising up the measuring tube, the tube must be arranged horizontally so that the liquid boils in the horizontal portion. Boiling can be ensured by

using a small heater if the natural heat leak from room temperature is not sufficient. Errors may occur because of unknown temperature gradients in the liquid and also in the vapour, whose density is often not negligible compared with that of the liquid, especially in helium systems.

For liquid helium in the absence of strong magnetic fields, the superconducting gauge is undoubtedly the most convenient and accurate, measuring level to within a few millimetres. The sensor consists of a length of Type II superconducting wire, which is heated so that it is superconducting below the liquid level, but normal above, so that the resistance is just proportional to the length of wire above the free surface. The state of the wire when in the vapour will again depend on the local heat transfer coefficient, but nevertheless a well-designed sensor appears to be unaffected by high velocity flows of cold gas. The heater is sometimes separate from the wire, sometimes the measuring current itself is sufficient.

Many types of flowmeter have been used at cryogenic temperatures, with varied success, although it is usual to measure the flow at room temperature if possible. The low viscosity of the liquids, and their low density, means that turbine meters are not responsive to changes in flow rate, and also may be damaged by overspeeding due to the large gas flows during cooldown of the system; a bypass may therefore be necessary. If the liquid is near saturation, vapour may be formed in the throats of orifice plates and venturi meters unless the pressure differential is so low that it is difficult to measure. Again, the measuring equipment may be damaged during cooldown because of the large pressure differentials which may be developed. Ultrasonics and thermal anemometry have been used with some success, but the equipment is expensive and difficult to install in a cryogenic environment. Except for very small pipelines, the vortex-shedding meter may be the best type to use.

A wide range of other instruments has been used in a cryogenic environment. Generally, instruments used for room-temperature applications can be adapted, with a careful choice of materials, unless the measuring phenomenon itself is very sensitive to temperature or does not exist in the cryogenic temperature range. Many types of transistors will operate satisfactorily right down to liquid helium temperatures [1.16, 1.25], and this fact has been exploited in the design of many instruments.

References

- 1.1 N. Kurti, 'Low Temperature Terminology', *Proc. XIII Int. Congr. Refrig.*, Vol. 1, pp. 593-597 (Int. Inst. Refrig., 1973).
- 1.2 N. Kurti, 'F'.
- 1.3 Data kindly
- 1.4 E. K. Farids
Gastech 81 1
1982).
- 1.5 A. O. Tisich
1-10 (1966).
- 1.6 E. F. Hamn
(1980); A. F.
there a crisi:
- 1.7 C. H. Rode
Cryog. Eng.
- 1.8 L. J. Neurin
pp. 32-43, F
'Supercondu
53.
- 1.9 B. J. Maddo
Cryog. Eng.
conducting s
598, Genov:
- 1.10 B. C. Belan
in the U.S.
(1975).
- 1.11 E. B. Forsy
Cryogenics)
- 1.12 *Cryogenics* ;
- 1.13 R. I. Scher
storage syst
123-132 (19
- 1.14 T. Ohtsuka
in Japan",
(1984).
- 1.15 J. H. P. Wa
presented at
- 1.16 R. K. Kirsch
- 1.17 H. M. Rose
- 1.18 T. van Du
Edward Arr
- 1.19 S. J. Williar
22, 129-201
- 1.20 J. Matisoo,
1980).
- 1.21 *The Times*.
- 1.22 P. Le Piver
Engng Conj
- 1.23 B. A. Hand
- 1.24 B. A. Hand
- 1.25 B. Lengeler
genics 14, 4

1. A SURVEY OF CRYOGENIC ENGINEERING

- 1.2 N. Kurti, 'From Cailletet and Pictet to microkelvin', *Cryogenics* **18**, 451-458 (1978).
- 1.3 Data kindly supplied by R. M. Thorogood.
- 1.4 E. K. Faridany, 'International trade in LNG: present projects and future outlook', *Proc. Gastech 81 LNG/LPG Conference*, pp. 21-35 (Gastech Ltd., Rickmansworth, England, 1982).
- 1.5 A. O. Tischler, 'The impact of the space age on cryogenics', *Adv. Cryog. Engng* **11**, 1-10 (1966).
- 1.6 E. F. Hammel, 'Helium: its past, present and future', *Adv. Cryog. Engng* **25**, 810-821 (1980); A. Francis, D. Keierleber and D. Swartz, 'Helium prospects for the future: is there a crisis?', *Adv. Cryog. Engng* **29**, 9-17 (1984).
- 1.7 C. H. Rode, 'Cryogenic system for a 100 km superconducting collider', *Proc. 10th Int. Cryog. Engng Conf.*, pp. 760-770, Helsinki, Finland (1984).
- 1.8 L. J. Neuringer, 'NMR in biology and medicine', *Proc. 10th Int. Cryog. Engng Conf.*, pp. 32-43, Helsinki, Finland (1984); M. F. Wood, I. L. MacDougall and P. H. Winson, 'Superconducting magnets for NMR imaging and in-vivo spectroscopy', *ibid.*, pp. 44-53.
- 1.9 B. J. Maddock and W. T. Norris, 'Superconductivity in electricity supply', *Proc. 7th Int. Cryog. Engng Conf.*, pp. 245-259, London, England (1978); J. G. Steel, 'Superconducting a.c. generators - a utility view', *Proc. 8th Int. Cryog. Engng Conf.*, pp. 590-598, Genova, Italy (1980).
- 1.10 B. C. Belanger, 'Superconducting and resistive cryogenic power transmission research in the U.S. - an opportunity for cryogenic innovation', *Adv. Cryog. Engng* **20**, 1-22 (1975).
- 1.11 E. B. Forsyth, 'Cryogenic engineering for the Brookhaven power transmission project', *Cryogenics* **17**, 3-7 (1977).
- 1.12 *Cryogenics* **25**, 50 (1985).
- 1.13 R. I. Schermer *et al.*, 'Design and operation of the 30 MJ superconducting magnetic storage system on the Bonneville Power Administration bus', *Adv. Cryog. Engng* **29**, 123-132 (1984).
- 1.14 T. Ohtsuka and Y. Kyotani, 'Recent progress on superconducting magnetic levitation in Japan', *Proc. 10th Int. Cryog. Engng Conf.*, pp. 750-759, Helsinki, Finland (1984).
- 1.15 J. H. P. Watson, 'Status report on magnetic separation using superconducting magnets', presented at *10th Int. Cryog. Engng Conf.*, Helsinki, Finland (1984).
- 1.16 R. K. Kirschman, 'Cold electronics: an overview', *Cryogenics* **25**, 115-122 (1985).
- 1.17 H. M. Rosenberg, *The Solid State*, 2nd edn, Clarendon Press (1978).
- 1.18 T. van Duzer and C. W. Turner, *Principles of Superconductive Devices and Circuits*, Edward Arnold (1981).
- 1.19 S. J. Williamson and L. Kaufman, 'Biomagnetism', *J. Magnetism and Magn. Materials* **22**, 129-201 (1981).
- 1.20 J. Matisoo, 'The superconducting computer', *Scientific American* **282** (5), 38-53 (May 1980).
- 1.21 *The Times*, London, 1 December 1983, p. 19.
- 1.22 P. Le Pivert, 'Cryosurgery: current issues and future trends', *Proc. 10th Int. Cryog. Engng Conf.*, pp. 551-557, Helsinki, Finland (1984).
- 1.23 B. A. Hands, 'Introduction to cryopump design', *Vacuum* **26**, 11-16 (1976).
- 1.24 B. A. Hands, 'Recent developments in cryopumping', *Vacuum* **32**, 603-612 (1982).
- 1.25 B. Lengeler, 'Semiconductor devices suitable for use in cryogenic environments', *Cryogenics* **14**, 439-447 (1974).

Journals

The most useful regular cryogenic publications are:

Cryogenics, a journal published by Butterworth Scientific Ltd., Guildford, England.
Advances in Cryogenic Engineering, which is published by Plenum Press and is the proceedings of the biennial Cryogenic Engineering Conference and the concurrent International Cryogenic Materials Conference held in the USA. It is referred to in this volume as *Adv. Cryog. Engng.*

Proceedings of the International Cryogenic Engineering Conference series (ICEC), published by Butterworth Scientific Ltd., Guildford, England, and predecessors.

Proceedings of the LNG and GasTech Conferences, which contain information on developments in LNG technology.

IC SQUID, proceedings of the International Conferences on SQUIDS.

International Institute of Refrigeration (IIR) conference proceedings.

Proceedings of the Applied Superconductivity Conference series.

General Bibliography

In reverse order of publication:

- R. F. Barron, *Cryogenic Systems*, 2nd edn, Oxford University Press (1985).
 K. D. Williamson, Jr. and F. J. Edeskuty (eds), *Liquid Cryogenics Vol. 1: Theory and Equipment*; Vol. 2: *Properties and Applications*, CRC Press (1983).
 A. Arkharov, I. Marfenina and Ye. Mikulin, *Theory and Design of Cryogenic Systems*, MIR Publishers (1981).
 G. K. White, *Experimental Techniques in Low-Temperature Physics*, 3rd edn, Clarendon Press (1979).
 A. C. Rose-Innes, *Low Temperature Laboratory Techniques. The Use of Liquid Helium in the Laboratory*, 2nd edn, English Universities Press (1973).
 C. A. Bailey (ed.), *Advanced Cryogenics*, Plenum Press (1971).
 G. G. Haselden (ed.), *Cryogenic Fundamentals*, Academic Press (1971).
 H. Weinstock (ed.), *Cryogenic Technology*, Boston Tech. Publ. (1969).
 R. H. Kropschot, B. W. Birmingham and D. B. Mann (eds), *Technology of Liquid Helium*, NBS Monograph 111 (1968).
 R. B. Scott, W. H. Denton and C. M. Nicholls (eds), *Technology and Uses of Liquid Hydrogen*, Pergamon Press (1964).
 J. H. Bell, *Cryogenic Engineering*, Prentice Hall (1963).
 R. W. Vance (ed.), *Cryogenic Technology*, John Wiley (1963).
 R. W. Vance and W. M. Duke (eds), *Applied Cryogenic Engineering*, John Wiley (1962).
 R. B. Scott, *Cryogenic Engineering*, Van Nostrand (1959).

Bibliography of Specific Topics

In alphabetical order of author:

- A. Barone and G. Paternò, *Physics and Applications of the Josephson Effect*, Wiley-Interscience (1982).
 N. R. Braton, *Cryogenic Recycling and Processing*, CRC Press (1980).

1. A SU

British C

Mech

J. R. Bu

A. J. Cr

B. Deav

T. van I

Arnol

R. C. F

Press,

D. Fishl

S. Fonei

Appli

R. A. H

(Engli

H. von

W. L. L

W. R. P

Topic

M. Reed

A. C. R

Press

R. P. Sl

B. B. S

Plenu

F. H. T

M. N. V

Non-sj

K. Men

Weid

D. Wils

(1979

- British Cryogenics Council, *Cryogenics Safety Manual - A Guide to Good Practice*, 2nd edn, Mechanical Engineering Publications, Bury St. Edmunds (1982).
- J. R. Bumby, *Superconducting Rotating Electrical Machines*, Clarendon Press (1983).
- A. J. Croft, *Cryogenic Laboratory Equipment*, Plenum Press (1970).
- B. Deaver and J. Ruvalds (eds), *Advances in Superconductivity*, Plenum Press (1983).
- T. van Duzer and C. W. Turner, *Principles of Superconductive Devices and Circuits*, Edward Arnold (1981).
- R. C. Ffooks, *Natural Gas by Sea*, Gentry Books, London (1979); *Gas Carriers*, Fairplay Press, London (1984).
- D. Fishlock (ed.), *A Guide to Superconductivity*, Macdonald-Elsevier (1969).
- S. Foner and B. B. Schwartz (eds), *Superconducting Machines and Devices - Large Systems Applications*, Plenum Press (1974).
- R. A. Haefter, *Kryo-Vakuumtechnik: Grundlagen und Anwendungen*, Springer-Verlag (1981) (English translation to be published by Oxford University Press).
- H. von Leden and W. G. Cahan, *Cryogenics in Surgery*, H. K. Lewis (1971).
- W. L. Lom, *Liquefied Natural Gas*, Applied Science Publishers (1974).
- W. R. Parrish, R. O. Voth, J. G. Hust, T. M. Flynn, C. F. Sindt and N. A. Olien, *Selected Topics on Hydrogen Fuel*, NBS Special Publication 419 (1975).
- M. Rechowicz, *Electric Power at Low Temperatures*, Clarendon Press (1975).
- A. C. Rose-Innes and E. H. Rhoderick, *Introduction to Superconductivity*, 2nd ed., Pergamon Press (1978).
- R. P. Shutt (ed.), *Bubble and Spark Chambers, Vol. 1*, Academic Press (1967).
- B. B. Schwartz and S. Foner (eds), *Superconductor Applications: SQUIDs and Machines*, Plenum Press (1977).
- F. H. Turner, *Concrete and Cryogenics*, Cement and Concrete Ass., England (1979).
- M. N. Wilson, *Superconducting Magnets*, Clarendon Press (1983).

Non-specialist Reading

- K. Mendelssohn, *The Quest for Absolute Zero; the Meaning of Low Temperature Physics*, Weidenfeld & Nicholson (1966).
- D. Wilson, *Supercold, an Introduction to Low Temperature Technology*, Faber & Faber (1979).

ATTACHMENT BL

IN THE UNITED STATES PATENT AND TRADEMARK OFFICE

In re Patent Application of

Applicants: Bednorz et al.

Serial No.: 08/479,810

Filed: June 7, 1995

For: NEW SUPERCONDUCTIVE COMPOUNDS HAVING HIGH TRANSITION
TEMPERATURE, METHODS FOR THEIR USE AND PREPARATION

Date: November 25, 2006

Docket: YO987-074BZ

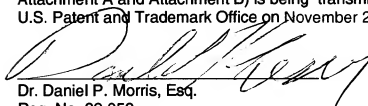
Group Art Unit: 1751

Examiner: M. Kopec

Commissioner for Patents
Box AF
P.O. Box 1450
Alexandria, VA 22313-1450

CERTIFICATE OF FIRST CLASS TRANSMISSION

I hereby certify that this Supplementary Response, (3 Pages Plus
Attachment A and Attachment B) is being transmitted by first class mail to the
U.S. Patent and Trademark Office on November 25, 2006.



Dr. Daniel P. Morris, Esq.
Reg. No. 32,053

FOURTEENTH SUPPLEMENTARY RESPONSE

In response to the Office Action dated October 20, 2005 please consider the
following:

IN THE UNITED STATES PATENT AND TRADEMARK OFFICE

In re Patent Application of

Date: January 30, 2008

Applicants: Bednorz et al.

Docket: YO987-074BZ

Serial No.: 08/479,810

Group Art Unit: 1751

Filed: June 7, 1995

Examiner: M. Kopec

For: NEW SUPERCONDUCTIVE COMPOUNDS HAVING HIGH TRANSITION
TEMPERATURE, METHODS FOR THEIR USE AND PREPARATION

Commissioner for Patents
Box AF
P.O. Box 1450
Alexandria, VA 22313-1450

SIXTEENTH SUPPLEMENTARY RESPONSE

Submitted at the Suggestion of the Examiner in response to the
Advisory Action dated November 15, 2007

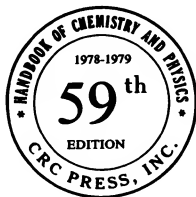
In response to the Advisory Action dated November 15, 2007 please consider the following:

ATTACHMENT B

VCE
tion
ogy,
VCE

CRC Handbook OF Chemistry and Physics

A Ready-Reference Book of Chemical and Physical Data



EDITOR

ROBERT C. WEAST, Ph.D.

*Vice President, Research, Consolidated Natural Gas Service Company, Inc.
Formerly Professor of Chemistry at Case Institute of Technology*

ASSOCIATE EDITOR

MELVIN J. ASTLE, Ph.D.

*Formerly Professor of Organic Chemistry at Case Institute of Technology
and
Manager of Research at Glidden-Durkee Division of SCM Corporation*

SES

In collaboration with a large number of professional chemists and physicists whose assistance is acknowledged in the list of general collaborators and in connection with the particular tables or sections involved.



CRC PRESS, Inc.
2255 Palm Beach Lakes Blvd., West Palm Beach, Florida 33409

Superconductivity*

B.W. ROBERTS

General Electric Research Laboratory, Schenectady, New York

The following tables on superconductivity include superconductive properties of chemical elements, thin films, a selected list of compounds and alloys, and high-magnetic-field superconductors.

The historically first observed and most distinctive property of a superconductive body is the near total loss of resistance at a critical temperature (T_c) that is characteristic of each material. Figure 1(a) below illustrates schematically two types of possible transitions. The sharp vertical discontinuity in resistance is indicative of that found for a single crystal of a very pure element or one of a few well annealed alloy compositions. The broad transition, illustrated by broken lines, suggests the transition shape seen for materials that are not homogeneous and contain unusual strain distributions. Careful testing of the resistivity limits for superconductors shows that it is less than 4×10^{-23} ohm-cm, while the lowest resistivity observed in metals is of the order of 10^{-13} ohm-cm. If one compares the resistivity of a superconductive body to that of copper at room temperature, the superconductive body is at least 10^{17} times less resistive.

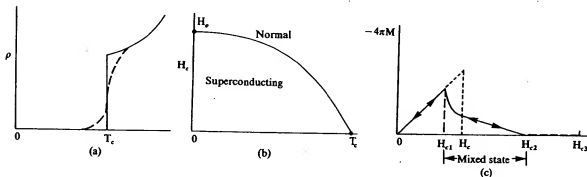


Figure 1. PHYSICAL PROPERTIES OF SUPERCONDUCTORS

- (a) Resistivity versus temperature for a pure and perfect lattice (solid line). Impure and/or imperfect lattice (broken line).
- (b) Magnetic-field temperature dependence for Type-I or "soft" superconductors.
- (c) Schematic magnetization curve for "hard" or Type-II superconductors.

The temperature interval ΔT_c , over which the transition between the normal and superconductive states takes place, may be of the order of as little as 2×10^{-5} °K or several °K in width, depending on the material state. The narrow transition width was attained in 99.9999 percent pure gallium single crystals.

A Type-I superconductor below T_c , as exemplified by a pure metal, exhibits perfect diamagnetism and excludes a magnetic field up to some critical field H_c , whereupon it reverts to the normal state as shown in the H-T diagram of Figure 1(b).

The difference in entropy near absolute zero between the superconductive and normal states relates directly to the electronic specific heat, γ : $(S_n - S_s)_{T \rightarrow 0} = -\gamma T$.

The magnetization of a typical high-field superconductor is shown in Figure 1(c). The discovery of the large current-carrying capability of Nb₃Sn and other similar alloys has led to an extensive study of the physical properties of these alloys. In brief, a high-field superconductor, or Type-II superconductor, passes from the perfect diamagnetic state at low magnetic fields to a mixed state and finally to a sheathed state before attaining the normal resistive state of the metal. The magnetic field values separating the four stages are given as H_{c1} , H_{c2} , and H_{c3} . The superconductive state below H_{c1} is perfectly diamagnetic, identical to the state of most pure metals of the "soft" or Type-I

*Prepared for Office of Standard Reference Data, National Bureau of Standards, by Standard Reference Data Center on Superconductive Materials, Schenectady, N.Y.

superconductor. Between H_{c1} and H_{c2} a "mixed superconductive state" is found in which fluxons (a minimal unit of magnetic flux) create lines of normal superconductor in a superconductive matrix. The volume of the normal state is proportional to $-4\pi M$ in the "mixed state" region. Thus at H_{c2} the fluxon density has become so great as to drive the interior volume of the superconductive body completely normal. Between H_{c2} and H_{c3} the superconductor has a sheath of current-carrying superconductive material at the body surface, and above H_{c3} the normal state exists. With several types of careful measurement, it is possible to determine H_{c1} , H_{c2} , and H_{c3} . Table 2-35 contains some of the available data on high-field superconductive materials.

High-field superconductive phenomena are also related to specimen dimension and configuration. For example, the Type-I superconductor, Hg, has entirely different magnetization behavior in high magnetic fields when contained in the very fine sets of filamentary tunnels found in an unprocessed Vycor glass. The great majority of superconductive materials are Type II. The elements in very pure form and a very few precisely stoichiometric and well annealed compounds are Type-I with the possible exceptions of vanadium and niobium.

Metallurgical Aspects. The sensitivity of superconductive properties to the material state is most pronounced and has been used in a reverse sense to study and specify the detailed state of alloys. The mechanical state, the homogeneity, and the presence of impurity atoms and other electron-scattering centers are all capable of controlling the critical temperature and the current-carrying capabilities in high-magnetic fields. Well annealed specimens tend to show sharper transitions than those that are strained or inhomogeneous. This sensitivity to mechanical state underlines a general problem in the tabulation of properties for superconductive materials. The occasional divergent values of the critical temperature and of the critical fields quoted for a Type-II superconductor may lie in the variation in sample preparation. Critical temperatures of materials studied early in the history of superconductivity must be evaluated in light of the probable metallurgical state of the material, as well as the availability of less pure starting elements. It has been noted that recent work has given extended consideration to the metallurgical aspects of sample preparation.

REFERENCES

References to the data presented in this section, to additional entries of superconductive materials, and to those materials specifically tested and found non-superconductive to some low temperature may be found in the following publications:

- "Superconductive Materials and Some of Their Properties", *Progress in Cryogenics*, B.W. Roberts, Vol. IV, Heywood and Co., 1964, pp. 160-231.
- "Superconductive Materials and Some of Their Properties", B.W. Roberts, National Bureau of Standards Technical Notes 408 and 482, U.S. Government Printing Office, 1966 and 1969.

SELECTED PROPERTIES OF THE SUPERCONDUCTIVE ELEMENTS

Conversion Factors

$$Oe \times 79.57 = A/m; \text{ katm} \times 1.013 \times 10^4 = N/m^2; kb \times 1.0 \times 10^4 = N/m^2$$

Element	$T_c(K)$	$H_c(\text{oersteds})$	$\theta_D(K)$	$\gamma(\text{mJmole}^{-1} \text{ deg} \cdot K^2)$
Al	1.175	104.93	420	1.35
Be	0.026			0.21
Cd	0.518, 0.52	29.6	209	0.688
Ga	1.0833	59.3	325	0.60
Ga (β)	5.90, 6.2	560		
Ga (γ)	7.62	950		
Ga (δ)	7.85	815		
Hg (α)	4.154	411	87, 71.9	1.81
Hg (β)	3.949	339	93	1.37
In	3.405	281.53	109	1.672
Ir	0.14, 0.11	19	425	3.27
La (α)	4.88	808, 798	142	10.0, 11.3
La (β)	6.00	1,096	139	11.3
Mo	0.916	90, 98	460	1.83
Nb	9.25	1,970	277, 238	7.80
Os	0.655	65	500	2.35
Pb	1.4			
Pb	7.23	803	96.3	3.0
Re	1.697	188, 211	415	2.35
Ru	0.493	66	580	3.0
Sb	2.6-2.7			
Sn	3.721	305	195	1.78
Ta	4.47	831	258	6.15
Tc	7.73, 7.78	1,410	411	4.84, 6.28
Th	1.39	159.1	165	4.31
Ti	0.39	56, 100	429, 412	3.32
Tl	2.332, 2.39	181	78.5	1.47
V	5.43, 5.31	1,100, 1,400	382	9.82
W	0.0154	1.15	550	0.90
Zn	0.875	55	319.7	0.633
Zr	0.53	47	290	2.78
Zr (ω)	0.65			

Thin Films Condensed at Various Temperatures

Element	$T_c(K)$
Al	1.18-5.7
Be	~0.3, ~9.6; 6.5-10.6 ^a ; 10.2 ^b
Bi	~2-~5, 6.11, 6.154, 6.173
Cd	0.53-0.91
Ga	6.4-6.8, 7.4-8.4, 8.56
In	3.43-4.5; 3.68-4.17 ^c
La	5.0-6.74
Mo	3.3-3.8, 4-6.7
Nb	6.2-10.1
Pb	~2-7.7
Re	~7
Sn	3.6, 3.84-6.0
Ta	<1.7-4.25, 3.16-4.8
Ti	1.3
Tl	2.64
V	5.14-6.02
W	<1.0-4.1
Zn	0.77-1.48

^aWith KCl.

^bWith Zn etioporphyrin.

^cIn glass pores.

SELECTED PROPERTIES OF THE SUPERCONDUCTIVE ELEMENTS (Continued)

Data for Elements Studied Under Pressure

Element	$T_c(K)$	Pressure
As	0.31-0.5 0.2-0.25	220-140 kb ~140-100 kb
Ba II	~1.3	55 kb
Ba III	3.05	85-88 kb
	~5.2	>140 kb
Bi II	3.916	25 katm
	3.90	25.2 katm
	3.86	26.8 katm
Bi III	6.55	~37 kb
	7.25	27-28.4 katm
Bi IV	7.0	43, 43-62 kb
Bi V	8.3, 8.55	81 kb
Bi VI	8.55	90, 92-101 kb
Ce	1.7	50 kb
Cs	~1.5	>~125 kb
Ga II	6.24, 6.38	>35 katm
Ga II'	7.5	>35 katm ($P \rightarrow 0$)
Ge	4.85-5.4	~120 kb
	5.35	115 kb
La	~5.5-11.93	0-~140 kb
P	4.7	>100 kb
	5.8	170 kb
Pb II	3.55, 3.6	160 kb
Sb	3.55	85 kb
	3.52	93 kb
	3.53	100 kb
	3.40	~150 kb
Se II	6.75, 6.95	~130 kb
Si	6.7, 7.1	120 kb
Sn II	5.2	125 kb
	4.85	160 kb
Sn III	5.30	113 kb
Te II	2.05	43 kb
	3.4	50 kb
Te III	4.28	70 kb
Te IV	4.25	84 kb
Tl, cub.	1.45	35 kb
Tl, hex.	1.95	35 kb
U	2.3	10 kb
Y	~1.2, ~2.7	120-170 kb

From Roberts, B. W., Properties of Selected Superconductive Materials, 1974 Supplement, NBS Technical Note 825, U.S. Government Printing Office, Washington, D.C., 1974, 10.

All compositions are denoted on an atomic basis, i.e., AB_n or AB_3 for compounds, unless noted. Solid solutions or odd compositions may be denoted as A_nB_{1-x} or A_nB . A series of three or more alloys is indicated as A_nB_{1-x} or by actual indication of the atomic fraction range, such as $A_{0-0.6}B_{1-0.4}$. The critical temperature of such a series of alloys is denoted by a range of values or possibly the maximum value.

The selection of the critical temperature from a transition in the effective permeability, or the change in resistance, or possibly the incremental changes in frequency observed by certain techniques is not often obvious from the literature. Most authors choose the mid-point of such curves as the probable critical temperature of the idealized material, while others will choose the highest temperature at which a deviation from the normal state property is observed. In view of the previous discussion concerning the variability of the superconductive properties as a function of purity and other metallurgical aspects, it is recommended that appropriate literature be checked to determine the most probable critical temperature or critical field of a given alloy.

A very limited amount of data on critical fields, H_c , is available for these compounds and alloys; these values are given at the end of the table.

SYMBOLS: n = number of normal carriers per cubic centimeter for semiconductor superconductors.

Substance	T_c , °K	Crystal structure type††	Substance	T_c , °K	Crystal structure type††
$Ag_{0.4}Zn_{1-x-y}$	0.5-0.845	Cubic	$Al_{1-0.4}Ge_{0.2}Nb_3$	20.7	A15
$AgBF_4O_8$	0.15		$AlLa_3$	5.57	DO ₁₉
$AgBi_2$	3.0-2.78		Al_2La	3.23	C15
$Ag_2F_{0.33}N_{0.75}O_{10.25}$	0.85-0.90		Al_3Mg_2	0.84	Cubic, f.c.
Ag_2FO_8	0.3	Cubic	$AlMo_3$	0.58	A15
Ag_2F	0.066		$AlMo_4Pd$	2.1	
$Ag_{0.3-0.3}Ga_{0.2-0.7}$	6.5-8		AlN	1.55	B4
Ag_2Ge	0.85		Al_2NNb_3	1.3	A13
$Ag_{0.438}Hg_{0.562}$	0.64	Hex., c.p.	$AlNb_3$	18.0	A15
$AgIn_2$	~2.4	C16	Al_2Nb_{1-x}	<4.2-13.5	D8 _h
$Ag_{0.1}In_{0.9}Te$ ($n = 1.40 \times 10^{22}$)	1.20-1.89	BI	Al_2Nb_{1-x}	12-17.5	A15
$Ag_{0.2}In_{0.8}Te$ ($n = 1.07 \times 10^{22}$)	0.77-1.00	BI	$Al_{0.27}Nb_{0.73-0.48}V_{0-0.25}$	14.5-17.5	A15
$AgLa$ (9.5 kbar)	1.2	B2	$AlNb_2V_{1-x}$	<4.2-13.5	
$AgNO_{1.1}$	1.04	Cubic	$AlOs$	0.39	B2
$AgPb_{1-x}$	7.2 max.		Al_2Os	5.90	
Ag_2Sn_{1-x} (film)	2.0-3.8		$AlPb$ (films)	1.2-7	
Ag_2Sn_{1-x}	1.5-3.7		Al_2Pt	0.48-0.55	C1
$AgTe_3$	2.6	Cubic	Al_2Re_{24}	3.35	A12
$AgTh_2$	2.26		Al_3Th	0.75	DO ₁₉
$Ag_{0.03}Tl_{0.97}$	2.67		$Al_2Ti_2V_{1-x-y}$	2.05-3.62	Cubic
$Ag_{0.94}Tl_{0.06}$	2.32		$Al_{0.108}V_{0.892}$	1.82	Cubic
Ag_2Zn_{1-x}	0.5-0.845	Cubic	Al_2Zn_{1-x}	0.5-0.845	
Al (film)	1.3-2.31		$AlZr_3$	0.73	LI ₂
Al (1 to 21 atm)	1.170-0.687		$AsBiPb$	9.0	
$AlAu_4$	0.4-0.7		$AsBiPbSb$	9.0	
Al_2CMo_3	10.0	Al	$As_{0.33}InTe_{0.67}$ ($n = 1.24 \times 10^{22}$)	0.85-1.15	BI
Al_2CMo_3	9.8-10.2	Like Al3	$As_{0.5}InTe_{0.5}$ ($n = 0.97 \times 10^{22}$)	0.44-0.62	BI
		Al3 + trace	$As_{0.10}Ni_{0.90}Pd_{0.44}$	1.39	C2
		2nd phase	$AsPb$	8.4	
Al_2CaSi	5.8	Cubic	$AsPd_2$ (low-temperature phase)	0.60	Hexagonal
$Al_{0.131}Cr_{0.088}V_{0.781}$	1.46		$AsPd_2$ (high-temp. phase)	1.70	C22
$AlGe_2$	1.75				
$Al_{0.5}Ge_{0.5}Nb$	12.6	A15			

††See key at end of table.

Substance	T_c , °K	Crystal structure type††	Substance	T_c , °K	Crystal structure type††
AsPd ₃	0.46	Complex	BW ₂	3.1	Cl6
AsRh	0.58	B31	B ₈ Y	6.5-7.1	
AsRh _{1.4-1.6}	<0.03-0.56	Hexagonal	B ₁₂ Y	4.7	
AsSn	4.10		BZr	3.4	Cubic
AsSn			B ₁₂ Zr	5.82	
(n = 2.14 × 10 ²²)	3.41-3.65	B1	BaBi ₃	5.69	Tetragonal
As ₂ Sn ₂₋₃	3.5-3.6, 1.21-1.17		Ba ₂ O ₇ Sr _{1-x} Ti (n = 4.2-11 × 10 ¹⁹)	<0.1-0.55	
As ₂ Sn ₄			Ba _{0.13} O ₃ W	1.9	Tetragonal
(n = 0.56 × 10 ²²)	1.16-1.19	Rhombohedral	Ba _{0.14} O ₃ W	<1.25-2.2	Hexagonal
Au ₃ Ba	0.4-0.7	D ₂	BaRh ₂	6.0	Cl5
AuBe	2.64	B20	Be ₂₂ Mo	2.51	Cubic, like Be ₂₂ Re
AuBi	1.80	Cl5			
Au ₂ Ca	0.34-0.38	Cl5 ₂	Be ₂ Nb ₂ Zr ₂	5.2	
AuGa	1.2	B31	Be _{0.98-0.92} Re _{0.02-0.08} (quenched)	9.5-9.75	Cubic
Au _{0.40-0.92} Ge _{0.60-0.08}	<0.32-1.63	Complex	Be _{0.957} Re _{0.043}	9.62	Cubic, like Be ₂₂ Re
AuIn	0.4-0.6	Complex			
AuLu	<0.35	B2	BeTc	5.21	Cubic
AuNb ₃	11.5	A15	Be ₂₂ W	4.12	Cubic, like Be ₂₂ Re
AuNb ₃	1.2	A2			
Au _{0-0.3} Nb _{1-0.7}	1.1-11.0	A15	Be ₁₃ W	4.1	Tetragonal
Au _{0.02-0.94} Nb ₃ Rh _{0.98-0.02}	2.53-10.9	A15	Bi ₃ Ca	2.0	
AuNb _{3(1-x)} V _{3x}	1.5-11.0	A15	Bi _{0.3} Cd _{0.13} Pb _{0.33} Sn _{0.12} (weight fractions)	8.2	
AuPb ₂	3.15			0.42-0.49	Cl5
AuPb ₂ (film)	4.3		BiCo	4.75	
AuPb ₃	4.40		Bi ₂ CS		
AuPb ₃ (film)	4.25	Cl5	Bi ₂ Cu _{1-x} (electrodeposited)	2.2	
Au ₂ Pb	1.18, 6-7	C2	BiCu	1.33-1.40	
AuSb ₂	0.58	B8 ₁	Bi _{0.019} In _{0.981}	3.86	
AuSn	1.25		Bi _{0.05} In _{0.95}	4.65	α-phase
Au ₂ Sn _{1-x} (film)	2.0-3.8	A3	Bi _{0.10} In _{0.90}	5.05	α-phase
Au ₂ Sn	0.7-1.1	Cubic	Bi _{0.15-0.30} In _{0.85-0.70}	5.3-5.4	α- and β-phases
Au ₂ Te ₂	1.62	Cl6	Bi _{0.34-0.48} In _{0.66-0.52}	4.0-4.1	
AuTh ₂	3.08		Bi ₃ In ₃	4.1	
AuTi	1.92	A15	BiIn ₂	5.65	β-phase
AuV ₃	0.74		Bi ₂ Ir	1.7-2.3	
Au ₂ Zn _{1-x}	0.50-0.845		Bi ₂ Ir (quenched)	3.0-3.96	
AuZn ₃	1.21	Cubic		3.6	
Au ₂ Zr ₂	1.7-2.8	A3	Bi ₂ K	3.58	Cl5
AuZr ₃	0.92	A15	BiLi	2.47	Li ₆ , α-phase
BCMo ₂	5.4	Orthorhombic	Bi ₄₋₉ Mg	0.7-~1.0	
Bi _{0.03} Cu _{0.51} Mo _{0.47}	12.5		Bi ₃ Mo	3-3.7	
BCMo ₂	5.3-7.0	Orthorhombic	BiNa	2.25	Li ₆
BHf	3.1	Cubic	BiNb ₃ (high pressure and temperature)	3.05	A15
Bi ₂ La	5.7		BiNi	4.25	B8 ₁
Bi ₁₂ Lu	0.48		Bi ₂ Ni	4.06	Orthorhombic
BMo	0.5 (extrapolated)		Bi _{1-x} Pb _{x-1}	7.26-9.14	
BMo ₂	4.74	Cl6	Bi _{1-x} Pb _{x-1} (film)	7.25-8.67	
BNb	8.25	B _f	Bi _{0.05-0.40} Pb _{0.95-0.60}	7.35-8.4	Hexagonal, c.p. to α-phase
BRe ₂	2.80, 4.6	D10 ₂			
Bi _{0.3} Ru _{0.7}	2.58				
Bi ₂ Sc	0.39				
BTa	4.0	B _f			
Bi ₆ Th	0.74		BiPbSb	8.9	

†† See key at end of table.

	Substance	T_c , °K	Crystal structure type††	Substance	T_c , °K	Crystal structure type††
	$\text{Bi}_{0.5}\text{Pb}_{0.31}\text{Sn}_{0.19}$ (weight fractions)	8.5		$\text{Co}_{0.44}\text{Mo}_{0.56}$	1.3	BI
	$\text{Bi}_{0.5}\text{Pb}_{0.25}\text{Sn}_{0.25}$	8.5		$\text{Co}_{0.5}\text{Mo}_{0.5}\text{Nb}_{1-x}$	10.8-12.5	BI
	BiPd_2	4.0		$\text{Co}_{0.6}\text{Mo}_{0.4}\text{Si}_3$	7.6	D8 ₈
al	$\text{Bi}_{0.4}\text{Pd}_{0.6}$	3.7-4	Hexagonal, ordered	$\text{CMo}_{0.2}\text{Ta}_{0.8}$	7.5	BI
	BiPd	3.7	Orthorhombic	$\text{CMo}_{0.5}\text{Ta}_{0.5}$	7.7	BI
al	Bi_2Pd	1.70	Monoclinic, α -phase	$\text{CMo}_{0.75}\text{Ta}_{0.25}$	8.5	BI
al	Bi_2Pd	4.25	Tetragonal, β -phase	$\text{CMo}_{0.8}\text{Ta}_{0.2}$	8.7	BI
	BiPdSe	1.0	C2	$\text{CMo}_{0.85}\text{Ta}_{0.15}$	8.9	BI
12Re	BiPdTe	1.2	C2	$\text{CMo}_{0.7}\text{Ti}_{0.3}$	10.2 max.	BI
	BiPt	1.21	B8 ₁	$\text{CMo}_{0.83}\text{Ti}_{0.17}$	10.2	BI
	BiPtSe	1.45	C2	$\text{CMo}_{0.9}\text{V}_{1-x}$	2.9-9.3	BI
	BiPtTe	1.15	C2	$\text{CMo}_{0.9}\text{Zr}_{1-x}$	3.8-9.5	BI
12Re	Bi_2Pt	0.155	Hexagonal	$\text{Co}_{1-0.9}\text{Nb}_{0.9-0.1}\text{Nb}$	8.5-17.9	
	Bi_2Rb	4.25	C15	$\text{Co}_{0.38}\text{Ni}_{1-0.62}\text{Ta}$	10.0-11.3	
	BiRe_2	1.9-2.2		CNb (whiskers)	7.5-10.5	
12Re	BiRh	2.06	B8 ₁	$\text{Co}_{0.988}\text{Nb}$	9.8	BI
al	Bi_3Rh	3.2	Orthorhombic, like NiB_3	CNb (extrapolated)	~14	
	Bi_4Rh	2.7	Hexagonal	$\text{Co}_{0.7-1.0}\text{Nb}_{0.3-0}$	6-11	BI
	Bi_2Sn	3.6-3.8		CNb ₂	9.1	
	BiSn	3.8		$\text{CMo}_{0.5}\text{Ta}_{1-x}$	8.2-13.9	
	Bi_2Sn_2	3.85-4.18		$\text{CNb}_2\text{Ti}_{1-x}$	<4.2-8.8	BI
	Bi_3Sr	5.62	Li_2	$\text{CNb}_{0.6-0.9}\text{W}_{0.4-0.1}$	12.5-11.6	BI
	Bi_3Te	0.75-1.0		$\text{CNb}_{0.1-0.9}\text{Zr}_{0.9-0.1}$	4.2-8.4	BI
	Bi_3Ti_3	6.4		CRb ₂ (gold)	0.023-0.151	Hexagonal
	$\text{Bi}_{0.26}\text{Ti}_{0.74}$	4.4	Cubic, disordered	$\text{CRCo}_{0.01-0.08}\text{W}$	1.3-5.0	
	$\text{Bi}_{0.26}\text{Ti}_{0.74}$	4.15	Li_2 , ordered?	$\text{CRCo}_{0.06}\text{W}$	5.0	
phases	Bi_2Y_3	2.25		CTa	~11 (extrapolated)	
	Bi_2Zn	0.8-0.9		$\text{Co}_{0.987}\text{Ta}$	9.7	
	$\text{Bi}_{0.5}\text{Zr}_{0.7}$	1.51		$\text{Co}_{0.848-0.987}\text{Ta}$	2.04-9.7	
	BiZr_3	2.4-2.8		CTa (film)	5.09	BI
	CCl_8	0.020-0.135	Hexagonal	CTa ₂	3.26	L_3
	C_6K (gold)	0.55		$\text{CTa}_{0.4}\text{Ti}_{0.6}$	4.8	BI
	CGaMo_2	3.7-4.1	Hexagonal, H-phase	$\text{CTa}_{1-0.4}\text{W}_{0-0.6}$	8.5-10.5	BI
	$\text{CHf}_{0.5}\text{Mo}_{0.5}$	3.4	BI	$\text{CTa}_{0.2-0.9}\text{Zr}_{0.8-0.1}$	4.6-8.3	BI
	$\text{CHf}_{0.3}\text{Mo}_{0.7}$	5.5	BI	CTc (excess C)	3.85	Cubic
	$\text{CHf}_{0.22}\text{Mo}_{0.75}$	6.6	BI	$\text{CTi}_{0.5-0.7}\text{W}_{0.5-0.3}$	6.7-2.1	BI
	$\text{CHf}_{0.6}\text{Nb}_{0.4}$	6.1	BI	CW	1.0	
	$\text{CHf}_{0.5}\text{Nb}_{0.5}$	4.5	BI	CW ₂	2.74	L_3
	$\text{CHf}_{0.4}\text{Nb}_{0.6}$	4.8	BI	CaF_2	5.2	Cubic, f.c.
	$\text{CHf}_{0.22}\text{Nb}_{0.75}$	5.6	BI	$\text{Ca}_2\text{O}_3\text{Sr}_{1-x}\text{Ti}$ ($n = 3.7-11.0 \times 10^{19}$)	6.15	C15
mbic	$\text{CHf}_{0.2}\text{Nb}_{0.8}$	7.0	BI	$\text{Ca}_{0.1}\text{O}_3\text{W}$	<0.1-0.55	
	$\text{CHf}_{0.9-0.1}\text{Ta}_{0.1-0.9}$	7.8	BI	CaPb	1.4-3.4	Hexagonal
	Cf (excess K)	5.0-9.0	BI	CaRh_2	7.0	
al,	C_6K	0.39	Hexagonal	$\text{Cd}_{0.3-0.5}\text{Hg}_{0.7-0.5}$	6.40	C15
	$\text{Co}_{0.40-0.44}\text{Mo}_{0.60-0.56}$	9-13	Hexagonal	$\text{Cd}_{0.3-0.5}\text{Hg}_{0.7-0.5}$	1.70-1.92	
	CMo	6.5, 9.26	Hexagonal	CdHg	1.77, 2.15	Tetragonal
	CMo_2	12.2	Orthorhombic	$\text{Cd}_{0.075-0.095}\text{In}_{1-x}$	3.24-3.36	Tetragonal
				$\text{Cd}_{0.97}\text{Pb}_{0.03}$	4.2	
				CdSn	3.65	
				$\text{Cd}_{0.17}\text{Ti}_{0.83}$	2.3	
				$\text{Cd}_{0.18}\text{Ti}_{0.82}$	2.54	
				CeCo_2	0.84	C15
				$\text{CeCo}_{1.67}\text{Ni}_{0.33}$	0.46	C15

†† See key at end of table.

Substance	$T_c, ^\circ K$	Crystal structure type††	Substance	$T_c, ^\circ K$	Crystal structure type††
$CeCo_{1.67}Rh_{0.33}$	0.47	C15	CuSse	1.5-2.0	C18
$Ce_2Gd_{1-x}Ru_2$	3.2-5.2	C15	CuSe ₂	2.3-2.43	C18
$CeIr_3$	3.34		CuSeTe	1.6-2.0	C18
$CeIr_3$	1.82		Cu_2Sn_{1-x}	3.2-3.7	
$Ce_{0.005}La_{0.995}$	4.6		Cu_2Sn_{1-x} (film)		
Ce_2La_{1-x}	1.3-6.3		(made at 10°K)	3.6-7	
$Ce_2Pr_{1-x}Ru_2$	1.4-5.3	C15	Cu_2Sn_{1-x} (film)		
Ce_2Pt_{1-x}	0.7-1.55		(made at 300°K)	2.8-3.7	
$CeRu_2$	6.0	C15	$CuTe_2$	<1.25-1.3	C18
$Co_2Fe_{1-x}Si_2$	1.4 max.	Cl	$CuTh_2$	3.49	C16
$CoHF_2$	0.56	E9 ₃	$Cu_{0.92}V$	3.9-5.3	A2
$CoLa_3$	4.28		Cu_2Zn_{1-x}	0.5-0.845	
$CoLu_3$	~0.35		Er_2La_{1-x}	1.4-6.3	
$Co_{0.99}Mo_{0.01}Re_{0.2}$	2-10		$Fe_{0.94}Mo_{0.06}Re_{0.2}$	1-10	
$Co_{0.02-0.10}Nb_{0.98-0.90}$	2.28-1.90	A15	$Fe_{0.05}Ni_{0.05}Zr_{0.90}$	~3.9	
$Co_2Ni_{1-x}Si_2$	1.4 max.	Cl	Fe_2Th_7	1.86	D10
$Co_2Rh_{0.5}Si_2$	2.5		Fe_2Ti_{1-x}	3.2 max.	Fe in α -Ti
$Co_2Rh_{1-x}Si_2$	3.65 max.		Fe_2Ti_{1-x}	3.7 max.	Fe in β -Ti
$Co_{0.3}Sc_{0.7}$	~0.35		$Fe_2Ti_{0.8}V_{1-x}$	6.8 max.	
$CoSi_2$	1.40, 1.22	Cl	FeU_6	3.86	D2 _c
Co_2Th_7	1.83	D10 ₂	$Fe_{0.7}Zr_{0.9}$	1.0	A3
Co_2Ti_{1-x}	2.8 max.	Co in α -Ti	$Ga_{0.5}Ge_{0.5}Nb_3$	7.3	A15
Co_2Ti_{1-x}	3.8 max.	Co in β -Ti	$GaLa_3$	5.84	
$CoTi_2$	3.44	E9 ₃	Ga_2Mo	9.5	
$CoTi_2$	0.71	A2	$GaMo_3$	0.76	A15
CoU	1.7	B2, distorted	Ga_2Mo	9.8	
CoU_6	2.29	D2 _c	GaN (black)	5.85	B4
$Co_{0.24}Y_{0.72}$	0.34		$GaNb_3$	14.5	A15
CoY_3	<0.34		$Ga_2Nb_2Sn_{1-x}$	14-18.37	A15
$CoZr_2$	6.3	Cl6	$Ga_{0.3}Pt_{0.3}$	2.9	Cl
$Co_{0.1}Zr_{0.9}$	3.9	A3	$GaPt$	1.74	B20
$Cr_{0.6}Ir_{0.4}$	0.4	Hexagonal, c.p.	$GaSb$ (120 kbar, 77°K, annealed)	4.24	A5
$Cr_{0.65}Ir_{0.35}$	0.59	Hexagonal, c.p.	$GaSb$ (unannealed)	~5.9	
$Cr_{0.7}Ir_{0.3}$	0.76	Hexagonal, c.p.	$Ga_{0.5}Sn_{1-x}$ (quenched)	3.47-4.18	
$Cr_{0.72}Ir_{0.28}$	0.83		$Ga_{0.5}Sn_{1-x}$ (annealed)	2.6-3.85	
Cr_3Ir	0.45	A15	Ga_2V_2	3.55	Tetragonal, Mn ₂ Hg ₅ type
$Cr_{0.9}Nb_{1-0.9}$	4.6-9.2	A2			
$Cr_{0.80}Os_{0.20}$	2.5	Cubic	GaV_3	16.8	A15
Cr_2Re_{1-x}	1.2-5.2		$GaV_{2.11-2.5}$	6.3-14.45	A15
$Cr_{0.40}Re_{0.60}$	2.15	D8 ₈	$GaV_{4.5}$	9.15	
$Cr_{0.8-0.6}Rh_{0.2-0.4}$	0.5-1.10	A3	$GaZr$	1.38	
Cr_3Ru (annealed)	3.3	A15	Gd_2La_{1-x}	<1.0-5.5	
Cr_2Ru	2.02	D8 ₈	$Gd_2Os_{0.5}Y_{1-x}$	1.4-4.7	
$Cr_{0.1-0.3}Ru_{0.9-0.3}$	0.34-1.65	A3	Gd_2Ru_{1-x}	3.6 max.	Cl5
Cr_2Ti_{1-x}	3.6 max.	Cr in α -Ti	$GdIr$	4.7	B31
Cr_2Ti_{1-x}	4.2 max.	Cr in β -Ti	Ge_2La	1.49, 2.2	Orthorhombic, distorted ThSi ₂ -type
$Cr_{0.1}Ti_{0.3}V_{0.6}$	5.6	β -phase			
$Cr_{0.0175}U_{0.9825}$	0.75	Hexagonal	$GeMo_3$	1.43	A15
$Cr_{0.32}O_3W$	1.12		$GeNb_2$	1.9	
$Cu_{0.15}In_{0.85}$ (film)	3.75		$GeNb_3$ (quenched)	6-17	A15
$Cu_{0.04-0.08}In_{1-x}$	4.4		$Ge_{0.29}Nb_{0.71}$	6	A15
$CuLa$	5.85		$Ge_2Nb_2Sn_{1-x}$	17.6-18.0	A15
Cu_2Pb_{1-x}	5.7-7.7		$Ge_{0.5}Nb_{0.5}Sn_{0.5}$	11.3	
CuS	1.62	B18			
CuS_2	1.48-1.53	C18			

††See key at end of table.

SELECTED SUPERCONDUCTIVE COMPOUNDS AND ALLOYS (Continued)

Substance	T_c , °K	Crystal structure type††	Substance	T_c , °K	Crystal structure type††
GePt	0.40	B31	InSb	2.1	
Ge ₃ Rh ₅	2.12	Orthorhombic, related to InNi ₂	(InSb) _{0.95-0.10} Sn _{0.05-0.90} (various heat treatments)	3.8-5.1	
			(InSb) _{0-0.07} Sn _{1-0.93}	3.67-3.74	
Ge ₂ Sc	1.3		In ₃ Sn	~5.5	
Ge ₃ Te ₄ ($n = 1.06 \times 10^{22}$)	1.55-1.80	Rhombohedral	In ₂ Sn _{1-x}	3.4-7.3	
Ge ₂ Tc _{1-x} ($n = 8.5-64 \times 10^{20}$)	0.07-0.41		In _{0.82-1} Tc ($n = 0.83-1.71 \times 10^{22}$)	1.02-3.45	BI
GeV ₃	6.01	BI	In _{1.006} Tc _{1.002}	3.5-3.7	BI
Ge ₂ Y	3.80	A15	In ₂ Te ₄ ($n = 0.47 \times 10^{22}$)	1.15-1.25	Rhombohedral
Ge _{1.62} Y	2.4		In ₂ Tl _{1-x}	2.7-3.374	
H _{0.33} Nb _{0.67}	7.28	Cubic, b.c.	In _{0.8} Tl _{0.2}	3.223	
H _{0.1} Nb _{0.9}	7.38	Cubic, b.c.	In _{0.62} Tl _{0.38}	2.760	
H _{0.05} Nb _{0.95}	7.83	Cubic, b.c.	In _{0.78-0.69} Tl _{0.22-0.31}	3.18-3.32	Tetragonal
H _{0.12} Ta _{0.88}	2.81	Cubic, b.c.	In _{0.69-0.62} Tl _{0.31-0.38}	2.98-3.3	Cubic, f.c.
H _{0.05} Ta _{0.92}	3.26	Cubic, b.c.	Ir ₂ La	0.48	C15
H _{0.04} Ta _{0.96}	3.62	Cubic, b.c.	Ir ₃ La	2.32	D10 ₂
HfN _{0.989}	6.6	BI	Ir ₃ La ₂	2.24	D10 ₂
Hf _{0-0.5} Nb _{1-0.5}	8.3-9.5	A2	Ir ₄ La	2.13	
Hf _{0.75} Nb _{0.25}	> 4.2		Ir ₂ Lu	2.47	C15
HfOs ₂	2.69	C14	Ir ₃ Lu	2.89	C15
HfRe ₂	4.80	C14	IrMo	< 1.0	A3
Hf _{0.14} Re _{0.86}	5.86	A12	IrMo ₂	8.8	A15
Hf _{0.99-0.96} Rh _{0.01-0.04}	0.85-1.51		IrMo ₃	6.8	D8 ₈
Hf _{0-0.55} Ta _{1-0.45}	4.4-6.5 ~	A2	IrNb ₂	1.9	A15
HfV ₂	8.9-9.6	C15	Ir _{0.4} Nb _{0.6}	9.8	D8 ₈
Hg ₂ In _{1-x}	3.14-4.55		Ir _{0.37} Nb _{0.63}	2.32	D8 ₈
HgIn	3.81		IrNb	7.9	D8 ₈
Hg ₃ K	1.20	Orthorhombic	Ir _{0.02} Nb ₂ Rh _{0.98}	2.43	A15
Hg ₃ K	3.18		Ir _{0.03} Nb ₂ Rh _{0.95}	2.38	A15
Hg ₄ K	3.27		Ir _{0.287} O _{0.14} Tl _{0.573}	5.5	E9 ₃
Hg ₄ K	3.42		Ir _{0.265} O _{0.035} Tl _{0.65}	2.30	
Hg ₃ Li	1.7	Hexagonal	Ir _x Os _{1-x}	0.3-0.98 (max.)-0.6	
Hg ₃ Na	1.62	Hexagonal	IrOsY	2.6	C15
Hg ₂ Na	3.05		Ir _{1.5} Os _{0.5}	2.4	C14
Hg ₂ Pb _{1-x}	4.14-7.26		Ir ₂ Sc	2.07	C15
HgSn	4.2		Ir _{2.5} Sc	2.46	C15
Hg ₂ Tl _{1-x}	2.30-4.109		IrSn ₂	0.65-0.78	C1
Hg ₂ Tl ₂	3.86		Ir ₂ Sn ₂	5.70	C15
Hg ₂ La _{1-x}	1.3-6.3		Ir ₂ Te ₃	~ 3	
InLa ₃	9.83, 10.4	LI ₂	Ir _{0.3} Te _{0.5}	1.18	C2
InLa ₃ (0-35, kbar)	9.75-10.55		IrTh	< 0.37	B ₇
In _{1-0.86} Mg _{0-0.14}	3.395-3.363		Ir ₂ Th	6.50	C15
InNb ₃ (high pressure and temp.)	4-8, 9.2	A15	Ir ₃ Th	4.71	
In _{0-0.3} Nb ₂ Sn _{1-0.7}	18.0-18.19	A15	Ir ₂ Th	1.52	D10 ₂
In _{0.3} Nb ₂ Zr _{0.5}	6.4		Ir ₃ Th	3.93	D2 ₂
In _{0.11} O ₂ W	< 1.25-2.8	Hexagonal	IrTi ₃	5.40	A15
In _{0.95-0.85} Pb _{0.05-0.15}	3.6-5.05		Ir ₂	1.39	A15
In _{0.98-0.91} Pb _{0.02-0.09}	3.45-4.2		IrW ₃	3.82	
InPb	6.65		Ir _{0.21} W _{0.72}	4.49	
InPd	0.7	B2	Ir ₂ Y	2.18, 1.38	C15
InSb (quenched from 170 kbar into liquid N ₂)	4.8	Like A5	Ir _{0.65} Y _{0.31}	1.98, 1.44	C15
			Ir _{0.70} Y _{0.30}	2.16	C15

††See key at end of table.

Substance	T_c , °K	Crystal structure type††	Substance	T_c , °K	Crystal structure type††
Ir ₂ Y	1.09	C15	Mo ₂ Si	1.30	A15
Ir ₂ Y ₃	1.61		MoSi _{0.7}	1.34	
Ir ₂ Y _{1-x}	0.3-3.7		Mo ₂ SiV _{0.5-x}	4.54-16.0	A15
Ir ₂ Zr	4.10	C15	Mo ₂ Tc _{0.5-x}	10.8-15.8	
Ir _{0.1} Zr _{0.9}	5.5	A3	Mo _{0.16} Ti _{0.84}	4.18, 4.25	
K _{0.27-0.31} O ₃ W	0.50	Hexagonal	Mo _{0.913} Ti _{0.087}	2.95	Cubic
K _{0.40-0.57} O ₃ W	1.5	Tetragonal	Mo _{0.04} Ti _{0.96}	2.0	
La _{0.55} Lu _{0.45}	2.2	Hexagonal, La type	Mo _{0.025} Ti _{0.975}	1.8	
La _{0.8} Lu _{0.2}	3.4	Hexagonal, La Type	Mo ₂ U _{1-x}	0.7-2.1	
LaMg ₂	1.05	C15	Mo ₂ V _{1-x}	0-~5.3	
LaN	1.35		Mo ₂ Zr	4.27-4.75	C15
LaOs ₂	6.5	C15	NNb (whiskers)	10-14.5	
LaPt ₂	0.46	C15	NNb (diffusion wires)	16.10	
La _{0.28} Pt _{0.72}	0.54	C15	NNb (film)	6-9	BI
LaRh ₃	2.60		Nb _{0.988} Nb	14.9	BI
LaRh ₃	1.62		Nb _{0.824-0.988} Nb	14.4-15.3	Cubic and tetragonal
LaRh ₃	2.58	D10 ₂	NNb _{0.70-0.795} Nb	11.3-12.9	
LaRh ₃	1.63	C15	NNb _{0.70-0.795} Nb	13.5-17.0	BI
LaRu ₂	6.5	D7 ₃	NNb _{0.70-0.795} Nb	6.0-11	
La ₂ S ₄	8.6	D7 ₃	N _{100-42 w/o} Nb _{0-18 w/o} Ti††	15-16.8	
La ₂ Se ₄	2.3	C _v	N _{100-75 w/o} Nb _{0-25 w/o} Zr††	12.5-16.35	
LaSi ₂	1.7-5.4		NNb _{0.71-1.2}	9.8-13.8	BI
La ₂ Y _{1-x}	1.04	B2	Nb _{0.95} Nb _{0.05} Zr _{0.15}	13.8	BI
LaZn	7.2	C14	Nb ₂ O ₇ Ti ₄	2.9-5.6	Cubic
LiPb	3.49	C15	Nb ₂ O ₇ V ₄	5.8-8.2	Cubic
LuOs ₂	1.27	C15	Nb _{0.34} Re	4-5	Cubic, f.c.
Lu _{0.275} Rh _{0.725}	0.49		NTa	12-14	BI
LuRh ₃	0.86	C14		(extrapolated)	
LuRu ₂	2.75	B2	NTa (film)	4.84	BI
Mg _{0.4-0.47} Tl _{0.53}	5.6		Nb _{0.6-0.987} Ti	<1.17-5.8	BI
Mg ₂ Nb	2.3 max.	Mn in α-Ti	Nb _{0.82-0.99} V	2.9-7.9	BI
Mn ₂ Ti _{1-x}	1.1-3.0	Mn in β-Ti	NZr	3.0-9.5	BI
Mn ₂ Ti _{1-x}	2.32	D2 ₂	Nb _{0.906-0.984} Zr	0.56	Tetragonal
MnU ₆	12	Hexagonal	Nb _{0.28-0.35} O ₃ W	7.2	
MoN	5.0	Cubic, f.c.	Nb _{0.28} Pb _{0.72}	1.25	
Mo ₂ N	0.016-9.2		NbO	2.52	A12
Mo ₂ Nb _{1-x}	7.2	A15	NbO ₂	1.05	A15
Mo ₂ Os	5.65	D8 ₈	Nb ₃ Os	1.89, 1.78	D8 ₈
Mo _{0.60} Os _{0.38}	5.31	DO ₂	Nb _{0.6} Os _{0.4}	2.42-2.30	A15
Mo ₃ P	3.52	A3	Nb ₃ Os _{0.02-0.10} Rh _{0.98-0.90}	1.60	D8 ₇ plus cubic
Mo _{0.5} Pd _{0.5}	10.0		Nb _{0.6} Pd _{0.4}	2.49-2.55	A15
Mo ₃ Re	1.2-12.2		Nb ₃ Pd _{0.02-0.10} Rh _{0.98-0.90}	4.21	D8 ₈
Mo ₂ Re _{1-x}	9.25, 9.89	A12	Nb _{0.62} Pt _{0.38}	10.9	A15
MoRe ₃	6.35	D8 ₈	Nb ₃ Pt	3.73	D8 ₈
Mo _{0.42} Re _{0.58}	11.1		Nb ₃ Pt _{0.02-0.98} Rh _{0.98-0.02}	2.52-9.6	A15
Mo _{0.52} Re _{0.48}	14.0		Nb _{0.38-0.18} Re _{0.62-0.82}	2.43-9.70	A15
Mo _{0.57} Re _{0.43}	10.6		Nb ₃ Rh	2.64	A15
Mo _{0.60} Re _{0.395}	1.97	A3	Nb _{0.60} Rh _{0.40}	4.21	D8 ₈ plus other
MoRh	1.5-8.2	Cubic, b.c.	Nb ₃ Rh _{0.98-0.90} Ru _{0.02-0.10}	2.42-2.44	A15
MoRh _{1-x}	9.5-10.5	A3	Nb ₂ Ru _{1-x}	1.2-4.8	
MoRu	7.18	D8 ₈	NbS ₂	6.1-6.3	Hexagonal, NbSe ₂ type
Mo _{0.61} Ru _{0.39}	1.66	A3			
Mo _{0.3} Ru _{0.8}	2.1				
Mo ₂ Sb ₄					

†w/o denotes weight percent.

††See key at end of table.

SELECTED SUPERCONDUCTIVE COMPOUNDS AND ALLOYS (Continued)

Substance	T_c , °K	Crystal structure type††	Substance	T_c , °K	Crystal structure type††
NbS ₂	5.0-5.5	Hexagonal, three-layer type	Os ₂ Zr	3.0	C14
Nb ₃ Sb _{0.7} Sn _{1.3}	6.8-18	A15	Os ₂ Zr _{1-x}	1.50-5.6	
NbSe ₂	5.15-5.62	Hexagonal, NbS ₂ type	FPb	7.8	
Nb _{1-1.05} Se ₂	2.2-7.0	Hexagonal, NbS ₂ type	FPd _{3.0-3.2}	<0.35-0.7	DO ₁₁
Nb ₃ Si	1.5	Li ₂	F ₃ Pd ₇ (high temperature)	1.0	Rhombohedral Complex
Nb ₃ SiSnV ₃	4.0		PRh	0.70	
Nb ₃ Sn	18.05	A15	PRh ₂	1.22	
Nb _{0.8} Sn _{0.2}	18.18, 18.5	A15	PW ₃	1.3	C1
Nb ₃ Sn _{1-x} (film)	2.6-18.5		Pb ₂ Pd	2.26	DO ₂
Nb ₃ Sn ₂	2.60	Orthorhombic	Pb ₄ Pt	2.95	C16
Nb ₃ Sn ₂	16.6	Tetragonal	Pb ₂ Rh	2.80	Related to C16
Nb ₃ SnTa ₂	10.8	A15	PtSb	2.66	C16
Nb ₃ SnTa ₂	16.4	A15	PbTe (plus 0.1 w/o Pb)†	6.6	
Nb _{1.3} SnTa _{0.5}	17.6	A15	PbTe (plus 0.1 w/o Ti)†	5.19	
Nb _{1.75} SnTa _{0.25}	17.8	A15	PbTi _{0.27}	5.24-5.27	
Nb _{1.3} SnTa _{0.7} (1-2)	6.0-18.0		PbTi _{0.17}	6.43	
Nb ₃ SnTaV	6.2	A15	PbTi _{0.12}	6.73	
Nb ₃ SnTa _{0.5} V _{0.5}	12.2	A15	PbTi _{0.075}	6.88	
Nb ₃ SnV ₂	5.5	A15	PbTi _{0.04}	6.98	
Nb ₃ SnV	9.8	A15	Pb _{1-0.26} Tl _{0-0.74}	7.06	
Nb _{1.3} SnV _{0.5}	14.2	A15	PbTi ₂	7.20-3.68	
Nb ₃ Ta _{1-x}	4.4-9.2	A2	PbZr ₅	3.75-4.1	
Nb ₃ Tc ₃	10.5	A12	Pd _{0.9} Pt _{0.1} Tc ₂	4.60	D8 ₈
Nb ₃ Ti ₁₋₂	0.6-9.8		Pd _{0.01} Ru _{0.01} Zr _{0.9}	0.76	A15
Nb _{0.6} Ti _{0.4}	9.8		Pd _{1.25} S (quenched)	1.65	C6
Nb ₃ U _{1-x}	1.95 max.		PdSb ₂	~9	
Nb _{0.88} Y _{0.12}	5.7	A2	PdSb	1.63	Cubic
Nb _{0.75} Zr _{0.25}	10.8		PdSbSe	1.25	C2
Nb _{0.66} Zr _{0.33}	10.8		PdSbTe	1.50	B8 ₂
Ni _{0.3} Tb _{0.7}	1.98	DI0 ₂	Pd ₂ Se	1.0	C2
NiZr ₂	1.52		Pd ₂ Se	1.2	C2
Ni _{0.1} Zr _{0.9}	1.5	A3	Pd _{2-x} Se	0.42	Tetragonal
Os ₃ Rb _{0.27-0.29} W	1.98	Hexagonal	Pd _{2-x} Se	0.66	Like Pd ₄ Te
Os ₃ SnTi	0.12-0.37		Pd _{2-x} Se	2.3	
(n = 1.7-12.0 × 10 ¹⁹)			Pd _{2-x} Se	2.5 max.	
Os ₃ SnTi	0.05-0.47		PdSi	0.93	B31
(n = 10 ¹⁸ -10 ²¹)			PdSn	0.41	B31
Os ₃ SnTi	0.47		PdSn ₂	3.34	
OTi	0.58		Pd ₃ Sn	0.41	C37
Os ₂ Se _{0.01} W	2-4	Hexagonal	Pd ₃ Sn ₂	0.47-0.64	B8 ₂
Os ₃ Tl _{0.30} W	2.0-2.14	Hexagonal	PdTe	2.3, 3.85	B8 ₁
OV ₃ Zr ₃	7.5	E9 ₃	PdTe _{1.02-1.08}	2.56-1.88	B8 ₁
OW ₃ (film)	3.35, 1.1	A15	PdTe ₂	1.69	C6
OsReY	2.0	C14	PdTe _{2.1}	1.89	C6
Os ₂ Sc	4.6	C14	PdTe _{2.3}	1.85	C6
OsTa	1.95	A12	Pd _{1.1} Te	4.07	B8 ₁
Os ₃ Th ₇	1.51	DI0 ₂	PdTh ₂	0.85	C16
Os ₂ W _{1-x}	0.9-4.1		Pd _{0.1} Zr _{0.9}	7.5	A3
OsW ₃	~3		PtSb	2.1	B8 ₁
Os ₂ Y	4.7	C14	PtSi	0.88	B31
			PtSn	0.37	B8 ₁
			PtTe	0.59	Orthorhombic
			PtTh	0.44	B _f
			Pt ₃ Th ₇	0.98	DI0 ₂
			Pt ₃ Th	3.13	

†w/o denotes weight percent.

††See key at end of table.

Substance	T_c , °K	Crystal structure type††	Substance	T_c , °K	Crystal structure type††
PtTi ₃	0.58	A15	Ru ₂ Y	1.52	C14
Pt _{0.02} U _{0.98}	0.87	β-phase	Ru ₂ Zr	1.84	C14
PtV _{2.5}	1.36	A15	Ru _{0.1} Zr _{0.9}	5.7	A3
PtV ₃	2.87-3.20	A15	SbSn	1.30-1.42,	BI or distorted
PtV _{3.5}	1.26	A15		1.42-2.37	BI
Pt _{0.5} W _{0.5}	1.45	A1	SbTi ₃	5.8	A15
Pt ₁ W _{1-x}	0.4-2.7		Sb ₂ Ti ₃	5.2	
Pt ₁ Y ₃	0.90		Sb _{0.01-0.03} V _{0.99-0.97}	3.76-2.63	A2
Pt ₁ Y	1.57, 1.70	C15	SbV ₃	0.80	A15
Pt ₁ Y ₂	0.82	D10 ₂	Si ₂ Th	3.2	C ₁₁ , α-phase
PtZr	3.0	A3	Si ₂ Th	2.4	C32, β-phase
Rc _{0.44} Ta _{0.56}	1.46	A12	SiV ₃	17.1	A15
Rc _{0.4} Ti _{0.6}	6.60	A12	Si _{0.9} V _{0.1} Al _{0.1}	14.05	A15
Rc ₁ Ti _{1-x}	6.6 max.		Si _{0.9} V _{0.1} Ba _{0.1}	15.8	A15
Rc _{0.76} V _{0.24}	4.52	D8 ₈	Si _{0.9} V _{0.1} Cu _{0.1}	16.4	A15
Rc _{0.92} V _{0.08}	6.8	A3	SiV _{2.5} Cr _{0.5}	11.3	A15
Rc _{0.6} W _{0.4}	6.0		Si _{0.9} V _{0.1} Cr _{0.1}	14.0	A15
Rc _{0.3} W _{0.7}	5.12	D8 ₈	SiV _{2.5} Mo _{0.5}	11.7	A15
Rc ₁ Y	1.83	C14	SiV _{2.5} Nb _{0.5}	12.8	A15
Rc ₁ Zr	5.9	C14	SiV _{2.5} Ru _{0.5}	2.9	A15
Rc _{0.4} Zr	7.40	A12	SiV _{2.5} Ti _{0.5}	10.9	A15
Rh _{1.5} Si _{1.5}	5.8	Cubic	SiV _{2.5} Zr _{0.5}	13.2	A15
Rh _{0.34} Sc _{0.66}	0.88, 0.92		Si ₂ W ₃	2.8, 2.84	
Rh ₁ Se _{1-x}	6.0 max.		Sn _{0.174-0.104} Ta _{0.826-0.896}	6.5-4.2	A15
Rh ₁ Sr	6.2	C15	SnTa ₃	8.35	A15, highly ordered
Rh _{0.4} Ta _{0.6}	2.35	D8 ₈			A15, partially ordered
RhTc ₁	1.51	C2	SnTa ₃	6.2	
Rh _{0.67} Tc _{0.33}	0.49		SnTaV ₃	2.8	A15
Rh ₁ Tc _{1-x}	1.51 max.		SnTa ₂ V	3.7	A15
RhTh	0.36	B _f	Sn ₂ Tc _{1-x}		
Rh ₁ Th ₇	2.15	D10 ₂	(n = 10.5-20 × 10 ²⁰)	0.07-0.22	BI
Rh ₁ Th	1.07		Sn ₂ Ti _{1-x}	2.37-5.2	
Rh ₁ Ti _{1-x}	2.25-3.95		SnV ₃	3.8	A15
Rh _{0.02} U _{0.98}	0.96		Sn _{0.02-0.057} V _{0.98-0.943}	2.87-~1.6	A2
RhV ₃	0.38	A15	Ta _{0.025} Ti _{0.975}	1.3	Hexagonal
RhW	~3.4	A3	Ta _{0.05} Ti _{0.95}	2.9	Hexagonal
RhY ₃	0.65		Ta _{0.05-0.75} V _{0.95-0.25}	4.30-2.65	A1
Rh ₁ Y ₃	1.48		Ta _{0.8-1} W _{0.2-0}	1.2-4.4	A2
Rh ₁ Y	1.07	C15	Tc _{0.1-0.4} W _{0.9-0.6}	1.25-7.18	Cubic
Rh ₁ Y	0.56		Tc _{0.56} W _{0.50}	7.52	α plus σ
RhZr ₂	10.8	C16	Tc _{0.45} W _{0.40}	7.88	σ plus α
Rh _{0.005} Zr (annealed)	5.8		Tc ₂ Zr	9.7	A12
Rh _{0.45} Zr _{1-0.55}	2.1-10.8		Th _{0-0.55} Y _{1-0.45}	1.2-1.8	C15
Rb _{0.1} Zr _{0.9}	9.0	Hexagonal, c.p.	Ti _{0.70} V _{0.30}	6.14	Cubic
Ru ₃ Sc	1.67	C14	Ti ₁ V _{1-x}	0.2-7.5	
Ru ₃ Th	3.56	C15	Ti _{0.5} Zr _{0.5} (annealed)	1.23	
RuTi	1.07	B2	Ti _{0.5} Zr _{0.5} (quenched)	2.0	
Ru _{0.05} Ti _{0.95}	2.5		V ₁ Zr	8.80	C15
Ru _{0.1} Ti _{0.9}	3.5		V _{0.36} Zr _{0.74}	~5.9	
Ru ₁ Ti _{0.6} V _{0.4}	4.0 max.		W ₂ Zr	2.16	C15
Ru _{0.45} V _{0.55}	4.0	B2			
RuW	7.5	A3			

†† See key at end of table.

 * See "H₂"

CRITICAL FIELD DATA

Substance	H_{c2} oersteds	Substance	H_{c2} oersteds
Ag ₂ F	2.5	InSb	1,100
Ag ₂ NO ₁₁	57	In _{0.8} Tl _{0.2}	252-284
Al ₂ CMO ₃	1,700	In _{0.8} Tl _{0.2}	252
BaBi ₂	740	Mg _{0.47} Tl _{0.53}	220
Bi ₂ Pt	10	Mo _{0.16} Tl _{0.84}	<985
Bi ₂ Sr	530	NbSb ₂	620
Bi ₂ Tl ₃	>400	PbTl _{0.27}	796
CdSn	>266	PbTl _{0.17}	849
CoSi ₂	105	PbTl _{0.12}	880
Cr _{0.1} Ti _{0.9} V _{0.6}	1,360	PbTl _{0.075}	864
In _{1-0.86} Mg _{0-0.14}	272.4-259.2	PbTl _{0.04}	

KEY TO CRYSTAL STRUCTURE TYPES

"Strukturbericht" type*	Example	Class	"Strukturbericht" type*	Example	Class
A1	Cu	Cubic, f.c.	C15 ₂	AuBe ₂	Cubic
A2	W	Cubic, b.c.	C16	CuAl ₂	Tetragonal, b.c.
A3	Mg	Hexagonal, close packed	C18	FeS ₂	Orthorhombic
A4	Diamond	Cubic, f.c.	C22	Fe ₂ P	Trigonal
A5	White Sn	Tetragonal, b.c.	C23	PbCl ₂	Orthorhombic
A6	In	Tetragonal, b.c. (f.c. cell usually used)	C32	AlB ₂	Hexagonal
A7	As	Rhombohedral	C36	MgNi ₂	Hexagonal
A8	Se	Trigonal	C37	Co ₂ Si	Orthorhombic
A10	Hg	Rhombohedral	C49	ZrSi ₂	Orthorhombic
A12	α-Mn	Cubic, b.c.	C54	TiSi ₂	Orthorhombic
A13	β-Mn	Cubic	C	Si ₂ Th	Tetragonal, b.c.
A15	"β-W" (WO ₃)	Cubic	DO ₃	BiF ₃	Cubic, f.c.
B1	NaCl	Cubic, f.c.	DO ₁₁	Fe ₂ C	Orthorhombic
B2	CsCl	Cubic	DO ₁₈	Na ₃ As	Hexagonal
B3	ZnS	Cubic	DO ₁₉	Ni ₃ Sn	Hexagonal
B4	ZnS	Hexagonal	DO ₂₀	NiAl ₃	Orthorhombic
B8 ₁	NiAs	Hexagonal	DO ₂₂	TiAl ₃	Tetragonal
B8 ₂	Ni ₂ In	Hexagonal	DO ₂	Ni ₃ P	Tetragonal, b.c.
B10	PbO	Tetragonal	D1 ₃	Al ₂ Ba	Tetragonal, b.c.
B11	γ-CuTi	Tetragonal	D1 ₄	PtSn ₄	Orthorhombic
B17	PrS	Tetragonal	D2 ₁	CaB ₆	Cubic
B18	CuS	Hexagonal	D2 ₂	MnU ₄	Tetragonal, b.c.
B20	FeSi	Cubic	D2 ₃	CaZn ₄	Hexagonal
B27	FeB	Orthorhombic	D5 ₂	La ₂ O ₃	Trigonal
B31	MnP	Orthorhombic	D5 ₃	Sb ₂ S ₃	Orthorhombic
B32	NaTi	Cubic, f.c.	D7 ₃	Th ₃ P ₄	Cubic, b.c.
B34	PdS	Tetragonal	D7 ₈	Ta ₃ B ₄	Orthorhombic
B ₇	δ-CrB	Orthorhombic	D8 ₁	Fe ₂ Zn ₁₀	Cubic, b.c.
B ₈	MoB	Tetragonal, b.c.	D8 ₂	Cu ₂ Zn ₈	Cubic, b.c.
B ₉	WC	Hexagonal	D8 ₃	Cu ₉ Al ₄	Cubic
B ₁	γ-MoC	Hexagonal	D8 ₄	Mn ₂ Si ₃	Hexagonal
C1	CaF ₂	Cubic, f.c.	D8 ₅	CrFe	Tetragonal
C1 _a	MgAgAs	Cubic, f.c.	D8 ₆	Mo ₂ B ₃	Rhombohedral
C2	FeS ₂	Cubic	D10 ₂	Fe ₂ Th ₃	Hexagonal
C6	ClI ₂	Trigonal	E2 ₁	CaTiO ₃	Cubic
C11b	MoSi ₂	Tetragonal, b.c.	E2 ₂	Fe ₂ W ₃ C	Cubic, f.c.
C12	CaSi ₂	Rhombohedral	L1 ₀	CuAu	Tetragonal
C14	MgZn ₂	Hexagonal	L1 ₂	Cu ₂ Au	Cubic
C15	Cu ₂ Mg	Cubic, f.c.	L2 _a	ThH ₂	Tetragonal, b.c.
			L3	Fe ₂ N	Hexagonal

*See "Handbook of Lattice Spacing and Structures of Metals", W.B. Pearson, Vol. 1, Pergamon Press, 1958, p. 79, and Vol. II, Pergamon Press, 1967, p. 3.

HIGH CRITICAL MAGNETIC-FIELD SUPERCONDUCTIVE COMPOUNDS AND ALLOYS

With Critical Temperatures, H_{c1} , H_{c2} , H_{c3} , and the Temperature of Field Observations, T_{obs}

Substance	T_c , °K	H_{c1} , kg	H_{c2} , kg	H_{c3} , kg	T_{obs} , °K†
Al_2CMo_3	9.8-10.2	0.091	156		1.2
$AlNb_3$		0.371			
$Ba_0.9Sr_{1-x}Ti$	<0.1-0.55	0.0039 max.			
$Bi_{0.9}Cd_{0.1}Pb_{0.25}Sn_{0.15}$			>24		3.06
Bi_1Pb_{1-x}	7.35-8.4	0.122 max.	>30 max.		4.2
$Bi_{0.98}Pb_{0.02}$	8.8		15		4.2
$Bi_{1-x}Pb_{0.25}Sn_{0.07}$			2.32		
$Bi_{0.992}Pb_{0.008}$		0.29	2.8		
$Bi_{0.99}Pb_{0.01}$		0.46	0.73		
$Bi_{0.99}Pb_{0.01}Sn_{0.016}$			>25		3.06
$Bi_{1-x}Sn_{0.07}$			0-0.032		3.7
Bi_2Ti_3	6.4		>5.56		3.35
C_6K (excess K)	0.55		0.160 (H⊥c)		0.32
			0.730 (H c)		0.32
C_6K	0.39		0.025 (H⊥c)		0.32
			0.250 (H c)		0.32
$C_{0.44}Mo_{0.56}$	12.5-13.5	0.087	98.5		1.2
CNb	8-10	0.12	16.9		4.2
$CNb_{0.8}Ta_{0.6}$	10-13.6	0.19	14.1		1.2
CTa	9-11.4	0.22	4.6		1.2
$Cd_2O_3Sr_{1-x}Ti$	<0.1-0.55	0.002-0.004			
$Cd_{0.1}Hg_{0.9}$		0.23	0.34		2.04
(by weight)					
$Cd_{0.03}Hg_{0.97}$		0.28	0.31		2.16
$Cd_{0.10}Tl_{0.30}V_{0.60}$	5.6	0.071	84.4		0
GaN	5.85	0.725			4.2
Ga_2Nb_{1-x}			>28		4.2
GaSb (annealed)	4.24		2.64		3.5
$GaV_{1.95}$	5.3		73***		0
$GaV_{2.1-3.5}$	6.3-14.45		230-300**		0
GaV_3		0.4	350***		0
			500**		
$GaV_{4.5}$	9.15		121*		0
$HfNb_3$			>52->102		1.2
$HfTa_3$			>28->86		1.2
$Hg_{0.95}Pb_{0.05}$		0.235	2.3		4.2
$Hg_{0.10}Pb_{0.89}$		0.23	4.3		2.93
$Hg_{0.12}Pb_{0.88}$	~6.75		>13		2.76
$In_{0.94}Pb_{0.06}$	3.45	0.1		0.12	2.94
$In_{0.96}Pb_{0.04}$	3.68	0.1	0.12	0.25	3.12
$In_{0.94}Pb_{0.06}$	3.90	0.095	0.18	0.35	
$In_{0.912}Pb_{0.087}$	4.2	~0.17	0.55	2.65	
$In_{0.916}Pb_{0.084}$		0.155	3.7		4.2
$In_{0.91}Pb_{0.09}$			2.8	5.5	4.2
$In_{1.000}Tl_{1.002}$	3.5-3.7		1.2*		0
$In_{0.99}Tl_{0.01}$		0.263	0.263		3.3
$In_{0.90}Tl_{0.10}$		0.257	0.257		3.25
$In_{0.83}Tl_{0.17}$		0.242	0.39		3.21
$In_{0.75}Tl_{0.25}$		0.216	0.50		3.16
LaN	1.35	0.45			0.76
La_2Se_4	6.5	~0.15	>25		1.3
La_2Se_4	8.6	~0.2	>25		1.25
$Mo_{0.52}Re_{0.48}$	11.1		14-21	22-33	4.2
			18-28	37-43	1.3
$Mo_{0.62}Re_{0.38}$	10.6		14-20	20-37	4.2
			19-26	26-37	1.3
$Mo_{0.93}Te_{0.07}$			~75*		0
$Mo_{0.9}Te_{0.1}$	4.18	0.028	98.7*		0
$Mo_{0.16}Te_{0.84}$			36-38		3.0
$Mo_{0.91}Ti_{0.09}$	2.95	0.060	~15		4.2
$Mo_{0.1-0.3}U_{0.9-0.7}$	1.85-2.06		>25		
$Mo_{0.17}Zr_{0.83}$			~30		
$N_{12.8}Nb_{87.2}$	15.2		>9.5		13.2
NNb (wires)	16.1		153*		0
			132		4.2
			95		8
			53		12
NNb_3O_{1-x}	13.5-17.0		~38		
NNb_3Zr_{1-x}	9.8-13.8		4->130		4.2
$Nb_{0.93}Nb_{0.07}Zr_{0.15}$			>130		4.2
$Nb_{0.98}Pb_{0.02}$		0.19	6.0		
$Nb_{0.91}Pb_{0.09}$		0.28	2.05		

†w/o denotes weight percent.

HIGH CRITICAL MAGNETIC-FIELD SUPERCONDUCTIVE COMPOUNDS AND ALLOYS (Continued)

Substance	T_c , °K	H_{c1} , kg	H_{c2} , kg	H_{c3} , kg	T_{ab} , °K†
Nb	9.15		2.020		1.4
Nb			1.710		4.2
Nb (unstrained)		0.4-1.1	3-5.5		4.2
Nb (strained)		1.1-1.8	3.40	6-9.1	4.2
Nb (cold-drawn wire)		1.25-1.92	3.44	6.0-8.7	4.2
Nb (film)		2.48	4.10	≈10	4.2
NbSc			>25		4.2
Nb ₃ Sn			>30		
		0.170	221		4.2
			70		14.15
			54		15
			34		16
			17		17
Nb _{0.1} Ta _{0.9}		0.084	0.154		4.195
Nb _{0.2} Ta _{0.8}			10		4.2
Nb _{0.65} -0.75Ta _{0.02} -0.10Zr _{0.15}			>70->90		4.2
Nb ₁ Ti _{1-x}			148 max.		1.2
			120 max.		4.2
Nb _{0.222} U _{0.778}		1.98	23		1.2
Nb ₁ Zr _{1-x}			127 max.		1.2
			94 max.		4.2
O ₃ SrTi	0.43	.0049*	.504*		0
O ₃ SrTi	0.33	.00195*	.420*		0
PbSb _{1-x} (quenched)			>1.5		4.2
PbSb _{1-x} (annealed)			>0.7		4.2
PbSb _{2.8-x} (quenched)			>2.3		4.2
PbSb _{2.8-x} (annealed)			>0.7		4.2
Pb _{0.87} Sn _{0.129}		0.45	1.1		
Pb _{0.965} Sn _{0.035}		0.53	0.56		
Pb _{1-x} Ti _x 0-0.74	7.20-3.68		2-6.9*		0
PbTi _{0.17}	6.73		4.5*		0
Ru _{0.26} W _{0.74}			>30		
Sb _{0.83} Sn _{0.07}			0.12		3.7
SiV ₃	17.0	0.55	156***		
Sn ₁ Te _{1-x}		0.00043-	0.005-		0.012-
		0.00236	0.0775		0.079
Ta (99.95%)			1.850		1.3
		0.425	1.425		2.27
		0.275	1.175		2.66
		0.090	0.375		3.72
Ta _{0.3} Nb _{0.7}			3.55		4.2
Ta _{0.65} -0.75Ti _{0.35} -1	4.4-7.8		>14-138		1.2
Ta _{0.4} Ti _{0.6}			138		1.2
Tc	~3.3	0.25*			0
Tc ₁ W _{1-x}	5.75-7.88		8-44		4.2
Ti				2.7	4.2
Ti _{0.12} V _{0.25}	5.3	0.029*	199*		0
Ti _{0.178} V _{0.225}	4.7	0.024*	172*		0
Ti _{0.615} V _{0.385}	7.07	0.050	~34		4.2
Ti _{0.516} V _{0.484}	7.20	0.062	~28		4.2
Ti _{0.415} V _{0.585}	7.49	0.078	~25		4.2
Ti _{0.12} V _{0.88}			17.3	28.1	4.2
Ti _{0.05} V _{0.95}			14.3	16.4	4.2
Ti _{0.04} V _{0.94}			8.2	12.7	4.2
Ti _{0.03} V _{0.97}			3.8	6.8	4.2
Ti ₁ V _{1-x}			108 max.		1.2
V	5.31	~0.8	~3.4		1.79
		~0.75	~3.15		2
		~0.45	~2.2		3
		~0.30	~1.2		4
V _{0.26} Zr _{0.74}	≈5.9	0.238			1.05
		0.227			1.78
		0.185			3.04
		0.165			3.5
W (film)	1.7-4.1		>34		1

†Temperature of critical field measurement.

*Extrapolated.

**Linear extrapolation.

***Parabolic extrapolation.

TABLES OF PROPERTIES OF SEMICONDUCTORS

Compiled by Dr. Brian Randall Pamplin

The term "semiconductor" is applied to a material in which electric current is carried by electrons or holes and whose electrical conductivity when extremely pure rises exponentially with temperature and may be increased from this low "intrinsic" value by many orders of magnitude by "doping" with electrically active impurities.

Semiconductors are characterised by an energy gap in the allowed energies of electrons in the material which separates the normally filled energy levels of the *valence band* (where "missing" electrons behave like positively charged current carriers "holes") and the *conduction band* (where electrons behave rather like a gas of free negatively charged carriers with an effective mass dependent on the material and the direction of the electrons' motion). This energy gap depends on the nature of the material and varies with direction in anisotropic crystals. It is slightly dependent on temperature and pressure, and this dependence is usually almost linear at normal temperatures and pressures.

The data is presented in three tables. Table I "General Properties of Semiconductors" lists the main crystallographic and semiconducting properties of a large number of semiconducting materials in three main categories; "Tetrahedral Semiconductors" in which every atom is tetrahedrally co-ordinated to four nearest neighbour atoms (or atomic sites) as for example in the diamond structure; "Octahedral Semiconductors" in which every atom is octahedrally co-ordinated to six nearest neighbour atoms—as for example in the halite structure; and "Other Semiconductors".

Table II gives more detailed information about some better known semiconductors, while Table III gives some information about the electronic energy band structure parameters of the best known materials.